UNIVERSITY OF BIRMINGHAM

DESIGN AND ANALYSIS OF SPREADING CODE AND TRANSCEIVER ARCHITECTURES FOR OPTICAL CDMA NETWORKS

BY

MOHAMMAD MASSOUD KARBASSIAN

A thesis submitted to
The University of Birmingham
for the degree of
DOCTOR OF PHILOSOPHY

COLLEGE OF ENGINEERING AND PHYSICAL SCIENCE
SCHOOL OF ELECTRONIC, ELECTRICAL AND COMPUTER ENGINEERING
May 2009

Abstract

In this thesis, firstly we have reviewed both previous and current state of optical CDMA (OCDMA) technologies. Search for appropriate spreading codes is one of the main challenges of OCDMA applications and hence is an important topic which is heavily addressed in the literature. Existing codes have restrictions on code-lengths, weights and correlation properties where the number of generated codes is severely limited.

Secondly, we have paid a particular attention in proposing a novel spreading code, hereby referred to as Double Padded Modified Prime Code (DPMPC) which suppresses the multiple-access interference (MAI) and also enhances the network capacity.

Then, we have applied the DPMPC to both coherent and incoherent time-spreading OCDMA transceivers and analysed their overall performances. We have also proposed novel transceivers which are power-efficient, simple and able to accommodate great number of simultaneous users. Accordingly, an advanced two-dimensional frequency-polarization modulation for OCDMA is introduced, for the first time, to elevate the system security as well as the performance.

Finally, the application of OCDMA in the passive optical network (PON) leading to the OCDMA-PON architecture is introduced including the optical line terminal and network units. Since Internet protocol (IP) is the dominant network protocol, IP-over-OCDMA network node configuration has also been proposed and analysed.

To my beloved parents

Acknowledgements

I would like to use this opportunity to express my sincere gratitude to my supervisor, *Dr. Hooshang Ghafouri-Shiraz*, for his continuous encouragement, advice and motivation that enabled me to achieve all goals to complete this research to the best of my standard. His insight and knowledge makes him a significant person to me. It is my great honour to be his student.

My profound love and appreciation go to my *parents* and *dearest sister, Mahnaz* for their constant support and kindness at every stage of my life. They always help me with their lucent thoughts that encouraged me to overcome all obstacles. Also many special thanks go to my beloved brother *Mohsen*, for his fruitful discussions, lightening vision, and for having an open ear on my down days.

At last but not least, I have to specially thank *Prof. Martin Russell* and the *School of Electronic, Electrical and Computer Engineering* that supported me financially throughout this research. Without them, I would not be able to pursue my further studies and this thesis was impossible. Also, many thanks go to the post graduate administrator, *Mrs Mary Winkles,* for her warm welcoming problem-solving attitude.

Table of Contents

List of Figures

List of Tables

List of Abbreviations

2D-ary	Two-Dimensional Array
ADSL	Asymmetric Digital Subscriber Line
APD	Avalanche Photo Diode
ASE	Amplified Spontaneous Emission
ASK	Amplitude Shift Keying
ASTN	Automatically Switched Transport Network
AWG	Arrayed Waveguide Grating
AWGN	Additive White Gaussian Noise
BER	Bit-Error Rate
CAT-5	Category-5 Cable
CATV	Community Access Television
CD	Coherent Detection
CDF	Cumulative Density Function
CDM	Code Division Multiplexing
CDMA	Code Division Multiple Access
CO	Central Office
CM	Cable Modem
CSMA/CD	Carrier Sense Multiple Access/Contention Detection
CQPolSK	Circular-Quad Polarization Shift Keying
DBA	Dynamic Bandwidth Allocation
DD	Direct Detection
DFB	Distribute Feedback
DiffServ	Differentiated Services
DMT	Discrete Multi-Tone

DPMPC	Double Padded Modified Prime Code
DSL	Digital Subscriber Line
DSLAM	DSL Access Multiplexer
DSP	Digital Signal Processing
DS-SS	Direct Sequence Spread Spectrum
DWDM	Dense Wavelength Division Multiplexing
EFM	Ethernet in the First Mile
E/O	Electro-Optical Conversion
FBG	Fibre Bragg Grating
FEC	Forward Error Correction
FIFO	First-In First-Out
FH-SS	Frequency-Hopping Spread Spectrum
FPolSK	Frequency-Polarization Shift Keying
FSK	Frequency Shift Keying
FTTB	Fibre to the Building
FTTC	Fibre to the Curb
FTTH	Fibre to the Home
FTTPC	Fibre to the Personal Computer
GbE	Gigabit Ethernet
Gbps	Giga Bits per Second
GMPLS	Generalised Multiprotocol Label Switch
GSS	Group Stream Sequence
HDTV	High Definition Television
HFC	Hybrid Fibre-Coax
HDSL	High-speed Digital Subscriber Line
IF	Intermediate Frequency
IM	Intensity Modulation
IP	Internet Protocol
ISDN	Integrated Service Data Network
ITU-T	International Telecommunication Union – Telecommunication
IQ	In-phase/Quadrature-phase

Kpbs	Kilo Bits per Second
LAN	Local Area Network
LCM	Liquid Crystal Modulator
LED	Light Emitting Diode
LPF	Low Pass Filter
LSP	Label Switched Path
M-ary	Multiple Array
MAC	Medium Access Control
MAI	Multiple Access Interference
Mbps	Mega Bits per Second
ML	Maximum Likelihood
MPC	Modified Prime Code
MPLS	Multiprotocol Label Switching
MQC	Modified Quadratic Congruence
MZI	Mach-Zehnder Interferometer
MZM	Mach-Zehnder Modulator
n-MPC	new-Modified Prime Code
NGN	Next Generation Network
O/E	Opto-Electronic Conversion
OBI	Optical Beating Interference
OCDM	Optical Code Division Multiplexing
OCDMA	Optical Code Division Multiple Access
OLT	Optical Line Terminal
OLS	Optical Label Swapping
OOC	Optical Orthogonal Code
OOK	On-OFF Keying
ONU	Optical Network Unit
OP	Optical Pulse
OPPM	Overlapping Pulse Position Modulation
OPS	Optical Packet Switched
OTDL	Optical Tapped Delay Line

OXC	Optical Cross Connect
P2P	Point-to-Point
P2MP	Point-to-Multi-Point
PBC	Polarization Beam Combiner
PBS	Polarization Beam Splitter
PC	Prime Code
PCS	Physical Coding Sublayer
PD	Photo-Detector
PDF	Probability Density Function
PER	Packet-Error Rate
PHY	Physical Layer
PIIN	Phase Induced Intensity Noise
PLOAM	Physical Layer Operation, Administration and Maintenance
PMD	Polarization Mode Dispersion
PN	Pseudo-Noise
PON	Passive Optical Network
PolSK	Polarization Shift Keying
POTS	Plain Old Telephone Service
PPM	Pulse Position Modulation
PSD	Power Spectral Density
PSK	Phase Shift Keying
QoS	Quality of Service
RF	Radio Frequency
ROADM	Reconfigurable Optical Add Drop Multiplexer
SAC	Spectral Amplitude Coding
SAN	Storage Area Network
SCMA	Sub-Carrier Multiple Access
SDH	Synchronous Data Hierarchy
SI	Self-Interference
SLA	Service Level Agreement
SMF	Single Mode Fibre-optic

SNR	Signal to Noise Ratio
SOA	Service Oriented Architecture
SONET	Synchronous Optical Network
SOP	State of Polarization
SPC	Spectral Phase Coding
SPON	Star Passive Optical Network
SSC	Spread Spectrum Communication
TDMA	Time Division Multiple Access
TQPolSK	Tetrahedron-Quad Polarization Shift Keying
UNI	User-Network Interface
URL	Uniform resource Locator
VDSL	Very high-bit-rate Digital Subscriber Line
VLAN	Virtual Local Area Network
VoD	Video-on-Demand
VPN	Virtual Private Network
WAN	Wide Area Network
WDM	Wavelength Division Multiplexing
WDMA	Wavelength Division Multiple Access

Chapter 1

Introduction

1.1 Introduction

In recent years the telecommunications backbone has experienced substantial growth however, the access network has changed little. The tremendous growth of Internet traffic has accentuated the aggravating lag of access network capacity. From the operators' side, the last-mile architecture still remains the bottleneck between high-capacity local area networks (LAN) and the backbone network. The last-mile network connects the service provider's central offices to businesses and residential subscribers. In the literature, this network is also referred to as the 'access network', the 'local loop' or even sometimes the 'first-mile' network, i.e. from the users' side. With the recent conversion of audio–visual media to high-definition formats, e.g. Blu-Ray and HDTV, bandwidth consumption can only continue to explode. Meanwhile, miniature laptops, iPhones and Blackberries are driving a wireless revolution.

Accordingly, subscribers demand access solutions which offer high-bandwidth media-rich Internet services as well as comparable prices with existing networks.

In the following, we briefly discuss challenges in the current transport/access networks in terms of network capacity and bandwidth with supported carrier distance. Accordingly, the motivations for optical communications and multiple-access techniques, particularly optical code-division multiple-access, are presented besides the aims and objectives of this research.

1.2 Challenges in Access Networks

Much of the focus and emphasis over the years has been on developing high capacity backbone networks. Backbone network operators currently provide multiple high capacity links with bandwidth of 10 Gbps each. However, current generation access network technologies such as digital subscriber line (DSL) provide 1.5 Mbps of downstream bandwidth and 128 kbps of upstream bandwidth at best. The access network is, therefore, truly the bottleneck for providing broadband services such as video-on-demand (VoD) to the end users [1].

In addition, DSL has a limitation that the distance of any DSL subscriber to a central office must be less than 5000 m because of signal distortions and losses. Typically, DSL providers do not provide services to distances more than 4000 m. Therefore, only an estimated 60% of the residential subscriber base can benefit DSL. Although variations of DSL, such as very high bit-rate DSL (VDSL) which can support up to 50 Mbps of downstream bandwidth, are gradually emerging. These technologies have much more

severe distance limitations; for example, the maximum distance which VDSL can be supported over is limited to 500 meters [2].

The other alternative available for broadband access to end users is through community access television (CATV) networks [3]. CATV networks provide Internet services by dedicating some radio frequency (RF) channels in coaxial cable for data.

However, CATV networks are mainly built for delivering broadcast services, so they do not fit well for distributing access bandwidth. At higher loads, the network's performance is usually frustrating to end users. Faster access network technologies are clearly desired for next generation broadband applications. The next generation access networks promises to bring fibre closer to the home (i.e. end users). The model of fibre-to-the-home (FTTH), fibre-to-the-curb (FTTC), fibre-to-the-building (FTTB), etc [4, 5] offers the potential for extraordinary access bandwidth to end users. These technologies aim at providing fibre directly to the home, or very near the home, from where technologies such as VDSL can take over. FTTx solutions are mainly based on the passive optical network (PON) architectures.

1.3 Motivations for Optical CDMA

Multiple access techniques are required to meet the demand for high-speed and large-capacity communications in the optical networks, which allow multiple users to share the huge fibre bandwidth. There are two major multiple access approaches: each user is allocated a specific time slot in time-division multiple-access (TDMA), or a specific frequency (wavelength) slot in wavelength division multiple-access (WDMA). Both techniques have been extensively explored and utilized in optical communication

systems [6-19]. Alternatively, optical code-division multiple-access (OCDMA) [20-41] is receiving increasing attention due to its potential for enhanced information security, simplified and decentralized network control, improved spectral efficiency, and increased flexibility in the granularity of bandwidth that can be provisioned. In OCDMA, different users whose signals may be overlapped both in time and frequency share a common communications medium; multiple-access is achieved by assigning unlike minimally interfering code sequences to different transmitters, which must subsequently be detected in the presence of multiple access interference (MAI) from other users.

However, the need to perform encoding and decoding for OCDMA poses one immediate challenge both because of the optical carrier frequency and the much higher bit-rate of multi gigabit/s per user which already approached the limit of electronic processing. Significant progresses of OCDMA research have been achieved worldwide in recent years; among them several different OCDMA schemes have been proposed based on different choices of sources [15, 27, 31, 42], coding schemes [20, 28, 43] and detections [37, 41, 44-48].

CDMA is well suited for bursty network environments, and the asynchronous nature of data transmission can simplify and decentralise network management and control. However, due to complex system requirements, full asynchronism is difficult to implement in practice while real-time simultaneous MAI suppression due to imperfect spreading codes is still a hot research topic and under investigation [31, 33, 36, 40, 47, 49-53]. Several challenging research topics are still missing for practical OCDMA realization and development. These include the high co-channel interference (i.e. MAI)

naturally present in almost all forms of OCDMA; low network capacity in terms of number of concurrent users; and codes that can support various traffic demands in terms of bandwidth and BER performances.

Furthermore, the motivation for OCDMA local area network (LAN) is reinforced by the expectancy of bursty LAN traffic patterns. OCDMA is recently viewed as a candidate technology for future PON access networks as well [4, 5, 17, 19, 50, 54-56]. The following is a brief description of the main assets that OCDMA exhibits from a networking perspective [32, 57]:

- Ideally, no channel control mechanism is required to avoid collisions or allocate bandwidth. In addition, optical network unit (ONU) are not required to report the instantaneous bandwidth requirements to the optical line terminal (OLT), thereby reducing round-trip time and delay.
- A new TDMA or WDMA user reduces free bandwidth irreversibly due to the bandwidth guaranteed under ONU service-level agreements (SLA), thus requiring changes to bandwidth allocations. For example, for every new user added in TDMA, the OLT may be required to run the admission control process. While in OCDMA, new user does not reduce the other users' bandwidth.
- OCDMA offers the capability to support high-speed symmetric traffic for a larger number of ONU than WDMA [5].
- OCDMA supports a larger number of users than TDMA or WDMA, especially 2D-OCDMA systems [58-61] where codes exploit both time and wavelength dimensions. It is also possible for an even larger number of codes to be assigned in OCDMA if an access protocol is used.

- Like WDMA, OCDMA offers a virtual point-to-point topology over the physical tree architecture. However, in doing so, WDMA requires an in-field WDM multiplexer or individual wavelength filters at the ONU. OCDMA requires the cheaper power splitter and/or correlator but incurs the larger power losses associated.
- Unlike WDMA and TDMA-WDM, OCDMA can accommodate a large number of low bit-rate users on the same optical medium. Moreover, using multi-rate OCDMA techniques, low and high bit-rate channels can be provisioned on the same link. Such aspects correspond to access traffic patterns and are highly desirable as they eliminate electronic grooming.

Moreover, significant CDMA properties of which simple, very high speed and cost effective optical communications can take advantage are also can be mentioned as [32]:

- **No Guard Time or Guard Bands**

In TDMA system when multiple users share the same channel there must be a way to ensure that they do not transmit at the same time to overlap each other's signal. Since there is no really accurate clock recovery a length of time must be allowed between the end of one user's transmission and the beginning of the next. Since the speed gets higher, this guard time comes to dominate the system throughput. In CDMA network, the stations simply transmit when they are ready. Also in WDMA system, unused frequency space is allocated between bands due to frequency overlapping avoidance through filtering process. These guard bands represent wasted bandwidth.

- **Easier System Management**

The users must have frequencies and/or time slots assigned to them through some central administration processes in WDMA and TDMA systems. All you need with CDMA is for communicating stations to have the assigned code.

Above all, we believe that to become viable, serious propositions must include the gradual migration paths from WDMA to OCDMA as is the case currently from TDMA to WDMA [62]. Such migration paths offer partial implementations that postpone some of the research elements required for full OCDMA-PON.

1.4 Aims and Objectives of This Research

The main aims of this research are as follow:

- To examine and develop realistic approaches to analyse the OCDMA concepts considering the most possible degrading parameters in the entire system.
- To design a flexible spreading code with significant correlation properties to suppress MAI effectively.
- To examine and develop reconfigurable transceiver architectures corresponding to the proposed novel spreading code in optical domain, along with channel coding and advanced optical modulations.
- To examine OCDMA as the access protocol in the optical networking and its compatibility to IP transmission in the current and future optical networks.

The specific objectives against which the success of the research should be judged are:

- To carry out theoretical performance evaluation of the OCDMA concepts.
- To design a novel spreading code with excellent correlation properties.
- To design transceiver architectures based on the proposed code and MAI cancellation techniques to enhance the network scalability and capacity.
- To examine the IP-over-OCDMA and OCDMA-PON architectures as the optical access network.

1.5 Thesis Organisation

The organisation of the thesis is as follows:

Chapter 2 introduces common multiple access techniques in optical domain and also the precious spread spectrum communication methods including direct sequence and frequency hopping. The current optical access network technologies along with the next generation architecture are presented and their existing challenges are also reported.

Chapter 3 is dedicated to describe current state of OCDMA technology including coding fundamentals in optical domain and its great merits in access networks. Introduction to different optical spreading codes like optical orthogonal codes (OOC) and prime codes (PC) including the novel prime spreading sequence family hereby referred to as double-padded modified prime code (DPMPC) are also presented. Their constructions, properties and applications are also discussed mathematically in details. The main body of Chapter 3 describes various encoding methods in time, wavelength and spectral domains.

As an incoherent scheme, pulse-position modulation (PPM) with detailed signalling format and architecture is analysed in Chapter 4. In the analysis, Manchester encoding has also been studied as a channel coding to enhance the MAI cancellation.

We have also analysed the DPMPC in overlapping PPM (OPPM) architecture in Chapter 5. Additionally, the network throughput, which is the amount of information transmitted per second by the user, as an important characteristic of a communications network is presented. Here also a new co-channel interference (i.e. MAI) cancellation technique which significantly improves the bit error probability of OCDMA networks is proposed and analysed.

Chapter 6 evaluates the coherent OCDMA techniques and examines the overall system performance in terms of the signal-to-noise ratio penalty as a function of simultaneous users accommodated to maintain an appropriate value of the BER for homodyne and heterodyne detections. As a coherent modulation, binary phase-shift keying (BPSK) format is deployed. In homodyne detection, two different phase modulations are studied including an external phase-modulator (i.e. Mach-Zehnder) and injection-locking method with distributed feed back (DFB) laser diode. The phase limitation and the performance for two methods plus MAI and receiver noise in a shot noise limited regime are investigated. The BER analysis of a heterodyne detection system using an external phase modulator is also examined in Chapter 6.

Chapter 7 proposes a novel MAI cancellation technique taking advantage of coherent modulation and incoherent detection which also simplifies the receiver configuration in synchronous frequency-shift keying (FSK) OCDMA network. In the theoretical

analysis, the system upper bounded bit-error rate (BER) is derived taking into account the Poisson effect on the I/O characteristics of the photo-detectors.

A novel incoherent transceiver structure for the optical modulation scheme deploying polarization shift keying (PolSK) in conjunction with OCDMA is proposed in Chapter 8. The system has been accurately analysed taking into account the presence of optical amplified spontaneous emission (ASE) noise, electronic receiver noise, photo-diode shot-noise and also MAI. The application of optical tapped-delay lines in the receiver as the CDMA-decoder is investigated as well. Furthermore, the new two-dimensional optical modulation scheme deploying hybrid frequency and polarization shift keying (F-PolSK) is also investigated to increase the security in Chapter 8.

Chapter 9 proposes a new IP transmission scheme over OCDMA network. The performance has been analyzed in terms of the users' channel utilization factor in the network. Moreover in Chapter 9, design for passive optical CDMA networks (OCDMA-PON) is proposed. The architectures for optical network units (ONU) and terminals (ONT) are also analysed. The network scalability in terms of fibre link distances as well as BER, considering main performance degrading issues are also investigated.

Finally, the study is concluded in Chapter 10. The significant results and remarks of this research are given as well as considering new challenges which are still remained and worthwhile to investigate as future research topics.

It should be noted that the analyses in this thesis have been performed by the aid of MATLAB technical programming language and the architectures in Chapter 4 and 7 have also been implemented and verified to date in OptiSystem™ (evaluation version provide by OptiWave™), the commercial optical communications software package.

Chapter 2

Multiple Access Techniques

2.1 Introduction

In order to make full use of the available bandwidth in optical fibres and to satisfy the bandwidth demand in future networks, it is necessary to multiplex low-rate data streams onto optical fibre to accommodate great number of subscribers. There is a need for technologies that allow multiple users to share the same frequency, especially as wireless telecommunications continues to increase in popularity. Currently, there are three common types of multiple access systems:

- Wavelength division multiple access (WDMA)
- Time division multiple access (TDMA)
- Code division multiple access (CDMA)

This Chapter reviews the basic multiple access techniques in optical domain and introduces the current state of optical access networks at the end of the Chapter.

2.1.1 Wavelength Division Multiple Access (WDMA)

In WDMA system, each channel occupies a narrow optical bandwidth (≥ 100 GHz) around a centre wavelength or frequency [7].

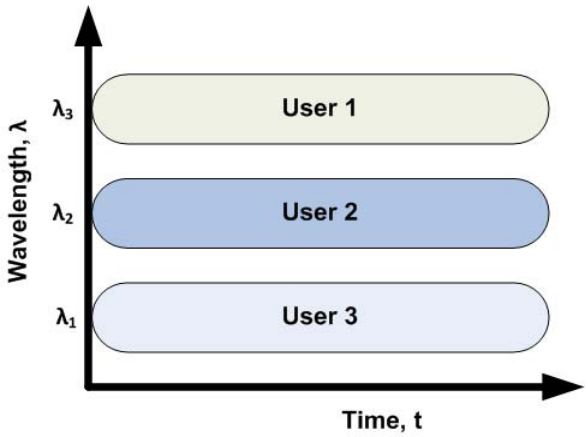

Figure 2.1 Resource sharing based on WDMA technique

The modulation format and speed at each wavelength can be independent of those of other channels as shown in Figure 2.1. Arrayed or tuneable lasers will be needed for WDMA applications [13]. Because each channel is transmitted at a different wavelength, they can be selected using an optical filter [12]. Tuneable filters can be realized using acousto-optics [63], liquid crystal [10], or fibre Bragg grating [43]. To increase the capacity of the fibre link using WDMA we need to use more carriers or wavelengths, and this requires optical amplifiers [64] and filters to operate over extended wavelength ranges. Due to greater number of channels and larger optical power the increased nonlinear effects in fibres causes optical crosstalk such as four-wave mixing [65] over wide spectral ranges. Another approach to increase the capacity of WDMA links is to use dense WDM (DWDM) [14], which will have to operate with reduced channel spacing (ITU-T recommendation G.692 defines 43 wavelength channels from 1530-1565 nm, with a spacing of 100 GHz). This requires a sharp optical

filter with linear phase response, wavelength stable components, and optical amplifiers with flat gain over wide bandwidths, and optical fibres must support hundreds of channels without distortion or crosstalk. With respect to channel switching, wavelength routing is the next switching dimension for DWDM, with interferometric crosstalk being an essential issue in the implementation of cross-connects based on space and wavelength [66]. Hence, the extent of wavelength routing that is realizable places fundamental limits on network flexibility, which in turn determines switch size and implementations complexity and costs.

2.1.2 Time Division Multiple Access (TDMA)

In TDMA system, each channel occupies a pre-assigned time slot, which interleaves with the time slots of other channels as shown in Figure 2.2.

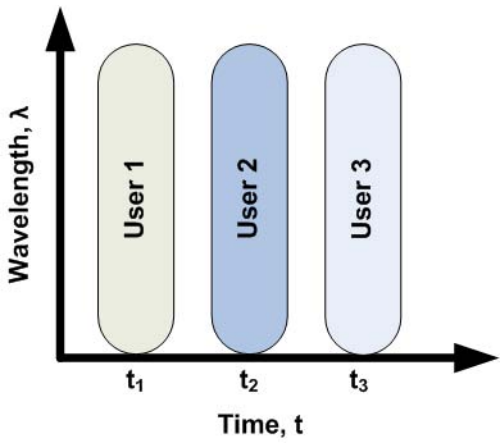

Figure 2.2 Resource sharing based on TDMA technique

Synchronous digital hierarchy (SDH) is the current transmission and multiplexing standard for high-speed signals, which is based on time division multiplexing [67]. Optical TDMA (OTDMA) networks can be based on a broadcast topology or incorporate optical switching [3]. In broadcast networks, there is no routing or switching within the

network. Switching occurs only at the periphery of the network by means of tuneable transmitters and receivers. The switch-based networks perform switching functions optically within the network in order to provide packet-switched services at very high bit-rates [68]. In an electrically time-multiplexed system, multiplexing is carried out in the electrical domain, before the electrical-to-optical conversion (E/O) and demultiplexing is performed after optical-to-electrical conversion (O/E). Major electronic bottlenecks occur in the multiplexer E/O, and the demultiplexer O/E, where electronics must operate at the full multiplexed bit-rate. Alternatively, in optically time-multiplexed systems where by moving the E/O and O/E converters to the baseband channels the electronic bottlenecks are alleviated [6]. OTDMA systems offer a large number of node addresses; however, the performance of OTDMA systems is ultimately limited by the time-serial nature of the technology. OTDMA systems also require strong centralized control to allocate time slots and to manage the network operation.

2.1.3 Code Division Multiple Access (CDMA)

CDMA is one of a family of transmission techniques generically called spread spectrum, explained in the following section. In this technique, the network resources are share among users which are assigned a code instead of time slot like TDMA or a wavelength like WDMA. Then, users are capable of accessing the resources using the same channel at the same time, as shown in the Figure 2.3.

The concepts of spread spectrum i.e. CDMA seem to contradict normal intuition, since in most communications systems we try to maximize the amount of useful signal we can fit into a minimal bandwidth.

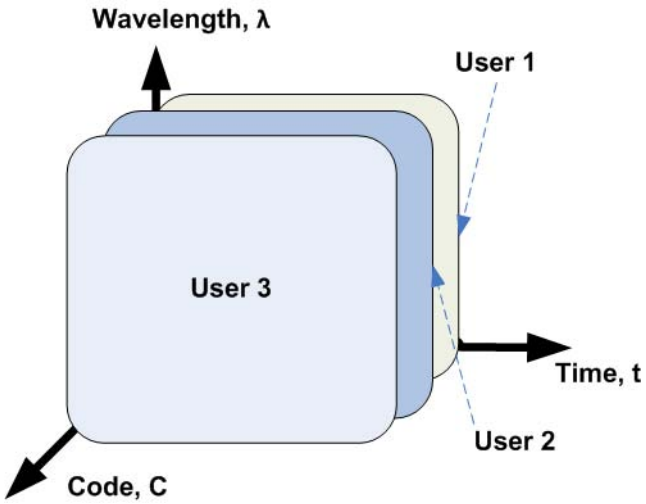

Figure 2.3 Resource sharing based on CDMA technique

In CDMA we transmit multiple signals over the same frequency band, using the same modulation techniques at the same time [69]. Traditional thinking would suggest that communication would not be possible in this environment. The following effects of spreading are worthwhile to mention:

- **Capacity Gain**

Using the Shannon-Hartly law for the capacity of a band-limited channel it is easy to see that for a given signal power the wider the bandwidth used, the greater the channel capacity. So if we broaden the spectrum of a given signal we get an increase in channel capacity and/or an improvement in the signal-to-noise ratio (SNR) [70].

The Shannon-Hartly law gives the capacity of a band-limited communications channel in the presence of Gaussian noise (most communications channel has Gaussian noise).

$$Capacity = B\log_2(1+SNR) \tag{2.1}$$

where $SNR = P_s/(2BN_0)$ and P_s represents the signal power, N_0 is the noise power and B denotes the available bandwidth.

It is easy to see that with P_s and N_0 held constant, capacity increases as bandwidth increases (though not quite as fast). Thus, for a given channel capacity, the required power decreases as utilized bandwidth increases. The wider the bandwidth the lower the power we need to use for a given capacity.

- **Security**

Spread spectrum was invented by military communications people for the purpose of battlefield communications. Spread spectrum signals have an excellent rejection of intentional jamming (jammer power must be very great to be successful). In addition, the direct sequence (DS) technique results in a signal which is very hard to distinguish from background noise unless you know the peculiar random code sequence used to generate the signal. Thus, not only are DS signals hard to jam, they are extremely difficult to decode (unless you have the key) and quite hard to intercept even if all you need to know is when something is being transmitted.

2.2 Spread Spectrum Communications

Spread spectrum communication (SSC) involves spreading the desired signal over a bandwidth much larger than the minimum bandwidth necessary to send the signal. It has become very popular in the realm of personal communications recently. Spread spectrum methods can be combined with CDMA methods to create multi-user communications systems with very good interference performance.

This section will cover the details behind the method of SSC, as well as analyse two main types of SS systems, direct-sequence spread spectrum (DS-SS) and frequency-hopping spread spectrum (FH-SS).

As stated before, spread spectrum systems afford protection against jamming and interference from other users in the same band as well as noise by spreading the signal to be transmitted and performing the reverse de-spread operation on the received signal at the receiver. This de-spreading operation in turn spreads those signals which are not properly spread when transmitted, decreasing the effect that spurious signals will have on the desired signal. Spread spectrum systems can be thought of as having two general properties: first, they spread the desired signal over a bandwidth much larger than the minimum bandwidth needed to send the signal, and secondly, this spreading is carried out using a pseudorandom noise (PN) sequence. In a general, we will see that the increase in bandwidth above the minimum bandwidth in a spread spectrum system can be thought of as applying gain to the desired signal with respect to the undesirable signals. We can now define the processing gain G_P as [71]:

$$G_P = \frac{BW_{car.}}{BW_{data}} \tag{2.2}$$

where $BW_{car.}$ is the bandwidth that the signal has been increased to (i.e. carrier bandwidth), and BW_{data} is the minimum bandwidth necessary to transmit the information or data signal. Processing gain can be thought of as the improvement over conventional communication schemes due to the spreading on the signal. Often, a better measure of this gain is given by the jamming margin, M_j [71]:

$$M_j(dB) = G_P(dB) - SNR_{\min} \tag{2.3}$$

This indicates the amount of interference protection offered before the signal is corrupted. The spreading function is achieved through the use of a PN sequence. The

data signal is combined with the PN sequence such that each data bit is encoded with several if not all the bits in the PN sequence. In order to achieve the same data rate as was desired before spreading, the new data must be sent at a rate equal to the original rate multiplied by the number of PN sequence bits used to encode each bit of data. This increase in bandwidth is the processing gain, which is a measure of the noise and interference immunity of this method of transmission.

To see how the spreading process helps protect the signal from outside interference, the types of possible interference are introduced: (i) noise, and (iii) interference from other users of the same frequency band. Noise can be considered as background additive white Gaussian noise (AWGN), and can be said to have power spectral density N_0. Since the noise is white, the spreading of the bandwidth does not have much of an effect here. The noise power is constant over the entire bandwidth, thus increasing the bandwidth actually lets more noise into the system, which might be seen as unfavourable. However, as discussed in Section 2.2.1 this is not a problem.

The major source of signal corruption comes from multi-user interference i.e. MAI. The technique of CDMA is to combat this type of interference. In a wireless communication network, all the signals propagate through the air by electromagnetic waves, thus there is no way to ensure that the intended user will receive only the desired signal. The intended user will receive all the signals being transmitted in the allocated frequency band. While, by assigning a specific spreading code to each user (i.e. ideally orthogonal to the other codes), the intended receiver will only detect the desired signal through correlating the received signal with the code of the transmission it wants to receive and then only the desired signal will remain.

2.2.1 Direct-Sequence Spread Spectrum (DS-SS)

DS-SS is the most common version of spread spectrum in use today, due to its simplicity and ease of implementation. In DS-SS, the carrier (data signal) is modulated by the PN sequence, which is of a much higher frequency than the desired data rate.

Let *f* be the frequency of the data signal, with appropriate pulse time $T = 1/f$. Let the PN sequence be transmitted at a rate f_c so that the increase in the data rate is f_c / f . The frequency f_c is known as the chip-rate, with each individual bit in the modulating sequence known as a chip.

Thus the width of each pulse in the modulating sequence is T_c, or chip duration. The Figure 2.4 illustrates the encoded signal, the data signal for one pulse width, and the PN sequence over the same time [72].

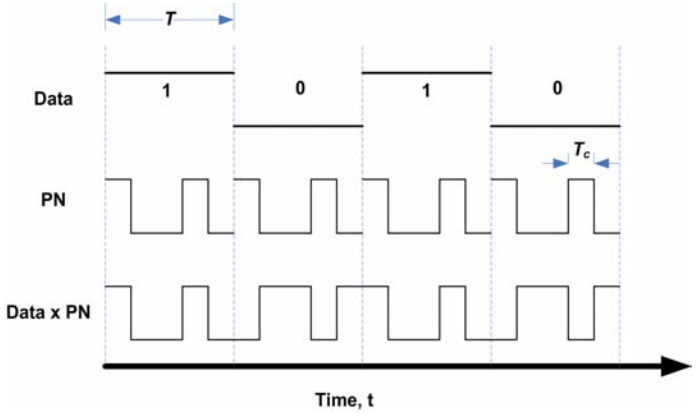

Figure 2.4 DS-SS signalling format

As a result, the frequency domain will look like the signal in Figure 2.5. Assuming that the data signal is *D(t)*, transmitted at frequency *f*, and the PN sequence is *PN(t)* at frequency f_c, then the transmitted signal is:

$$S(t) = D(t) \cdot PN(t) \tag{2.4}$$

The PN sequence is designed such that it has very good autocorrelation properties, for example:

$$R_{PN}(\tau) = \begin{cases} 1 & \tau = 0, N, 2N \\ 1/N & otherwise \end{cases} \quad (2.5)$$

where $R_{PN}(\tau) = \int_{-\infty}^{+\infty} PN_1(t) \cdot PN_2(t+\tau)dt$ is the correlation function and *N* is the length of the PN sequence.

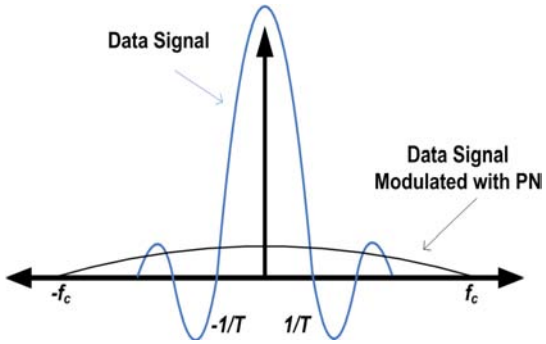

Figure 2.5 Data signal and DS-SS modulated data signal in frequency domain

Therefore, when the signal is correlated with the PN sequence at the receiver, the received signal will be recovered exactly (assuming that there is synchronisation between the send and receive PN sequences) as:

$$S(t).PN(t) = D(t) \cdot PN(t) \cdot PN(t) = D(t) \quad (2.6)$$

Now, if we allow both noise *N(t)* and jamming signal *J(t)* with finite power distributed evenly across the frequency band, the received signal at the receiver input *Y(t)*, is:

$$Y(t) = D(t) \cdot PN(t) + J(t) + N(t) \quad (2.7)$$

Now, when the signal is correlated with the PN sequence, the data signal portion of *Y(t)* is de-spread giving us the original *D(t)*. However, correlating *J(t)* and *N(t)* with the

PN sequence results in spreading signal over the frequency band f_c, whereas the signal *D(t)* has returned to its original frequency $f = 1/T$. So a filter following the signal correlation can recapture the signal *D(t)* with a reduced amount of jamming power. The jamming power that can pass through the filter is now decreased by a factor f_c/f, which was introduced earlier as the processing gain G_P, i.e. $G_P = BW_{Car.}/BW_{data} = f_c/f$. So we see that the data signal has been made immune to the effect of a malicious third party jammer as well. As stated earlier, even though a factor of f_c/f more noise was let into the system by the increased bandwidth, the effect of that noise was also reduced by G_P due to the processing gain of the system, and thus the effect of AWGN has not been increased by this DS-SS system [71].

2.2.2 CDMA and DS-SS

In a CDMA system, each user is identified by its own code, and in order to prevent users from interacting with each other, these codes are designed to be orthogonal to each other (the cross-correlation function between any two of these codes is ideally zero). In practice, perfect orthogonality is hard to achieve, in this Chapter we assume perfect orthogonality in order to explain the CDMA theory. Each user's signal is being encoded with a PN sequence and its own orthogonal code. Therefore, the transmitted signal *S(t)* can be expressed as:

$$S_i(t) = D_i(t) \cdot PN(t) \cdot C_i(t) = D_i(t) \cdot P_i(t) \tag{2.8}$$

where $C_i(t)$ denotes the CDMA code of the i^{th} user whose data signal is $D_i(t)$, and $P_i(t)$ denotes the combination of the PN sequence and the orthogonal code for the i^{th} user. Ideally, this allows a large number of users to use the same bandwidth, because

not only we have the intentional interference rejection properties but we also have a multi-user interference rejection. Assume that there are *N* users with *N* orthogonal codes in this system, all using the same frequency band. Thus the i^{th} receiver's signal is:

$$Y_i(t) = D_i(t) \cdot P(t) + \sum_{k=1, k\neq i}^{N} D_k(t+\theta) \cdot P_k(t+\theta) \tag{2.9}$$

where θ is a random delay. When this is correlated with the PN sequence and the i^{th} orthogonal code, the result will become zero (the result of the orthogonality), and only the signal due to the desired transmission will remain. The basic transmitter and receiver structure for DS-SS are shown in Figure 2.6. The transmitter just multiplies the data signal with the PN sequence and the CDMA code, and then modulates this resulting signal up to the carrier frequency, and the receiver just performs the reverse operation and integrates the received signal. However, all this assumes perfect synchronization between transmitter and receiver.

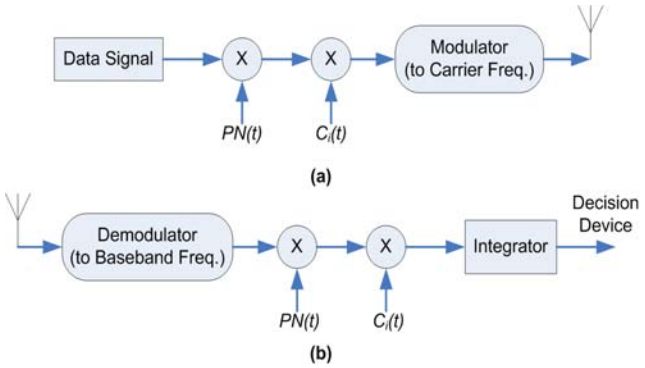

Figure 2.6 DS-SS basic transceiver (a) transmitter (b) receiver

2.2.3 Frequency-Hopping Spread Spectrum (FH-SS)

In FH-SS the signal itself is not spread across the entire large bandwidth while the wide bandwidth is divided into *N* sub-bands and the signal hops from one band to the other in a pseudorandom manner instead. The centre frequency of the signal changes from

one sub-band to another, as shown in Figure 2.7. As we can see, a large frequency band of width $N \cdot f_b$ at f_c is divided into *N* sub-bands of width f_b. The bandwidth f_b must be enough to transmit the data signal *D(t)*, and at a predetermined time interval, the centre frequency of the data signal changes from one sub-band to another pseudo randomly [73].

Figure 2.7 shows the data signal hops from band *N* at $f_c + (N/2) f_b$ to band 2 at $f_c - (N/2 - 1) f_b$ and to band *N-2*, and so on. Usually, the width of each sub-band is set so that the amount of signal that overlaps with adjacent sub-bands is minimal, and is thus approximately the bandwidth of the original data signal.

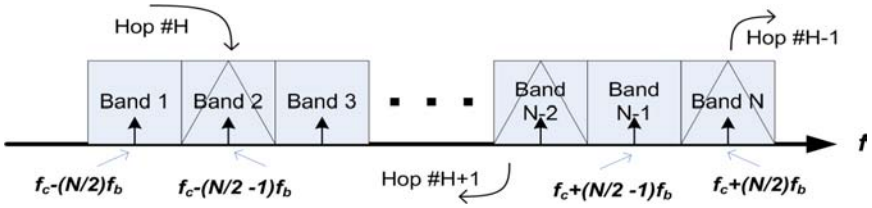

Figure 2.7 FH-SS signalling format

Two different kinds of FH-SS are used: slow FH and fast FH. In slow FH-SS, several bits are sent for each hop, so the signal stays in a particular sub-band for a long time relative to the data-rate. In fast FH-SS, the signal switches sub-bands several times for each bit transmitted, so the signal stays in a sub-band for a very short time relative to the data-rate. There are people who say that slow FH is not really a spread spectrum technique, since this does not really spread the system, since the time spent in one sub-band is very large, the corresponding width of the band can be small, thus possibly violating the first principle of a spread spectrum system, namely that the spread bandwidth must be much greater than the non-spread bandwidth.

In the fast FH, the performance of the system with respect to AWGN is not affected as in the DS. The noise power seen at the receiver is approximately the same as that in the un-hopped case, since each sub-band is approximately the same size as the original data signal's bandwidth. Here, if we again assume that the jamming signal $J(t)$ is distributed uniformly over the entire band, it is clear that the only portion of the jamming signal that affects the data is the part within the bandwidth of f_b, and thus the jamming signal is reduced by the factor of the processing gain G_P which is:

$$G_P = \frac{BW_{car.}}{BW_{data}} = \frac{N \cdot f_b}{f_b} = N \tag{2.10}$$

Thus in the FH, the protection afforded is equal to the number of frequency bands. In case of interference in certain frequency bands, the probability of a bit being in error is then given by $P_{be} = J/N$, where J is the number of channels interfered, and N is the total number of frequencies available to the hopping.

However, fast FH allows us to very simply decrease the BER. If we choose to have a large number of chips per bit (here a chip represents a hop), then we can use a simple majority function to determine what the transmitted bit was. We assume that the number of available hop channels is larger than the number of channels being interfered. If the simple majority function is being used, then the formula for the error-rate becomes [73]:

$$P_e = \sum_{x=r}^{c} C_r^c \cdot p^x \cdot q^{c-x} \tag{2.11}$$

where $C_r^c = \binom{c}{r} = \frac{c!}{(c-r)!\cdot r!}$ and it is read the combination of *r* out of *c* which is the number of chips per bit (hops per bit), *r* is the number of chip errors necessary to cause a bit-error, *p* is the probability of one bit-error (i.e. $P_{be} = J/N$), and *q* is the probability of no error for a chip, or *1-p*. By increasing the number of chips per bit from 1 to 3 and assuming *r*=2 for example, we find that the error-rate is now:

$$P_e = \binom{3}{2}(p^2 - p^3) + \binom{3}{3}p^3 = 3p^2 - 2p^3 = 3\times10^{-4} - 2\times10^{-6} \approx 3\times10^{-4} \qquad (2.12)$$

Thus by just increasing the hopping-rate from once per bit to three times per bit, the bit-error rate can be decreased dramatically.

Since the PN sequence determines the hopping sequence, the data signal is modulated to the PN sequence generator's frequencies and switched by the frequency synthesizer where it is finally transmitted. The basic structure of the transmitter is shown in Figure 2.8(a). At the receiver, shown in Figure 2.8(b), the frequency synthesizer demodulates the signal down to a baseband frequency, and then the signal is filtered so that only the desired data signal is passed through, and finally the signal is decoded. Again, to get multiple users using the same wide frequency band, CDMA techniques must be used.

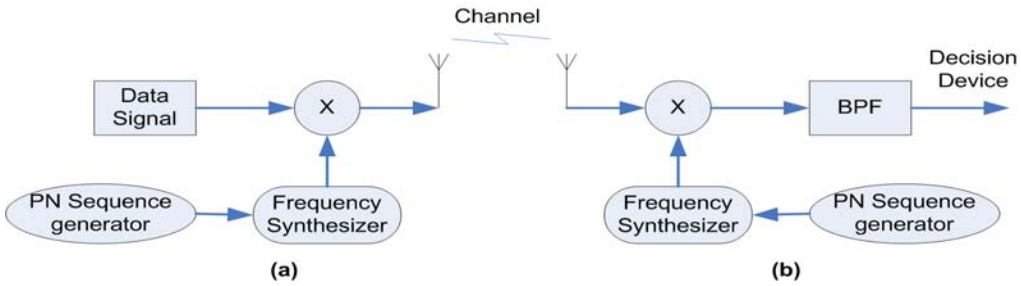

Figure 2.8 FH-SS basic transceiver (a) transmitter (b) receiver

2.2.4 CDMA and FH-SS

The frequency-hopping CDMA scheme provides each user with an orthogonal hop sequence i.e. no two users occupy the same sub-band at the same time. In this way, multiple users can be accommodated without any chance of them interfering with each other, since ideally only one user will be in a frequency sub-band during a given hop, and thus the receiver, due to its band-pass filter, will be able to detect the intended signal. Thus, in order to support multiple users, the transceiver given in Figure 2.8 must be modified to incorporate an orthogonal code sequence to determine the centre frequencies of the hopping sequences as the input to the frequency synthesizer.

2.3 Optical Access Networks

In the past decade we have witnessed significant development in the area of optical networking. Such advanced technologies as dense wavelength-division multiplexing (DWDM), optical amplification, optical path routing e.g. optical cross connect (OXC), reconfigurable optical add-drop multiplexer (ROADM), and high-speed switching have found their way into the wide-area networks (WANs), resulting in a substantial increase of the telecommunications backbone capacity and greatly improved reliability.

At the same time, enterprise networks converged on 100 Mbps fast Ethernet architecture [74]. Some LANs even moved to 1 Gbps data-rates, courtesy of a new gigabit Ethernet (GbE) standard recently adopted by the Institute of Electrical and Electronics Engineers (IEEE 802.3).

An increasing number of households have more than one computer. Home networks allow multiple computers to share a single printer or a single Internet connection. Most often, a home network is built using a low-cost switch or a hub that can interconnect 4 to 16 devices. Builders of new houses now offer an option of wiring a new house with a category-5 (CAT-5 or RJ45) cable [75]. Older houses have an option of using existing phone wiring, in-house power lines, or an evermore popular wireless network, based on the IEEE 802.11 standard. Different flavours of this standard can provide up to 11 Mbps bandwidth or up to 54 Mbps bandwidth, with distance being a trade-off. Whether it is a wireless or wired solution, home networks are kind of tiny LANs providing hi-speed interconnection for multiple devices.

These advances in the backbone, enterprise, and home networks coupled with the tremendous growth of Internet traffic have accentuated the frustrating delay of access network capacity. The last-mile (from provider's point of view) still remains the bottleneck between high-capacity LANs and the backbone network.

2.3.1 Existing Solutions

The most widely deployed broadband solutions today are digital subscriber line (DSL) and cable modem (CM) networks. Although they are improvements compared to 56kbps old dial-up lines, they are unable to provide enough bandwidth for emerging services such as full duplex video conferencing.

2.3.1.1 Digital Subscriber Line (DSL)

DSL uses the same twisted pair as telephone lines and requires a DSL modem at the customer premises and DSL access multiplexer (DSLAM) in the central office. The basic

premise of the DSL technology is to divide the spectrum of the line into several regions with the lower 4 kHz being used by plain old telephone service (POTS) equipments, while the higher frequencies are being allocated for higher-speed digital communications. There are four basic types of DSL connections [2].

The basic DSL is designed with integrated services data network (ISDN) compatibility in mind. It has 160 kbps symmetric capacity and affords users with either 80 or 144 kbps of bandwidth, depending on whether the voice circuit was supported or not. The high-speed digital subscriber line (HDSL) is made compatible with a T1 rate of 1.544 Mbps. The original specification required two twisted pairs. However, a single-line solution was standardized by International Telecommunication Union (ITU G.991.1).

2.3.1.2 Asymmetric DSL (ADSL)

The ADSL is the most widely deployed flavour of DSL. It uses one POTS line and has an asymmetric line speed. In the downstream direction, the line rate could be in the range of 750 kbps to 1.5 Mbps on the loops of 5,000 meters. On shorter loops, the rate can be as high as 6 Mbps. In the upstream direction, the rate could be in the range of 128 to 750 kbps. The actual rate is chosen by the ADSL modem based on the line circumstances.

Finally, the very high-speed digital subscriber line (VDSL) can have a symmetric or an asymmetric line speed. It achieves much higher speed than HDSL or ADSL, but operates over much shorter loops. The rates could range from 13 Mbps for 1500 meters loops to 52 Mbps over 300 meters loops [2].

While the maximum ADSL transmission capacity is 1.5 Mbps, in reality it could go much lower depending on the line conditions. Twisted-pair wires admit a number of

impairments, most significant of which are crosstalk, induced noise, bridged taps, and impulse noise. To cope with such impairments, the ADSL employs a multi-carrier modulation approach known as discrete multi-tone (DMT). A DMT system transmits data on multiple subcarriers in parallel. DMT adapts to line conditions by varying the bit-rate on each subcarrier channel. A good channel may carry as many as 15 bits/symbol/s, while a really noisy channel may carry no data at all [2].

The asymmetric nature of the ADSL was prompted by observation of user traffic at the time. While the downstream traffic was a result of downloading large files and web pages, the upstream traffic primarily consisted of short commands, uniform resource locator (URL) requests, and/or server login queries. Consequently, the ADSL adopted a *10:1* ratio of the downstream bandwidth to the upstream bandwidth; with AT&T even advocating for as high as a *100:1* ratio [19].

It is interesting to note that the highly asymmetric nature of the traffic is a thing of the past. New and emerging applications tend to skew the ratio toward greater symmetry. Such applications as video conferencing or storage-area networks (SAN) require symmetric bandwidth in both directions. A big impact on traffic symmetry can be attributed to peer-to-peer applications. It is reported that the recent ratio of downstream to upstream traffic is approximately *1.4:1* [75]. This is one of the concerns during this research as it can be achieved through CDMA data link.

2.3.1.3 Community Access Television (CATV) Networks

The CATV networks were originally designed to deliver analogue broadcast TV signals to subscriber TV sets. Following this objective, the CATV networks adopted a tree topology and allocated most of its spectrum for downstream analogue channels.

Typically, CATV is built as a hybrid fibre-coax (HFC) network with fibre running between either a head-end or a hub (optical node) and the final drop to the subscriber through coaxial cables as illustrated in Figure 2.9. The coaxial part of the network uses repeaters (amplifiers) to split the signal among many subscribers.

The major limitation of CATV architecture for carrying modern data services is that this architecture was originally designed only for broadcast analogue services. Out of a total cable spectrum width of about 740 MHz, the 400 MHz band is allocated for downstream analogue signals, and the 300 MHz band is allocated for downstream digital signals. Upstream communications are left with about a 40 MHz band or about 36 Mbps of effective data throughput per optical node. This very modest upstream capacity is typically shared among 500 to 1000 subscribers, resulting in frustratingly low speed during peak hours [19].

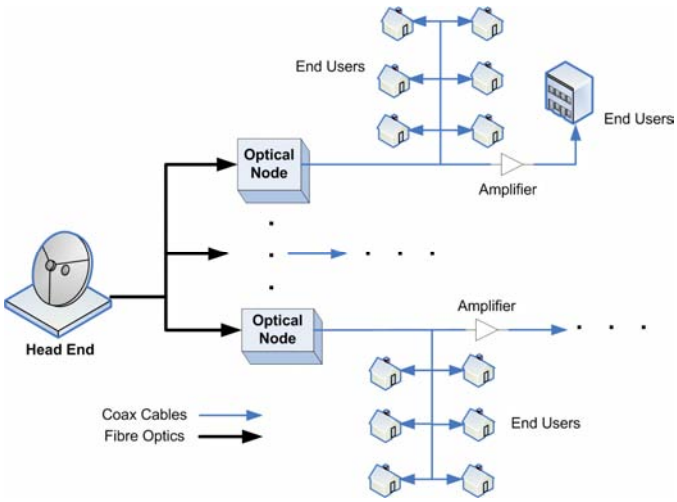

Figure 2.9 Hybrid fibre-coax architecture

2.3.2 Next Generation Networks (NGN)

Optical fibre is capable of delivering bandwidth-intensive, integrated voice, data, and video services at distances beyond 20 km in the subscriber access network. A

straightforward way to deploy optical fibre in the local access network is to use a point-to-point (P2P) topology, with dedicated fibre runs from the central office to each subscriber as shown in Figure 2.10(a). While this is a simple architecture, in most cases it is cost prohibitive because it requires significant outside fibre plant deployment as well as connector termination space in the local exchange.

As it can be observed from Figure 2.10, considering *N* subscribers at an average distance of L km from the central office, a P2P architecture, Figure 2.10(a), requires *2N* transceivers and *N×L* total fibre length, even by assuming that a single fibre is used for bidirectional transmission [17]. To reduce fibre deployment, it is possible to deploy a remote switch (concentrator) close to the neighbourhood. This will reduce the fibre consumption to only *L* km by assuming negligible distance between the switch and customers, whereas it will actually increase the number of transceivers to *2N + 2*, as there is one more link added to the network, illustrated in Figure 2.10(b). In addition, curb-switched network architecture requires electric power as well as backup power at the curb switch. Currently, one of the most significant operational expenditures for local exchange carriers is that of providing and maintaining electric power in the local loop. Therefore, it is logical to replace the tough active curb side switch with an inexpensive passive optical splitter [18].

2.3.2.1 Passive Optical Network (PON)

A passive optical network (PON) is a technology viewed by many as an attractive solution to the first-mile problem [74, 76]; a PON minimizes the number of optical transceivers, central office terminations and fibre deployment. A PON is a point-to-multipoint (P2MP) optical network with no active elements in the signals' path from

source to destination. The only interior elements used in PON are passive optical components, such as optical fibre, splices, and splitters. An access network based on a single fibre PON only requires *N + 1* transceivers and *L* km of fibre.

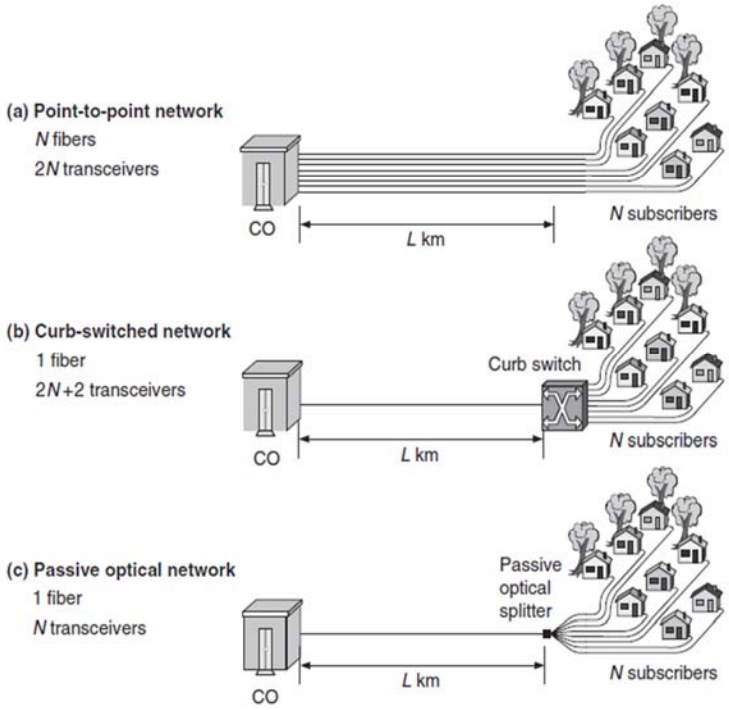

Figure 2.10 Fibre to the home deployment scenarios [19]

An optical line terminal (OLT) at the central office is connected to many optical network units (ONU) at remote nodes through one or multiple *1:N* optical splitters. The network between the OLT and the ONU is passive i.e. it does not require any power supply. An example of a PON using a single optical splitter is shown in Figure 2.10(c). The presence of only passive elements in the network makes it relatively more faults tolerant and decreases its operational and maintenance costs once the infrastructure has been laid down. A typical PON uses a single wavelength for all downstream transmissions (from OLT to ONUs) and another wavelength for all upstream transmissions (from ONUs to OLT), multiplexed on a single fibre.

PON technology is getting more and more attention by the telecommunication industry as the first-mile solution. Advantages of using PON for local access networks are numerous, among them [18, 19, 74, 76]:

- A PON-based local loop can operate at distances of up to 20 km, which considerably exceeds the maximum coverage afforded by various flavours of DSL.
- Only one strand of fibre is needed in the trunk (i.e. private exchange box), and only one port per PON is required in the central office. This allows for a very dense central office equipments and low power consumption.
- PON provides higher bandwidth due to deeper fibre penetration. While the fibre-to-the-building (FTTB), fibre-to-the-home (FTTH), or even fibre-to-the-PC (FTTPC) solutions have the ultimate goal of fibre reaching all the way to customer premises, fibre-to-the-curb (FTTC) may be the most economical deployment today.
- PON eliminates the necessity of installing multiplexers and demultiplexers in the splitting locations, thus relieving network operators from the dreadful task of maintaining them and providing power to them. Instead of active devices in these locations, PON has passive components that can be buried in the ground at the time of deployment.
- PON allows easy upgrades to higher bit-rates or additional wavelengths. Passive splitters and combiners provide complete path transparency.

2.4 Summary

In this Chapter we have discussed and introduced briefly common multiple-access techniques in optical domain along with the precious spread spectrum communication methods including most popular ones: direct sequence and frequency hopping. The current states of the networking solutions and also the next generation architectures have been presented have been reported. Accordingly, due to the daily increase of users in information highway, flexible user allocation, easier traffic routing and transmission, higher security, enhanced service management and QoS are required to be considered in the next generation networks.

Chapter 3

Optical CDMA Review

3.1 Introduction

Interest in OCDMA has been steadily growing during recent decades and this trend is accelerating due to the optical fibre penetration in the first-mile and the establishment of passive optical network (PON) technology as a pragmatic solution for residential access. In OCDMA, an optical code represents a user address and signs each transmitted data bit. We define optical coding as the process by which a code is inscribed into, and extracted from, an optical signal. Although a prerequisite for OCDMA, optical coding has a wide range of novel and promising applications, such as access protocol and label switching. Most previous reviews of OCDMA have focused on physical-layer (PHY) implementations and present an overview of networking applications. This Chapter is an overview of both OCDMA and optical coding through their major applications. A novel spreading code is also proposed here.

3.1.1 Coding Fundamentals in Optical Domain

Optical code-division multiplexing (OCDM) is a procedure by which each communication channel is distinguished by a specific optical code rather than a wavelength like WDM or a time slot like TDM. An encoding operation optically transforms each data bit before transmission. The encoding and decoding operations alone constitute optical coding. OCDMA is the use of OCDM technology to arbitrate channel access among multiple network nodes in a distributed fashion. Encoding involves multiplying the data bit by a code sequence either in the time domain, the wavelength domain, or a combination of both. The latter method is called two-dimensional coding (2D-coding) [58-61]. Time-domain coding that manipulates the phase of the optical signal requires phase-accurate coherent sources. Alternatively, positive encoding manipulates the power of the optical signal but not its phase and typically uses incoherent sources. In wavelength-domain coding, transmitted bits consist of a unique subset of wavelengths forming the code. 2D-coding combines both wavelength selection and time spreading. A data bit is encoded as consecutive chips of different wavelengths, the unique wavelength sequence constituting the code. Regardless of the coding domain, the coding operation broadens the spectrum of the data signal, hence the designation of spread spectrum as discussed in Section 2.2. Note that encoding can also be performed in the space-domain [77], whereby the code determines the positions of chips within a dense fibre array or a multi-core fibre.

An OCDMA local area network (LAN) is based on a broadcast medium as illustrated in Figure 3.1. Signals from different encoders are coupled and each decoder receives the sum of the encoded signals. If a given encoder transmits a signal, only the decoder

with the same code is capable of recovering it. Unwanted signals appear as noise to the decoder and are called multiple-access interference (MAI). MAI is the principal source of noise in OCDMA and is the limiting factor to system performance. In a well-designed OCDMA LAN where MAI is overcome, users can successfully communicate asynchronously regardless of network traffic as shown in Figure 3.1.

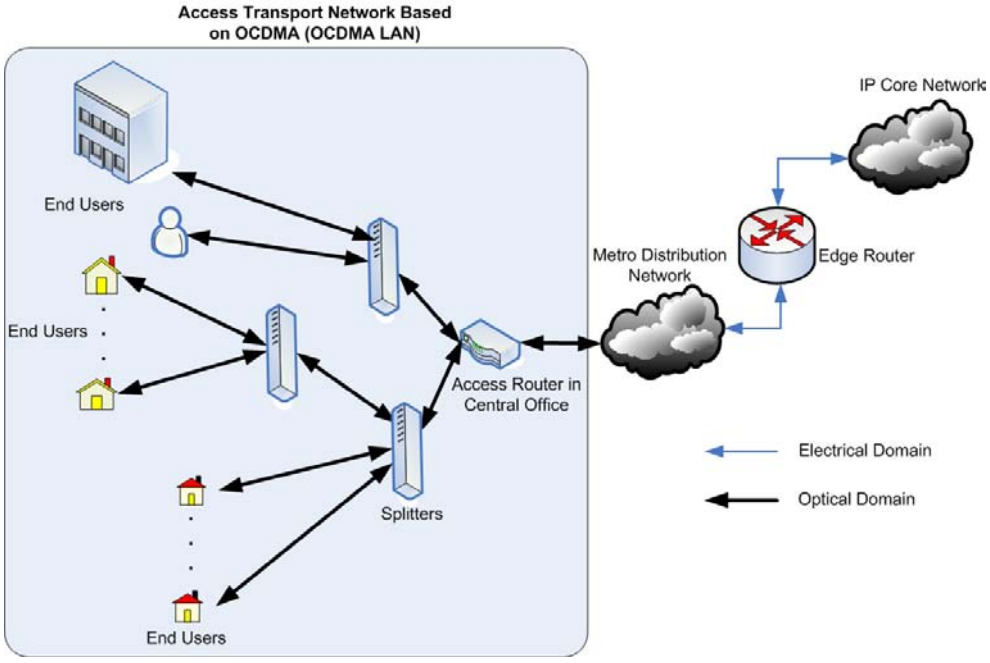

Figure 3.1 Architecture of LAN based on optical CDMA

Decoding a signal encoded by the same code represents a logical auto-correlation of a single code. Otherwise, the operation represents a cross-correlation between two different codes. Code design aims at generating codes with high auto-correlation and low cross-correlation properties. More particular requirements on code design arise from the use of specific transmission media or components. Various code families have been proposed to address such requirements [24, 25, 38, 49, 59, 60, 78-83]. Code-length is an important feature of code and system design. A larger code length

improves correlation properties among codes, hence raising system performance in terms of MAI, bit-error rate (BER), and throughput [32, 72, 73].

Employing incoherent versus coherent light sources is often used to classify OCDMA systems because that choice has important cost and performance implication [28]. Note that the choice of coherent sources does not always imply that chips are phase rather than power modulated. In addition, whether the encoding occurs in fibre, in a planar lightwave circuit, or in an out-of-fibre external device has an important impact on system design [84].

Throughout this thesis, we distinguish multiplexing techniques (xDM) from multiple accesses (xDMA) to make the entire scheme more apparent. The former focus on transport and the latter denotes distributed access methods. For example, in an OCDMA-over-WDM network, all nodes require an OCDMA transceiver while, each wavelength is used as a medium for a number of OCDMA channels.

3.2 Optical Spreading Codes

In OCDMA system, main purpose is to recognize the intended users' signals in the presence of other users' signals. Another aim is to accommodate more possible subscribers in the system. In this case, the suitable optical sequence codes with the best orthogonal characteristic should be employed. In terms of the correlation properties, spreading sequences are selected with the features of maximum auto-correlation and minimum cross-correlation in order to optimize the differentiation between correct signal and interference.

Firstly, optical orthogonal codes are reviewed in this Chapter. Then, the family of prime codes are discussed and analysed. Furthermore, the novel coding scheme is introduced and analysed in the next Chapter where it is employed in various OCDMA schemes throughout the thesis.

3.2.1 Optical Orthogonal Codes (OOC)

An important type of temporal codes is the OOC proposed for intensity modulation or direct-detection (IM-DD) OCDMA systems [58, 60, 78, 81, 85-88]. These are very sparse codes, meaning that the code weight is very low, thus limiting the efficiency in practical coding and decoding. Moreover, the number of codes that can be supported is very low as compared to a code set with the same length used in radio communications (PN codes for example). To get more codes we need to increase the length of the code, demanding the use of very short pulse optical sources having pulse-width much smaller than the bit duration.

The required temporal OCDMA codes must satisfy the following conditions:

i. The peak auto-correlation function of the code should be maximized.
ii. The side lobes of the auto-correlation function of the code should be minimized.
iii. The cross-correlation between any two codes should be minimized.

Conditions (i) and (iii) insure that the MAI is minimized, while condition (ii) simplifies the synchronisation process at the receiver.

The correlation $R_{C_iC_j}(\tau)$ of two signature signals $C_i(t)$ and $C_j(t)$ is defined as:

$$R_{C_iC_j}(\tau) = \int_{-\infty}^{+\infty} C_i(t) \cdot C_j(t+\tau)dt \quad \text{for} \quad i, j = 0,1,2... \tag{3.1}$$

where the signature signal $C_k(t)$ is defined as:

$$C_k(t) = \sum_{n=-\infty}^{+\infty} c_k(n) \cdot u_{T_c}(t - nT_c) \quad \text{for} \quad k = 1,2,... \tag{3.2}$$

$c_k(n) \in \{0,1\}$ is the periodic sequence of period *N* and chip duration of T_c. The discrete correlation function of any two code sequences $c_i(n)$ and $c_j(n)$ are then given by:

$$R_{c_i c_j}(m) = \sum_{n=0}^{N-1} c_i(n) \cdot c_j(n+m) \quad \text{for} \quad m = ...,-1,0,1,... \tag{3.3}$$

The sum in the argument of $c_i(n+m)$ is calculated modulo *N*, we represent this operation from now on as $[x]_y$ which is read *x* modulo *y*. In the discrete form, the above conditions are rewritten as:

- The number of *one*s in the zero-shift discrete auto-correlation function should be maximized.
- The number of coincidences of the non-zero shift discrete autocorrelation function should be minimized.
- The number of coincidences of the discrete cross-correlation function should be minimized.

An OOC is usually represented by a quadruple, $(N, W, \lambda_a, \lambda_c)$ where *N* is the sequence length; *W* is the sequence weight (number of *one*s); λ_a is the upper bound on the auto-correlation for non-zero shift and λ_c is the upper bound on cross-correlation. The conditions for OOCs are then:

$$R_{c_i c_j}(m) = \sum_{n=0}^{N-1} c_i(n) \cdot c_j(n+m) \le \lambda_c \quad \text{for} \quad \forall m \tag{3.4}$$

and

$$R_{c_i c_j}(m) = \sum_{n=0}^{N-1} c_i(n) \cdot c_j(n+m) \le \lambda_a \quad \text{for} \quad [m]_n \neq 0 \tag{3.5}$$

When $\lambda_c = \lambda_a = \lambda$, the OOC is represented by (N, W, λ) and called optimal OOC. $|C|$ shows the cardinality of the code sequences i.e. the size of the code which refers to the number of code words contained in the code family. The largest possible size of the set with conditions of (N, W, λ) denotes $\Phi(N, W, \lambda)$. By the aid of Johnson bound [85], it is known that Φ should satisfy [78]:

$$\Phi(N, W, \lambda) \le \frac{(N-1)(N-2).....(N-\lambda)}{W(W-1)(W-2).....(W-\lambda)} \tag{3.6}$$

In case of $\lambda_c = \lambda_a = 1$, i.e. strict OOC, it can be shown that the number of codes is upper-bounded by:

$$|C| \le \left\lfloor \frac{(N-1)}{W(W-1)} \right\rfloor \tag{3.7}$$

where $\lfloor x \rfloor$ denotes the integer portion of the real number *x*.

An example of a strict OOC $(13, 3, 1)$ code set is *C={1100100000000, 1010000100000}*. It is clear that the auto-correlation is thus equal to the code-weight of 3, and the non-zero shift auto-correlation and the cross-correlation is less than or equal to *one*. The same code set can be represented using the set notation of {(1,2,5);(1,3,8)}*mod*(13), where the elements in the set represent the position of the pulses (i.e. 1s) in the code sequence of code-length 13.

Assuming an OCDMA system with OOC coding and an avalanche photo-detector (APD), the compound effect of APD noise, thermal noise and MAI was evaluated in [89]. The complex statistics of the APD, described in [90], was not used but instead a simplifying Gaussian approximation was considered in [91]. It was shown that when the noise

effects are considered, the performance of OCDMA based on OOCs can be two orders of magnitude worse than that of the ideal case. Also the improvement in BER by using hard-limiters is not significant because the MAI during the *zero* data bit transmission cannot be completely suppressed as in the noise-free case.

Although synchronisation is beyond the scope of this thesis, it is important to point out briefly to some of the works done on the topic. In the above, asynchronous operation was assumed but synchronisation of OOC systems will be a major requirement to introduce burst and packet-based systems. Also performance degradation of OOC systems will be severe if synchronisation is not maintained. A simple synchronisation method was considered in [92] and more recently a multiple search method that reduces the mean synchronisation time was proposed and analysed in [93].

The main disadvantage of OOCs is the limited number of users for a reasonable code length and weight, therefore, two dimensional OOC codes that use the wavelength-time dimensions were proposed and their performance analysis and construction methods were thoroughly investigated [58, 60].

3.2.2 Prime Code Families

From the practical point of view, two aforementioned primary goals of OCDMA system must be achieved. Again, receiver could correctly recognize the desired users' signals among the interfering signals, and more possible subscribers could be accommodated in the system. Therefore, according to three designed conditions described in Section 3.2.1, the above two goals of OCDMA transceivers should be accomplished with the aid of employing the suitable optical codes sequences with best orthogonal characteristics.

In the last decades, various optical spreading sequences for OCDMA networks have been investigated and experimented [24, 25, 38, 49, 59, 60, 78-83]. However, we only focus our attention on prime code families including prime codes (PC), modified prime codes (MPC), and the recent one new modified prime codes (n-MPC) along with the novel proposed double padded modified prime code (DPMPC). Their construction method and properties are also investigated in the following sub-sections.

3.2.2.1 Prime Codes (PC)

Prime sequences were first proposed in [24] which were previously developed for an optical fibre network using asynchronous OCDMA s with relaxed requirements. Then, the brief introduction including prime codes construction principle, correlation properties, advantages and limitations is discussed.

A. Construction Principle

Compared with OOCs, the generation process of prime codes is relatively simple. The construction of PC is divided into two steps. Firstly, it is aimed to build a set of prime sequences $S_x = (S_{x0}, S_{x1}, ..., S_{xj}, ..., S_{x(P-1)})$ from the Galois Field, $GF(P) = (0, 1, 2, ..., j, ... P-1)$ where *P* is a prime number, $P \in (3, 5, 7, 11, ...)$. This *S* sequence could be obtained by multiplying every element *j* with *x* both from the $GF(P)$, and then modulo with *P*. Hence, the number of *P* distinct PC sequences could be derived. The elements of prime sequence are given by:

$$S_{xj} = x \cdot j (\mathrm{mod}\, P) \tag{3.8}$$

where $x, j \in \{0,1,..., P-1\}$.

Secondly, each prime sequence S_x is then mapped into a binary code sequence $C_x = (C_{x0}, C_{x1}, ..., C_{xj}, ..., C_{x(P^2-1)})$ with code-length P^2 according to the following rule:

$$C_{xi} = \begin{cases} 1 & for \quad i = S_{xj} + jP \ , \ j = 0,1,...,P-1 \\ 0 & otherwise \end{cases} \tag{3.9}$$

Therefore, one set of prime code sequences could be accomplished by using the above approach.

B. Example of a PC Set

An example of a PC set where *P=5* is displayed in Table 3.1 in order to clearly interpret the development process of the sequences.

Table 3.1 PC sequences where *P=5*

Groups *x*	*i* 0 1 2 3 4	Sequence	PC Sequences
0	0 0 0 0 0	S_0	C_0 = 10000 10000 10000 10000 10000
1	0 1 2 3 4	S_1	C_1 = 10000 01000 00100 00010 00001
2	0 2 4 1 3	S_2	C_2 = 10000 00100 00001 01000 00010
3	0 3 1 4 2	S_3	C_3 = 10000 00010 01000 00001 00100
4	0 4 3 2 1	S_4	C_4 = 10000 00001 00010 00100 01000

It is apparent from Table 3.1 that PC set with code-length P^2 and code-weight *P* has *P* distinct sequences.

C. PC Correlation Properties

The auto- and cross-correlation functions for any pair of code sequences C_n and C_m with discrete format are as follows:

$$R_{C_nC_m} = C_n \cdot C_m = \begin{cases} P, & if \quad m = n, \quad auto-correlation \\ 1, & if \quad m \neq n, \quad cross-correlation \end{cases} \tag{3.10}$$

where $m, n \in \{1, 2, ..., P\}$.

It is easily seen from the correlation function that the auto-correlation peak value by setting $n = m$ is bounded by *P*. At the same time, the cross-correlation constraint is equal to *one* at each synchronised time *T* i.e. equivalent to the bit duration or the code-length.

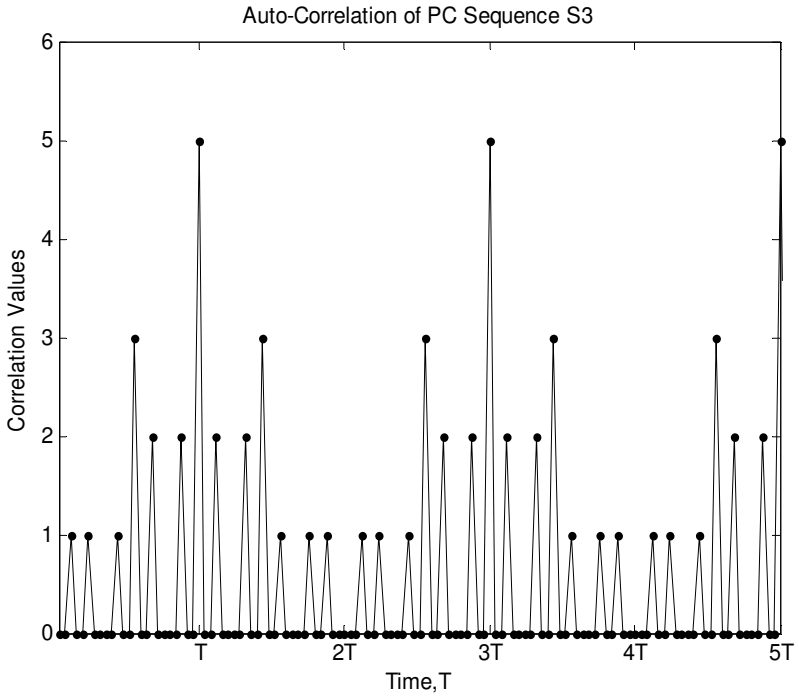

Figure 3.2 Auto-correlation values of PC sequence of S_3, where *P=5* following the data stream of 10101

Figure 3.2 displays the auto-correlation values of PC sequence S_3, and the peak values equals 5 as expected. Meanwhile, the cross-correlation values of PC sequences S_3 and S_2 for the same data stream is illustrated in the Figure 3.3. The peak value of cross-correlation function is bounded by *one* at each synchronised time *T* when the signal follows the data stream 10101 as illustrated in the Figures.

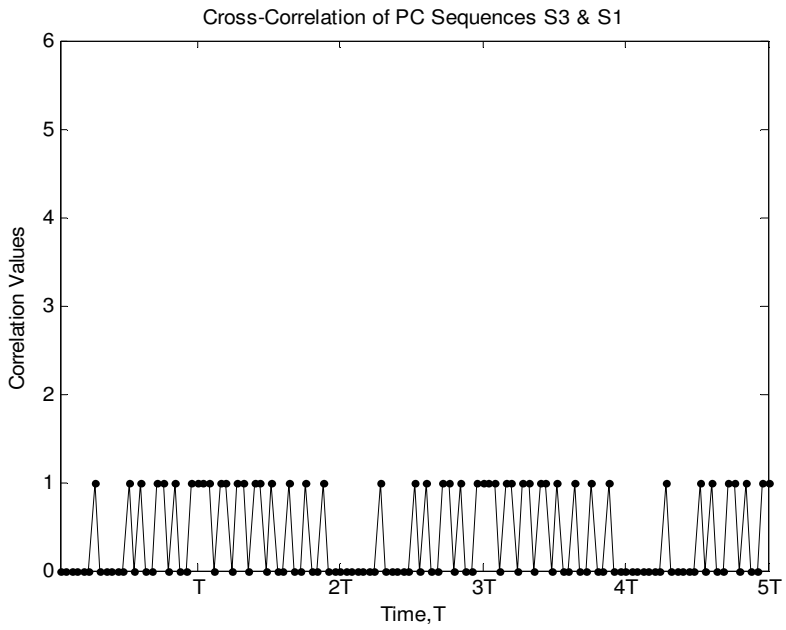

Figure 3.3 Cross-correlation values of PC sequences of S_3 and S_1, where *P=5* following the data stream of 10101

D. Disadvantages of PC Sequences

The major drawback associated with PC sequences is the limited number of available sequences. Therefore, the corresponding number of possible subscribers is insufficient in the probable network design based on PC sequences.

3.2.2.2 Modified Prime Code (MPC)

In order to overcome the limitation of PCs, a modified version of PC sequence named the modified prime code (MPC) is recalled. These optical sequences have the ability to support more users simultaneously transmitted in the system with the lower MAI.

A. Construction Principle

One set of MPC sequences could be achieved through *P-1* times shifting of the pervious PC sequences. Therefore, the available number of signature code sequences could be extended to P^2 with *P* groups of *P* sequences, where *P* is a prime number [94].

Firstly, the original PC sequence generator S_{xj} is left (or right) rotated. Then, the new time-shifted sequences $S_{x,t} = (S_{xt0}, S_{xt1}, ..., S_{xtj}, ..., S_{xt(P-1)})$ are obtained in terms of the following function, where *t* represents the number of times as S_x has been left (or right) rotated [24]. Hence, this method could result in a significant increase in the number of possible subscribers.

$$C_{xti} = \begin{cases} 1 & for \quad i = S_{xtj} + jP \quad j = 0,1,...,P-1 \\ 0 & otherwise \end{cases} \tag{3.11}$$

Finally, by applying this method a set of MPC sequences can be generated.

B. Example of an MPC Set

Similarly, one example of MPC is exhibited in Table 3.2. In this case, the prime number *P* also equals 5.

Table 3.2 implies that the MPC sequences with code-length P^2 and code-weight *P* has P^2 distinct code sequences. Hence, in the OCDMA system using MPC, the number of possible subscribers could be significantly extended up to P^2, which is a factor of *P* larger than that of PC.

C. MPC Correlation Properties

The auto- and cross-correlation functions for any pair of code sequences C_n and C_m in a discrete manner are as follows [24]:

$$R_{C_m C_n} = C_m \cdot C_n = \begin{cases} P, & \text{if } m = n \\ 0, & \text{if } m \neq n, m \text{ and } n \text{ share the same group} \\ 1, & \text{if } m \neq n, m \text{ and } n \text{ are from different groups} \end{cases} \tag{3.12}$$

where $m, n \in \{1,2,...,P^2\}$.

Table 3.2 MPC sequences where *P=5*

Group *x*	*i* 0 1 2 3 4	Sequence	MPC Sequences
0	0 0 0 0 0	$S_{0,0}$	$C_{0,0}$ = 10000 10000 10000 10000 10000
	4 4 4 4 4	$S_{0,1}$	$C_{0,1}$ = 00001 00001 00001 00001 00001
	3 3 3 3 3	$S_{0,2}$	$C_{0,2}$ = 00010 00010 00010 00010 00010
	2 2 2 2 2	$S_{0,3}$	$C_{0,3}$ = 00100 00100 00100 00100 00100
	1 1 1 1 1	$S_{0,4}$	$C_{0,4}$ = 01000 01000 01000 01000 01000
1	0 1 2 3 4	$S_{1,0}$	$C_{1,0}$ = 10000 01000 00100 00010 00001
	1 2 3 4 0	$S_{1,1}$	$C_{1,1}$ = 01000 00100 00010 0000110000
	2 3 4 0 1	$S_{1,2}$	$C_{1,2}$ = 00100 00010 00001 10000 01000
	3 4 0 1 2	$S_{1,3}$	$C_{1,3}$ = 00010 00001 10000 01000 00100
	4 0 1 2 3	$S_{1,4}$	$C_{1,4}$ = 00001 10000 01000 00100 00010
2	0 2 4 1 3	$S_{2,0}$	$C_{2,0}$ = 10000 00100 00001 01000 00010
	2 4 1 3 0	$S_{2,1}$	$C_{2,1}$ = 00100 00001 01000 00010 10000
	4 1 3 0 2	$S_{2,2}$	$C_{2,2}$ = 00001 01000 00010 10000 00100
	1 3 0 2 4	$S_{2,3}$	$C_{2,3}$ = 01000 00010 10000 00100 00001
	3 0 2 4 1	$S_{2,4}$	$C_{2,4}$ = 00010 10000 00100 00001 01000
3	0 3 1 4 2	$S_{3,0}$	$C_{3,0}$ = 10000 00010 01000 00001 00100
	3 1 4 2 0	$S_{3,1}$	$C_{3,1}$ = 00010 01000 00001 00100 10000
	1 4 2 0 3	$S_{3,2}$	$C_{3,2}$ = 01000 00001 00100 10000 00010
	4 2 0 3 1	$S_{3,3}$	$C_{3,3}$ = 00001 00100 10000 00010 01000
	2 0 3 1 4	$S_{3,4}$	$C_{3,4}$ = 00100 10000 00010 01000 00001
4	0 4 3 2 1	$S_{4,0}$	$C_{4,0}$= 10000 00001 00010 00100 01000
	4 3 2 1 0	$S_{4,1}$	$C_{4,1}$= 00001 00010 00100 01000 10000
	3 2 1 0 4	$S_{4,2}$	$C_{4,2}$= 00010 00100 01000 10000 00001
	2 1 0 4 3	$S_{4,3}$	$C_{4,3}$= 00100 01000 10000 00001 00010
	1 0 4 3 2	$S_{4,4}$	$C_{4,4}$= 01000 10000 00001 00010 00100

Therefore, it should be noted from the above function the interesting group correlation proprieties associated with MPC sequences. Namely, the cross-correlation value of two code sequences within the same group is strictly orthogonal. However, for sequences located in two different groups, the cross-correlation value is bounded by *one*. Additionally, the auto-correlation peak value equals *P* by setting $n = m$.

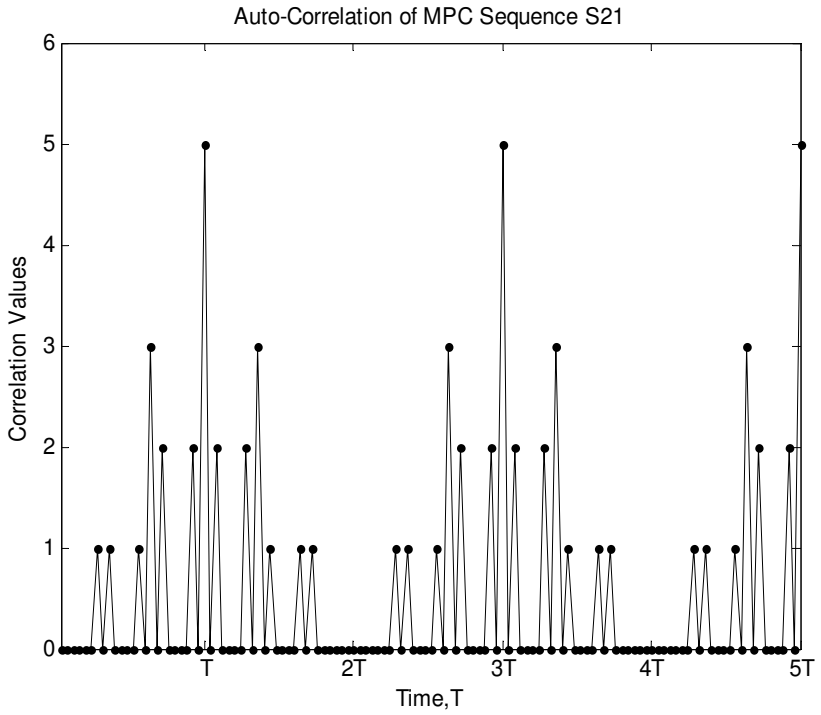

Figure 3.4 Auto-correlation values of MPC sequence of $S_{2,1}$, where *P=5* following the data stream of 10101

Figure 3.4 illustrates the auto-correlation property of MPC sequence $S_{2,1}$,and the maximum peak value equals 5 at each synchronised time *T* i.e. equivalent to the bit duration or the code-length when the sequences follow the data stream 10101.

Similarly, the cross-correlation values of MPC sequences placed in the same group $S_{2,0}$ and $S_{2,1}$ for the same data stream is displayed in the Figure 3.5. As one can see, the value of cross-correlation function is equal to *zero* at each synchronised time *T*.

Finally, Figure 3.6 suggests that for the MPC sequences within two different groups $S_{1,0}$ with $C_{2,1}$ the cross-correlation values equal *one* at each synchronised time *T*. Therefore, smaller cross-correlation values exist between two code sequences; the lower MAI is involved correspondingly.

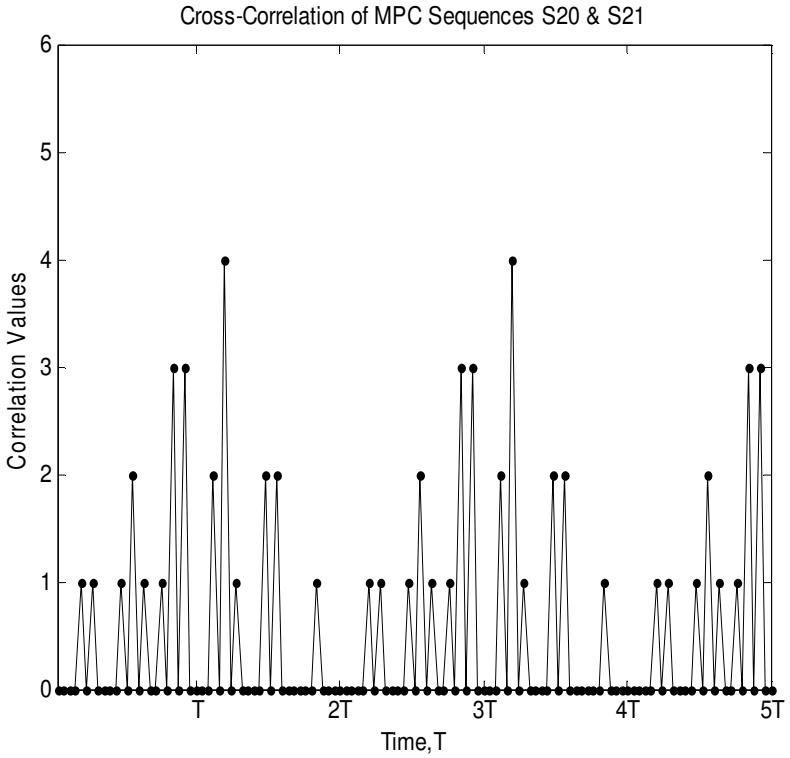

Figure 3.5 Cross-correlation values of MPC sequences of $S_{2,0}$ and $S_{2,1}$, where *P=5* within the same group, following the data stream of 10101

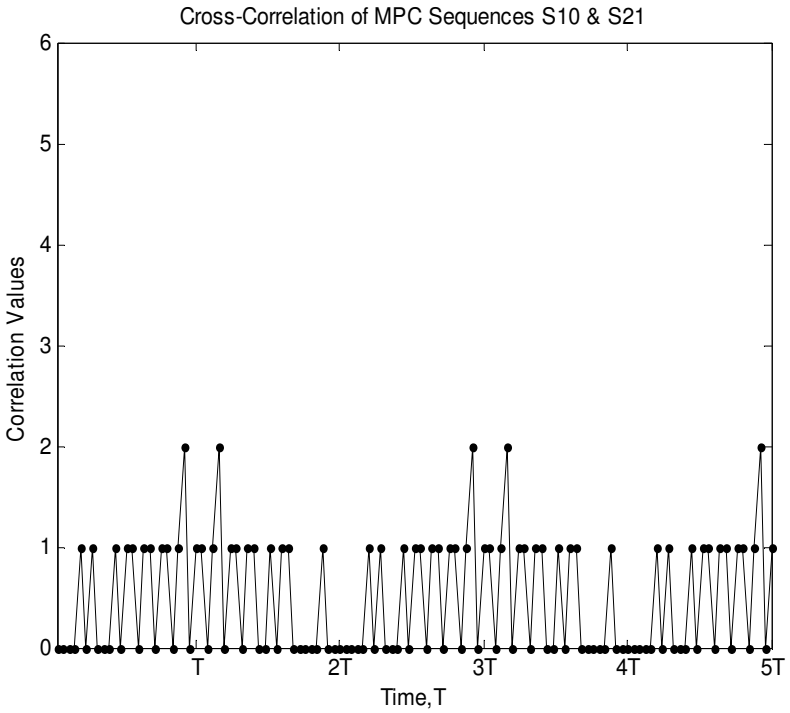

Figure 3.6 Cross-correlation values of MPC sequences of $S_{1,0}$ and $S_{2,1}$, where *P=5* within the different groups, following data stream of 10101

D. Advantages of MPC Sets

MPC sequences with relative large number of available code sequences and lower cross-correlation values are identified as a suitable candidate, especially for synchronous OCDMA to accommodate a greater number of subscribers under the same bandwidth-expansion. On the other hand, as aforementioned, code-length plays a significant role in raising the system performance in terms of MAI, BER, and throughput. Therefore, investigating longer codes that maintain the desired properties can be beneficial.

3.2.2.3 new-Modified Prime Code (n-MPC)

A. Construction Principle

The n-MPC has been proposed in [95] and generated through repeating the last sequence stream of the previous MPC sequence and rotating in the same group with the aid of a sub-sequence of length *P*. This kind of code has *P* groups, each of which has *P* code sequences. The length of each code is P^2+P and the weight is $P+1$. The total number of available sequences is P^2.

B. Example of an n-MPC Set

Table 3.3 shows an example of the n-MPC for $P=5$.

C. n-MPC Correlation Properties

The auto- and cross-correlation function for any pair of codes C_n and C_m is given at each synchronised time *T* by [95]:

$$R_{C_m C_n} = C_m \cdot C_n = \begin{cases} P+1, & \text{if } m = n \\ 0, & \text{if } m \neq n, m \text{ and } n \text{ share the same group} \\ 1, & \text{if } m \neq n, m \text{ and } n \text{ are from different groups} \end{cases} \quad (3.13)$$

where $m, n \in \{1,2,...,P^2\}$.

Table 3.3 n-MPC sequences where *P=5*

Group *x*	*i* 0 1 2 3 4	Sequence	MPC Sequences	Padded Sequence
0	0 0 0 0 0	$S_{0,0}$	$C_{0,0}$ = 10000 10000 10000 10000 *10000*	***01000***
	4 4 4 4 4	$S_{0,1}$	$C_{0,1}$ = 00001 00001 00001 00001 00001	*10000*
	3 3 3 3 3	$S_{0,2}$	$C_{0,2}$ = 00010 00010 00010 00010 00010	00001
	2 2 2 2 2	$S_{0,3}$	$C_{0,3}$ = 00100 00100 00100 00100 00100	00010
	1 1 1 1 1	$S_{0,4}$	$C_{0,4}$ = 01000 01000 01000 01000 ***01000***	00100
1	0 1 2 3 4	$S_{1,0}$	$C_{1,0}$ = 10000 01000 00100 00010 00001	00010
	1 2 3 4 0	$S_{1,1}$	$C_{1,1}$ = 01000 00100 00010 00001 10000	00001
	2 3 4 0 1	$S_{1,2}$	$C_{1,2}$ = 00100 00010 00001 10000 01000	10000
	3 4 0 1 2	$S_{1,3}$	$C_{1,3}$ = 00010 00001 10000 01000 00100	01000
	4 0 1 2 3	$S_{1,4}$	$C_{1,4}$ = 00001 10000 01000 00100 00010	00100
2	0 2 4 1 3	$S_{2,0}$	$C_{2,0}$ = 10000 00100 00001 01000 00010	01000
	2 4 1 3 0	$S_{2,1}$	$C_{2,1}$ = 00100 00001 01000 00010 10000	00010
	4 1 3 0 2	$S_{2,2}$	$C_{2,2}$ = 00001 01000 00010 10000 00100	10000
	1 3 0 2 4	$S_{2,3}$	$C_{2,3}$ = 01000 00010 10000 00100 00001	00100
	3 0 2 4 1	$S_{2,4}$	$C_{2,4}$ = 00010 10000 00100 00001 01000	00001
3	0 3 1 4 2	$S_{3,0}$	$C_{3,0}$ = 10000 00010 01000 00001 00100	00001
	3 1 4 2 0	$S_{3,1}$	$C_{3,1}$ = 00010 01000 00001 00100 10000	00100
	1 4 2 0 3	$S_{3,2}$	$C_{3,2}$ = 01000 00001 00100 10000 00010	10000
	4 2 0 3 1	$S_{3,3}$	$C_{3,3}$ = 00001 00100 10000 00010 01000	00010
	2 0 3 1 4	$S_{3,4}$	$C_{3,4}$ = 00100 10000 00010 01000 00001	01000
4	0 4 3 2 1	$S_{4,0}$	$C_{4,0}$ = 10000 00001 00010 00100 01000	00100
	4 3 2 1 0	$S_{4,1}$	$C_{4,1}$ = 00001 00010 00100 01000 10000	01000
	3 2 1 0 4	$S_{4,2}$	$C_{4,2}$ = 00010 00100 01000 10000 00001	10000
	2 1 0 4 3	$S_{4,3}$	$C_{4,3}$ = 00100 01000 10000 00001 00010	00001
	1 0 4 3 2	$S_{4,4}$	$C_{4,4}$ = 01000 10000 00001 00010 00100	00010

The auto- and cross-correlation properties of the n-MPC for the data stream 10101 are illustrated in Figures 3.7 to 3.9 where *P=5*. Figure 3.7 implies the auto-correlation values of the n-MPC sequence which is *P+1=6* at the synchronised time *T*. Meanwhile, Figure 3.8 plots the cross-correlation values of the n-MPC sequences within the same group which are '0'. While, Figure 3.9 suggests that for n-MPC from different groups,

cross-correlation values are equal to '1' at synchronous instants *T* i.e. equivalent to the bit duration or the code-length.

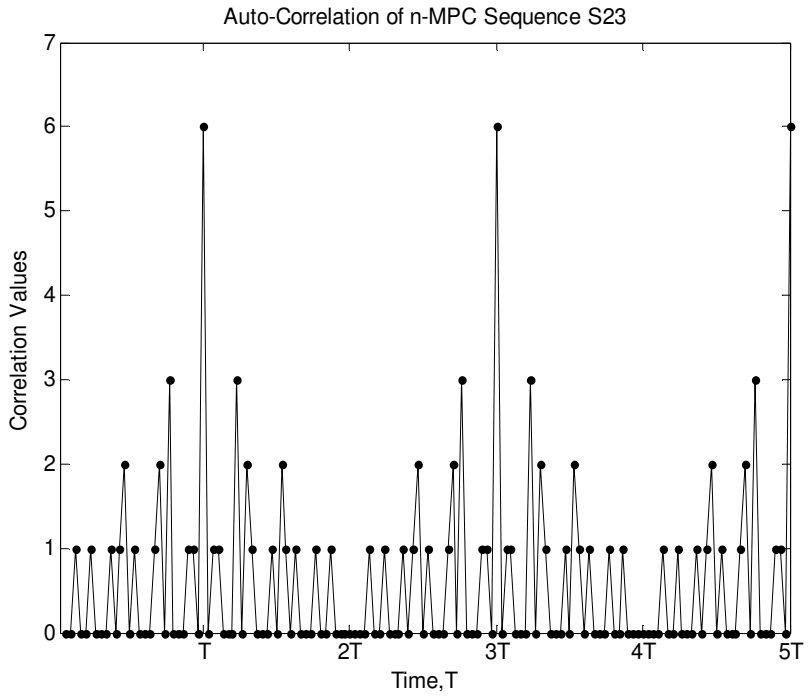

Figure 3.7 Auto-correlation values of n-MPC sequence of $S_{2,3}$, where *P=5* following the data stream of 10101

D. Advantages of n-MPC Sequences

The conclusion can be drawn that increased code-length can enhance the correlation properties that finally improve the detection process. However, the code-length is also a trade-off between network performance and throughput.

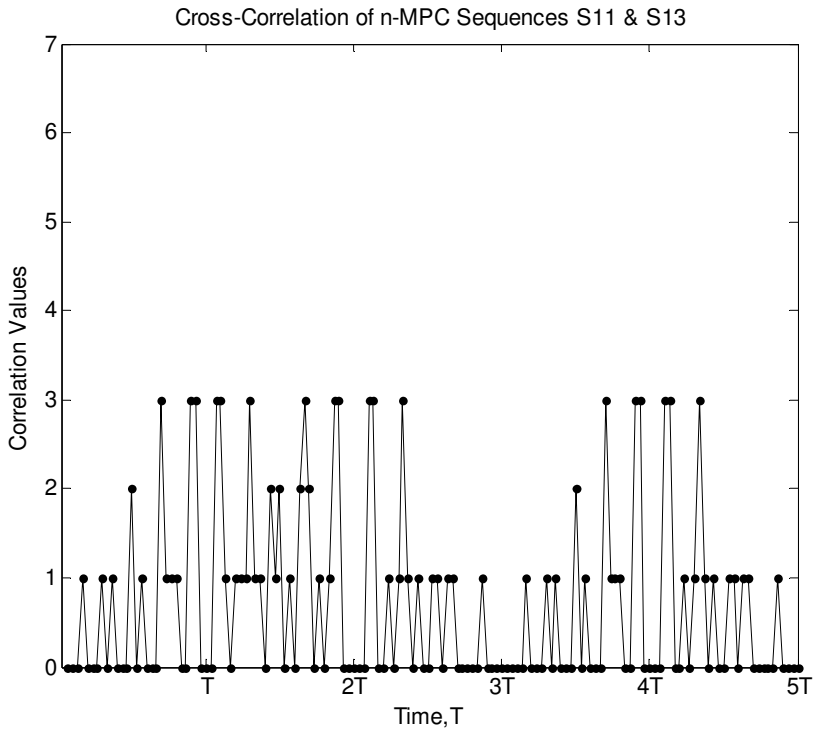

Figure 3.8 Cross-correlation values of n-MPC sequences $S_{1,1}$ and $S_{1,3}$ within the same group where *P=5*, following the data stream of 10101

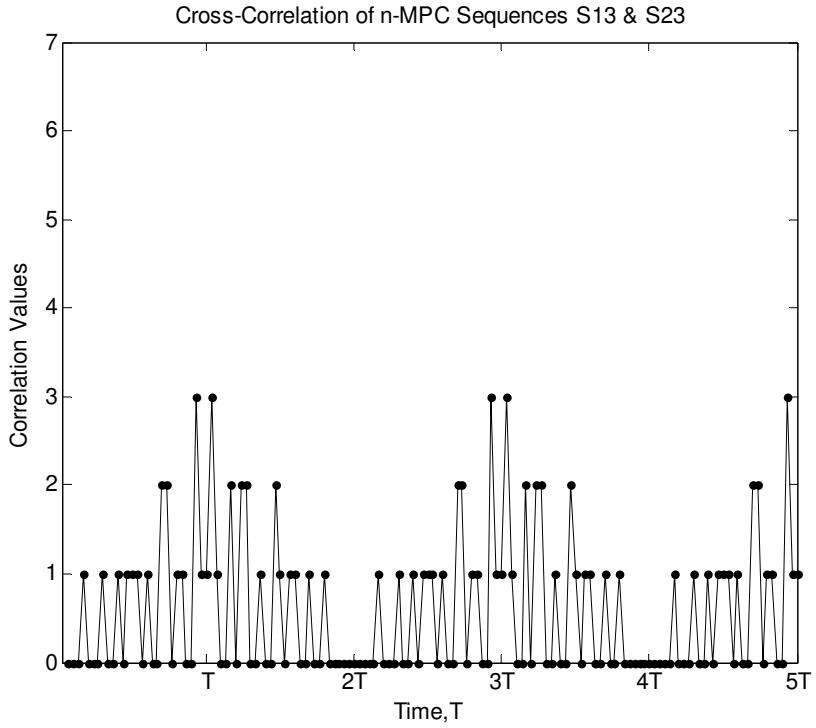

Figure 3.9 Cross-correlation values of n-MPC sequences of $S_{1,3}$ and $S_{2,3}$, within the different groups where *P=5*, following the data stream of 10101

3.2.2.4 Double-Padded Modified Prime Code (DPMPC)

By studying the aforementioned spreading codes, it is observed that the code-length and accordingly correlation properties still need to be enhanced. This implies an increase in the chip-rate (processing gain in spreading) which makes the spreading code more secure (i.e. less or no interception) and also permit the OCDMA system to mitigate the MAI by increasing the difference between cross and auto-correlation values. Having these features in mind as motivations, the new spreading code used as the address sequences for the application in optical CDMA communications has been designed and constructed.

A. Construction Principle

The DPMPC is simply generated after one more step padding of n-MPC by repeating the final sequence-stream of the previous MPC sequence. In fact, the padding order can also be applied vice versa, whereas if the padding order changes during the code generation, the cross-correlation value also changes into undesirable values (increases); therefore, the padding order has to be followed for the whole code sequences. Finally, the two sequences are padded into each MPCs and consequently the code enlarges by *2P* as compared with MPC and by *P* as compared with n-MPC. It is necessary to note that the padded sequences cannot only be the final sequence-stream of MPC but also they can be any stream of MPC sequences. This is due to the uniqueness of each MPC sequence-stream that makes each code matchless against each other. This code-family has also *P* groups, each of which has *P* sequence codes.

The length of each code is P^2+2P and the weight is $P+2$ with the total number of available sequences of P^2.

B. Example of a DPMPC Set

Table 3.4 shows an example of the DPMPC for $P=5$. Referring to Table 3.4 each code consists of two parts, MPC and group sequence-stream (GSS) parts. For example, for code $C_{1,0}$ the MPC part is *10000 01000 00100 00010 00001* and its GSS part is *00001 00010* which are the last sequence-stream of $C_{1,0}$ itself and $C_{1,4}$ in the same group. That is shown as $C_{10} \rightarrow 10000\,01000\,00100\,00010\,00001 + 00001\,00010.$

Table 3.4 DPMPC sequences where $P=5$

Group *x*	*i* 0 1 2 3 4	Sequence	MPC Part	GSS Part
0	0 0 0 0 0	$S_{0,0}$	$C_{0,0}$ = 10000 10000 10000 10000 *10000*	*10000* ***01000***
	4 4 4 4 4	$S_{0,1}$	$C_{0,1}$ = 00001 00001 00001 00001 *00001*	*00001* *10000*
	3 3 3 3 3	$S_{0,2}$	$C_{0,2}$ = 00010 00010 00010 00010 00010	00010 00001
	2 2 2 2 2	$S_{0,3}$	$C_{0,3}$ = 00100 00100 00100 00100 00100	00100 00010
	1 1 1 1 1	$S_{0,4}$	$C_{0,4}$ = 01000 01000 01000 01000 ***01000***	01000 00100
1	0 1 2 3 4	$S_{1,0}$	$C_{1,0}$ = 10000 01000 00100 00010 00001	00001 00010
	1 2 3 4 0	$S_{1,1}$	$C_{1,1}$ = 01000 00100 00010 00001 10000	10000 00001
	2 3 4 0 1	$S_{1,2}$	$C_{1,2}$ = 00100 00010 00001 10000 01000	01000 10000
	3 4 0 1 2	$S_{1,3}$	$C_{1,3}$ = 00010 00001 10000 01000 00100	00100 01000
	4 0 1 2 3	$S_{1,4}$	$C_{1,4}$ = 00001 10000 01000 00100 00010	00010 00100
2	0 2 4 1 3	$S_{2,0}$	$C_{2,0}$ = 10000 00100 00001 01000 00010	00010 01000
	2 4 1 3 0	$S_{2,1}$	$C_{2,1}$ = 00100 00001 01000 00010 10000	10000 00010
	4 1 3 0 2	$S_{2,2}$	$C_{2,2}$ = 00001 01000 00010 10000 00100	00100 10000
	1 3 0 2 4	$S_{2,3}$	$C_{2,3}$ = 01000 00010 10000 00100 00001	00001 00100
	3 0 2 4 1	$S_{2,4}$	$C_{2,4}$ = 00010 10000 00100 00001 01000	01000 00001
3	0 3 1 4 2	$S_{3,0}$	$C_{3,0}$ = 10000 00010 01000 00001 00100	00100 00001
	3 1 4 2 0	$S_{3,1}$	$C_{3,1}$ = 00010 01000 00001 00100 10000	10000 00100
	1 4 2 0 3	$S_{3,2}$	$C_{3,2}$ = 01000 00001 00100 10000 00010	00010 10000
	4 2 0 3 1	$S_{3,3}$	$C_{3,3}$ = 00001 00100 10000 00010 01000	01000 00010
	2 0 3 1 4	$S_{3,4}$	$C_{3,4}$ = 00100 10000 00010 01000 00001	00001 01000
4	0 4 3 2 1	$S_{4,0}$	$C_{4,0}$ = 10000 00001 00010 00100 01000	01000 00100
	4 3 2 1 0	$S_{4,1}$	$C_{4,1}$ = 00001 00010 00100 01000 10000	10000 01000
	3 2 1 0 4	$S_{4,2}$	$C_{4,2}$ = 00010 00100 01000 10000 00001	00001 10000
	2 1 0 4 3	$S_{4,3}$	$C_{4,3}$ = 00100 01000 10000 00001 00010	00010 00001
	1 0 4 3 2	$S_{4,4}$	$C_{4,4}$ = 01000 10000 00001 00010 00100	00100 00010

Similarly, by padding the final sequence-stream of MPC of $C_{1,0}$ which is *00001* to the MPC part of $C_{1,1}$ and last sequence-stream of $C_{1,1}$ which is *10000*, DPMPC of $C_{1,1}$ is generated.

C. DPMPC Correlation Properties

The auto- and cross-correlation function for any pair of codes C_n and C_m is given at each synchronised time *T* i.e. equivalent to the bit duration or the code-length by:

$$R_{C_m C_n} = C_m \cdot C_n = \begin{cases} P+2, & \text{if } m = n \\ 0, & \text{if } m \neq n, m \text{ and } n \text{ share the same group} \\ 1, & \text{if } m \neq n, m \text{ and } n \text{ are from different groups} \end{cases} \quad (3.14)$$

where $m,n \in \{1,2,\ldots P^2\}$. Figures 3.10 – 3.12 illustrate the correlation values of various DPMPC sequences.

In Figure 3.10, the auto-correlation values of $S_{2,1}$ at each synchronised position are displayed. It can also be seen in Figures 3.11 and 3.12 that the cross-correlation values of different codes at time *T* is *zero* for the codes in the same group and *one* for those which are in the different groups. As an example, data stream of *11010* is followed by the code sequences to show how it exactly works.

D. Advantages of DPMPC Sequences

The DPMPC expands the code-length by remaining the excellent correlation property of the PC families. This attribute helps the OCDMA stays more secure as well. As discussed earlier in Section 3.1.1 and also will be discussed later, the code-length is an important feature of a code that can raise the system performance by reducing MAI and consequently error-rate.

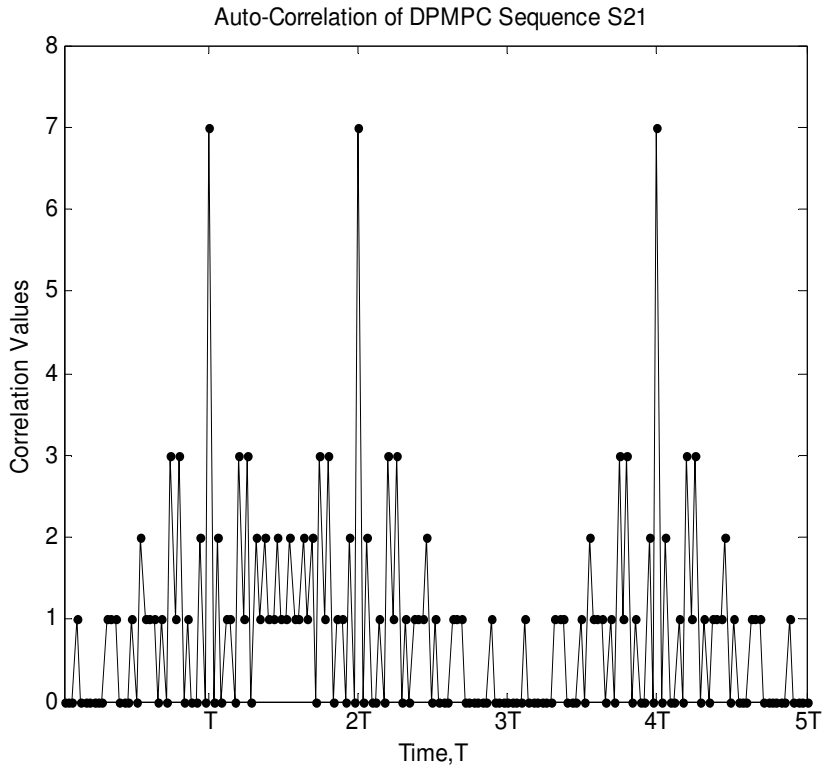

Figure 3.10 Auto-correlation values of DPMPC sequence of $S_{2,1}$ where *P=5* following the data stream of 11010

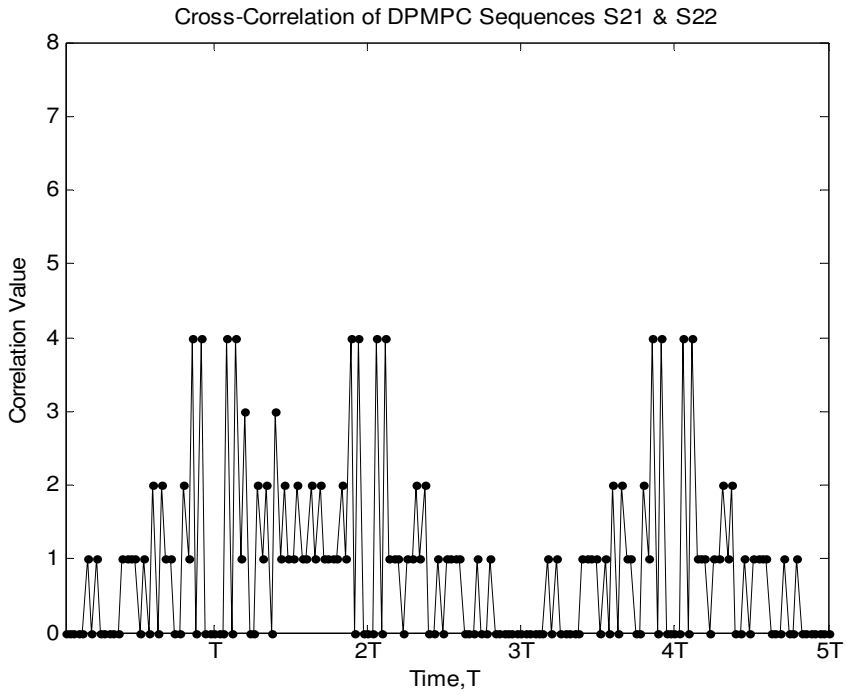

Figure 3.11 Cross-correlation values of DPMPC sequences $S_{2,1}$ and $S_{2,2}$ within the same group where *P=5*, following the data stream of 11010

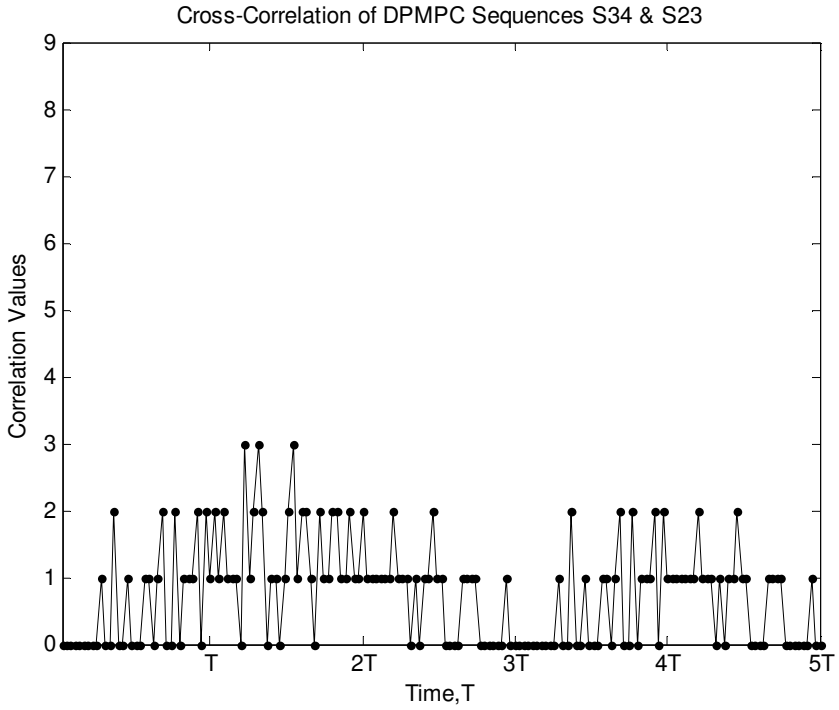

Figure 3.12 Cross-correlation values of DPMPC sequences of $S_{3,4}$ and $S_{2,3}$, within the different groups where *P=5*, following the data stream of 11010

On the other hand, as observed from Figure 3.10, the auto-correlation peaks increased and accordingly enhance the difference between auto- and cross-correlation values. This feature assists the detection process significantly and reduces MAI remarkably. It should be mentioned that the longer code brings complexity in the system implementations and decrease the system throughput at the cost of better correlation property and security.

Table 3.5 compares the prime code families in terms of code-length, cardinality, code-weight and correlation properties. It is shown that the DPMPC has greater code-length, higher weight while maintaining the same good correlation properties.

Table 3.5 Comparisons of the prime code families

Code Family	Code-Length	Code-Weight	Cardinality	Correlation Properties	
				Auto-	Cross-
PC	P^2	P	P	P	1
MPC	P^2	P	P^2	P	0 or 1
n-MPC	P^2+P	$P+1$	P^2	$P+1$	0 or 1
DPMPC	P^2+2P	$P+2$	P^2	$P+2$	0 or 1

3.3 CDMA Techniques in Optical Domain

A variety of approaches to OCDMA have been suggested [20, 25, 28, 31, 96]. They share a common strategy of distinguishing data channels not by wavelength or time slot, but by distinctive spectral or temporal code (or signature) impressed onto the bits of each channel. Carefully designed receivers isolate channels by code-specific detection. There is no global optimum topology for fibre optic LAN interconnection yet. Thus each topology has its own advantages and disadvantages, which may become significant or insignificant depending on the specific application [97, 98].

In intensity on-off Keying (OOK) system, each user information source modulates the laser diode directly [15, 27] or indirectly using an external modulator [48]. The optical signal is encoded optically in an encoder that maps each bit into a very high rate (i.e. code-length x data-rate) optical sequences. The encoded lightwave from all active users are broadcasted in the network by a star coupler. The star coupler can be a passive or active device. The optical decoder or matched filter at the receiving node is matched to the transmitting node giving a high correlation peak that is detected by the photo-detector. Other users using the same network at the same time but with different codes give rise to MAI. This MAI can be high enough to make the LAN useless if the code used in the network does not satisfy specific cross-correlation properties.

Other factors affecting the performance of the network are shot noise and thermal noise at the receiver.

Generally, OCDMA systems can be classified to incoherent or coherent schemes. Incoherent schemes are based on intensity-modulation/direct-detection (IM-DD) scheme that incorporates non-coherent detection of super-imposed optical power of all users. The operation of direct-detection makes the procedure simple and the receiver is cost effective. The photo-detector detects the power of the optical signal but not the instantaneous phase variations of the optical signal. Thus, only incoherent signal processing techniques can be used to process the signature sequences composed of only *one*s and *zero*s restricting the type of codes that can be used in incoherent OCDMA systems [20]. In coherent OCDMA, the phase information of the optical carrier is crucial for the de-spreading process. Due to the nature of optical fibre transmission and its nonlinear effects the complexity of the coherent OCDMA receiver makes this approach more difficult to realize. However, the performance of the coherent scheme is much better than incoherent one since the receivers are more signal-to-noise ratio (SNR) sensitive [28, 44, 99, 100].

Alternatively, OCDMA can be classified into temporal and spectral according to the way the optical signal is encoded as briefly introduced in the following sub-sections. Temporal OCDMA performs the coding in time domain by using very short optical pulses e.g. 10 ps at data-rate 1 Gbps and code-length of 100, using optical tapped-delay lines (OTDL) to compose the coded optical signal. Spectral OCDMA, on the other hand, encodes the phase or intensity of the spectral content of a broadband optical

signal by using phase or amplitude masks. Wavelength-hopping can be considered as a temporal-spectral coding where the coding is done in both dimensions.

3.3.1 Wavelength-Hopping Coding

Fast wavelength-hopping OCDMA system can be implemented by fibre Bragg grating (FBG) [15, 101-103]. Multiple Bragg gratings are used to generate the CDMA hopping frequencies (i.e. wavelengths). Due to the linear first-in-first-reflected nature of multiple Bragg gratings, the time-frequency hopping pattern is determined by the order of the grating frequencies in the fibre. The order of the grating frequencies in the decoder is the reverse of that in the encoder to achieve the matched filtering operation. Figure 3.13 shows the encoder and decoder in a star-coupled network. If the central wavelength of the incoming lightwave equals the Bragg wavelength, it will be reflected by the FBG, or it will be transmitted. With proper written CDMA coding pattern, the reflected light field from FBG will be spectrally encoded onto an address code. To reduce the effect of the MAI, codes with minimum cross-correlation properties are required [25]. These codes fall into the category of one-coincidence sequences and are characterised by the following three properties:

- All of the sequences are of the same length;
- In each sequence, each frequency is used at most once; and
- The maximum number of hits between any pair of sequences for any time shift equals *one*.

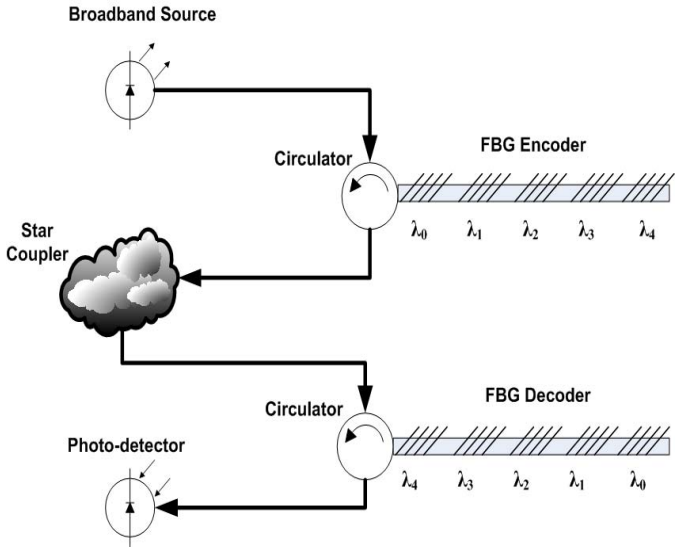

Figure 3.13 Principle of FBG encoder and decoder

3.3.2 Spectral Phase Coding (SPC)

Figure 3.14(a) shows an encoder and decoder of the spectral phase encoding system. The information source modulates the very short laser pulses. The generated short pulses are Fourier transformed and the spectral components are multiplied by the code corresponding to a phase shift of 0 or π [21, 104]. Fourier transform can be implemented by the Grating and lens pair as shown in Figure 3.14(b).

As a result of phase encoding, the original optical ultra-short pulse is transformed into a low intensity signal with longer duration. The liquid crystal modulator (LCM) can be utilised to set the spectral phase to maximum-sequence phase [105]. The LCM has a fully programmable linear array and individual pixels can be controlled by applying drive levels resulting in phase shifts of 0 or π. By a phase mask, the dispersed pulse is partitioned into N_c frequency chips by the aid of a phase mask that can be a LCM. Each chip is assigned a phase shift depending on the users address code sequences.

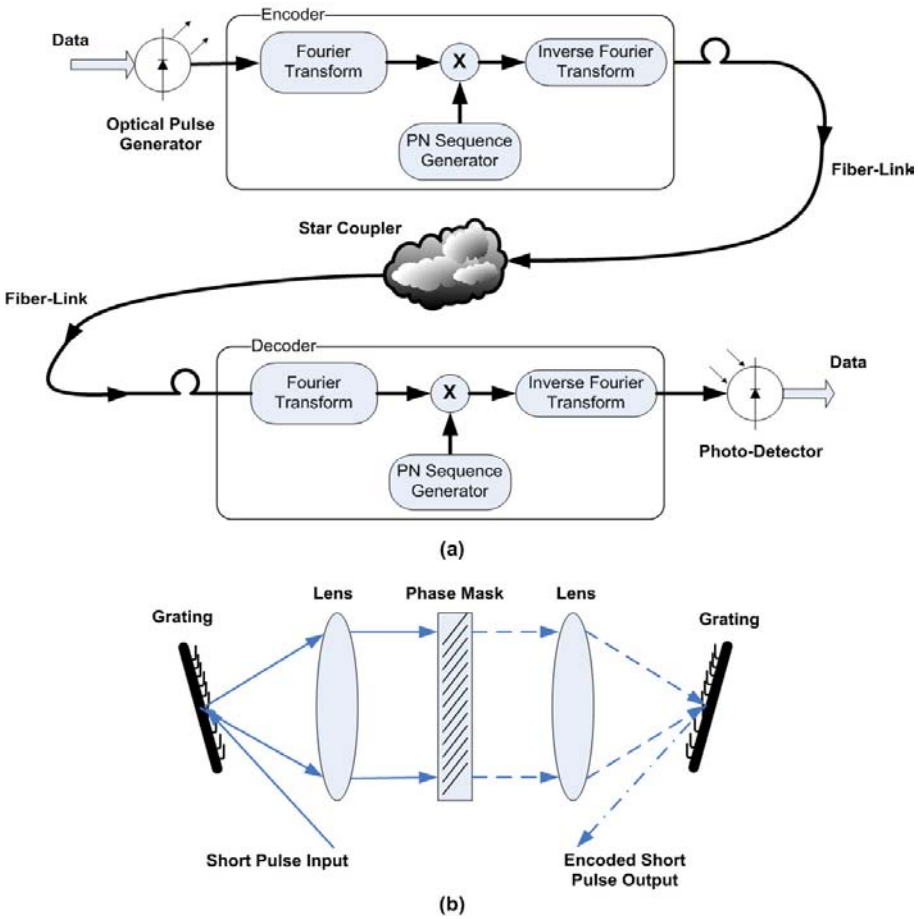

Figure 3.14 (a) Principle of SPC-OCDMA (b) Structure of optical Fourier transform and SPC

3.3.3 Spectral Amplitude Coding (SAC)

In SAC-OCDMA format, frequency components of the signal from a broadband optical source are encoded by selectively blocking or transmitting them in accordance with a signature code [26, 28]. Compared to SPC-OCDMA, SAC-OCDMA is less expensive due to incoherent optical source. For the access environment, where cost is one of the most decisive factors, the SAC-OCDMA seems therefore to be a promising candidate.

Figure 3.15 shows the principle structure of a SAC-OCDMA system. The receiver filters the incoming signal through the same direct decoder filter $A(w)$ at the transmitter as well as its complementary decoder $\overline{A}(w)$. The outputs from these decoders are detected by two photo-detectors connected in a balanced structure. For an interfering

signal, depending on the assigned signature code, a part of its spectral components will match the direct decoder, and the other part will match the complementary decoder. Since the output of the balanced receiver represents the difference between the two photo-detector outputs, the interfering channels will be cancelled whereas the matched channel is demodulated, i.e. MAI is cancelled in this SAC-OCDMA system.

Several signature code sets have been proposed for a SAC-OCDMA, including *M*-sequence [103], Hadamard [32], and modified-quadratic congruence (MQC) codes [106]. Each of these signature code sets can be represented by (N, W, λ), denoting its length, weight, and in-phase cross correlation respectively. In the *M*-sequence code set, $W = (N+1)/2$ and $\lambda = (N+1)/4$; the weight and in-phase cross correlation of the Hadamard code set are $N/2$ and $N/4$, respectively.

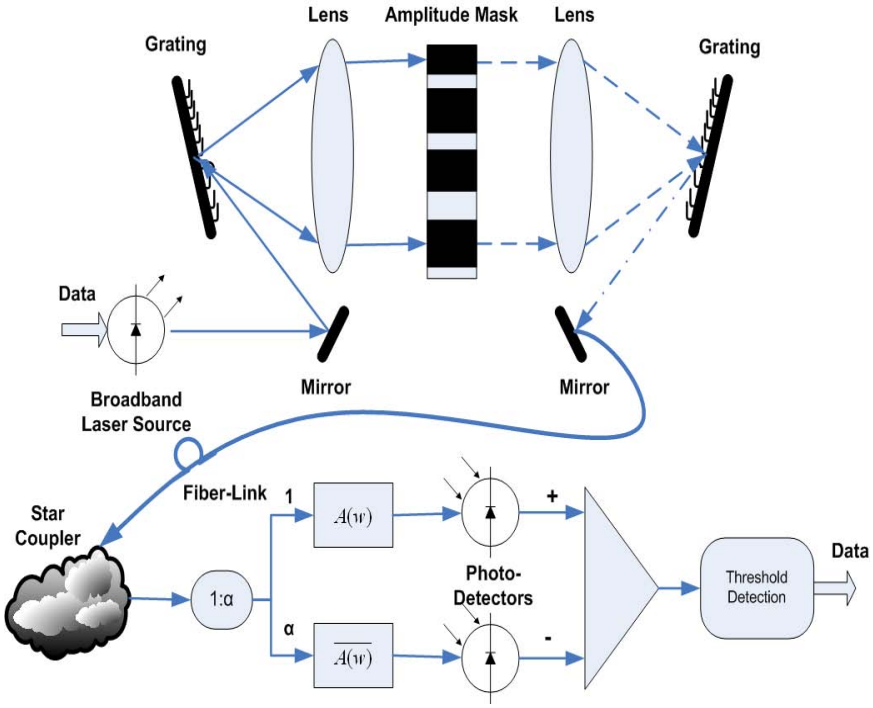

Figure 3.15 Principle of the SAC-OCDMA scheme

In MQC code, $\lambda = 1$ and for a prime number *P*, we have code-length of $N = P^2 + P$ and weight of $W = P + 1$. Let $C_d = [C_d(0), C_d(1), ..., C_d(N-1)]$ and $C_k = [C_k(0), C_k(1), ..., C_k(N-1)]$ be two *(0,1)* signature codes, then the correlation properties are given by:

$$R_{c_d c_k} = \sum_{i=0}^{N-1} C_d(i) \cdot C_k(i) = \begin{cases} W & d = k \\ \lambda & d \neq k \end{cases} \tag{3.15}$$

The correlation between $\overline{C}_d$ (a complementary of C_d) and C_k is then:

$$R_{\overline{c}_d c_k} = \sum_{i=0}^{N-1} \overline{C}_d(i) \cdot C_k(i) = W - C_{c_d c_k} = \begin{cases} 0 & d = k \\ W - \lambda & d \neq k \end{cases} \tag{3.16}$$

To completely cancel MAI, it is necessary to set a ratio between the optical powers that arrive at the two photo-detectors that can be $\alpha = \lambda / W - \lambda$ [28]. The cancellation of the interfering signal (i.e. $d \neq k$) by the balanced receiver thus can be seen as:

$$R_{c_d c_k} - \alpha R_{\overline{c}_d c_k} = 0 \tag{3.17}$$

Since a broadband optical source is used in frequency-domain encoding, optical beating interference (OBI) or beat noise is the major performance degrading factor. OBI occurs when a photo-detector simultaneously receives two or more optical signals at nearly the same wavelength. One of the solutions to the beat noise in coherent SAC-OCDMA is to employ an optical spreading code set with the lowest possible weight and the longest possible length for a given bit-rate [25].

A lower code-weight causes a lower SNR which means the received optical power is low because it is further reduced by a ratio of α in one of the branches as shown in Figure 3.15. That makes OBI low enough to ignore. In case of increased optical power,

a low-weight but longer code causes a higher SNR (i.e. better performance), due to the lower in-phase cross-correlation which finally results in again lower OBI [50].

Another major degrading factor in spectral-coded schemes, SPC and SAC, is phase-induced intensity noise (PIIN) that is highly proportional to the electric current generated by the photo-detectors as [28]:

$$\delta_{PIIN} = I^2 \cdot B \cdot \tau_c \tag{3.18}$$

where I is the photocurrent, *B* is the receiver's noise-equivalent electrical bandwidth and τ_c is the coherence time of source.

3.3.4 Time Spreading Coding

The temporal OCDMA signal can be generated by the splitting and combining of very short optical pulses. A high-peak optical pulse is encoded into a low intensity pulse train using parallel OTDLs at the transmitter in a star-coupled architecture. The decoding is performed by intensity correlation at the receiver using matched parallel OTDLs [40, 49, 53].

Incorrectly positioned pulses in the pulse train will form a background interference signal. The research in these incoherent OCDMA scheme led to the invention of a few major code groups such as OOC and PC families, as introduced in Section 3.2. In order to reduce crosstalk (i.e. MAI), these codes are all designed to have long code-length and low code-weight so that reduces temporal overlap between pulses from different users at the intensity correlator output. On the other hand, there should be a trade-off, since the long code-length can cause the inefficient spectral. Even with very carefully designed codes, co-channel interference due to non-orthogonal code

sequences gives a severe performance penalty. The BER is usually quite high and the number of allowable active users becomes very limited [20, 22, 23, 36, 40, 78].

Due to the extremely fast growth in bandwidth demand in the recent years, it is now necessary to make full use of the entire bandwidth capacity available in optical fibres. However, at the time that OCDMA systems using delay-line networks have been proposed, it was believed that the terabit communication capacity in fibre-optics would never be fully utilised. Even multi-gigabit networks were highly respected at that time. Although optics has been used for carrying signals, all the switching and multiplexing operations were performed in the electronic domain. Optoelectronic (OE) and electro-optic (EO) conversions occur at the terminal equipment. The OE-EO conversion was regarded as the bottleneck to high-speed multiplexing. Therefore, due to recent progress in photonics technologies, ultra-fast switching, multiplexing and signal processing in optical domain are feasible, and accordingly temporal OCDMA has been drawn a lot of attention nowadays to make use of the redundant bandwidth in optical fibres to alleviate the electronic processing overhead at the networks interface.

3.4 Synchronous vs. Asynchronous OCDMA

As noted in Section 3.2.2, synchronous OCDMA (S-OCDMA) dramatically improves efficiency in the trade-offs between code-length, MAI and address space. Since, in S-OCDMA, the receiver examines the correlator output only at one instant in the chip-interval, code sets for S-OCDMA are described by the triple, (N, W, λ).

In general, an OOC set of C_a with $(N, W, \lambda_a, \lambda_c)$, with cardinality of $|C_a|$ designed for asynchronous OCDMA (A-OCDMA) can be used as an OOC set of C_s

with $(N, W, \max(\lambda_a, \lambda_c))$, with cardinality $|C_s| = n.|C_a|$ for S-OCDMA. Since, each of the *n* time-shifts of each code sequence of C_a can be used as a unique code sequence in C_s with the same correlation properties.

In contrast, DPMPC can also be utilized in A-OCDMA; however, less number of subscribers is then accommodated due to lack of time-shifting feature used in the synchronous one. On the contrary, in the OOC which are normally applied to A-OCDMA, we have to set the weight (i.e. no. of 1s) and code sequence independently and keep the number of spreading codes small to attain good correlation property. Table 3.5 shows the OOCs with frame-length of $F = 32$ and weight of $\omega = 4$ [78]. Since the total number of OOC sequences is given by the integer part of $(F-1)/(\omega^2 - \omega)$, hence there are only two codes to satisfy the cross-correlation value of *one*. To assure this condition, the distance of any two 1s should be different in all codes as shown in Table 3.5. Therefore, to increase the number of spreading codes in OOC, either the frame-length has to increase or the weight has to decrease. In practice, in order to make 25 codec sequences with weight of 7, the code-length needs to be 1051. Therefore, OOC's frame-length needs to be 30 times larger than DPMPC ($((\omega^2 - \omega) \times 25 + 1) / (P^2 + 2P) = 30$ where $P = 5$ and $\omega = 7$) that accordingly decreases the bit-rate dramatically. When the OOC weight decreases, its correlation properties degrade. Consequently, the DPMPC whose weight is the same as OOC is more effective in S-OCDMA scheme, besides it can offer better correlation properties and more spreading sequences in shorter frame-length.

Table 3.6 OOC with $F = 32$ and $\omega = 4$

No. of chips between the subsequent 1s	Optical Orthogonal Codes (OOC)
9,3,15,5	10000000010010000000000000010000
4,7,19,2	10001000000100000000000000000010

The effect of channel interference (i.e. MAI) is inherent in direct-detection OCDMA, when the number of simultaneous active users increases, the optical pulses from the intended user and the interfering users overlap and BER tends to have an error-floor. Therefore, it is required to reduce the probability of overlapped pulses from interfering users to mitigate the effect of co-channel interference. The probability of overlapping pulses has been reduced by changing the modulation scheme OOK to *M-ary* pulse-position modulation (PPM) due to the variable pulse positions of pulse occurrence in PPM, although error-floor still exist [34, 36, 40], as discussed in details in next Chapter as well.

3.5 Summary

An overview of coding fundamentals in optical domain has been briefly introduced and discussed. OCDMA potentials as an access protocol in the optical networking concept have been investigated along with two major optical spreading codes, i.e. OOC and PC sets, with their applications and properties in details. We have also reviewed most common encoding techniques in optical spread spectrum communications in time, frequency and spectra domains with considering their merits and drawbacks. In addition, in this Chapter we introduced a novel spreading code sequences hereby referred to as double padded modified prime code (DPMPC) and analysed its features. In the following Chapters throughout the thesis, DPMPC is considered as the spreading

code and novel transceiver architectures and multiple access interference (MAI) cancellation techniques are going to be proposed and analysed within the applications of optical transport network in mind.

It should be noted that the most common wavelengths in the optical communications are at around 1.55 µm and 1.31 µm due to the least attenuation (loss) in the fibre-optic [31, 33, 36, 40, 47, 49-53]. Accordingly, throughout this thesis, we have also considered the analyses mainly at these wavelengths.

Chapter 4

Analysis of DPMPC in PPM-OCDMA Network

4.1 Introduction

Both on-off keying (OOK) and pulse-position modulations (PPM) OCDMA are two popular modulation schemes in incoherent OCDMA networks. PPM as an energy efficient modulation excels OOK if the average power rather than chip-time is the constraining factor [39]; however in practical OCDMA systems the chip-time is important, whereas power issues come to critical point in mobile and personal devices as well. In this Chapter, Manchester codes are systematically assigned to users as source coding for further improvement of the system performance and also we have assumed that the multiple access interference (MAI) is dominant noise in the system.

In this Chapter, the bit-error rate (BER) with respect to the double padded modified prime code (DPMPC) in incoherent synchronous PPM-OCDMA system will be analysed and derived. The PPM-OCDMA system without interference canceller becomes

unreliable as the number of simultaneous subscribers increases. The reason is that MAI increases rapidly as the number of active users increases. Even though increasing the multiplicity *M* and the prime number *P* is helpful for improving the overall system performance, however it is not realistic to increase *M* and *P* continuously. Moreover, the increment on *M* and *P* will increase the system complexity. If the amount of MAI can be removed or reduced, the system performance can be improved remarkably and more active users are accommodated in the network. Hence, the systems have been studied with MAI canceller and along with Manchester encoding. Finally, in order to realise the preference of DPMPC, the performances of various codes like new modified prime code (n-MPC) and modified prime code (MPC), introduced in Section 3.2.2, are demonstrated and compared for better understanding.

4.2 PPM-OCDMA Signalling

The *M-ary* PPM-OCDMA signalling format is shown in Figure 4.1. One frame with a duration of *T* seconds consists of *M* time slots, each of which is τ seconds wide, where $T = M\tau$. Where *P* is the prime number, P^2+2P chips of a DPMPC sequence with chip time T_c constitute a slot. Each symbol is represented by a train of optical pulses placed in one of *M* adjacent time slots. Therefore, for an *M-ary* PPM-OCDMA communication system, there are *M* possible pulse positions within the symbol frame *T*. In a single time frame, each user is allowed to transmit only one of the *M* symbols. A pre-assigned unique spreading sequence can be used to distinguish different users; although several of them can transmit the same symbol in a frame. When a user transmits a symbol, the unique spreading sequence of the desired user will occupy the corresponding time

slot. For a proper spread, the spreading sequence with length L_c must be exactly fitted into time slot τ (also called the spreading interval), where $\tau = T_c \cdot L_c$.

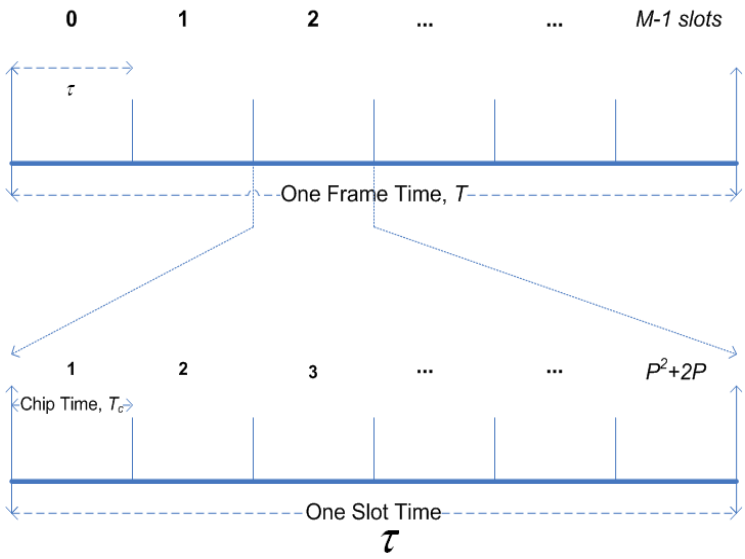

Figure 4.1 *M-ary* PPM-OCDMA signalling format with DPMPC

4.3 PPM-OCDMA Transceiver Architecture

4.3.1 PPM-OCDMA Transmitter Architectures

4.3.1.1 Simple Transmitter

A typical transmitter model for an incoherent PPM-OCDMA system is shown in Figure 4.2, which consists of information source, optical PPM encoder and OCDMA encoder [36]. In the following, the main function of each block in the transmitter is described.

- Information Source

The total number of information sources depends on the entire number of available sequences, where *N* out of total number of users are the active ones. Each user transmits continuous data symbols. Referring to Figure 4.2, take DPMPC as an example considering $P = 3$ and $M = 3$, hence the maximum number of active users is $P^2 = 9$.

Assuming that active intended user #2 sends data in slot *0*, user #6 sends data in slot *1* and user #8 also sends data in slot *2*.

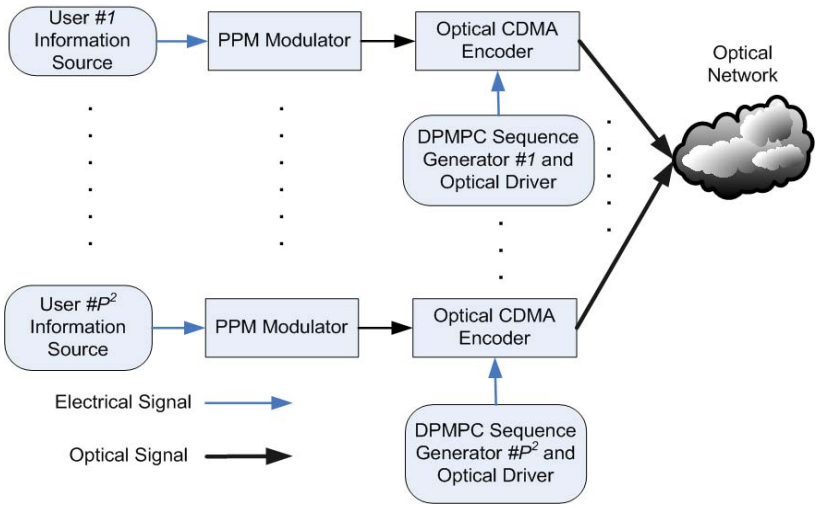

Figure 4.2 Incoherent PPM-OCDMA transmitters structure

- PPM Modulator

The output symbol of each information source is modulated into one of *M* time slots, and generates an optical PPM signal with the tall narrow shape using a laser pulse of width T_c and certain time delay reference to a certain point. The time delay depends on the amplitude of the data symbol transmitted from the source user. The position of laser pulses for intended users #2, #6 and #8 are displayed in Figure 4.3, which are the output waveforms of PPM encoder.

- Optical CDMA Encoder

The optical PPM signal is then passed to an OCDMA encoder, where it is spread into a train of shorter laser pulses with chip width T_c. The train of shorter laser pulses is the spreading sequence of the desired user. The spreading sequence is one of DPMPC sequences in the analysis. An OCDMA encoder can be implemented by using optical

tapped-delay lines (OTDL), which includes delayers, combiners and a splitter. Figure 4.4 shows an example of OCDMA encoder model.

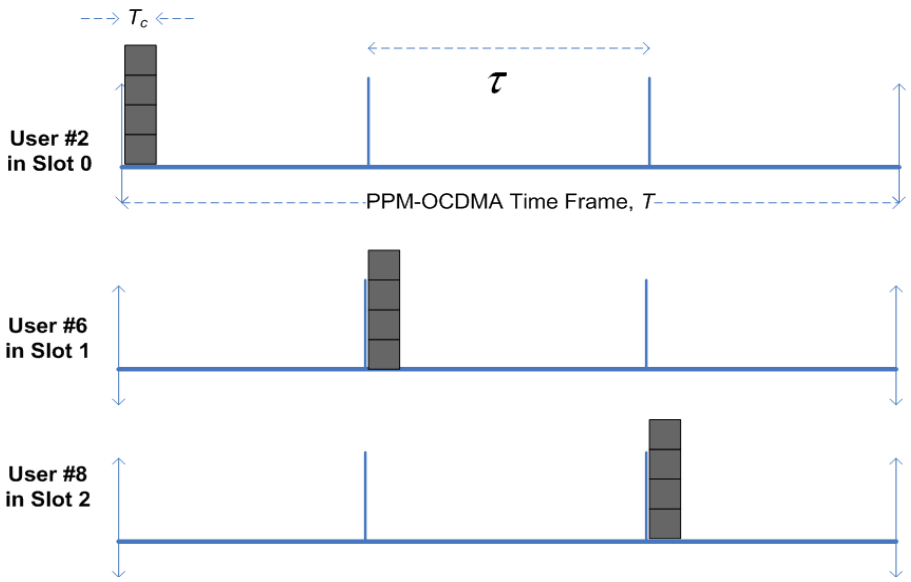

Figure 4.3 Example of PPM signals for users #2, #6 and #8 when *M=3*

Assuming that the intended user #2, #6 and #8 are arbitrarily assigned the signature sequences of $C_{0,0}$=*100 100 100 100 010*, $C_{1,0}$=*100 010 001 001 010* and $C_{2,0}$=*100 001 010 010 001* respectively as an example for the rest of our study. Then the three spreading sequences and the corresponding PPM-OCDMA signals are displayed in Figure 4.5. At the end, there is the summation of all formatted signals, which are illustrated in Figure 4.6 then the outcome is passed into the optical fibre as a communication channel.

4.3.1.2 Transmitter with MAI Cancellation

The transmitter model for PPM-CDMA system with interference cancellation is similar to that shown in Figure 4.2. The only difference is that the maximum number of accommodated users will be P^2-P, not P^2. Since the last sequence code of each group is

reserved as the reference correlator at the receiver which will be discussed later, they then cannot be allocated to any user. Assuming *N* active users are in the system, and each user transmits continuous data symbols. Then, the idle users are P^2-*P*-*N*.

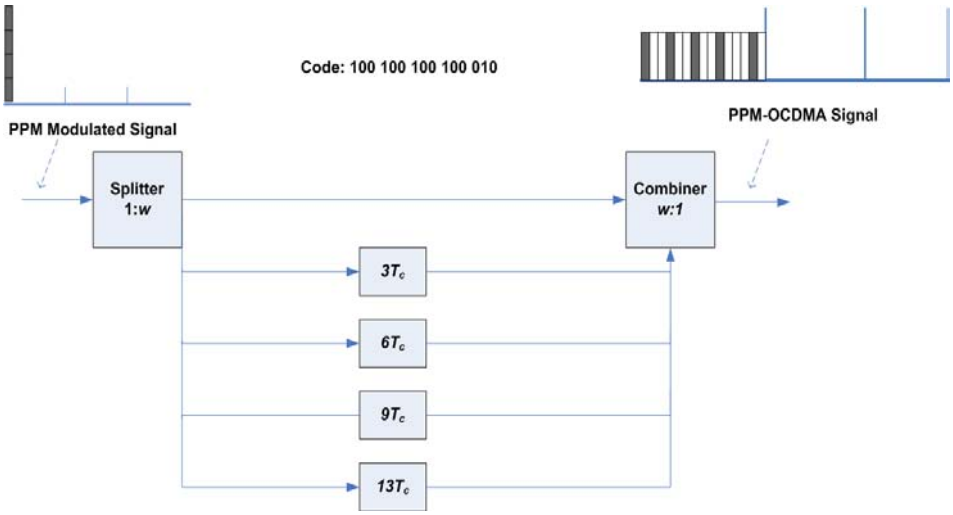

Figure 4.4 OTDLs for encoding *100 100 100 100 010* as a signature code

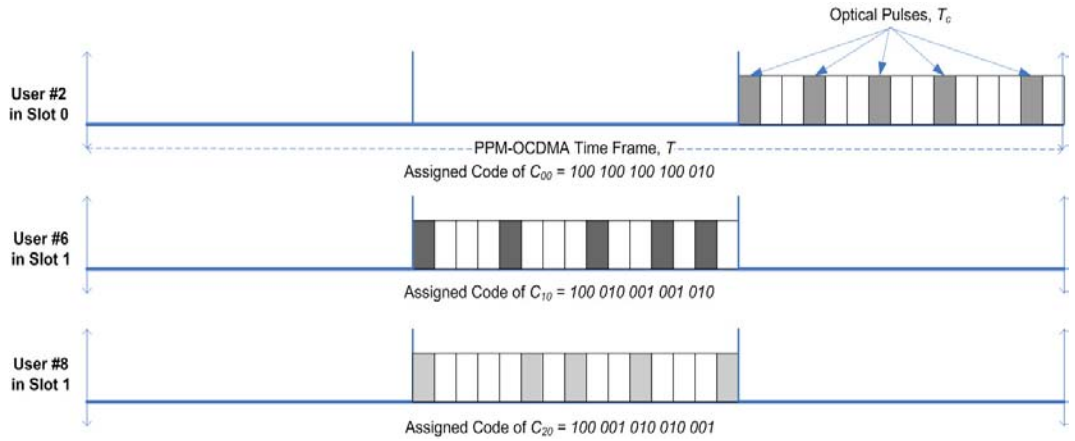

Figure 4.5 Signalling model for *3-ary* PPM-OCDMA, e.g. three users #2, #6 & #8 have signature codes: *100100100100010*, *100010001001010* and *100001010010001* respectively

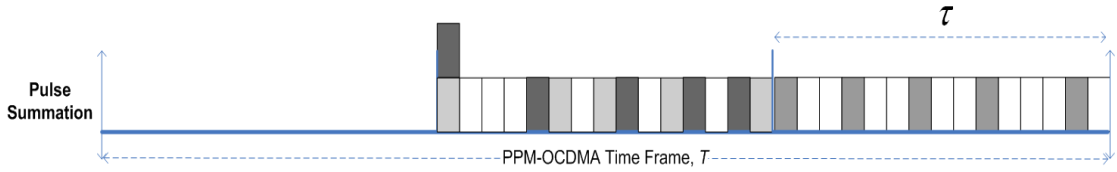

Figure 4.6 Example of the combination of PPM-OCDMA signals in an optical channel

4.3.1.3 Transmitter with MAI Cancellation and Manchester Encoding

Manchester encoding is a type of data communications in which: (i) Data and clock signals are combined to form a single self-synchronizing data stream. (ii) Each encoded bit contains a transition at the midpoint of a bit period. (iii) The direction of transition is determined by whether the bit is a *zero* or *one*. And (iv) the first half is the true bit value and the second half is the complement of the true bit value. Therefore, the rules of Manchester encoding are as follows: (a) if the original data is a logic *zero*, the Manchester code is a transition of *zero* to *one* at one time period; (b) if the original data is a logic *one*, the Manchester code is a transition of *one* to *zero* at one time period.

In our analysis, we define both first- and second- half time period denoting a true bit value. Manchester encoding is systematically allocated to different users in the system; it is indicated that the first half users i.e. $(P+1)/2$ groups (out of *P* groups) are assigned to transmit data by using the first half-chip interval $[0\ ,\ T_c/2]$, while the rest half users from the remaining $(P-1)/2$ groups share the second half-chip interval $[T_c/2\ ,\ 0]$. This coding scheme ensures that the two groups of users will not interfere with each other and thus will help to reduce multi-user interference [53], referring to the signal model example for *P=3* and *M=3* analysed in Figures 4.5 and 4.6, Figures 4.7 and 4.8 illustrate the signal formats for the system with Manchester coding. The spreading sequences $C_{0,0}$ and $C_{1,0}$ for user #2 and user #6 are respectively located in the first half-chip interval, while spreading sequence $C_{2,0}$ for user #8 is allocated in the second half-chip interval.

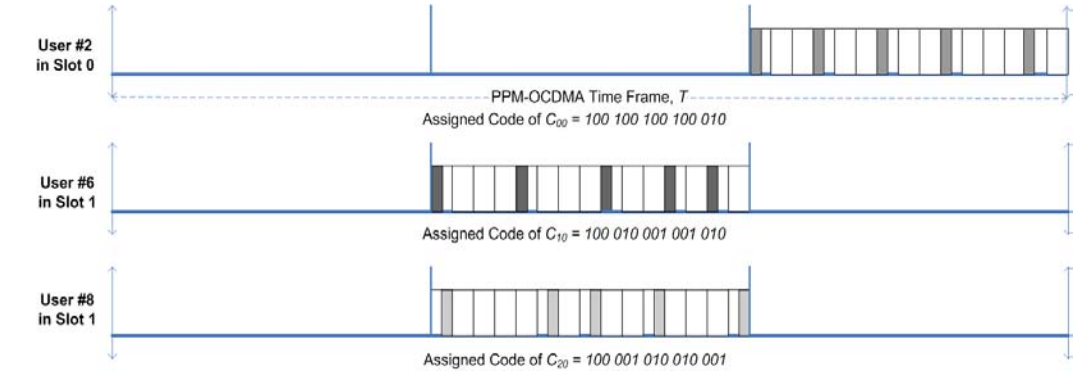

Figure 4.7 Signalling model for *3-ary* PPM-OCDMA system with Manchester codes, the three active users #2, #6 & #8 have signature codes: *100100100100010*, *100010001001010* and *100001010010001* respectively for example

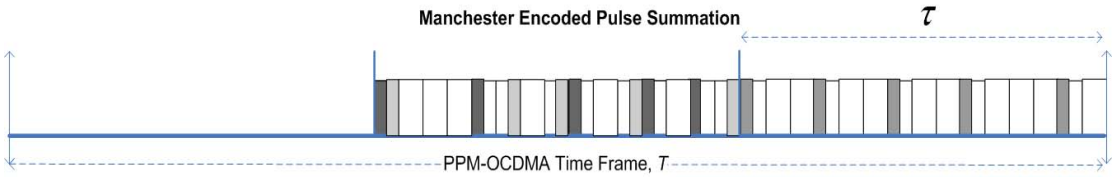

Figure 4.8 Example of the combination of Manchester-coded PPM-OCDMA signals in an optical channel

4.3.2 PPM-OCDMA Receiver Architectures

4.3.2.1 Simple Receiver

The receiver of the incoherent PPM-OCDMA without interference cancellation and Manchester codes is shown in Figure 4.9. The main function of each block is explained in details as following.

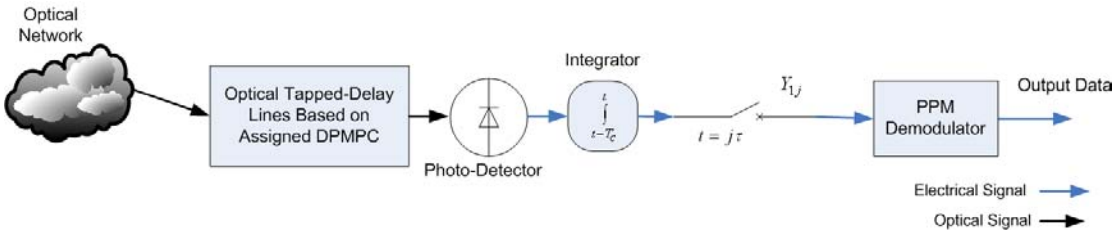

Figure 4.9 Incoherent PPM-OCDMA receiver model

- Optical Tapped-delay Line (OTDL)

The received PPM-OCDMA signal from optical fibre, which includes all the users' information and noise, is correlated by its own spreading sequence by OTDL. An OTDL could be regarded as an optical matched filter. The mark positions in the spreading sequence determine the structure of the OTDL as also shown in Figure 4.4. The amount of delays is not only dependent on the spreading sequence but also on the marks positions within the chip intervals. The correlated spreading sequence is the same one pre-assigned at the transmitter. If the incoming signal is encoded with the correct address, the output of the optical matched filter will yield an auto-correlation peak, otherwise smaller cross-correlation amplitude is generated.

- Photo-detector

The photo-detector is used to convert the demultiplexed optical signal into electrical signal, which is proportional to the photon-counts.

- Integrator

The integration is performed over the entire chip duration T_c. Sampling the integrated signal is done at the moment of $j \cdot \tau$ only, where $j \in \{1,2,...M\}$. It should be mentioned that in a direct-detection PPM-OCDMA system, the synchronization is carried out at the end of each time slot. It then intends to sample at the last chip position of the DPMPC, where maximum auto-correlation can be obtained within spreading slot τ of the time frame T.

- PPM Detector

Thereafter, the photon-count of each time slot is sent to the decision mechanism. The obtained *M-ary* samples are passed through PPM decoder, which is a comparator over the *M* samples. The slot containing the maximum photon-counts is declared as the correct true bit value.

4.3.2.2 Receiver with MAI Cancellation

The incoherent PPM-OCDMA receiver model with MAI cancellation is shown in Figure 4.10.

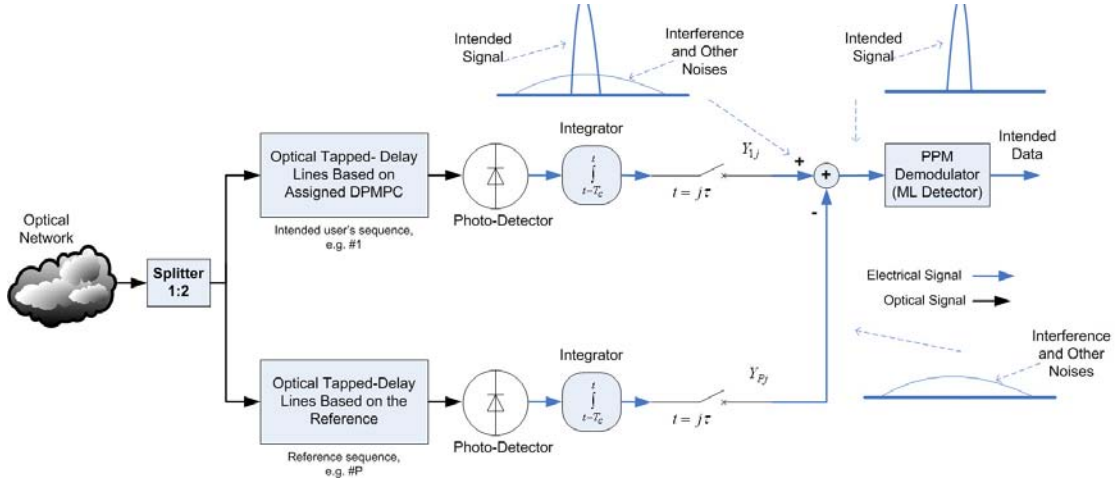

Figure 4.10 Incoherent PPM-OCDMA receiver structure with MAI cancellation

The MAI cancellation technique has been proposed in [49] based on the correlation properties of MPC. The same scheme is used here while DPMPC is employed as spreading code instead. The idea is to pre-reserve a code to provide interference estimation. The estimated interference is then subtracted from the received signal after photo-detection.

As it can be observed from Figure 4.10, the received signal, which consists of intended data, MAI and noise, is divided into two equal parts by a 1×2 optical splitter, then the

split signals are fed into two optical matched filters. The upper portion named the main branch is used to extract useful signal while the lower portion called the reference branch is used to estimate the amount of MAI. In the main branch the injected signal is correlated with its own spreading sequence, while in the reference branch, the fed signal is correlated with the reference spreading sequences which are the last sequence code from each group preserved at the beginning. The mark positions of the desired user's spreading sequence determine the structure of OTDL in the main branch, and the mark positions of reference spreading sequence determine the structure of OTDL in the reference branch. In practice, since the output of the photo-detectors follows the Poisson process, and the photo-detectors used in the branches have the same characteristics, the MAI and noises, e.g. shot and thermal noises, are cancelled out after subtraction. If the incoming signal is encoded with the correct address, the output of the optical matched filter will yield an auto-correlation peak. Otherwise, cross-correlation amplitude is generated. Moreover, based on the correlation properties of DPMPC, the detection will outperform where the correlation values differ remarkably.

All of the correlation outputs are then converted to electrical signals using photo-detector. Integration is performed over entire chip duration, while synchronisation is applied at the moment of $j \cdot \tau$ only, where $j \in \{1, 2, \ldots M\}$. They are sampled at the last chip position.

Based on the group correlation property of DPMPC, the photon-count $Y_{p,j}$ is only composed of MAI which is the same interference in the main branch. The MAI cancellation is achieved by subtracting the photon-count $Y_{p,j}$ in the reference branch

from the photon-counts $Y_{1,j}$ in the main branch at the moment $j \cdot \tau$. Then *M* subtractions are passed through a PPM decoder, where comparison is performed. The slot (corresponding to a particular symbol) with the maximum subtraction value is declared to be the transmitted true bit value.

4.3.2.3 Receiver with MAI Cancellation and Manchester Encoding

Figure 4.11 displays the incoherent PPM-OCDMA receiver model with interference cancellation and Manchester encoding.

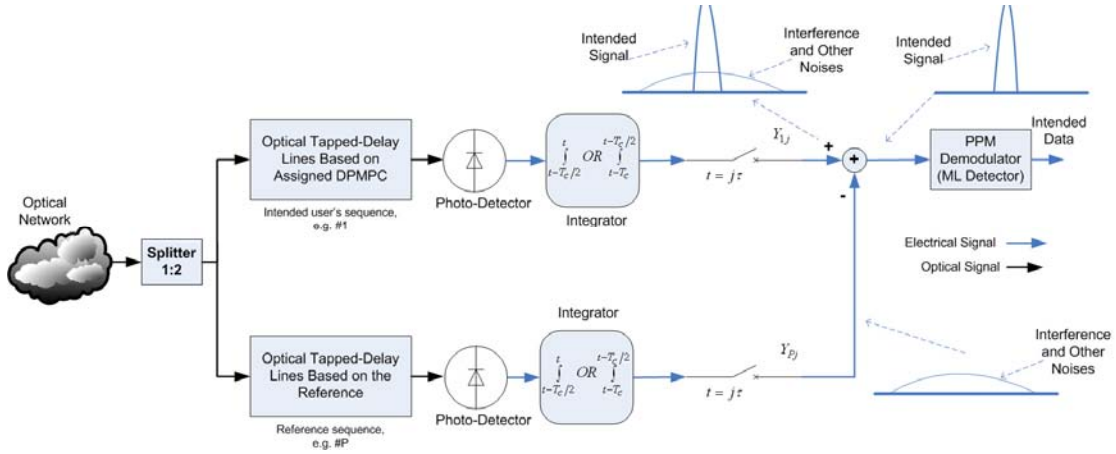

Figure 4.11 Incoherent Manchester-encoded PPM-OCDMA receiver structure with MAI cancellation

The essential principle of receiver model with interference cancellation and Manchester codes are similar to the system with interference cancellation but the only remarkable difference is the range of integrations.

The electrical signals (after photo-detection) of the users in group 1 to group $(P+1)/2$ will be integrated over the first half-chip intervals for both main and reference branches; while the integration is performed over the second half-chip intervals for the remaining users from group $(P-1)/2$ to group *P*. In Figure 4.11 the integration is either from $t-T_c$ to $t-T_c/2$ which is the first half-chip duration or from $t-T_c/2$ to t which

makes the second half-chip duration. The integrated signal is sampled at the moment of $j \cdot \tau$ only, where $j \in \{1,2,\ldots M\}$.

4.4 PPM-OCDMA Performance Analysis

Using DPMPC as the spreading sequences, the network described in Figure 4.2 for prime number *P* and multiplicity *M* is analysed. Since the entire available sequence code is P^2, the total number of subscribers equals P^2. It is assumed that *N* out of P^2 are active users and the remaining users are idle. We define a random variable $\gamma_n, n \in \{1,2,\ldots, P^2\}$ as follows:

$$\gamma_n = \begin{cases} 1, & if\ user\ \#n\ is\ Active \\ 0, & if\ user\ \#n\ \ is\ Idle \end{cases} \tag{4.1}$$

Thus $\sum_{n=1}^{P^2} \gamma_n = N$.

4.4.1 Analysis of Simple Receiver

Assuming that user #2 is the intended user. Let the random variable *T* represents the number of active users in the 1st group and variable *t* is the realization of *T*.

$$T = \sum_{n=1}^{P^2} \gamma_n \tag{4.2}$$

The probability distribution of *T*, given that user #2 is active for any $t \in \{t_{\min}, t_{\min+1}, \ldots, t_{\max}\}$, where $t_{\min} = \max(N + P - P^2, 1)$ and $t_{\max} = \min(N, P)$ is expressed as [34]:

$$P_T(t) = \frac{\binom{P^2 - P}{N - t} \cdot \binom{P-1}{t-1}}{\binom{P^2 - 1}{N - 1}} \tag{4.3}$$

where $C_b^a = \binom{a}{b} = \frac{a!}{(a-b)!\cdot b!}$ and it is called combination of *b* out of *a*. Let the collection of the photon-counts $(Y_{n,0}, Y_{n.1},..., Y_{n,M-1})$ be denoted by the Poisson random vector Y_n for user #*n*. $\mathbf{Q}$ denotes the average photon-counts per pulse where $\mathbf{Q}=\mu\cdot \ln M/(P+2)$ and μ is a parameter proportional to the received signal power [41]. Defining an interference random vector $k=(k_0,k_1,...,k_{M-1})^T$ of size *M*, where the random variable k_j represents the number of optical interference pulses introduced to time slot j. The vector $u=(u_0,u_1,...,u_{M-1})^T$ is the realization of vector k. Given $T=t$, k is a multinomial random vector with probability:

$$P_{k|T}(u_0,u_1,...,u_{M-1}\mid t)=\frac{1}{M^{N-t}}\cdot\frac{(N-t)!}{u_0!u_1!....u_{M-1}!} \tag{4.4}$$

where $\sum_{j=0}^{M-1} u_j = N-t$.

The bit-error probability can be lower bounded depending on the PPM modulation scheme [40] as follows:

$$P_b = \frac{M}{2(M-1)}\sum_{t=t_{\min}}^{t_{\max}} P_E\cdot P_T(t) \tag{4.5}$$

Taking $\mathbf{Q}\to\infty$, by modifying and rewriting the probability according to the DPMPC properties, the lower-bounded BER is derived as [40]:

$$\begin{aligned} P_E \geq & \sum_{u_1=P+3}^{N-t}\binom{N-t}{u_1}\frac{1}{M^{u_1}}\cdot\left(1-\frac{1}{M}\right)^{N-t-u_1}\cdot\sum_{u_0}^{\min(u_1-P-3,N-t-u_1)}\binom{N-t-u_1}{u_0} \\ & \cdot\frac{1}{(M-1)^{u_0}}\cdot\left(1-\frac{1}{M-1}\right)^{N-t-u_0-u_1}+0.5\sum_{u_1=P+2}^{\frac{N-t+P+2}{2}}\binom{N-t}{u_1}\frac{1}{M^{u_1}}\cdot\left(1-\frac{1}{M}\right)^{N-t-u_1}\cdot\binom{N-t-u_1}{u_1-P-2}\cdot \\ & \frac{1}{(M-1)^{u_1-P-2}}\cdot\left(1-\frac{1}{M-1}\right)^{N-t-2u_1+P+2} \end{aligned} \tag{4.6}$$

4.4.2 Analysis of Receiver with MAI Cancellation and Manchester Encoding

As discussed earlier, the last sequence code in each group is preserved as the reference sequence, thus the total number of reference codes is *P*. Then the entire available spreading sequences are $P^2 - P$ so the idle users are $P^2 - P - N$. In this system, 4.3 for any $t \in \{t_{\min}, t_{\min+1}, ..., t_{\max}\}$, is rewritten as follows:

$$P_T^1(t) = \frac{\binom{P^2 - 2P + 1}{N - t} \cdot \binom{P - 2}{t - 1}}{\binom{P^2 - P - 1}{N - 1}} \tag{4.7}$$

where $t_{\min} = \max\left(N + 2P - P^2 - 1, 1\right)$ and $t_{\max} = \min\left(N, P - 1\right)$.

The interference cancellation with Manchester codes shown in Figure 4.11, a new random variable *R* for the number of active users from group 2 to group $(P+1)/2$ is defined. Denoting that *r* is the realization of *R*, the probability of which for any $r \in \{r_{\min}, r_{\min+1}, ..., r_{\max}\}$, given $T = t$, can be written as:

$$P_{R|T}(r \mid t) = \frac{\binom{\frac{P^2 - 2P + 1}{2}}{r} \cdot \binom{\frac{P^2 - 2P + 1}{2}}{N - t - r}}{\binom{P^2 - 2P + 1}{N - t}} \tag{4.8}$$

where $r_{\min} = \max\left(0, N - t - \frac{P^2 - 2P + 1}{2}\right)$, $r_{\max} = \min\left(\frac{P^2 - 2P + 1}{2}, N - t\right)$ [36].

Given $T = t$ and $R = r$, the probability of interference vector k is then given as:

$$P_{k|(T,R)}(u_0, u_1, ...u_{M-1} \mid t, r) = \frac{1}{M^r} \cdot \frac{r!}{u_0!.u_1!....u_{M-1}!} \tag{4.9}$$

An upper-bounded bit-error probability based on the PPM modulation scheme can be derived as:

$$P_b = \frac{M}{2(M-1)} \sum_{t=t_{\min}}^{t_{\max}} \sum_{r=r_{\min}}^{r_{\max}} P_E \cdot P_{R|(t,r)} \cdot P_T^1(t) \tag{4.10}$$

where an upper-bounded BER can be modified according to DPMPC coding and achieved by:

$$P_E \le (M-1) \sum_{u_1=0}^{r} \binom{r}{u_1} \cdot \left(\frac{1}{M}\right)^{u_1} \cdot \left(1-\frac{1}{M}\right)^{r-u_1} \cdot \sum_{u_0=0}^{r-u_1} \binom{r-u_1}{u_0} \cdot \left(\frac{1}{M-1}\right)^{u_0} \cdot \left(1-\frac{1}{M-1}\right)^{r-u_0-u_1} \cdot \exp\left[-\mathbf{Q}.\frac{(P+2)^2}{4.(P+2+u_0+u_1}\right] \tag{4.11}$$

It is important to note that, if $\mathbf{Q} \to \infty$, then $P_E = 0$.

4.4.3 Analysis of Receiver with MAI Cancellation

The system with only MAI cancellation is very similar to the structure discussed in previous section. The integration in this system is carried out over the entire chip time rather than half chip time. The contribution of MAI is the users from group 2 up to group *P*. Following the BER probability given in 4.5, the upper-bounded BER is given as:

$$P_b = \frac{M}{2(M-1)} \sum_{t=t_{\min}}^{t_{\max}} P_E \cdot P_T^1(t) \tag{4.12}$$

where the error probability is modified to DPMPC coding as:

$$P_E \le (M-1) \sum_{u_1=0}^{N-t} \binom{N-t}{u_1} \cdot \left(\frac{1}{M}\right)^{u_1} \cdot \left(1-\frac{1}{M}\right)^{N-t-u_1} \cdot \sum_{u_0=0}^{N-t-u_1} \binom{N-t-u_1}{u_0} \cdot \left(\frac{1}{M-1}\right)^{u_0} \left(1-\frac{1}{M-1}\right)^{N-t-u_0-u_1} \cdot \exp\left[-\mathbf{Q}.\frac{(P+2)^2}{4.(P+2+u_0+u_1)}\right] \tag{4.13}$$

4.5 Discussion of Results

The DPMPC has been applied into three structures and the overall performances are discussed in details for: (i) Simple receiver; (ii) Receiver with only MAI cancellation and (iii) Receiver with both MAI cancellation and Manchester encoding. In order to demonstrate the DPMPC potential, MPC and n-MPC (Section 3.2.2) are also applied into the above three structures. When DPMPC is analysed, the equations 4.3-4.6 are used for structure (i), equations 4.7-4.11 are applied in receiver (iii) and equations 4.7, 4.12 and 4.13 are also used in the system (ii). The corresponding equations for n-MPC and MPC can be found in [34, 80] respectively.

4.5.1 BER against Received Signal Power

Figure 4.12 illustrates the BER performances of all three codes in three introduced receiver structures against the average photons per pulse (μ) which is a parameter proportional to received signal power. The full-load communication has been assumed in the analysis which means the total number of active users are present $N=P^2-P$. The prime number P and multiplicity M are set to 11 and 8 respectively, thus the total number of active users are 110. The lower-bounded BER for receiver (i) is considered when $\mu=\infty$ (i.e. relatively high power), therefore the constant BER is achieved as a lower-bounded BER as shown in Figure 4.12. It is obvious that the higher received signal power, the lower BER is achieved. The $BER=10^{-9}$ is also depicted as a reference for better explanation.

In Figure 4.12, at $\mu=100$, the lower-bounded error-rates obtained from the simple receiver structures are 1.5×10^{-3} for MPC, 7.2×10^{-4} for n-MPC and 3.3×10^{-4} for the

DPMPC which is the smallest error-rate. Also, upper-bounded error-rates in receivers with MAI cancellation are 1.7×10^{-6} for MPC coding, 7.1×10^{-7} for n-MPC encoded, and finally 3×10^{-7} for DPMPC. Furthermore, the upper-bounds of error-rates of Manchester coded receivers with MAI cancellation can be expected as 2.2×10^{-9} for MPC, 1×10^{-9} for n-MPC and again 2.8×10^{-10} for DPMPC. As one can observe, the performance improvement by employing DPMPC is remarkable.

Since μ increases, more optical power is transmitted to represent the presence of a PPM pulse, thus the presence and absence of a pulse are more distinguishable. It can also been seen that, the overall performance with the MAI canceller improves more notable than the simple receivers.

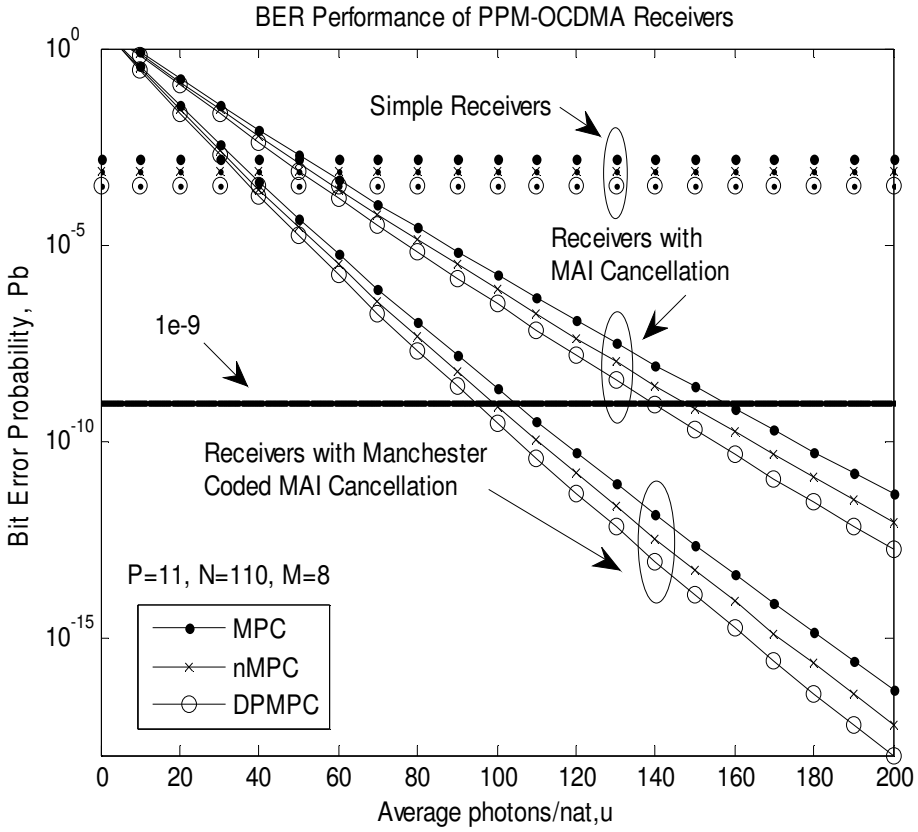

Figure 4.12 Performance of the PPM-OCDMA receivers using different codes against the average number of photons per pulse μ, when *M=8, P=11* and *N=110*

It can be seen that, there is no advantage with the MAI canceller for smaller value of received signal power ($\mu < 40$). Furthermore, the BER performance can be improved further by applying Manchester codes in the PPM-OCDMA cancellation system.

Also, Figure 4.13 shows the performance analysis in a higher multiplicity of PPM modulation (i.e. *M=16*). It is apparent that lower BER is achieved with higher multiplicity and less received power μ. Higher multiplicity offers more pulse positions to expand the capacity whereas it restricts the system complexity.

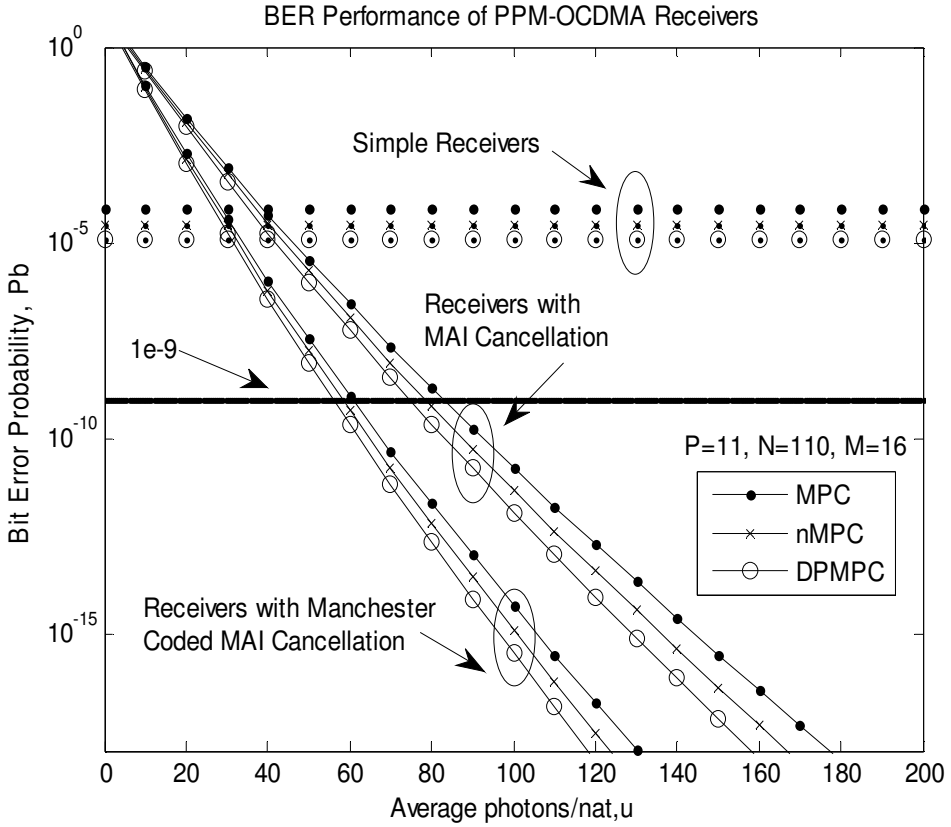

Figure 4.13 Performance of the PPM-OCDMA receivers using different codes against the average number of photons per pulse μ, when *M=16, P=11* and *N=110*

4.5.2 BER against Number of Active Users

Figure 4.14 plots the BER performances of various receivers using different coding schemes when $\mu = 100$, *P=11* and *M=8* against the number of active users in the

network. In this analysis, the upper-bounds of BER for receivers with MAI cancellation and Manchester coded MAI cancellation are considered when $\mu = 100$, while the lower-bound of BER for simple receiver when $\mu = \infty$ (i.e. relatively high received signal power) is taken into account for only n-MPC and DPMPC. The results indicate that the DPMPC can accommodate greater number of users. To examine the results, when *N=60*, the error-rate at the simple receiver using n-MPC is 1.1×10^{-3} while using DPMPC it is 4.4×10^{-4} as shown in Figure 4.14. The simple receivers' structures are unable to support users greater than 60, since the BER soars very high ($BER \approx 1$).

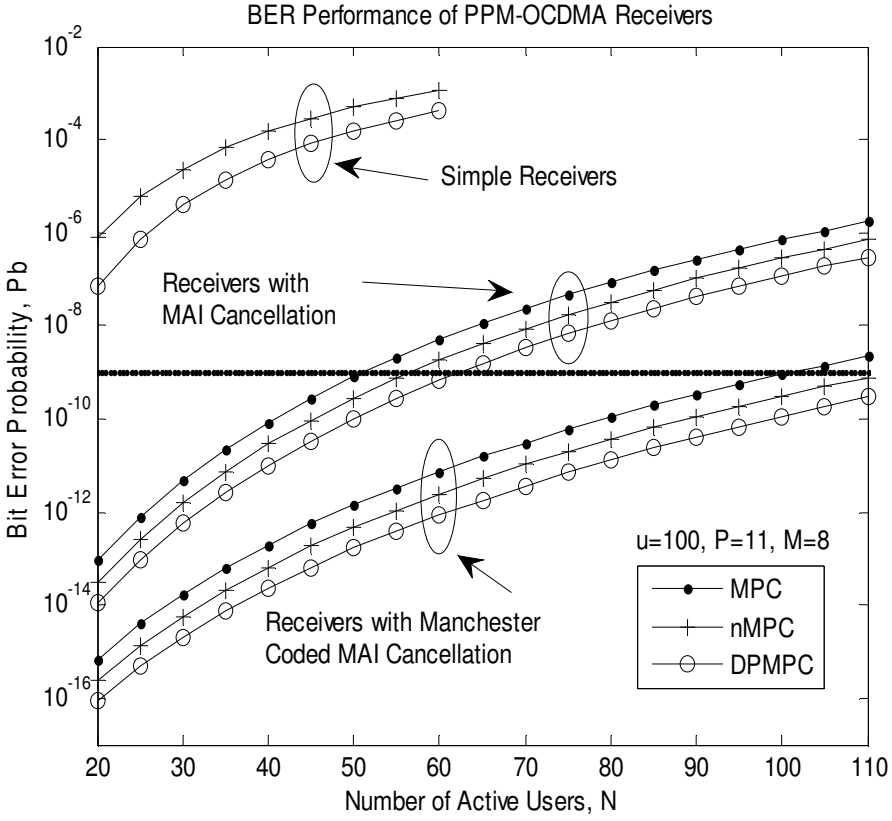

Figure 4.14 Performance of the PPM-OCDMA receivers using different codes against the number of users, *N* when μ*=100, P=11* and *M=8*

Furthermore in Figure 4.14, the BER at the receivers with MAI cancellation have been improved remarkably. The error-rate at receiver with MAI using n-MPC is 1.77×10^{-9},

whereas the one using DPMPC has BER of 6.6×10^{-10}. The scheme with Manchester coding has been much enhanced to have BER of less than 10^{-11} regardless of coding scheme, however among them DPMPC is still outperforming.

It can be noticed that the bit-error probability increases as the number of subscribers increases in these three receivers. The reason is that the interference increases as the number of active users increases. The interference canceller can effectively remove the MAI and improve the BER performance. It can also be seen that the error-rate can become better when Manchester codes are applied to the system as well as the interference cancellation. It is also seen in Figure 4.14 that the simple receivers are unable to support more than 60 users under this given condition due to the interference growth.

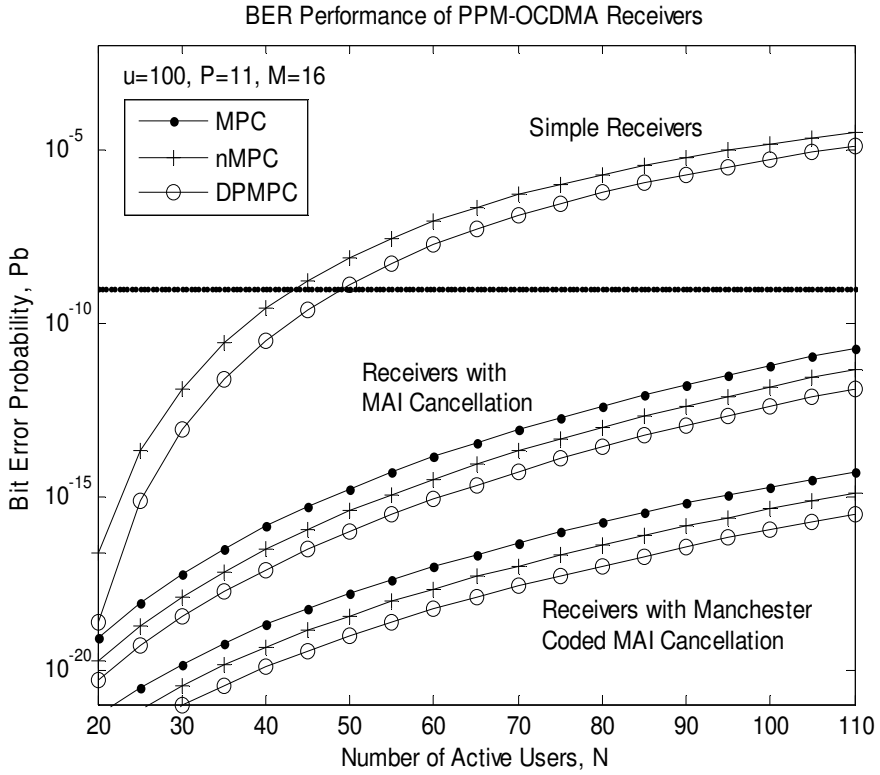

Figure 4.15 Performance of the three PPM-CDMA receivers using different codes against the number of users, *N* when $\mu = 100, P = 11$ and *M=16*

The same results are expected from the receivers when multiplicity increases (i.e. *M=16*) as presented in Figure 4.15. The *BER = 10^{-9}* is also depicted to assist the eye. The higher multiplicity makes the system implementation difficult. It has been found that when the system design limits the multiplicity, Manchester encoding offers its benefits to elevate the outcomes.

4.5.3 BER against Prime Number

The BER performance of receivers with MAI cancellation and Manchester coded receivers with MAI cancellation are compared against prime number *P* in Figure 4.16. Due to the indicated outperformance of other two receivers than simple receivers, only receivers (ii) and (iii) are presented. In this analysis, the receivers are evaluated in the case of full-load i.e. $N = P^2 - P$, *M=8* and $\mu = 100$. It is apparent that the error-rate is very low in case of employing DPMPC rather than other coding schemes especially when *P* is small.

We now examine the BER of various receivers with different coding schemes. At the receivers with MAI cancellation when *P=13*, the error-rate is 8.6×10^{-6} for MPC, 4.3×10^{-6} for n-MPC and 2.1×10^{-6} for DPMPC, the improvement is notable indeed. At the Manchester coded receivers with MAI cancellation, the error-rate can be expected as 1.1×10^{-8} for MPC, 4.9×10^{-9} for n-MPC and finally 2.1×10^{-9} for DPMPC which means 2.34 times enhancement as compared to n-MPC.

It is also expected that the performance becomes better with higher multiplicity as presented in the previous Figures. Although in practice, the implementations may be restricted by accurate time slots in high value multiple array PPM signalling. It is

important to mention that the time slots cannot be increased arbitrary due to limited electronic circuitry. Therefore, when we are limited to increase multiplicity, Manchester coding can be a good option to enhance the performance; however with a cost of network bandwidth.

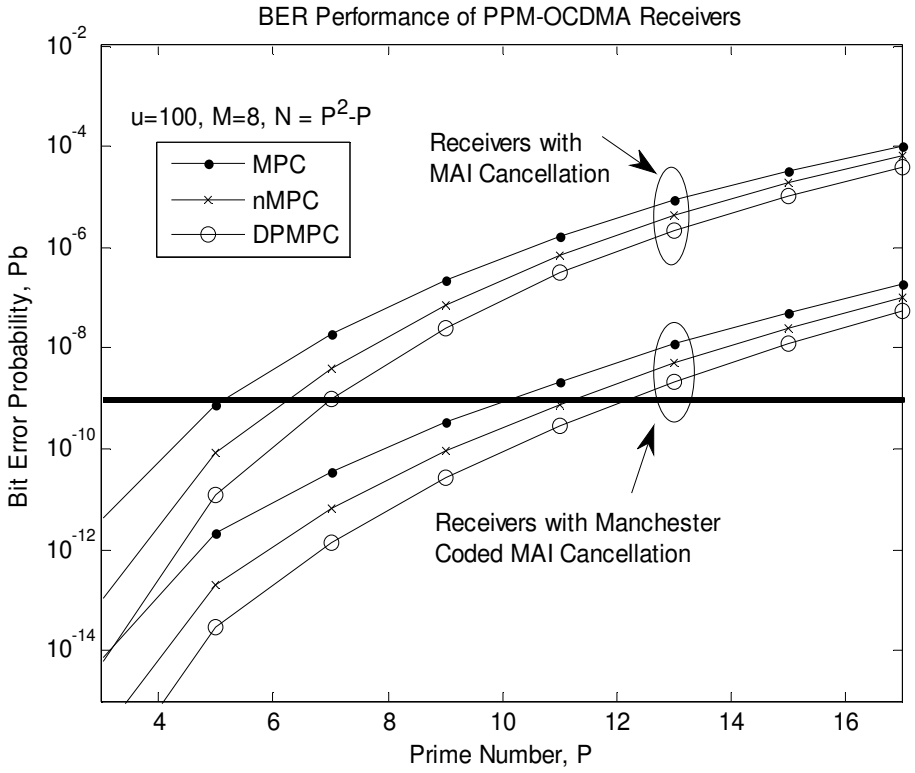

Figure 4.16 Performance of the PPM-OCDMA receivers using different codes against prime number *P* when $\mu = 100,\ N = P^2 - P$ and *M = 8*

4.6 Conclusion

In this Chapter, our proposed double padded modified prime code (DPMPC) has been applied to incoherent synchronous PPM-OCDMA network. Three different types of receivers, including (i) simple receiver (ii) receiver with MAI cancellation and (iii) receiver with Manchester coded MAI cancellation, have been analysed. The lower bound of error-rate for the receiver (i) and the upper-bounded BER for receivers (ii) and (iii) have been derived. In a nutshell, the results presented here indicate that the

receivers with this novel coding scheme are able to accommodate greater number of users, while they still maintain low BER and less power consumption. As a validation, this scheme has been published [P1, P2][1] as well as implemented and verified by OptiSystem™ optical communications commercial software package [107].

[1] See 'List of Publications'

Chapter 5

Analysis of DPMPC in Overlapping PPM-OCDMA Network

5.1 Introduction

Although PPM is a power-efficient modulation scheme, it is not convenient for a PPM system to achieve high throughput due to the requirement of bandwidth expansion [37]. In the past few years, interest has been given to overlapping PPM (OPPM) which is an alternative signalling format to the conventional PPM in incoherent optical channels. OPPM can be considered as a generation of PPM signalling format, where overlapping is allowed between pulse positions. Besides, OPPM can achieve higher throughput than a PPM system without the need of bandwidth expansion due to the fixed-assigned time slots. Moreover, OPPM retains the advantages of PPM in terms of power efficiency and implementation simplicity.

In this Chapter, a synchronous OPPM-OCDMA signalling format and system is analysed where double padded modified prime code (DPMPC) has been employed as a spreading code. Then, the transmitter and receiver models for different architectures are investigated in details in terms of bit-error rate (BER) performance. Based on the properties of the novel code, a multiple-access interference (MAI) cancellation technique is proposed for the OPPM-OCDMA network, unlike the conventional method to put hard-limiter(s) before and behind the OCDMA correlators to eliminate the floor interference at the receivers [46]. Since the Manchester codes have the capability to further improve the system performance, they are applied to OPPM-OCDMA transceivers as well. As the overlapping is allowed, there is self-interference at the synchronisation instants at OPPM-OCDMA receivers, thus the entire process is also taken into account with the self-interference. The numerical results are obtained under the assumption that the dominant noise source in the network is MAI and both photodiode dark current noise and thermal noise contributions are negligible. Finally, the throughputs for both OPPM- and PPM-OCDMA networks are discussed and evaluated.

5.2 OPPM-OCDMA Signalling

An *M-ary* OPPM modulation deploys *M* time slots making duration of *T* time frame. The modulated signal is permitted to spread over a spreading interval with τ slot duration, which is again subdivided into *P* smaller subintervals each of width τ/P where *P* is a prime number. An overlap of $(M - \gamma) \cdot \tau$, where $\gamma \in \{1, 2 \ldots M\}$, is allowed between any two adjacent spreading intervals where γ is the overlapping index [35].

Encoding an optical OPPM signal, the spreading sequence of length *L* (taking the DPMPC $L = P^2 + 2P$) must be exactly fitted into the time slot τ; thus τ/P can be appropriate as chip duration of T_c. If a wrapped signal is allowed, the time frame *T* must satisfy the following condition:

$$T = M\tau = \frac{M}{\gamma} L \cdot T_c \tag{5.1}$$

Figure 5.1 illustrates *8-ary* OPPM-OCDMA signalling format of DPMPC sequence of $C_{0,0}$ where *P=3* for example and better understanding, where $\gamma = 5$ (i.e. $\gamma = L/P = P + 2$). Shifting the position within the time frame *T* for different numbers of subintervals can form different slots. Let us assume that the initial position represents slot 0. Right-shifting the time slot for one subinterval forms slot 1 and so on. When the time slot reaches to the end of the time frame, it is broken into two blocks. The right-hand-side block is wrapped back to the beginning of the time frame, while the left-hand-side block is put in the end of the time frame. Those slots with characteristic that have a part of signals wrapped back to the beginning of the time frame are called *wrapped slots* while the slots without that property are named *unwrapped slots*. It is apparent from Figure 5.1 that the unwrapped slots are 0 to 3 and the wrapped slots are 4 to 7. When the OPPM signal is wrapped, the spreading sequence also follows the OPPM signal.

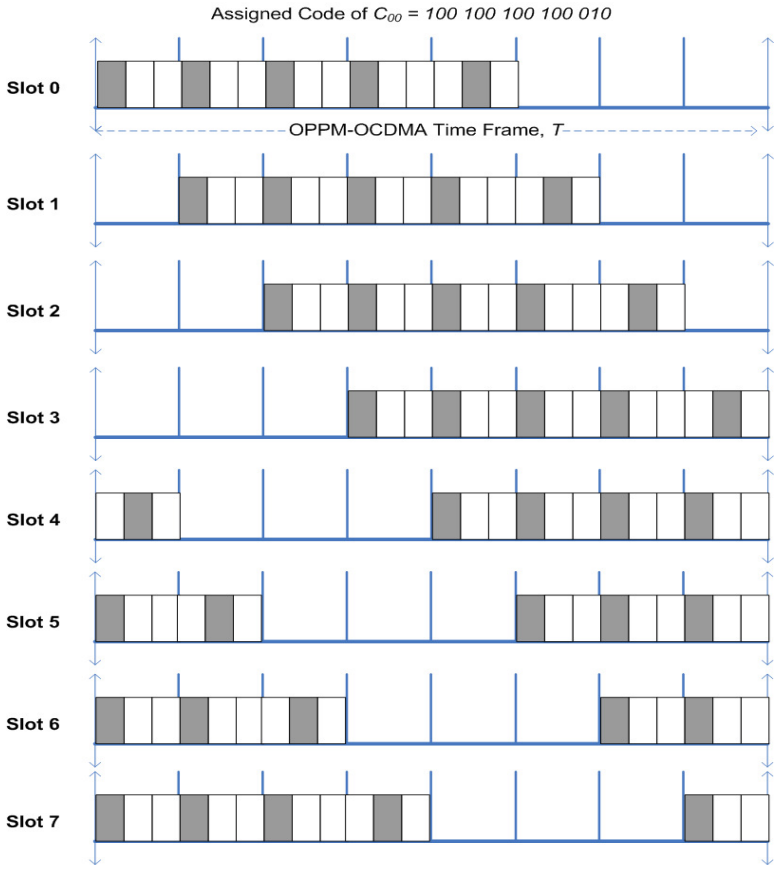

Figure 5.1 OPPM-OCDMA signalling for *P=3*, *γ=5* and *M=8* for DPMPC signature of $C_{0,0}$ = *100 100 100 100 010*

5.3 OPPM-OCDMA Transceiver Architecture

5.3.1 OPPM-OCDMA Transmitter Architectures

5.3.1.1 Simple Transmitter

A transmitter model for incoherent OPPM-OCDMA network is shown in Figure 5.2. It consists of information source, OPPM modulator and OCDMA encoder [40]. The main responsibility of each block is similar to the transmitter model for PPM-OCDMA network explained in Chapter 4.

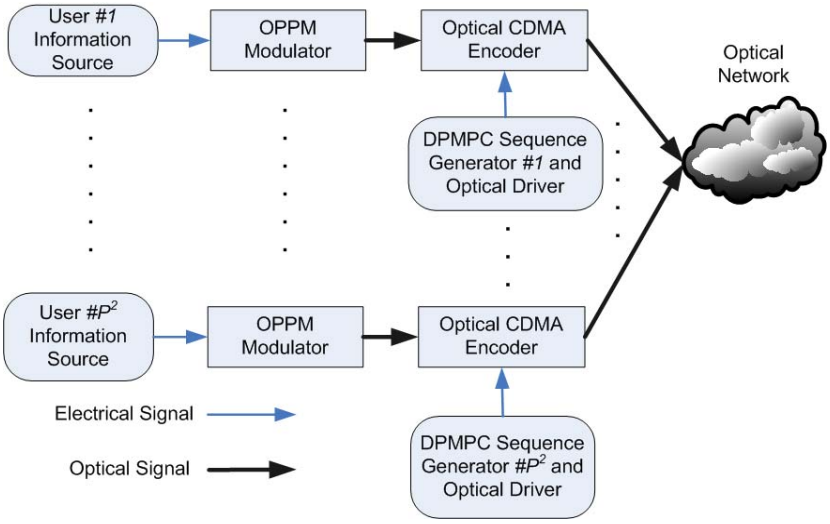

Figure 5.2 Incoherent OPPM-OCDMA transmitters structure

- Information Source

Information source is responsible to provide the optical pulses representing data stream from users. The total number of information sources depends on total number of available sequences P^2, where N users out of them are active users. In Figure 5.2, taking DPMPC, given $P=3$ and $M=8$, so the maximum number of active users is $P^2= 9$.

- OPPM Modulator

Each data stream is then fed into OPPM modulators, where a tall narrow laser pulse of width T_c is generated and time delayed in accordance to the data symbol to generate *M-ary* OPPM signalling. The time delay depends on the amplitudes of the data symbol transmitted from the information source. Figure 5.3 shows the outputs of optical OPPM modulator for user #2, user #5 and user #7 in slots 0, 2 and 4 respectively.

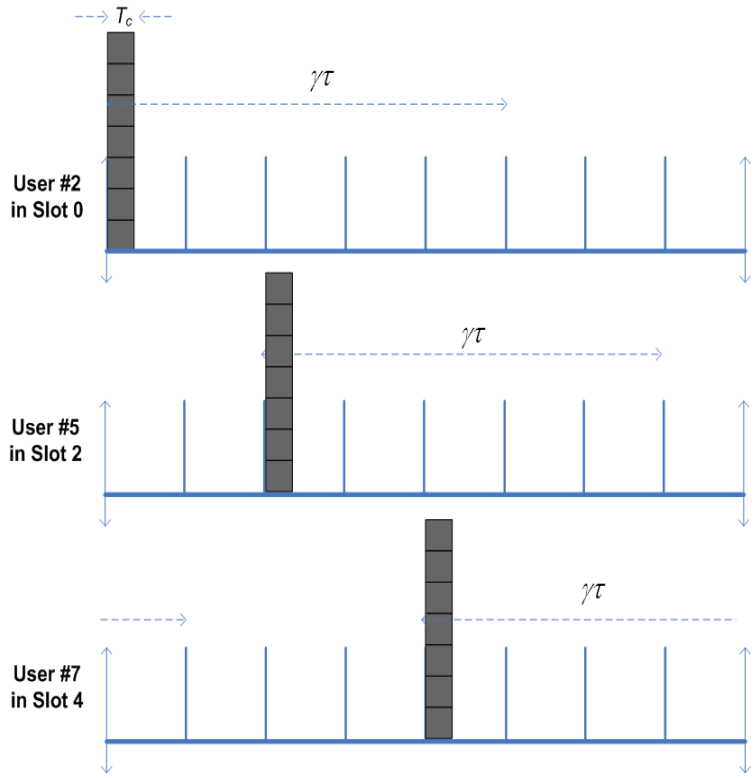

Figure 5.3 OPPM signalling for users #2, #5 and #7 at *P=3, γ=5* and *M=8*

- Optical CDMA Encoder

The outputs of modulator are then passed to the OCDMA encoder, where it is spread into shorter optical pulse with the same width T_c reference to the signature sequence and it is only allowed to occur within the spreading intervals τ. The structure of optical tapped-delay line (OTDL) as and OCDMA encoder for an unwrapped signal and a wrapped signal are shown in Figures 5.4(a) and 5.4(b) respectively.

As shown in Figure 5.5, user #2 sends data in slot 0 encoded with signature code $C_{0,0}$=*100 100 100 100 010*; user #5 transmits data in slot 2 with signature code $C_{1,2}$=*001 100 010 010 100*; and user #7 sends data in slot 4 which is encoded by signature code $C_{2,1}$=*001 010 100 100 010*.

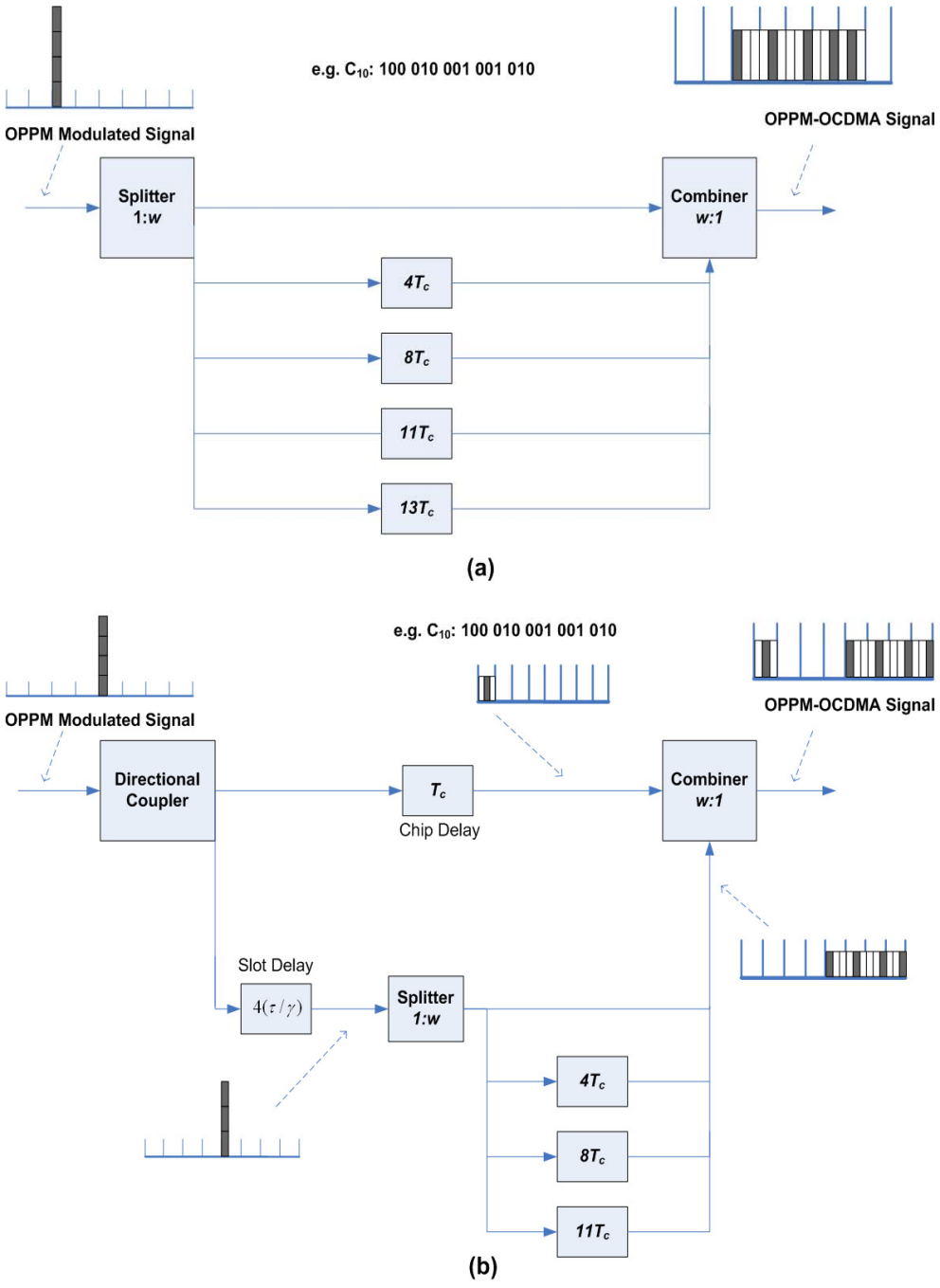

Figure 5.4 OCDMA encoder, assuming a signature code *100 010 001 001 010* (a) an unwrapped signal (b) a wrapped signal

Finally, all the signals are combined together to form an optical signal, which is transmitted across the optical channels to the receivers, which are illustrated in Figure 5.6.

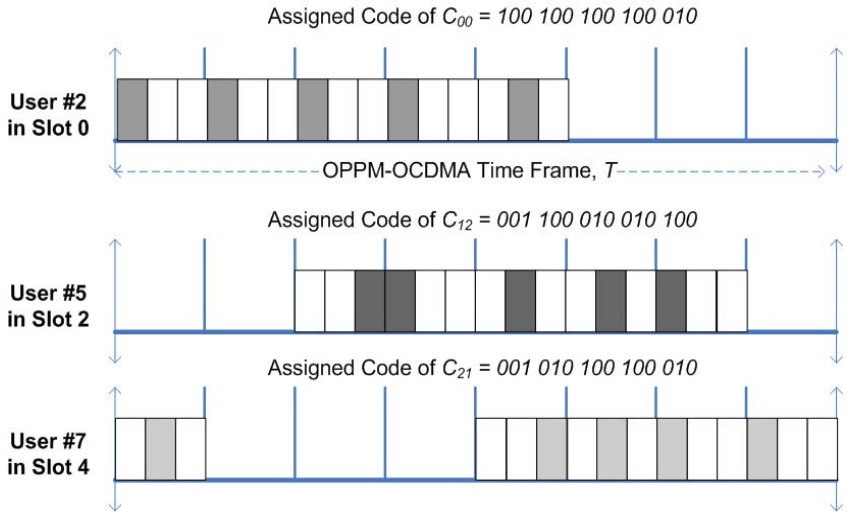

Figure 5.5 OPPM-OCDMA signalling for *P=3, γ=5* and *M=8* with assigned codes

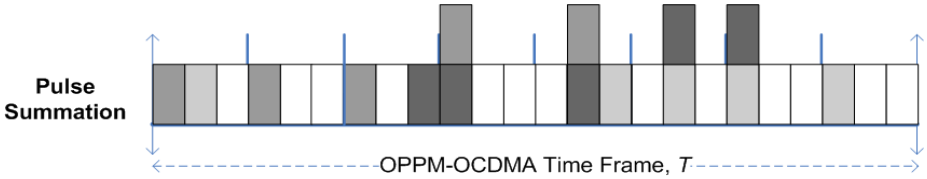

Figure 5.6 OPPM-OCDMA signalling combination in the optical channel

5.3.1.2 Transmitter with MAI Cancellation

The transmitter model of OPPM-CDMA system with interference cancellation is similar to that discussed in Figure 5.2. The last spreading sequence of each DPMPC group is again pre-reserved as a reference at the receiver, so the total available signature codes becomes $P^2 - P$. Assuming *N* active users are in the network, and each user transmits *M-ary* continuous data symbols. Therefore, the idle users are $P^2 - P - N$.

5.3.1.3 Transmitter with MAI Cancellation and Manchester Encoding

It should be pointed out that Manchester encoding is introduced to further improve the system performance, although it extends the bandwidth. As introduced in Section 4.3.1.3, the first half users from group 1 to group *(P+1)/2* are assigned the first half-

chip interval [0, $T_c/2$], while the rest of users share the second half-chip interval [$T_c/2$, T_c]. It ensures that the two groups of users will not interfere with each other and thus will help to reduce MAI among users from different groups. As a comparison with the signals model for *P=3,* $\gamma = 5$ and *M=8* in Figures 5.5 and 5.6, Figures 5.7 and 5.8 demonstrate the signals model for the transmitter with Manchester coded MAI cancellation. The spreading sequence $C_{0,0}$ for user #2 is assigned in the first half-chip interval, while spreading sequence $C_{1,2}$ and $C_{2,1}$ for users #5 and #7 are using the second half-chip intervals.

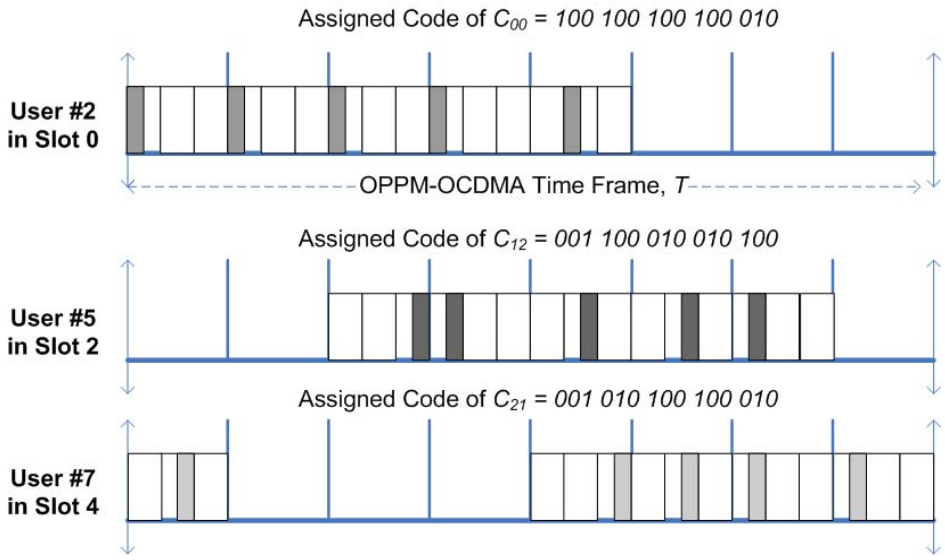

Figure 5.7 Manchester–coded OPPM-OCDMA signalling format with assigned sequences

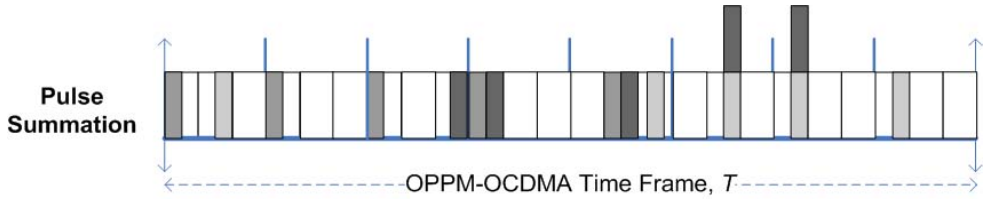

Figure 5.8 Manchester-coded OPPM-OCDMA signalling combination in the optical channel

5.3.2 OPPM-OCDMA Receiver Architectures

5.3.2.1 Simple Receiver

A receiver model for incoherent OPPM-OCDMA is presented in Figure 5.9 as introduced in [35].

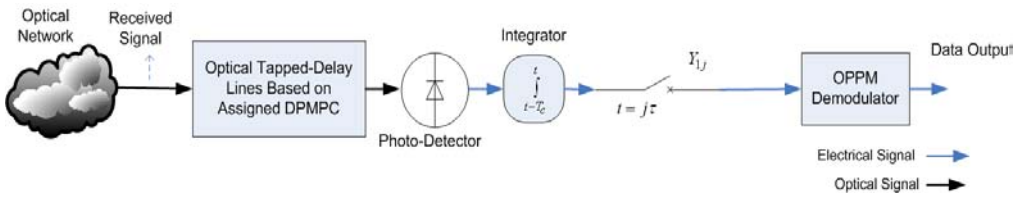

Figure 5.9 Incoherent OPPM-OCDMA receivers simple architecture

- Optical Tapped-delay Line (OTDL)

The received signal from *N* active users is correlated with the unique spreading sequence by the OTDL, acts as an optical correlator [36]. The mark positions of the spreading sequence determine the structure of the OTDL. The number of delays is not only dependent on the spreading sequence but also on the positions of the marks within the chip intervals as shown in Figure 5.4 for encoding process. If it is encoded with its own spreading sequence of the optical correlator, the output of the optical correlator will yield an auto-correlation peak. Otherwise a cross-correlation value is obtained and rejected.

- Photo-detector

The output is then converted to an electrical signal by the photo-detector. The electrical signal is proportional to the collected photon counts.

- OPPM Demodulator

This part demodulates the electric signal containing the photon-counts collected over the chip duration from the integrator. Finally, the time slot contains the sufficient power is declared to be the intended result by the maximum likelihood detection rule.

5.3.2.2 Receiver with MAI Cancellation

The MAI cancellation technique is similar with the one introduced in Section 4.3.2.2. One sequence from each DPMPC group is preserved as a reference to estimate the MAI noise. The estimated interference is then subtracted from the received signal after photo-detection [49]. Figure 5.10 shows the OPPM-OCDMA receiver structure with MAI cancellation.

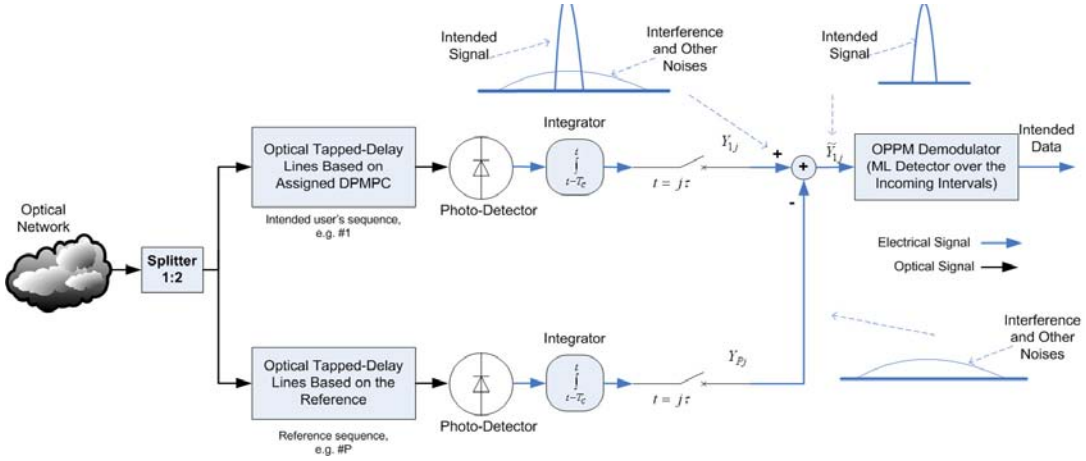

Figure 5.10 Incoherent OPPM-OCDMA receiver architecture with MAI cancellation

The received signal, consisting of a desired signal, MAI and noises, is fed into a 1×2 optical splitter where it is divided into two equal signals. Like the PPM-OCDMA receiver model, the upper portion, main branch, is used to extract intended data; while the lower portion, reference branch, is used to estimate the MAI. The signal in the main branch is correlated with the same signature sequence which characterizes the desired user; while in the reference branch, the signal is correlated with the

reference sequence which is the last sequence in each group preserved initially. If the injected signal is encoded with the correct address code, the output of the OTDL will yield an auto-correlation peak. Otherwise, cross-correlation value is generated. In the photo-detector, optical signals are converted to electrical signals. The electric signals will be integrated over the entire chip duration, synchronised at each interval. Sampling is performed at the end of each mark position of each slot. According to the property of the DPMPC, the photon-count $Y_{P,j}$ the reference branch is mainly composed of MAI. In the main branch, the intended signal and MAI constitute the photon-counts $Y_{1,j}$ as shown in Figure 5.10.

Interference cancellation is carried out by subtracting $Y_{P,j}$ from $Y_{1,j}$. In practice, since the output of the photo-detectors follows the Poisson process, and the photo-detectors used in the branches have the same characteristics, the MAI and noises, e.g. shot and thermal noises, are cancelled out after subtraction as seen in Figure 5.10. All the subtraction is then passed to the decision unit based on maximum likelihood detection which is a comparator device selecting the interval which contains the greatest power among all the *M* intervals.

5.3.2.3 Receiver with MAI Cancellation and Manchester Encoding

A block diagram of receiver model for the incoherent OPPM-OCDMA with Manchester coded MAI cancellation is presented in Figure 5.11.

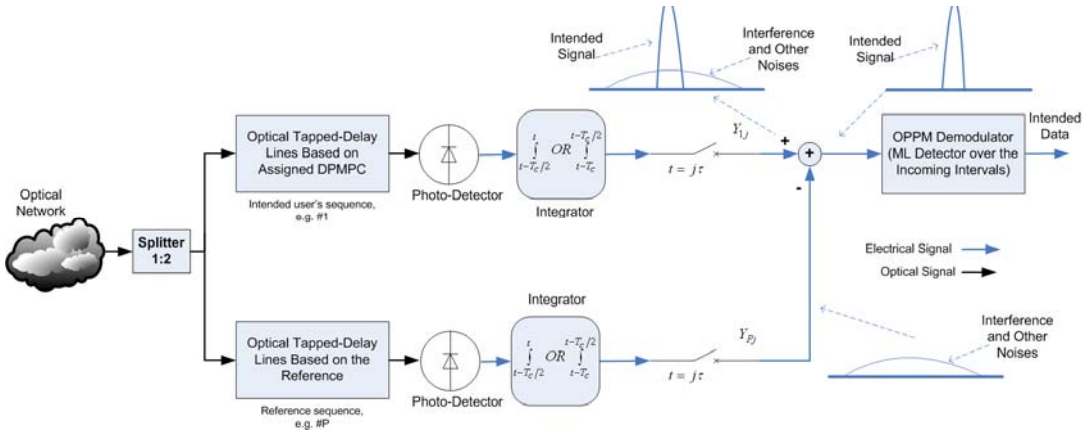

Figure 5.11 Incoherent OPPM-OCDMA receivers architecture with MAI cancellation and Manchester encoding

Apart from the fact that the integration range is different, the main function of each device for the system with interference cancellation and Manchester codes is the same as the receiver with interference only.

The optical signals are converted to electrical signals by the photo-detectors. Following this, the electric signals will be integrated over the first half-chip or the second half-chip which are determined by the users in each group. The active users from group 1 to group *(P+1)/2* will be integrated over the first half-chip intervals $[t-T_c, t-T_c/2]$ for both the main and reference branches; while the integration is performed over the second half-chip intervals $[t-T_c/2, t]$ for the remaining subscribers from group *(P-1)/2* to group *P*. Later, the integrated signal is sampled at the end of each subinterval.

5.4 OPPM-OCDMA Performance Analysis

Now here, by employing DPMPC in an incoherent OPPM-OCDMA system, the receivers' performance in terms of bit-error rate (BER) will be derived. We define the random Poisson vector $Y_{1,j}$, denoting the photon-counts collected at the receiver, where $j \in \{0,1,2,\ldots M-1\}$. $Y_{1,j}$ is contributed by two parts: the intended signals and the

interference introduced by other users. Index *i* is declared to be the true one if $Y_{1,i} > Y_{1,j}$ for every $i \neq j$. $S_{1,i} = 1$ represents intended user, e.g. #1, transmitting signal in slot *i*. The probability of error is as [35]:

$$P[E|i] = \Pr\left\{Y_{1,j} \geq Y_{1,i},\ some\ \ j \neq i \,\middle|\, S_{1,i} = 1\right\} \tag{5.2}$$

Hence,

$$P[E] = \Pr\left\{Y_{1.j} \geq Y_{1,0},\ some\ \ j \neq 0 \,\middle|\, S_{1,0} = 1\right\} \tag{5.3}$$

Then the BER based on the *M-ary* modulation format becomes [34]:

$$P_b = \frac{M}{2(M-1)} P_E \tag{5.4}$$

5.4.1 Analysis of Simple Receiver

The entire sequence codes are P^2, assuming that *N* out of them are active users. Thus the idle users are $P^2 - N$. A random variable *T* denotes the number of active users in the first group and *t* is the realisation of *T*. The probability distribution function (PDF) of *T* for any $t \in \{t_{\min}, t_{\min+1}, ..., t_{\max}\}$, where $t_{\min} = \max\left(N + P - P^2, 1\right)$ and $t_{\max} = \min\left(N, P\right)$ can be written as:

$$P_T(t) = \frac{\binom{P^2 - P}{N - t} \cdot \binom{P-1}{t-1}}{\binom{P^2 - 1}{N-1}} \tag{5.5}$$

Since different users may contribute different number of interfering pulses to user #1, assuming that user #1 is encoded within first group sequence codes, the *N* active users are divided into two categories to further investigate: (i) the first group active users whose signature codes are in the same group as the desired user; (ii) the non-first group users whose signature codes are in the other groups.

(i) Interference due to the first group users

The number of interfering users in the first group is denoted by a random variable *H*, and *h* is the realisation of *H*. Since the overlapped symbols are allowed, the interfering slots are $\kappa = |M - \gamma|$ out of *M* slots (see Figure 5.5 when *M=8* and overlapping index $\gamma = 5$) which can introduce an interfering pulse to user #1 in the first group, the conditional PDF of interference in first group can be expressed as follows:

$$P_{H|T}(h|t) = \binom{t-1}{h} \cdot \left(\frac{\kappa}{M}\right)^{h} \cdot \left(1 - \frac{\kappa}{M}\right)^{t-1-h} \tag{5.6}$$

where $h \in \{0, 1, \ldots t-1\}$.

When the interfering signature codes are left-rotated (or right-rotated) for *jP* chips from the code of the desired user, the number of interfering pulses introduced to the desired users are then either *j* or $\gamma - j$, where $j \in \{1, 2, 3, \ldots, \gamma\}$ [35]. Denote the number of interfering pulses caused by the first group users by *L*, and variable *l* is the realisation of *L*. The conditional PDF of *L* is then as follows:

$$P_{L|HT}(l|h,t) = \frac{1}{\kappa^{h}} \tag{5.7}$$

And $l \in \{l_{\min}, l_{\min+1}, \ldots, l_{\max}\}$ where $l_{\min} = \sum_{j=1}^{h} \min(\gamma - j, j)$ and $l_{\max} = \sum_{j=1}^{h} \max(\gamma - j, j)$, in other words:

$$l \equiv l_{\min} + \left\lfloor \frac{l_{\max} - l_{\min}}{\kappa^{h}} \times \rho \right\rfloor \tag{5.8}$$

where $\rho \in \{1, \ldots, \kappa^{h}\}$ and $\lfloor x \rfloor$ returns the integer of *x*.

(ii) Interference due to the non-first group users

The non-first group users introduce interfering pulses to the desired user with the probability of γ/M (γ is the overlapping index). A random variable *U* denotes the number of non-first group interfering users, and the variable *u* is the realisation of *U*. The conditional PDF of *U* is then written as:

$$P_{U|T}(u|t)=\binom{N-t}{u}\cdot\left(\frac{\gamma}{M}\right)^{u}\cdot\left(1-\frac{\gamma}{M}\right)^{N-t-u} \tag{5.9}$$

where $u\in\{0,1...,N-t\}$.

Thus P_E is described based on the interferences and modulation scheme as:

$$\begin{aligned} P_E &= P_e\left\{Y_{1,j}\geq Y_{1,0}, some\ \ j\neq 0 \middle| S_{1,0}=1, T=t, U=u, H=h\right\}\cdot P(H=h)\cdot P(U=u)\cdot P(T=t) \\ &\geq (M-1)\cdot P_e\left\{Y_{1,1}\geq Y_{1,0} \middle| S_{1,0}=1, T=t, U=u, H=h\right\}\cdot P(H=h)\cdot P(U=u)\cdot P(T=t) \\ &= (M-1)\cdot P_1\cdot P_{L|HT}\cdot P_{H|T}(h|t)\cdot P_{U|T}(u|t)\cdot P_T(t) \end{aligned} \tag{5.10}$$

where P_1 is defined as follow [37]:

$$P_1=\sum_{y_1}^{\infty}e^{-\mathbf{Q}(u+1)}\cdot\frac{[\mathbf{Q}.(u+1)]^{y_1}}{y_1!}\cdot\sum_{y_0}^{y_1}e^{-\mathbf{Q}(u+P+2)}\cdot\frac{[\mathbf{Q}.(u+P+2)]^{y_0}}{y_0!} \tag{5.11}$$

where **Q** denotes the average photon-counts per pulse, $\mathbf{Q}=\mu\cdot\log\frac{M}{P+2}$ [41].

The BER can be finally expressed based on the modulation format and above interference analysis as:

$$P_b=\frac{M}{2}\sum_{t_{\min}}^{t_{\max}}\sum_{u=0}^{N-t}\sum_{h=0}^{t-1}\sum_{\rho=0}^{2^h}P_1\cdot P_{L|HT}\cdot P_{H|T}\cdot P_{U|T}\cdot P_T \tag{5.12}$$

5.4.2 Analysis of Receiver with MAI Cancellation

As aforementioned, the last sequence code from each group is initially preserved as the reference sequence; thus the total number of reference codes is P. Then the entire

available spreading sequences are $P^2 - P$. The idle users are $P^2 - P - N$. In this case, 5.5 for any $t \in \{t_{\min}, t_{\min+1}, \ldots t_{\max}\}$ where $t_{\min} = \max\left(N + 2P - P^2 - 1, 1\right)$ and $t_{\max} = \min\left(N, P-1\right)$ is rewritten as follows:

$$P_T^1(t) = \frac{\binom{P^2 - 2P + 1}{N - t} \cdot \binom{P-2}{t-1}}{\binom{P^2 - P - 1}{N-1}} \tag{5.13}$$

A Poisson random vector Y_1 is used to represent the photon-counts collected from the main branch, while Y_P denotes the photon-counts received from the reference branch. Then vector $\tilde{Y}_1$ is defined as $\tilde{Y}_1 = Y_1 - Y_P$. Hence, we have [37]:

$$\begin{aligned} P_E &= P_r\left\{\tilde{Y}_{1,j} \geq \tilde{Y}_{1,0}, some\ j \neq 0 \middle| S_{1,0} = 1\right\} \\ &\geq (M-1) \cdot P_r\left\{\tilde{Y}_{1,1} \geq \tilde{Y}_{1,0} \middle| S_{1,0} = 1, T = t, U = u, H = h\right\} \cdot P(H = h) \cdot P(U = u) \cdot P(T = t) \\ &= (M-1) \cdot P_1 \cdot P_{L|HT} \cdot P_{H|T}(h|t) \cdot P_{U|T}(u|t) \cdot P_T^1(t) \end{aligned} \tag{5.14}$$

where $P_1 \leq \exp\left[-\mathbf{Q}\frac{(P+2)^2}{4.(P+2+2u+l)}\right]$.

Thus the BER can be written based on the interference analysis and modulation format as:

$$P_b = \frac{M}{2} \sum_{t_{\min}}^{t_{\max}} \sum_{u=0}^{N-t} \sum_{h=0}^{t-1} \sum_{\rho=0}^{2^h} \exp\left[-\mathbf{Q}\frac{(P+2)^2}{4.(P+2+2u+l)}\right] \cdot P_{L|HT} \cdot P_{H|T} \cdot P_{U|T} \cdot P_T^1 \tag{5.15}$$

5.4.3 Analysis of Receiver with MAI Cancellation and Manchester Encoding

In the receiver with Manchester coded MAI cancellation shown in Figures 5.11, a new random variable *W* for the number of active users from group 2 up to group $(P+1)/2$ is

defined. Variable *w* is the realisation of *W* for any $w \in \{w_{\min},...,w_{\max}\}$ can be written as [53]:

$$P_{W|T}(w|t) = \frac{\binom{(P^2-2P+1)/2}{w} \cdot \binom{(P^2-2P+1)/2}{N-t-w}}{\binom{P^2-2P+1}{N-t}} \tag{5.16}$$

where $w_{\min} = \max\{0, N-t-(P^2-2P+1)/2\}$, $w_{\max} = \min\{N-t, (P^2-2P+1)/2\}$.

Then, the conditional PDF of variable *U*, non-first group interferers, is written as:

$$P^1_{U|T}(u|t) = \binom{w}{u} \cdot \left(\frac{\gamma}{M}\right)^u \cdot \left(1-\frac{\gamma}{M}\right)^{w-u} \tag{5.17}$$

where $u \in \{0,1,2...w\}$.

Hereafter, the BER based on the modulation scheme and interference analysis is expressed as follow:

$$P_b = \frac{M}{2} \sum_{t_{\min}}^{t_{\max}} \sum_{w_{\min}}^{w_{\max}} \sum_{u=0}^{N-t} \sum_{h=0}^{t-1} \sum_{\rho=0}^{2^h} \exp\left[-Q\frac{(P+2)^2}{4.(P+2+2u+l)}\right] \cdot P_{L|HT} \cdot P_{H|T} \cdot P^1_{U|T} \cdot P^1_T \tag{5.18}$$

5.4.4 Analysis of Self-Interferences (SI)

Since the synchronisation is performed at the last chip of a code sequence, then the self-interference arise due to incomplete orthogonal code sequences. This subsection is devoted to investigate the effect of SI at synchronous incoherent OPPM-OCDMA transceivers. The SI and MAI as dominant degrading factors have been considered at the receivers. Referring to 5.4, the BER is given by:

$$P_b = \frac{M}{2(M-1)} P_E \tag{5.19}$$

5.4.4.1 Analysis of SI at Simple Receiver

Recalling that the random Poisson vector $Y_{1,j}$ denotes the photon-counts collected by receiver #1, where $j \in \{0,1,\ldots M-1\}$. Index *i* is declared to be the true one if $Y_{1,i} > Y_{1,j}$ for every $i \neq j$. $S_{1,i} = 1$ represents user #1 transmitting data at slot *i*. When the spreading sequence shifts, the probability of SI is $q = 1/P^2$. Hence, the probability of error P_E can be as discussed previously:

$$P_E = P_1 \cdot P\{T = t\} \cdot P\{U = u\} \cdot P\{H = h\} \tag{5.20}$$

where $P\{T = t\}, P\{U = u\}$ and $P\{H = h\}$ have been introduces in sections 5.4.1 - 5.4.3. The PDF of P_1 is then introduced as:

$$\begin{aligned} P_1 &= \sum_{j=0}^{M-1} P_r\left\{Y_{1,j} \geq Y_{1,0}, some \quad j \neq 0 \middle| S_{1,0} = 1, T = t, U = u, H = h, L = l\right\} \\ &\leq (M-\gamma) \cdot P_r\left\{Y_{1,1} \geq Y_{1,0} \middle| S_{1,0} = 1, T = t, H = h, U = u, L = l, v_0 = 0\right\} \\ &\quad + \sum_{j=1}^{\gamma-1} P_r\left\{Y_{1,j} \geq Y_{1,0} \middle| S_{1,0} = 1, T = t, H = h, U = u, L = l, v_j = k_j\right\} \end{aligned} \tag{5.21}$$

For any $j \in \{1, 2, \ldots, M-1\}, v_j \in \{0, 1\}$ denotes the number of pulses that cause SI in the slot j due to the transmitted data at slot *0* by the intended user. In the first term of *P_1*, there is no SI, due to $v_0 = 0$, $P_r = [v_0 = 0] = 0$. While the second term causes the actual SI due to the remaining $\gamma - 1$ interfering slots [35]. These slots interfere with slot 0 at the probability of $P_r\{v_j = 1\} > 0$. Hence, P_1 can be derived as:

$$\begin{aligned} P_1 &= (M-\gamma) \cdot P_r\left\{Y_{1,1} > Y_{1,0} \middle| S_{1,0} = 1, T = t, U = u, H = h, L = l, v_1 = 0\right\} \\ &\quad + (\gamma-1) \cdot q \cdot P_r\left\{Y_{1,j} > Y_{1,0} \middle| S_{1,0} = 1, T = t, U = u, H = h, L = l, v_1 = 1\right\} \\ &\quad + (\gamma-1) \cdot (1-q) \cdot P_r\left\{Y_{1,j} > Y_{1,0} \middle| S_{1,0} = 1, T = t, U = u, H = h, L = l, v_1 = 1\right\} \\ &= (M-\gamma) \cdot P_{r1} + (\gamma-1) \cdot q \cdot P_{r2} + (\gamma-1) \cdot (1-q) \cdot P_{r1} \\ &= (M-1) \cdot P_{r1} + (\gamma-1) \cdot q \cdot (P_{r2} - P_{r1}) \end{aligned} \tag{5.22}$$

where

$$\begin{aligned} P_{r1} &= P_r\left\{Y_{1,1} > Y_{1,0} \,\middle|\, S_{1,0}=1, T=t, U=u, H=h, L=l, v_1=0\right\} \\ &= \sum_{y_1=0}^{\infty} e^{-\mathbf{Q}(u+l)} \cdot \frac{\left[\mathbf{Q}\cdot(u+l)\right]^{y_1}}{y_1!} \cdot \sum_{y_0=0}^{y_1} e^{-\mathbf{Q}(u+P+2)} \cdot \frac{\left[\mathbf{Q}\cdot(u+P+2)\right]^{y_0}}{y_0!} \end{aligned} \tag{5.23}$$

and

$$\begin{aligned} P_{r2} &= P_r\left\{Y_{1,1} > Y_{1,0} \,\middle|\, S_{1,0}=1, T=t, U=u, H=h, L=l, v_1=1\right\} \\ &= \sum_{y_1=0}^{\infty} e^{-\mathbf{Q}(u+l+1)} \cdot \frac{\left[\mathbf{Q}\cdot(u+l+1)\right]^{y_1}}{y_1!} \cdot \sum_{y_0=0}^{y_1} e^{-\mathbf{Q}(u+P+2)} \cdot \frac{\left[\mathbf{Q}\cdot(u+P+2)\right]^{y_0}}{y_0!} \end{aligned} \tag{5.24}$$

Therefore, the error probability P_b can be obtained as follow:

$$\begin{aligned} P_b &= \frac{M}{2(M-1)} P_E \\ &= \frac{M}{2(M-1)} \cdot P_1 \cdot P\{T=t\} \cdot P\{U=u\} \cdot P\{H=h\} \\ &= \frac{M}{2(M-1)} \cdot \sum_{t=t_{\min}}^{t_{\max}} \sum_{u=0}^{N-t} \sum_{h=0}^{t-1} \sum_{\rho=0}^{\kappa^h} \left[(M-1)\cdot P_{r1} + (\gamma-1)\cdot q\cdot(P_{r2}-P_{r1})\right] \cdot P_{L|HT} \cdot P_{H|T} \cdot P_{U|T} \cdot P_T \end{aligned} \tag{5.25}$$

5.4.4.2 Analysis of SI at Receiver with MAI Cancellation

Since the last signature codes from DPMPC groups are preserved as the reference correlation, the total number of available spreading sequence becomes $P^2 - P$. Consequently, the probability of self-interference at this receiver becomes $q = 1/\left(P^2 - P\right)$. A Poisson random vector Y_1 is used to represent the photon-counts collected from the main branch, while Y_P denotes the photon-counts received from the reference branch. The vector $\tilde{Y}_1$ is defined as $\tilde{Y}_1 = Y_1 - Y_P$. Then, error probability P_E is defined as:

$$\begin{aligned} P_E &= \sum_{j=0}^{M-1} P_r\left\{\tilde{Y}_{1,1} > \tilde{Y}_{1,i},\ some\, j \neq i \,\middle|\, S_{1,i}=1, T=t, U=u, H=h, L=l\right\} \cdot P(T=t)\cdot P(U=u)\cdot P(H=h) \\ &\le \sum_{j=0}^{M-1} P_r\left\{\tilde{Y}_{1,1} > \tilde{Y}_{1,0},\ some\, j \neq 0 \,\middle|\, S_{1,0}=1, T=t, U=u, H=h, L=l\right\} \cdot P(T=t)\cdot P(U=u)\cdot P(H=h) \end{aligned} \tag{5.26}$$

By further analysis, we have:

$$
\begin{aligned}
P_E &= \sum_{j=0}^{M-1} P_r\left\{\tilde{Y}_{1,1} > \tilde{Y}_{1,0},\ some\, j \neq 0 \middle| S_{1,0}=1, T=t, U=u, H=h, L=l\right\} \\
&\leq (M-\gamma)\cdot P_r\left\{\tilde{Y}_{1,1} > \tilde{Y}_{1,0}, some\, j \neq 0 \middle|\ S_{1,0}=1, T=t, U=u, H=h, L=l, v_1=0\right\} \\
&+(\gamma-1)\cdot q\cdot P_r\left\{\tilde{Y}_{1,1} > \tilde{Y}_{1,0}, some\, j \neq 0 \middle|\ S_{1,0}=1, T=t, U=u, H=h, L=l, v_1=1\right\} \\
&+(\gamma-1)\cdot (1-q)\cdot P_r\left\{\tilde{Y}_{1,1} > \tilde{Y}_{1,0}, some\, j \neq 0 \middle|\ S_{1,0}=1, T=t, U=u, H=h, L=l, v_1=0\right\} \\
&= (M-\gamma)\cdot P^1{}_{r1} + (\gamma-1)\cdot q\cdot P^1{}_{r2} + (\gamma-1)\cdot (1-q)\cdot P^1{}_{r1} \\
&= (M-(\gamma+1)\cdot q)\cdot P^1{}_{r1} + (\gamma-1)\cdot q\cdot P^1{}_{r2}
\end{aligned}
\tag{5.27}
$$

The term in the right-hand-side of the last inequality is due to the $M-1-(\gamma-1)$ slots which do not cause SI with slot 0, where:

$$
P^1_{r1} = P_r\left\{\tilde{Y}_{1,1} > \tilde{Y}_{1,0},\ some\ \ j \neq 0 \middle|\ S_{1,0}=1, T=t, U=u, H=h, L=l, v_1=0\right\} \tag{5.28}
$$

$$
P^1_{r2} = P_r\left\{\tilde{Y}_{1,1} > \tilde{Y}_{1,0}, some\, j \neq 0 \middle|\ S_{1,0}=1, T=t, U=u, H=h, L=l, v_1=1\right\} \tag{5.29}
$$

Since the slots are uniformly distributed, these probabilities are the same and then we define $\theta(u,t)$ as follow:

$$
\theta(u,t) = P^1_{r2} = P^1_{r1} = P_r\left\{\tilde{Y}_{1,1} > \tilde{Y}_{1,0}, some\, j \neq 0 \middle|\ S_{1,0}=1, T=t, U=u, H=h, L=l, v_1=1\right\} \tag{5.30}
$$

We can further simplify the calculations by using the Chernoff Bound [37], and then we have:

$$
\begin{aligned}
\theta(u,t) &= P_r\left\{Y_{1,1} - Y_{P,1} > Y_{1,0} - Y_{P,0} \middle|\ S_{1,0}=1, T=t, U=u, H=h, L=l, v_1=1\right\} \\
&\leq E\left[z^{[Y_{1,1}-Y_{P,1}-Y_{1,0}-Y_{P,0}]} \middle| S_{1,0}=1, T=t, U=u, H=h, L=l, v_1=1\right]
\end{aligned}
\tag{5.31}
$$

where $E[\ ]$ is the conditional expectation operator and $z>1$ is the number of interfering slots. The natural logarithm computation is carried out on $\theta(u,t)$ and expectation term is performed as follows:

$$
Ln\theta(u,t) \leq \mathbf{Q}\cdot(u+l+1)\cdot(z-1) - \mathbf{Q}\cdot(u+1)\cdot\left(1-z^{-1}\right) - \mathbf{Q}\cdot(P+2+u)\cdot\left(1-z^{-1}\right) - \mathbf{Q}\cdot u(1-z) \tag{5.32}
$$

Now, by setting $z-1=\delta,\ \delta>0$ and integer, we have then $1-z^{-1}\leq 1$ whereas $\delta-\delta^2\leq 0$, thus by considering new boundaries, we obtain the lower-bounded [37]:

$$1 - z^{-1} \geq \delta - \delta^2 \tag{5.33}$$

By substituting 5.33 in 5.32, we have:

$$\begin{aligned} Ln\ \theta(u,t) &= \mathbf{Q}(u+l+1)(\delta) - \mathbf{Q}(u+l)(\delta - \delta^2) - \mathbf{Q}(u+P+2)(\delta - \delta^2) - \mathbf{Q}(u)(-\delta) \\ &= \mathbf{Q}(2u+l+P+2)(\delta^2) - \mathbf{Q}(P+2)\delta \end{aligned} \tag{5.34}$$

By minimising 5.34 regarding δ, it is obtained as:

$$\delta = \frac{P+2}{2(P+2+2u+l)} \tag{5.35}$$

Therefore, by substituting 5.35 into 5.34, we have:

$$Ln\ \theta(u,t) = \mathbf{Q}(2u+l+P+2)\left(\frac{P+2}{2(P+2+2u+l)}\right)^2 - \mathbf{Q}(P+2)\left(\frac{P+2}{2(P+2+2u+l)}\right) \tag{5.36}$$

and bringing 5.36 back to exponential format, we obtain:

$$\theta(u,t) \leq \exp\left[-\mathbf{Q}\frac{(P+2)^2}{4(P+2+2u+l)}\right] \tag{5.37}$$

Hereafter,

$$P_{r2}^1 = \theta(u,t) \leq \exp\left[-\mathbf{Q}\frac{(P+2)^2}{4(P+2+2u+l)}\right] \tag{5.38}$$

Similarly for P_{r1}^1:

$$P_{r1}^1 \leq \exp\left[-\mathbf{Q}\frac{(P+2)^2}{4(P+2+2u+l)}\right] \tag{5.39}$$

Hence, the upper-bounded BER of the receiver with MAI and SI becomes:

$$\begin{aligned} P_b &= \frac{M}{2(M-1)} \cdot P_E \\ &= \frac{M}{2(M-1)} \cdot P_E \cdot P\{T=t\} \cdot P\{U=u\} \cdot P\{H=h\} \\ &= \frac{M}{2} \sum_{t=t_{\min}}^{t_{\max}} \sum_{u=0}^{N-t} \sum_{h=0}^{t-1} \sum_{\rho=0}^{\kappa^h} \left[P_{r1}^1 + (\gamma-1) \cdot q \cdot \left(P_{r2}^1 - P_{r1}^1\right)\right] \cdot P_{L|HT} \cdot P_{H|T} \cdot P_{U|T} \cdot P_T^1 \end{aligned} \tag{5.40}$$

where the probabilities of other elements in 5.40 have been introduced in Sections 5.4.2 and 5.4.3.

5.4.4.3 Analysis of SI at Receiver with MAI Cancellation and Manchester Encoding

This receiver is very similar to the receiver with MAI discussed previously. The only difference is that active users are divided into two groups, referring to Section 5.4.3, and then the upper-bounded BER can be obtained considering MAI and SI as:

$$P_b = \frac{M}{2} \sum_{t=t_{\min}}^{t_{\max}} \sum_{w=w_{\min}}^{w_{\max}} \sum_{u=0}^{N-t} \sum_{h=0}^{t-1} \sum_{\rho=0}^{\kappa^h} \left[P_{r1}^1 + (\gamma - 1) \cdot q \cdot \left(P_{r2}^1 - P_{r1}^1 \right) \right] \cdot P_{L|HT} \cdot P_{H|T} \cdot P_{U|T}^1 \cdot P_{W|T} \cdot P_T^1 \qquad (5.41)$$

5.5 Discussion of Results

Now, this section presents the three transceivers' performance based on the above DPMPC analysis. To better understand the results, the performances are compared with latest developed prime code families i.e. n-MPC in details. The analysis for n-MPC in incoherent OPPM-OCDMA system can be found in [80]. Firstly, the performance in terms of BER for receivers when only MAI considered as an interference are investigated, secondly the receivers affected by both MAI and SI are examined.

5.5.1 BER Performance of Receivers with MAI and without SI

The DPMPC has been applied into three structures and the overall performances are discussed in details: (i) Simple receiver; (ii) Receiver with only MAI cancellation and (iii) Receiver with both MAI cancellation and Manchester encoding.

This section presents the results of the receivers when MAI has been considered as dominant degrading interference. The simple receiver is examined based on the

Section 5.4.1; Section 5.4.2 is used for the receiver with MAI cancellation and finally third receiver type is estimated by equations in Section 5.4.3.

Figure 5.12 shows the BER evaluation for DPMPC, n-MPC and MPC codes employed in incoherent OPPM-OCDMA simple receivers against the average photons per pulses, μ. Prime number *P* and number of active users *N* are set to be 7 and 42 (i.e. full-load) respectively. Two different multiplicities of *M= 8* and *16* are investigated at the receivers. As it can be observed from Figure 5.12, the performance is getting better as μ increases. DPMPC outperforms other codes due to greater difference correlation values discussed previously. It is also indicated that multiplicity plays a significant role to improve the performance but compromise the structure complexity; e.g. for $\mu = 70$ and *M=16* BER of n-MPC is 0.0081, MPC is 0.0094 while DPMPC's is 0.0065.

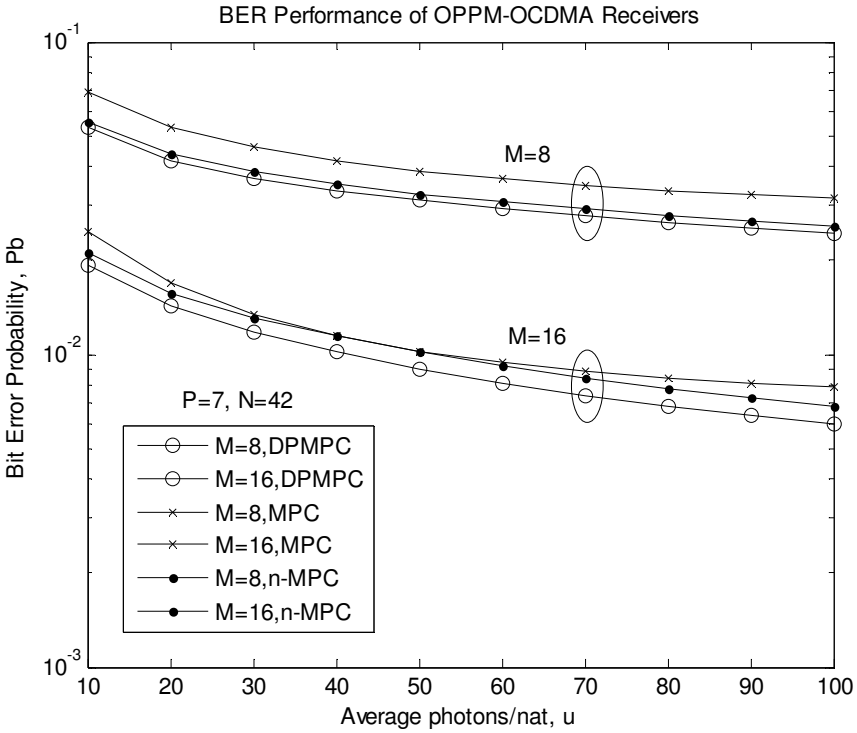

Figure 5.12 BER Performance of OPPM-OCDMA simple receivers using different codes against the average photons per pulse μ, when *P=7, N=42* and *M=8* and *16*

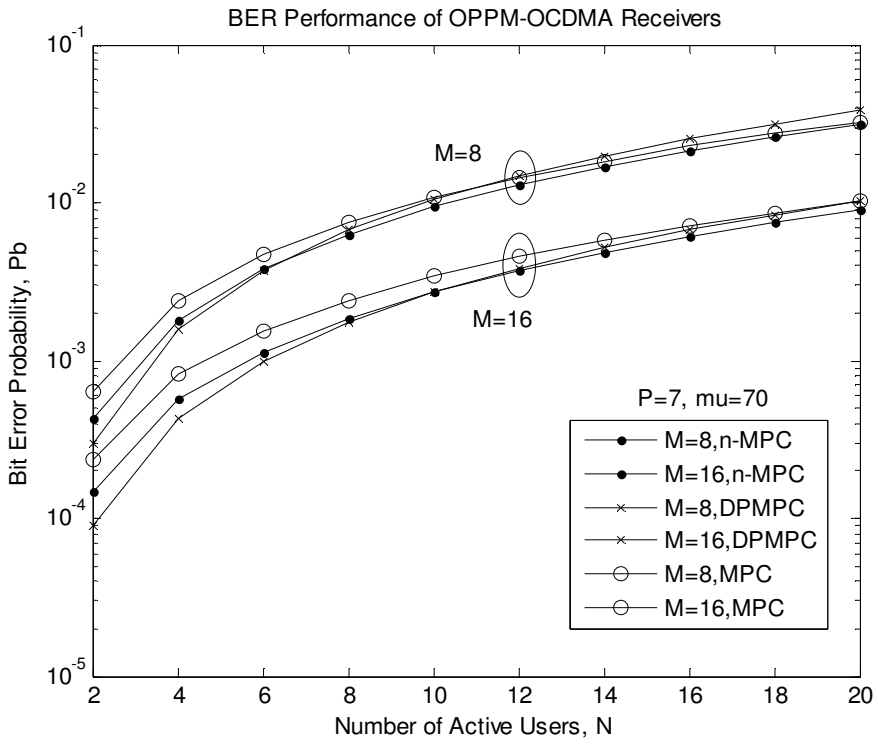

Figure 5.13 BER Performance of OPPM-OCDMA simple receivers using different codes against the number of active users *N*, when *P=7,* $\mu = 70$, *M=8* and *16*

BER performance of simple receivers using DPMPC, MPC and n-MPC, under a given condition, is illustrated on Figure 5.13 against the number of active users. It is observable that increasing number of users increases the BER due to raising more interference and makes the system unreliable. Again, multiplicity has an effective role in the receivers' performance; however the overall performances of the simple receivers, shown in Figures 5.12 and 5.13, are so defective to compare with the $BER = 10^{-9}$ requirement in the optical communications that the results indicate the necessity of interference cancellation.

To examine other receivers, now we only evaluate the performance of DPMPC and n-MPC code families since n-MPC has already outperformed MPC [95]. The $BER = 10^{-9}$ is also drawn on the Figures for clear understanding.

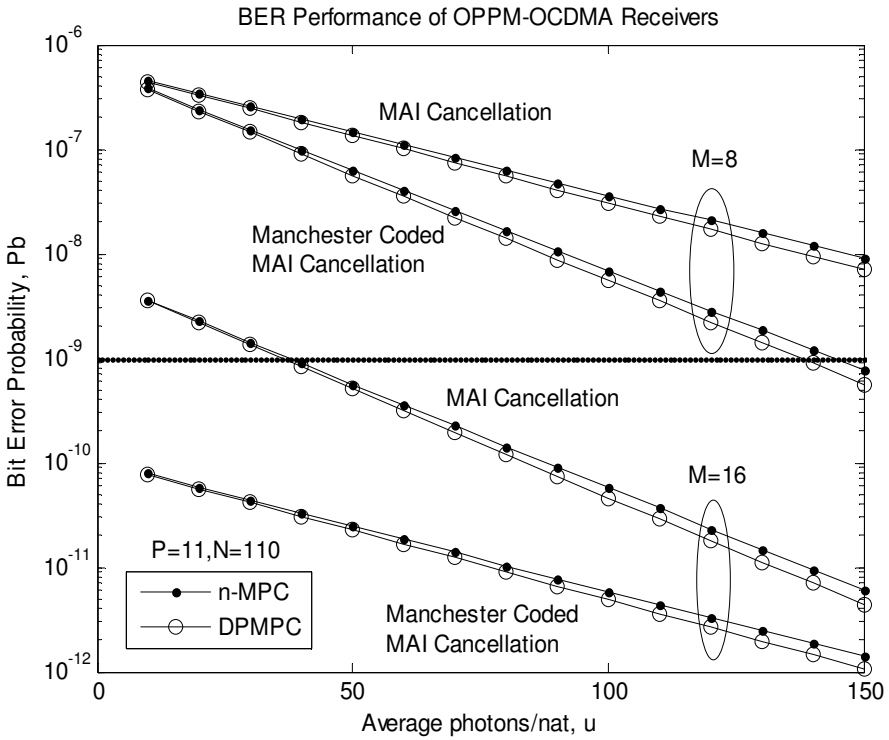

Figure 5.14 BER Performance of OPPM-OCDMA receivers considering MAI using different codes against the average photons per pulse μ, when *P=11, N=110, M=8* and *16*

Figure 5.14 gives an idea about how the average photon-count influences the BER performance. The prime number *P*, and number of active users *N* are set on 11 and full-load of 110 respectively. On the other hand, average photon-count (μ) is a parameter proportional to signal power, accordingly as can be seen BER decreases when received signal's power increases. It has been expected that using interference reduction with Manchester encoding improves the system quality and now it is indicated by the results which are more enhanced than simple receivers and receivers with only MAI cancellation. It is also observed from Figure 5.14 that the receivers with MAI reduction and Manchester coded MAI canceller are also power efficient. Apparently, by increasing μ and *M* a very reliable communication link can be

guaranteed, although the raise is not infinite and they should reach optimum values depending on the system specification at the transceivers design stage.

Figure 5.15 illustrates the performance of the incoherent OPPM-OCDMA receivers with MAI cancellation and Manchester coded one against the number of active users when *P=7*, *M=8, 16* and $\mu = 100$. The interesting issue is where the minimum error probability lays down, the area is in the range of 50 to 60 percent of the total number of users, $N=P^2-P$, depending on the prime number *P* for the receiver with Manchester coded MAI cancellation, shown in Table 5.1 for various number of *P* and their minimum measured BER and in Figure 5.15. Accordingly, if the number of maximum supported active users is set on 55% (as an average, N_{eff}) of total users in the access network, transceivers will apparently have much enhanced performance. It is noted that the maximum supported active users in the current networks is usually set on 10-20 percent of total users due to capital expenditure cost of the network design and implementation [108].

Table 5.1 Minimum BER for the number of active users considering only MAI at receivers with Manchester coded MAI cancellation, when *M=16* and $\mu = 100$

P	BER_{min} *of n-MPC*	BER_{min} *of DPMPC*	N_{eff}	N_{Full}	*Supported No. of Active Users* (N_{eff}/N_{Full})*%*
5	1.84×10^{-12}	8.51×10^{-13}	*12*	*20*	*60*
7	9.26×10^{-17}	3.46×10^{-17}	*24*	*42*	*57.1*
11	6.85×10^{-22}	4.8×10^{-22}	*60*	*120*	*50*
13	5.17×10^{-27}	3.25×10^{-27}	*84*	*156*	*53.8*
17	6.23×10^{-35}	7.23×10^{-36}	*140*	*272*	*51.47*

By comparing the BER values at the effective points, N_{eff}, it can be observed that the BER differences are remarkable and it can compensate the network capacity.

Furthermore, the multiplicity *M* has its independent effect on improving the BER; however the implementation will be very complicated due to the precise timing and switching design. The performance behaviour, shown in Figures 5.14 and 5.15 when *M= 8* and *16,* indicated that by increasing *M* the network capacity is recovered as well as the overall performance under a given condition specially with DPMPC.

5.5.2 BER Performance of Receivers with MAI and SI

In this section, the receivers are examined against the number of active users *N*, and the average number of photons per pulse μ, when both the multiple-access and self-interferences are taken into account. Obviously, simple receivers will even degrade more due to higher level of interferences; therefore, here we study two types of receivers including (i) with only MAI cancellation and (ii) with Manchester coded MAI cancellation. The evaluations for different receivers are based on the analysis mentioned in Section 5.4.4 for DPMPC.

Figure 5.16 shows the receivers BER, when the conditions are set on *P=11, N=110* (i.e. full-load) and *M=8* and *16*, against the average number of photons per pulse μ. As it can be seen, the higher the received signal power, the more reliable communication is established. At the start point both codes performs very good, while by increasing μ, DPMPC causes the lower error-rates. It is said that the difference can be compensated by the system capacity as well as signal power. It means that by using DPMPC we can have the same BER in a fixed signal power which is possible with higher power by using n-MPC.

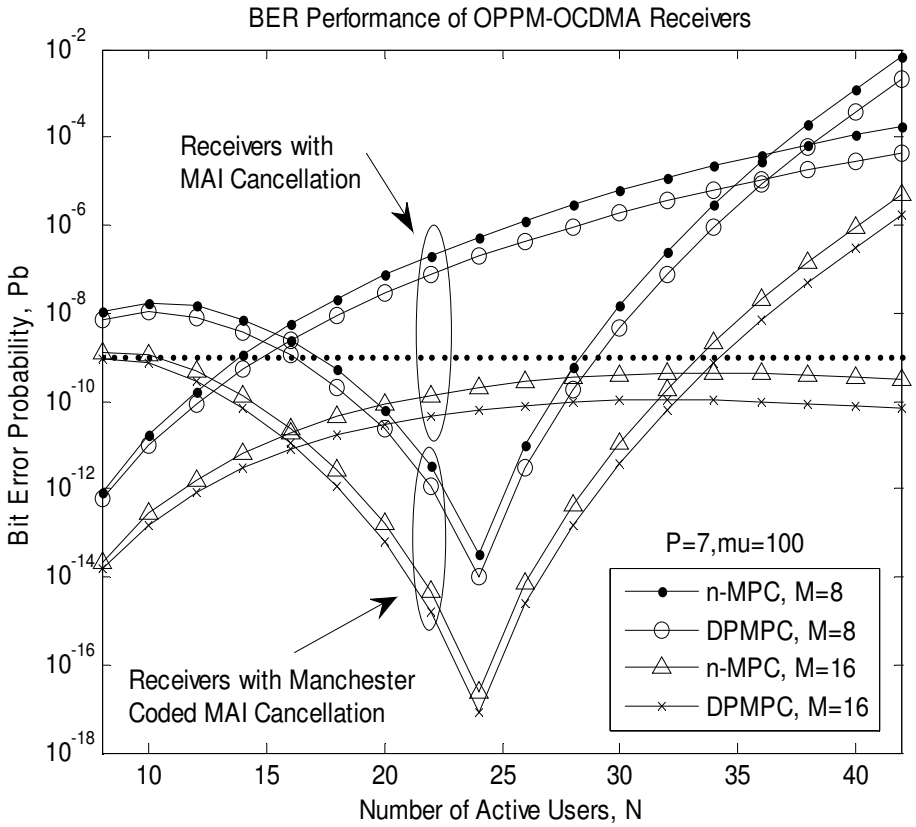

Figure 5.15 BER Performance of OPPM-OCDMA receivers considering MAI using different codes against the number of active users *N*, when *P=7,* $\mu = 100$, *M=8* and *16*

For example when $\mu = 50$, BER of the receivers with DPMPC equals the receivers with n-MPC when $\mu = 55$. Furthermore, we pick the receivers with only MAI when *M=16* and $\mu = 100$ for examination from Figure 5.16, the BER of receiver employing DPMPC is 1.8×10^{-10} while it is 2.9×10^{-10} for n-MPC, i.e. 37% improvement.

Obviously, as discussed before, multiplicity gives more options to time-slot for accommodating more signals. It is apparent in Figure 5.16 that superior performance is achieved by higher level of multiplicity *M*. As higher multiplicity makes the system implementation complex, applying Manchester encoding is an excellent choice to accommodate more interference-reduced users. Regarding the fact that BER of less than 10^{-9} is acceptable in optical communication, it is also drawn to assist the eye.

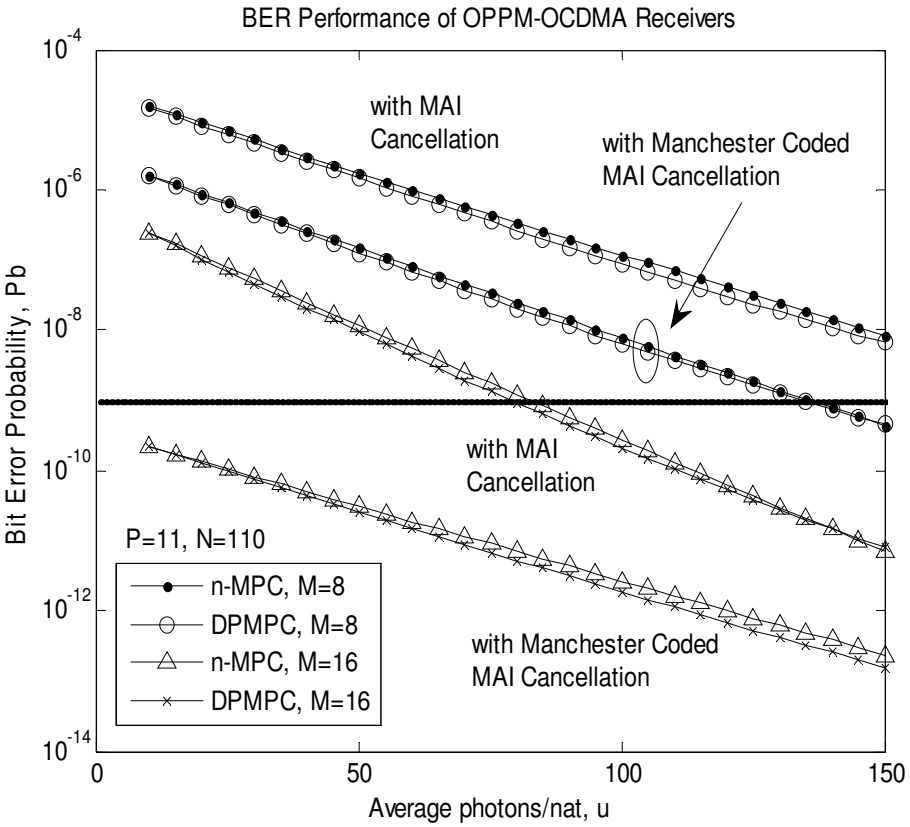

Figure 5.16 BER Performance of OPPM-OCDMA receivers considering MAI and SI using different codes against the average photons per pulse μ, when *P=11, N=110, M=8* and *16*

Finally, Figure 5.17 illustrates the incoherent OPPM-OCDMA receivers performing against the number of active users *N*, when *P=7,* $\mu = 100$, *M=8* and *16*. The effective number of users N_{eff} denotes where the minimum error probability occurs at the receivers with Manchester coded MAI reduction, referring to Table 5.2 for various *P*.

Table 5.2 Minimum BER for the number of active users considering MAI and SI at receivers with Manchester coded MAI cancellation, when *M=16* and $\mu = 100$

P	BER_{min} *of n-MPC*	BER_{min} *of DPMPC*	N_{eff}	N_{Full}	*Supported No. of Active Users* (N_{eff}/N_{Full})%
5	8.6×10^{-12}	1.2×10^{-12}	*12*	*20*	*60*
7	3.3×10^{-16}	1.3×10^{-16}	*24*	*42*	*57.1*
11	6.9×10^{-20}	4.5×10^{-20}	*60*	*120*	*50*
13	5.3×10^{-25}	3.1×10^{-25}	*84*	*156*	*53.84*
17	6.8×10^{-29}	4.1×10^{-29}	*140*	*272*	*51.47*

It is observed that by increasing the number of active users, interferences increases then the receivers operate under unstable communication, whereas DPMPC is still superior to n-MPC, especially in scheme of using cancellation technique plus Manchester encoding. For example, we pick the receiver with Manchester coded MAI cancellation, when *M=8* at N_{eff} from Figure 5.17, the BER for the receiver employing n-MPC is 9.8×10^{-13}, while it is 3.7×10^{-13} for DPMPC i.e. 62% improvement.

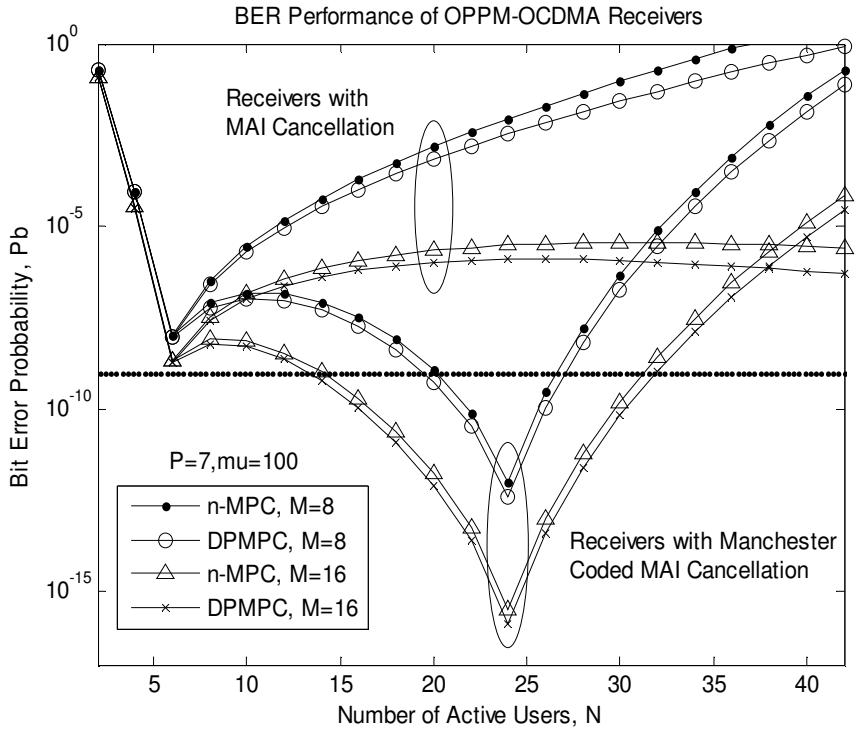

Figure 5.17 BER Performance of OPPM-OCDMA receivers considering MAI and SI using different codes against the number of active users *N*, when *P=7, M=8, 16* and $\mu = 100$

To compare the error-rates of the receivers considering only MAI in Section 5.5.1 with the receivers considering MAI and SI, it is observed that the performance is further degraded by self-interference. However, the overall BER is still in a reasonable range by employing DPMPC along with the MAI cancellation technique and Manchester coding which have much contributed with the transceivers' enhancement.

5.6 Analysis of Throughput

In practice, one of the important parameters of the performance evaluation is the data-rate. For a given user, throughput is the rate of data transmission given by the amount of information transmitted per second by the user.

5.6.1 OPPM-OCDMA Throughput

Referring to Section 5.2, T is the duration of each *M-ary* time frame, with chip duration of T_c. The spreading sequence of length *L* must be exactly fitted into time slot τ, where $\tau = LT_c$. γ is the overlapping index. The throughput of OPPM-OCDMA is defined as R_{T-OPPM} data packet per time slot [34, 37]:

$$R_{T-OPPM} = \frac{\ln M}{T} = \frac{\ln M}{M\,\tau/\gamma} = \frac{\gamma \ln M}{MLT_c} \tag{5.42}$$

Since the pulse-width T_c is always fixed, for the sake of convenience the throughput-pulse-width product R_{O-OPPM} is defined as follows:

$$R_{O-OPPM} = R_{T-OPPM} \cdot T_c = \frac{\gamma \ln M}{MLT_c} \cdot T_c = \frac{\gamma \ln M}{ML} \tag{5.43}$$

It is noted that the throughput-pulse-width product R_{O-OPPM} is proportional throughput R_{T-OPPM} for a fixed pulse width of T_c. In addition, the users-throughput product, denoted by *NR*, as the product of the number of users times R_0 is defined by:

$$NR_{OPPM} = N \cdot R_{O-OPPM} = N \cdot \frac{\gamma \ln M}{ML} \tag{5.44}$$

NR is the measure of the total data-rate from all users transmitted within the channel. In practice, we are interested in characterising the maximum throughput that can be achieved when keeping the bit-error probability below a prescribed threshold.

Therefore, the parameters γ, M and L are allowed to vary to optimise the throughput under the constraint that $P_b \le \varepsilon$. In doing so, we have:

$$R_{O-OPPM,\max} = \max_{\substack{\gamma,M,L \\ P_b \le \varepsilon}} R_{O-OPPM} \quad , \quad NR_{OPPM,\max} = \max_{\substack{\gamma,M,L \\ P_b \le \varepsilon}} NR_{OPPM} \tag{5.45}$$

5.6.2 PPM-OCDMA Throughput

Under a given conditions in incoherent PPM-OCDMA transceiver, the throughput R_{T-PPM} is given by [34]:

$$R_{T-PPM} = \frac{\ln M}{T} = \frac{\ln M}{M\tau} = \frac{\ln M}{MLT_c} \tag{5.46}$$

The throughput-pulse-width product R_{O-PPM} in the PPM-OCDMA is expressed as:

$$R_{O-PPM} = R_{T-PPM} \cdot T_c = \frac{\ln M}{MLT_c} \cdot T_c = \frac{\ln M}{ML} \tag{5.47}$$

Similarly, in PPM-OCDMA transceiver, the users-throughput product can be written as:

$$NR_{PPM} = N \cdot R_{O-PPM} = N \cdot \frac{\ln M}{ML} \tag{5.48}$$

Now, by considering DPMPC in the PPM- and OPPM-OCDMA systems, the throughput-pulse-width product could be further rewritten as:

$$R_{O-OPPM} = \frac{\gamma \ln M}{ML} = \frac{(P+2)\cdot \ln M}{M \cdot \left(P^2 + 2P\right)} \tag{5.49}$$

$$R_{O-PPM} = \frac{\ln M}{ML} = \frac{\ln M}{M \cdot \left(P^2 + 2P\right)} \tag{5.50}$$

And the users-throughput products can be expressed as the following:

$$NR_{OPPM} = N.\frac{\gamma \ln M}{ML} = \frac{N \cdot (P+2)\cdot \ln M}{M \cdot \left(P^2 + 2P\right)} \tag{5.51}$$

$$NR_{PPM} = N.\frac{\ln M}{ML} = \frac{N \cdot \ln M}{M \cdot \left(P^2 + 2P\right)} \tag{5.52}$$

As it can be seen from the 5.51 and 5.52, under the given condition, OPPM system supports *P+2* (i.e. γ) times higher throughput than PPM scheme. In other words, OPPM is offering the higher throughput without the bandwidth expansion as it is required in the PPM system. Where the bandwidth increase is challenging or impossible due to the components or bandwidth limitations, OPPM modulation is able to provide higher throughput by introducing an overlapping index in which the spreading is performed over number of slots rather than only one slot as compared with PPM modulation. This implies to support the greater number of users i.e. system capacity enhancement without bandwidth expansion.

5.7 Conclusion

In this Chapter, proposed DPMPC has been employed into incoherent synchronous overlapping PPM-OCDMA network. Three types of receivers including (i) simple receiver (ii) receiver with MAI cancellation and (iii) receiver with MAI cancellation and Manchester coding, have been analysed and examined. The lower-bounded BER for the receiver (i) and the upper-bounded BER for receivers (ii) and (iii) have been derived. In this analysis, the MAI was assumed the dominant noise while background noise and photodiodes dark currents were negligible. However, the self-interference has been taken into account. I should be noted that the overall system performance in terms of around 50% lower BER, almost 30% capacity enhancements and increase in the network throughput without bandwidth expansion is a trade-off with the system complexity, signal multiplicity and overlapping index for physical implementation.

The published results [P1, P2][1] indicated that the receivers employing this novel coding scheme with MAI cancellation are able to accommodate greater number of users, while they still maintain low BER and less power consumption. Manchester coding has also produced the enhanced performance and showed when the multiplicity restricts the system implementation; Manchester coding is able to recover this limitation at the cost of transceivers bandwidth.

[1] See 'List of Publications'

Chapter 6

Analysis of DPMPC in Coherent OCDMA Network

6.1 Introduction

Recently, coherent time spreading OCDMA which employs either direct time spreading using super structures fibre Bragg grating [101] and arrayed waveguide grating [109] or spectrally phase coding time spreading by spatial lightwave modulator [110] has attracted a lot of attention because of the overall superior performance over incoherent schemes. Several architectures have been considered for the use of CDMA within an optical fibre, the most common systems use direct-detection with bipolar codes such as Gold sequences [111]; while, unipolar prime code families, particularly the introduced novel one, double-padded modified prime code (DPMPC), has more flexible code-length and is partially orthogonal. To retain the advantage of $\{0,1\}$ codes as a power saving option, we consider in this Chapter unipolar signalling and coherent binary phase shift keying (BPSK) modulation. The capacity of the system using prime

codes is limited by the maximum achievable bit-rate of the electronic circuitry that generates the pseudo-noise (PN) sequences. Here, we concentrate on a maximum attainable chip-rate of 10 Gchips/s and a desired bit-rate of hundreds of Mbps. This imposes a limit on the length of the spreading sequences which must be in the order of hundreds of chips per bit.

In this Chapter, the signal-to-noise ratio (SNR) of a coherent homodyne and heterodyne OCDMA architectures employing the DPMPC sequences and two phase modulation methods are examined. The phase modulation methods include using either Mach-Zehnder interferometer (MZI) as an external phase modulator or distributed feedback (DFB) laser diode's driving current as an injection-locking method along with the dual-balanced detection structure. We have also evaluated the performance penalty imposed on the OCDMA system as a result of the limited phase excursion of $\pm 0.42\pi$ as a result of injection-locking modulation [111].

Furthermore, we also analyse the coherent BPSK-OCDMA scheme with heterodyne detection. The external phase modulation method is considered for heterodyne detection. In the analysis, the system SNR with respect to the number of simultaneous active users is investigated considering both the receiver noise and multiple-access interference (MAI).

6.2 Coherent Homodyne BPSK-OCDMA Architecture

This section is dedicated to describe the architecture of the coherent BPSK-OCDMA network. In the coherent OCDMA system based on the external phase modulation shown in Figure 6.1, the outgoing data is first BPSK encoded generating the in-phase

and quadrature phase (IQ) signals in electrical domain. Then, the encoded BPSK-signal phase modulates the lightwave through MZI as an external phase modulator. The use of an external MZI modulator for this application was verified experimentally in [112]. Finally, the signals are CDMA encoded by means of DPMPC sequences and multiplexed via star couplers and transmitted over a star passive optical network (SPON) as a network infrastructure. This corresponds to multiplication of the optical carrier and enables the system employing codes based on in-phase correlations. At the intended receiver as shown in Figure 6.1, the inverse process takes place where another MZI is used to demodulate the received signal using the same DPMPC sequence used for encoding at the transmitter end. Referring to the DPMPC correlation properties, Section 3.2.2.4, the signal that has been multiplied by the same code will de-spread, while signals multiplied by different codes will be further spread in the frequency domain and hence removed. In practice, the received signal is required to be filtered to reject unwanted crosstalks outside the receiver bandwidth. The intended demodulated signal and tiny co-channel interference (i.e. reduced through de-spreading process) is photo-detected in dual-balanced structure to remove noises and direct-current (dc) values to reliably detect IQ signal.

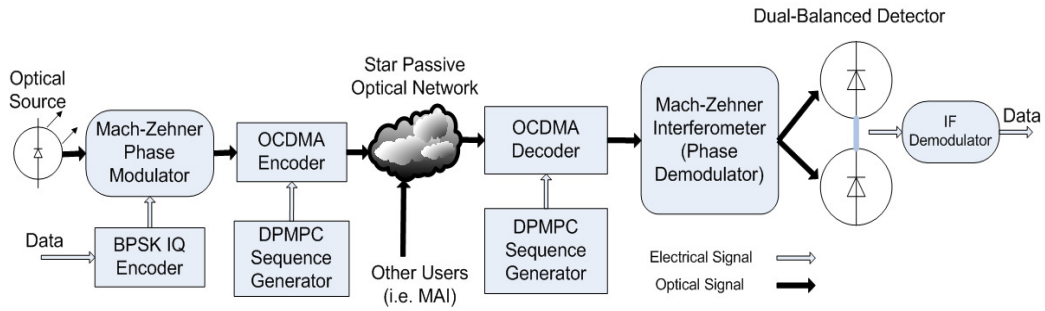

Figure 6.1 Coherent homodyne BPSK-OCDMA transceiver with MZI phase modulator

Figure 6.2 illustrates the coherent OCDMA system based on the injection-locking of the DFB laser diodes' driving current for the phase modulation. Two quality current-driven DFB laser diodes are used at the transmitter as an optical source and at the receiver as a local oscillator. The signal is phase-modulated by controlling the injection current of the DFB laser at the transmitter. The optical signal is then CDMA encoded by assigned DPMPC sequence and transmitted over the network. At the receiver end the synchronized local oscillator is combined coherently with the received OCDMA signal. In CDMA detection process, the portion of the received signal encoded with the same DPMPC sequence at the transmitter (i.e. intended data for the intended receiver) is de-spread, whereas signals encoded with other sequences (i.e. MAI) are further spread and reduced. The coherently mixed optical signals are incident on a dual-balanced detector whose electrical output conserves the phase information. The generated bipolar electrical signal is integrated over a bit interval and the result is compared to a threshold to form the final bit estimation based on the maximum likelihood (ML) decision rule.

When phase modulation is achieved by an MZI modulator, the chip-rate can increase to the maximum value of 10 Gchips/s; in contrast, the injection current adjusted to achieve phase modulation has the maximum chip-rate of about 1 Gchips/s due to the limited phase excursion [44, 111, 113]. Therefore, there is already an apparent limitation on the overall system performance.

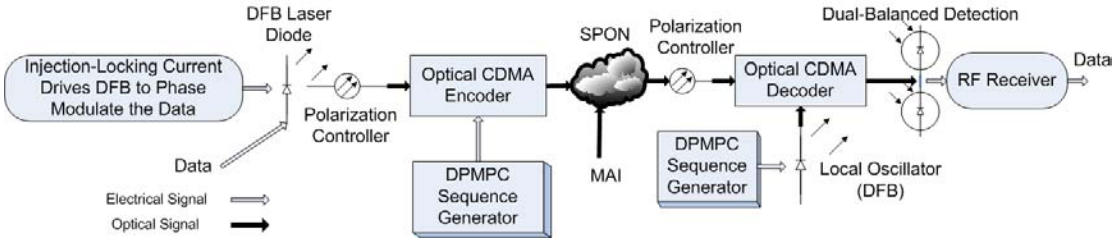

Figure 6.2 Coherent homodyne BPSK-OCDMA transceiver with injection-locking DFB laser

6.2.1 Analysis of Phase Modulation with MZI

According to Figure 6.1, to extract the information contained in the phase of the optical carrier, the coherent detection is employed. For estimation and removal of dc values in the baseband signal, a dual-balanced detector is a reasonable option [44]. The receiver operates under the shot noise limited regime by considering the local oscillator power so sufficient that both dark current and receiver thermal noise can become negligibly small.

First of all, we require examining the equations that manage the electrical output of a dual-balanced detector in a CDMA system. Let *K* be the number of active users and $S_i(t-\tau_i)$ be the signature sequence of the i^{th} user. Let τ_i be the relative time-delay between the i^{th} user and the desired user (e.g. user #1). We employ DPMPC spreading sequences and assume all users have the same polarization and average power given by $\hat{S}^2$. $C_i(t)$ denotes the piecewise-constant function which is the product of the data-bit and code sequence bit values of the i^{th} user at time *t*. The initial phase offset of the i^{th} user is a random variable θ_i uniformly distributed over the interval $(0, 2\pi)$.

Since $C_i(t)$ phase-modulates the lightwave and assumes either 0 or 1 (as product of two bit values) to generate the optical signal phase, it appears in the phase argument to show the signal behaviour. Hence, the received signal with amplitude $\hat{S}$ is:

$$s(t) = \sqrt{2}\hat{S}\sum_{i=1}^{K}\cos(\omega_c t + C_i(t)\cdot(\pi/2) + \theta_i) \tag{6.1}$$

The local oscillator will also be phase-modulated by the spreading sequence of the desired user, thus $S_1(t)$ (i.e. $S_i(t-\tau_i)$ where *i*=1 and $\tau_i = 0$) appears in the phase argument as well, thus the local oscillator signal with amplitude $\hat{L}$ is also given by:

$$l(t) = \sqrt{2}\hat{L}\sum_{i=1}^{K}\cos(\omega_c t + S_1(t)\cdot(\pi/2) + \theta_{LO}) \tag{6.2}$$

where θ_{LO} is the initial phase offset of the local oscillator. Now, the product of $l(t)$ and $s(t)$ at the receiver is:

$$l(t)\cdot s(t) = 2\cdot\hat{L}\cdot\hat{S}\cdot\sum_{i=1}^{K}\cos(\omega_c t + S_1(t)\cdot(\pi/2) + \theta_{LO})\cdot\cos(\omega_c t + C_i(t)\cdot(\pi/2) + \theta_i) \tag{6.3}$$

Hence:

$$\begin{aligned} l(t)\cdot s(t) = 2\cdot\hat{L}\cdot\hat{S}\cdot\sum_{i=1}^{K}[&\frac{1}{2}\cos(\omega_c t + S_1(t)\cdot(\pi/2) + \theta_{LO} + \omega_c t + C_i(t)\cdot(\pi/2) + \theta_i) \\ &+\frac{1}{2}\cos(\omega_c t + S_1(t)\cdot(\pi/2) + \theta_{LO} - \omega_c t - C_i(t)\cdot(\pi/2) - \theta_i)] \end{aligned} \tag{6.4}$$

The summation part, which generates the higher frequency of $2\omega_c t$, is filtered through dual-detection receiver as it is out of detectors' frequency range. The remaining part of $l(t)\cdot s(t)$ as well as the output of the dual-detector is:

$$\Re\cdot l(t)\cdot s(t) = \Re\cdot\hat{L}\cdot\hat{S}\cdot\sum_{i=1}^{K}\cos\left[\left(S_1(t) - C_i(t)\right)\cdot(\pi/2) + \theta_{LO} - \theta_i\right] \tag{6.5}$$

$\Re = \eta e/h\nu$ is the photo-detectors responsivity where η is the quantum efficiency of each detector, *h* is Planck's constant, *e* is the fundamental charge of an electron, and ν is the employed optical frequency. Note that we assume the local oscillator tracks the phase of the desired user, thus we use $\theta_{LO} = \theta_1 = 0$. As mentioned earlier, when a

relatively sufficient power from local oscillator is employed, the receiver operates under shot noise limited regime and its noise has one-sided power spectral density of [44, 111, 113]:

$$N_0 = 2\Re\,\hat{L}^2 \tag{6.6}$$

Integral of the detector output, i.e. 6.5, over a bit interval *T*, results in as the following:

$$\begin{aligned} S_{out} &= \Re\sum_{i=1}^{K}\int_0^T l(t)\cdot s(t)dt + \sqrt{N_0}\int_0^T n(t)dt \\ &= \Re\hat{L}\hat{S}b_0^1 T + \sqrt{\Re T}\cdot\hat{L} + \Re\hat{L}\hat{S}\sum_{i=2}^{K}\left[b_{-1}^i R_{i,1}(\tau_i) + b_0^i\hat{R}_{i,1}(\tau_i)\right]\cos\theta_i \end{aligned} \tag{6.7}$$

where b_0^1 represents the information bit being detected, b_{-1}^i and b_0^i are overlapping of the previous and the following bits of the i^{th} user. The continuous-time partial cross-correlation functions $R_{i,j}(\tau)$ and $\hat{R}_{i.j}(\tau)$ are defined as:

$$\begin{aligned} R_{i,j}(\tau) &= \int_o^{\tau} s_i(t-\tau)\cdot s_j(t)dt \\ \hat{R}_{i.j}(\tau) &= \int_{\tau}^{T} s_i(t-\tau)\cdot s_j(t)dt \end{aligned} \tag{6.8}$$

where $\tau = \tau_i - \tau_j$ and $\tau_1 = 0$. The noise $n(t)$ in 6.7 can be assumed a Gaussian random variable with zero mean and unit variance [111]; all data bits are independent, equi-probable and the delays are independent and uniformly distributed over a bit interval. The first term in 6.7 is due to the desired user, while the second term is additive white Gaussian noise (AWGN), and the third is the multiuser interference (i.e. MAI) which is distributed normally while a reasonable number of active users are involved. The variance of each term in the MAI sum mentioned in [44, 111, 113] is $T^2/3N$, where *N* is the length of the signature sequence ($2T^2/3N$ corresponds to the correlation and $1/2$ is due to the phase offset). Finally, the signal-to-noise ratio (SNR) of the coherent

homodyne BPSK-OCDMA with MZI phase modulator is derived regarding the number of active users *K* as:

$$SNR(K) = \frac{\Re^2 \hat{L}^2 \hat{S}^2 T^2}{\Re^2 \hat{L}^2 \hat{S}^2 T^2 \frac{K-1}{3N} + \Re T \hat{L}^2} = \frac{1}{\frac{K-1}{3N} + \frac{1}{\Re \hat{S}^2 T}} \tag{6.9}$$

Note that for single-user $SNR(1) = \Re \hat{S}^2 T = E_b / N_0$ where E_b is the signal energy of one bit. The bit-error rate (BER) of BPSK signalling with Gaussian noise, related to the above SNR, is then:

$$BER_{BPSK}(K) = Q\left(\sqrt{2 \times SNR(K)}\right) = \frac{1}{2} erfc\sqrt{SNR(K)} \tag{6.10}$$

where *Q(x)* and *erfc(x)* are Q-function and complementary-error-function respectively.

Figure 6.3 shows the comparison of BER against the single-user SNR for DPMPC sequences when *P*= 23 and Gold-sequence of 511 chips as used in [47, 101, 109, 110, 113]. If we pose the limit of 100 Gchips/s to the chip-rate and want to keep the bit-rate sufficiently high (hundreds of Mbps), we are limited to spreading sequences having lengths in the order of hundreds. As Gold sequences have $N = 2^n - 1$ chips long, with *n* being an odd integer, we are limited to *n*= 9, i.e. a length of 511; while, with DPMPC there are two further steps, where *P* equals 23 and 29 with code-lengths $\left(N = P^2 + 2P\right)$ of 575 and 899, respectively. Also the desired BER threshold of 10^{-9} is indicated in Figure 6.3 as a reference.

The parameter *r* shown in the inset of Figure 6.3 which ranges from 50% to 10% denotes the percentage of the total possible number of active users involved in the communication according to the coding scheme. For example, 10% of users (53 users) are accommodated with guaranteed BER of 4×10^{-10} at single-user SNR of 15 dB when

P=23; while 10% of users (50 users) with Gold-sequence of 511 chips are accommodated with BER of 1.3×10^{-9}. As the result shows for a given value of *r* when the signal power increases the system BER decreases; however, for higher values of *r* the system BER degrades due to MAI growth. Also it can be seen, the performance using the DPMPC surpasses the overall performance of Gold-sequences in different conditions.

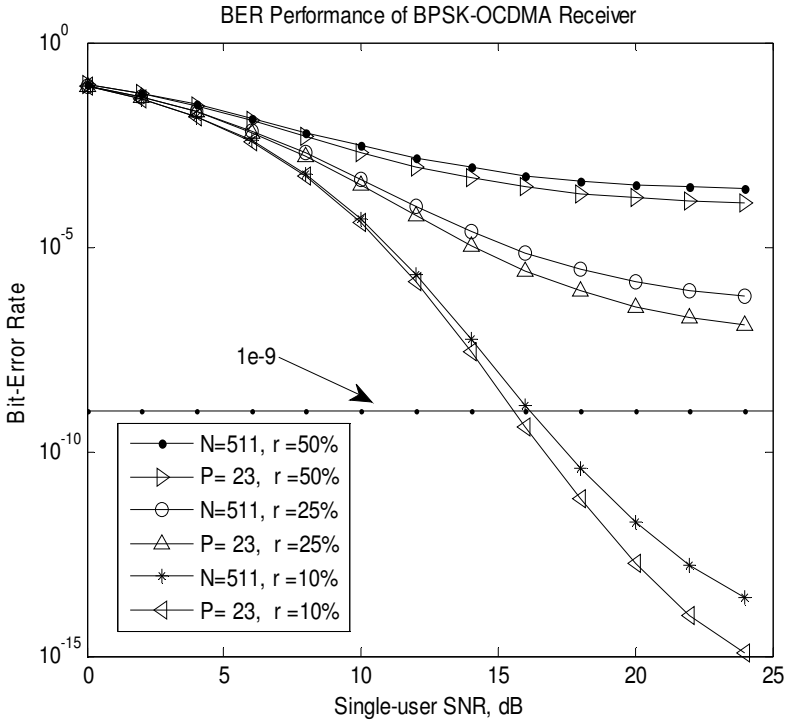

Figure 6.3 BER performance of homodyne BPSK-OCDMA with MZI against single-user SNR

Figure 6.4 explains the system behaviour against the number of active users for different single-user SNRs (shown on the graphs as EbN) and compares DPMPC with *P*=23 and Gold-sequences with 511 chips. It is clearly shown that (i) as the single-user SNR increases the BER decreases, (ii) the system performance is limited by MAI and (iii) the system employed DPMPC can accommodate greater number of active users than that of Gold-sequence.

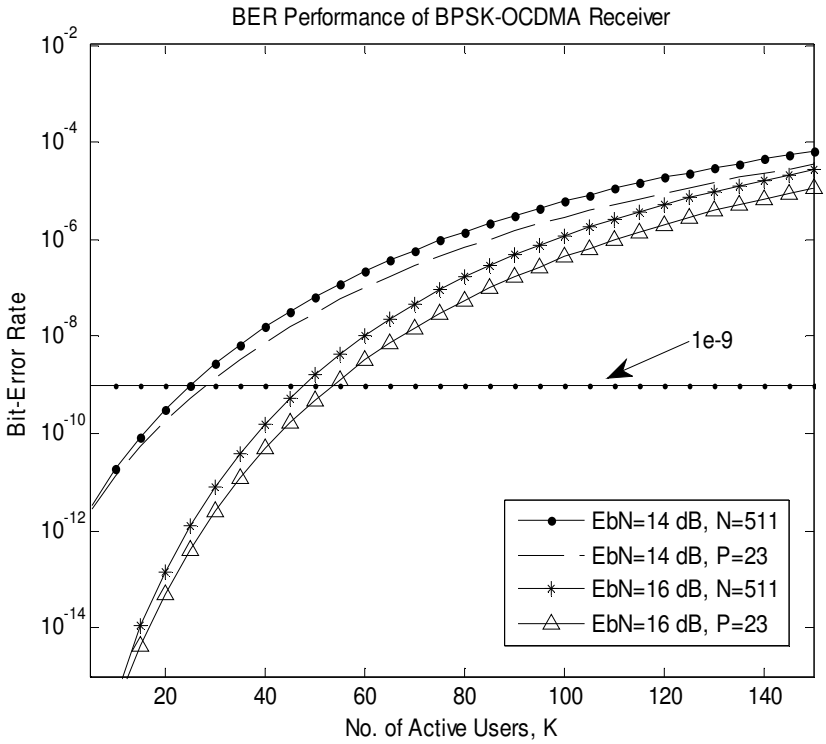

Figure 6.4 BER performance of homodyne BPSK-OCDMA with MZI against the number of active users, *K*

For example, the system with DPMPC when $EbN = 16dB$ can tolerate maximum of 55 simultaneous active users maintaining $BER = 10^{-9}$, while 45 users can be supported in the other one. Needless to say, one more step of *P*=29 still remained that can definitely enhance the network capacity to compare with commonly used Gold-sequence.

6.2.2 Analysis of Phase Modulation with DFB Injection-Locking

In previous section, we have studied matched-filtering during coherent detection with a dual-balanced detector followed by an integrator which leads to a baseband electrical signal consisting of the de-spread signal with AWGN and MAI. In homodyne detection the local oscillator is at the same frequency as that of the carrier and the output electrical signal is at baseband. Now, we discuss the phase modulation by

injection-locking of the driving current of DFB laser based on the architecture shown in Figure 6.2.

To examine the effect of the phase limitation on the modulation process, the injection current of DFB laser diode is modulated to accomplish PSK signalling at the transmitter with phase excursion being limited to $\pm 0.42\pi$ and modulation speed of 1 Gchip/s. At the receiver the signal is demodulated by the injection-locking current of the second DFB laser as a local oscillator shown in Figure 6.2. As it is no longer feasible to track the desired user's initial phase offset by injection-locking method, another tracking method is assumed, therefore it is still $\theta_1 = \theta_{LO} = 0$ and since $\pm 0.42\pi = \pm \pi/2 \mp 0.08\pi$, the received signal can be expressed as [111]:

$$s(t) = \sqrt{2}\hat{S}\sum_{i=1}^{K}\cos(\omega_c t + C_i(t)\cdot(\pi/2 - 0.08\pi) + \theta_i) \tag{6.11}$$

The local oscillator signal is then:

$$l(t) = \sqrt{2}\hat{L}\sum_{i=1}^{K}\cos(\omega_c t + S_1(t)\cdot(\pi/2 - 0.08\pi) + \theta_{LO}) \tag{6.12}$$

The output of the dual-balanced detector under these circumstances is:

$$\begin{aligned}\Re\cdot l(t)\cdot s(t) &= 2\Re\hat{L}\hat{S}\cdot\sum_{i=1}^{K}\cos\left[\left(S_1(t) - C_i(t)\right)\cdot(\pi/2 - 0.08\pi) + \theta_{LO} - \theta_i\right] \\ &= \Re\hat{L}\hat{S}\cdot\sin^2(0.08\pi)\cdot\sum_{i=1}^{K}\cos(\theta_{LO} - \theta_i) \\ &+ \Re\hat{L}\hat{S}\cdot\cos^2(0.08\pi)\cdot\sum_{i=1}^{K}\cos((S_1(t) - C_i(t))\cdot(\pi/2) + \theta_i) \\ &+ \Re\hat{L}\hat{S}\cdot\sin(0.16\pi)\cdot\sum_{i=1}^{K}\sin((S_1(t) - C_i(t))\cdot(\pi/2) + \theta_i)\end{aligned} \tag{6.13}$$

Due to the phase limitation, two new terms in the output of the dual-balanced detector appear. The first term in 6.13 is constant in time and accounted as dc component which can be estimated and removed at the dual-balanced detector. The

last term in 6.13 involves the weighted-sum of the difference of two codes (essentially a new pseudo-code). The weighted-sum is bounded by the sum over the pseudo-codes, which in turn is negligible compared to that of the second term; since, the code-length becomes arbitrarily larger than the number of active users (i.e. *N >> K*). Hence, the output can be approximated by the only second term plus noise [44, 111]. By integrating over a bit interval *T*, the output signal can be obtained as:

$$\begin{aligned} S_{out} &= \Re \hat{L}\hat{S} \cdot \cos^2(0.08\pi) \cdot \sum_{i=1}^{K} \int_0^T \cos((S_1(t) - C_i(t)) \cdot (\pi/2) + \theta_i) dt + \sqrt{N_0} \int_0^T n(t) dt \\ &= \Re \hat{L}\hat{S} b_0^1 T \cdot \cos^2 0.08\pi + \sqrt{\Re T} \cdot \hat{L} \\ &\quad + \Re \hat{L}\hat{S} \cdot \cos^2 0.08\pi \cdot \sum_{i=2}^{K} \left[b_{-1}^i R_{i,1}(\tau_i) + b_0^i \hat{R}_{i,1}(\tau_i) \right] \cdot \cos\theta_i \end{aligned} \quad (6.14)$$

Using the same Gaussian approximation for the MAI, the SNR becomes:

$$SNR(K) = \frac{\left(\Re \cos^2 0.08\pi\right)^2 \cdot \hat{L}^2 \hat{S}^2 T^2}{\left(\Re \cos^2 0.08\pi\right)^2 \cdot \hat{L}^2 \hat{S}^2 T^2 \cdot \frac{K-1}{3N} + \Re T \hat{L}^2} = \frac{1}{\frac{K-1}{3N} + \frac{1}{\Re \hat{S}^2 T \cdot \cos^4 0.08\pi}} \quad (6.15)$$

By comparing 6.9 and 6.15, it is noticed that the only difference is the *cosine* term. The phase excursion causes the system power loss of $10\log\theta$, where θ is the phase limitation [111]. It caused the degradation of 1.2 dB when the phase limitation is 0.42π since the limitation applies to both modulator and demodulator. Therefore, it is expected a power loss of 0.6 dB for a single user at either of transmitter or receiver.

As illustrated in Figure 6.5, the BER of both modulation methods have been evaluated against the single-user SNR (i.e., $EbN = E_b / N_0$) when *r* = 10% when *P*=23 (i.e., 53 users). The system with external phase modulation outperforms since there is no restriction on phase excursion as well as the chip-rates. Additionally, it can be observed from Figure 6.5 that the difference between two graphs is 1.2 dB at any point

of the same BER value, e.g. by reaching to the value of $BER = 10^{-9}$, EbN at external modulation method is required to be 15.8 dB while it is 17 dB for EbN at injection-locking method.

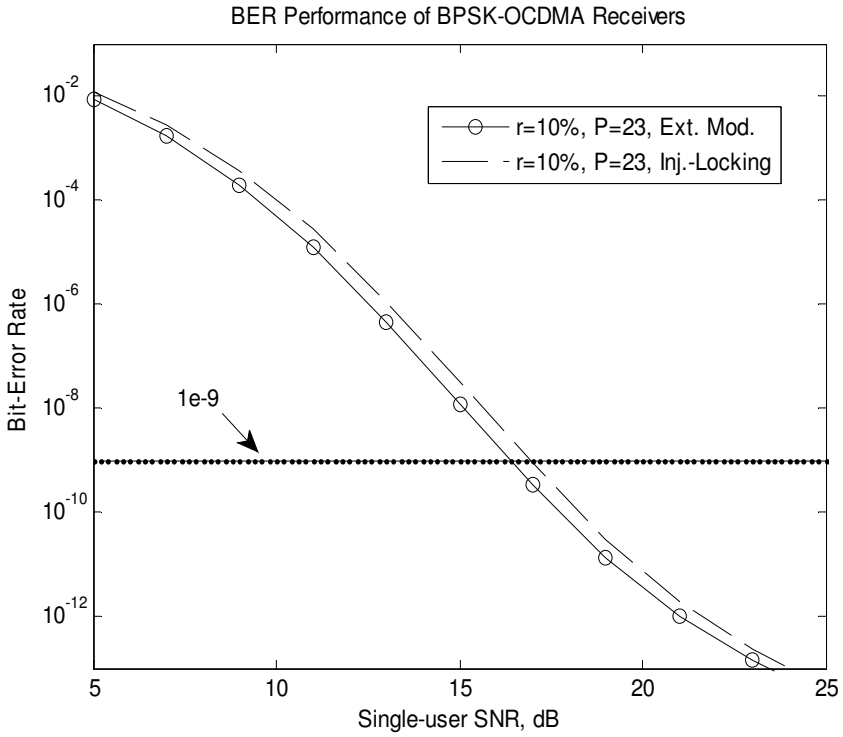

Figure 6.5 BER comparisons of homodyne BPSK-OCDMA with different phase modulations against single-user SNR, EbN

The behaviour of these two methods is also illustrated in Figure 6.6 against the number of active users *K* when $EbN = 16\ dB$ and *P*=23. The external modulation indicates remarkably enhanced performance particularly at the lower number of simultaneous active users.

As it can be seen at $BER = 10^{-9}$, the system employing DPMPC and MZI can support 55 users, while 50 users are accommodated in the system with injection-locking phase modulation method, i.e. 10% capacity degradation.

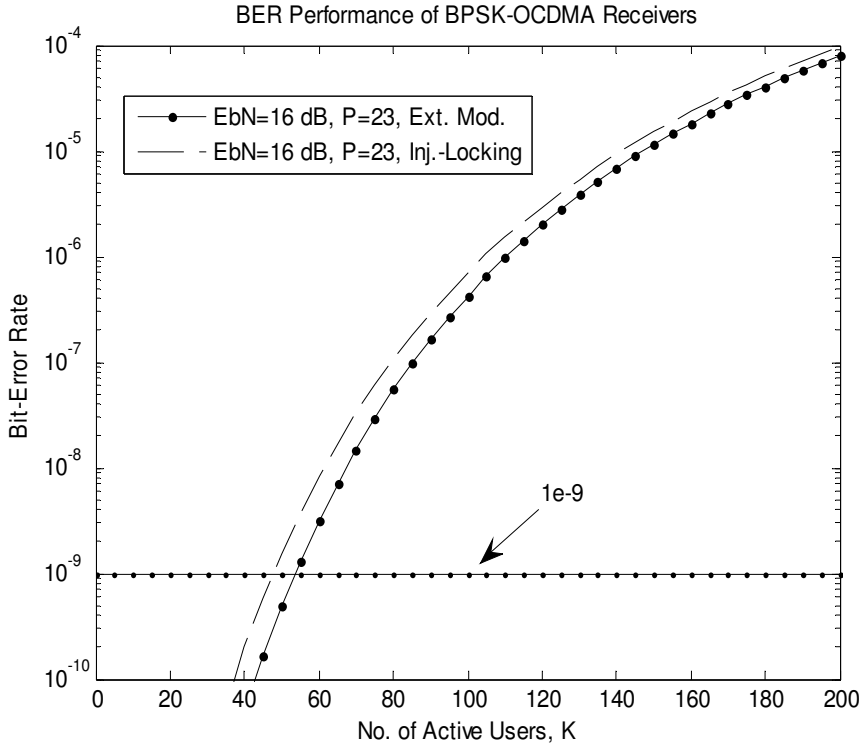

Figure 6.6 BER comparisons of homodyne BPSK-OCDMA with different phase modulations against the number of active users, *K*

6.3 Coherent Heterodyne BPSK-OCDMA Architecture

In this section, we study the coherent heterodyne BPSK-OCDMA architecture employing DPMPC and comparing with commonly used Gold-sequences. As a reference configuration, we consider an SPON with *Z* transmitters and *Z* receivers employing the BPSK modulation as their basic structures are shown in Figure 6.7. Each incoming bit is encoded by means of a DPMPC sequence, acting as the address of the destination.

Let x_i be the DPMPC sequence identifying the i^{th} receiver and call the '1' or '0' symbols forming the DPMPC sequence *chips*. The following rule is applied in the BPSK scheme: either x_i or $\overline{x_i}$ is transmitted, depending on whether a '1' or a '0' data bit is to be sent, where $\overline{x_i}$ is derived from x_i by inverting each chip in the sequence.

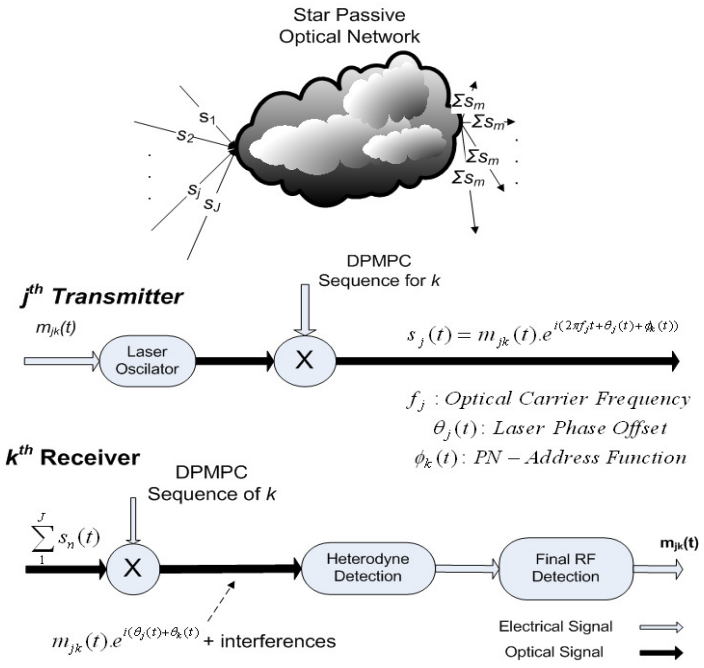

Figure 6.7 Transceiver architecture for heterodyne BPSK-OCDMA from $j \rightarrow k$

The signals from all the transmitters are then summed up and broadcast to every receiver. The receivers perform a correlation between the received signal and their own prime code sequence (address); all the signals except the properly encoded one, will be decoded as interfering noise, whereas the latter will give rise to a correlation peak. Hence, several simultaneous transmissions, addressed to different receivers are possible. Because the cross-correlation between DPMPC sequences in different groups is not *zero* (but it is as low as *one*), the interfering signals will reduce the noise margin of the receivers.

The spreading and de-spreading operations can be performed directly on the optical domain by means of a lithium-niobate crystal phase modulator [114], driven by the incoming data and the pseudo-noise sequence. After the de-spreading, the signal is heterodyne-detected and processed based on the decision rule (i.e. ML) according to the chosen modulation scheme. A block diagram of the system is shown in Figure 6.8.

Because of the spreading, the maximum achievable bit-rate is limited by the speed of the electronic circuitry which generates the prime code sequences. Since we are considering MZI as an external phase modulator, we are able to pose the limit of 10 Gchips/s to the chip-rate and intend to keep the bit-rate sufficiently high. Obviously, a synchronous network (i.e. one in which all the transceivers are bit synchronised) shows very good results in terms of the number of allowed simultaneous users.

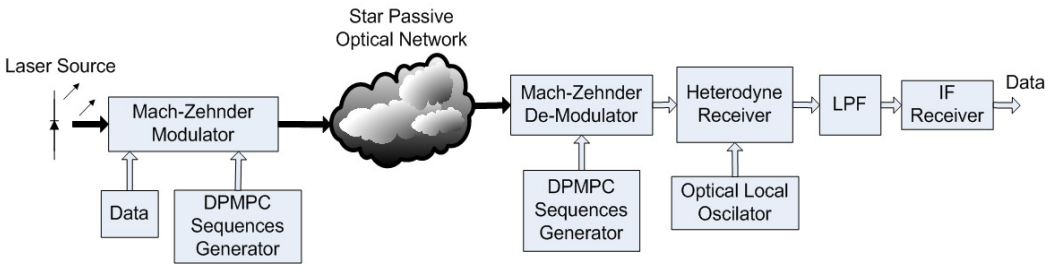

Figure 6.8 Transceiver structure of heterodyne BPSK-OCDMA

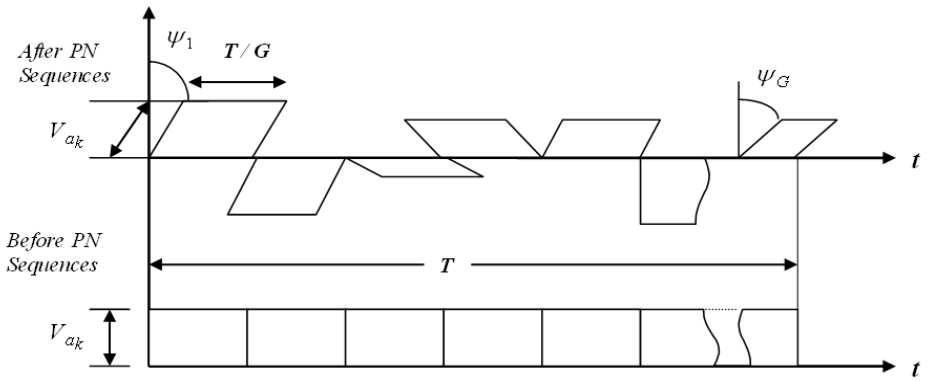

Figure 6.9 PN-sequence applied to a unit energy pulse for direct phase modulation

The spreading is taken to be the form of a pseudo-random rotation of the modulating signal's phase during each chip interval T_c as depicted in Figure 6.9 according to the pseudo-random bit sequence (DPMPC) associated with the intended receiver (user). The receiver de-spreads the received signal using the exact pseudo-noise (PN) sequence by subtracting the same phase pattern used in the spreading process. After

de-spreading, it is as if no spreading had been done. As aforementioned, spreading and de-spreading can be done directly on the optical signal by using lithium-niobate crystal phase modulators. For proper de-spreading the PN sequence used in the receiver must be synchronised with the one used in the transmitter as in detail illustrated in Figure 6.7 for $user\ j \rightarrow user\ k$ transmission process. This synchronisation is one of the tasks to be performed by the call-start-up procedure, together with carrier-frequency acquisition. These are important functions; however, we will not discuss them in this Chapter, where the focus is on the key issue of the performance of an ongoing call under the (conservative) assumption that other users are actively engaged in a call.

6.3.1 Analysis of Phase Modulation with MZI

Here we take a more detailed look at the way in which a nominally transparent channel is provided between a generic pair of users $j \rightarrow k$ given a background of communications between other users. We use the complex representation for signals, thus let v_j denotes the laser output at the j^{th} transmitter destined for the k^{th} receiver before the DPMPC sequence multiplier, shown in Figure 6.7. $v_j(t)$ can be expressed as:

$$v_j(t) = u_j(t) \cdot e^{i\omega_j t} \tag{6.16}$$

where $u_j(t)$ is the modulating signal and ω_j is the optical angular frequency (i.e. $\omega_j = 2\pi f_j$).

Let $\{a_k(t)\}_{k=1}^{J}$ denotes the set of addressing sequences of the *J* receivers which is the same as the set of DPMPC sequences. The chip-time T_c is supposed to divide the symbol time *T* perfectly. As the quotient *G* ($G = T/T_c$) is called *spread spectrum*

processing gain and since the chip duration is denoted by T_c, we mathematically represent each $a_k(t)$ as:

$$a_k(t) = \sum_{l=1}^{N} e^{i\phi_{lk}} \cdot h(t - lT_c) \tag{6.17}$$

where

$$h(t) = \begin{cases} 1, & 0 \le t \le T_c \\ 0, & otherwise \end{cases} \tag{6.18}$$

with Fourier transform of:

$$H(\omega) = 2T_c e^{-i\omega T_c/2} \frac{\sin(\omega T_c/2)}{\omega T_c/2} \tag{6.19}$$

Although the phase variables are known by the communicators, for analytical purposes they can be treated as random variables. The phase variables in the array $\{\phi_{lk}\}$ where $1 < l < N$, $1 \le k \le J$ are assumed to have the properties of the independent and identically distributed random variables on the interval $[-\pi, \pi)$. It should be noted that $a_k(t) \cdot a_k^*(t) = 1$ for $\forall k : 1 \le k \le J$ and that $a_k(t) \cdot a_{k'}^*(t)$ $(k \ne k')$ is statistically the same as $a_k(t)$ $\forall k : 1 \le k \le J$. The accumulation of all *J* signals equals:

$$\gamma = \sum_{m=1}^{J} u_m(t) \cdot e^{i\omega_m t} \cdot a^{(m,k)}(t) \tag{6.20}$$

By $\{(\cdot)^{(m,k)}\}_{m=1}^{J}$ we mean any permutation of the integer 1 through *J* where $(\cdot)^{(m,k)}$ conveys who is communicating to whom i.e. m^{th} transmitter is communicating to k^{th} receiver, moreover γ is assumed to be received at each receiver. At k^{th} receiver, we have upon acquisition of the transmitter frequency ω_j:

$$\sum_{m=1}^{J} u_m(t).e^{i(\omega_m - \omega_j)t} \cdot a^{(m,k)}(t) \cdot a_k^*(t) \;=\; u_j(t) + \sum_{m=1}^{J}{}^{j} e^{i(\omega_m - \omega_j)t} \cdot u_m(t) \cdot b_m(t) \tag{6.21}$$

where $\sum^{j}$ means the j^{th} summand is omitted and the set of $b_m(t)$, $\forall m: 1 \le m \le J$, is a statistically independent copy of the set of $a_m(t)$ $\forall m: 1 \le m \le J$. The signal $u_j(t)$ has been received unaltered except for the additive noise of:

$$\sum_{m=1}^{J}{}^{j} e^{i(\omega_m - \omega_j)t} . u_m(t) . b_m(t) \tag{6.22}$$

Next, we look at quantifying the background noise level. Let the consecutive random phases of the desired pulse during an arbitrary symbol time be ψ_n, $n \in \{1, 2, ..., G\}$ and the corresponding phases of a generic interferer be ϕ_n, $n \in \{1, 2, ..., G\}$. Let us assume that the interferer is displaced by a frequency f_l ($\omega_l = 2\pi f_l$) from the desired transmission. At the end of a symbol period during which the l^{th} transmitter has sent a '1', the unwanted contribution from the *l* interferer, after the matched filter, is:

$$i_l = \frac{2}{T} \sum_{n=1}^{G} \int_{(n-1)T/G}^{nT/G} e^{i(\phi_n - \psi_n)} \cdot e^{i\omega_l t} dt = \frac{2}{G} \sum_{n=1}^{G} e^{i\zeta_n} \cdot \frac{\sin(\omega_l T / 2G)}{\omega_l T / 2G} \tag{6.23}$$

where ζ_n is distributed in the same way as ϕ_n or ψ_n. By the central limit theorem [114], the limit of large *G*, right-hand-side of 6.23 is Gaussian distributed. So, if g_l denotes a complex Gaussian variant of unit variance, we can say that the right-hand-side of 6.23 is approximately distributed as the variant of:

$$x_l = 2G^{-1/2} \left[\sin(\omega_l T / 2G) / (\omega_l T / 2G) \right] \cdot g_l \tag{6.24}$$

In the following the main guidelines for the BPSK modulation is outlined. Let us assume the l^{th} signal is from the intended user. According to Figure 6.8, the signal is heterodyne detected, thus the receiver output after multiplication contains both unwanted optical signal and required intermediate frequency (IF) signal which is selected through the filter. The IF signal level is proportional to the phase shift of the

incoming signal; the higher the difference in phase between the two states, the higher difference between the two output voltage levels from the receiver will be. Decisions are made by the IF receiver (see Figure 6.8) on the basis of the IF signal level achieved from the following variable $Z(T)$ [42, 114]:

$$Z(T) = \frac{\Re}{2N}\left[N \cdot d_i + \sum_{i=1, i\neq l}^{K} d_i \cdot X_{li}\right] + n_B(T) \tag{6.25}$$

where *K* is the number of simultaneous transmissions, *N* is the length of the PN sequences (DPMPC), d_i is the i^{th} transmitter data bit, $n_B(t)$ is the sampled baseband Gaussian noise process and X_{li} is a random variable representing the cross-correlation between the DPMPC sequences used by the i^{th} and l^{th} transmitters. If we define the new random variable *W*, as:

$$W = \sum_{i=1, i\neq l}^{K} d_i \cdot X_{li} \tag{6.26}$$

Its probability density function (PDF) can be obtained from the PDF of the random variable X_{li}. According to DPMPC correlation properties, Section 3.2.2.4, in-phase cross-correlation values are *zero* or *one* in that the intended user interferes with other users in either the same or the different groups respectively. Obviously, the *zero* value does not cause the interference due to perfectly orthogonal sequences, while the *one* value causes the interference which is just among intended user and $P^2 - P$ users from different groups (P^2 whole sequences or users and *P* sequences from the same group of intended user which are orthogonal), therefore cross-correlation values are uniformly distributed among interfering users, thus the PDF of *W* becomes:

$$P(W = i) = \frac{i}{P^2 - P} \tag{6.27}$$

where $P(W=i)$ is the probability that *W* assumes the value *i* (the number of actively involved users in the transmission). Based on the knowledge of the PDF of *W* where representing the interference, the following expression for the BER can be obtained, conditioned to a number of simultaneous transmissions, *K* [42, 114]:

$$BER_K = \frac{1}{2}\sum_{i=0}^{W_m} erfc\left[\frac{N-i}{N}\cdot\sqrt{r}\right]\cdot P(W=i) \tag{6.28}$$

where W_m, is the largest value assumed by the random variable which depends on the number of active users, *W* denoting the interference and *r* is the SNR, i.e.:

$$r = \frac{E_b}{N_0} = \frac{\eta P_r}{2hf\,B_{IF}} \tag{6.29}$$

where η is the photo-detector's quantum efficiency ($\eta = 0.9$), P_r is the received signal power, *h* is the Planck constant, *f* is the employed optical frequency $(\lambda = 1.55\,\mu m)$ and B_{IF} is the IF bandwidth. In order to minimize the laser phase noise or chirp, the bandwidth of the IF receiver in Figure 6.8 should be practically wider than a matched filter, i.e. the low-pass filter (LPF) in Figure 6.8, whose noise bandwidth would be generally equal to the bit-rate. In case of widening the matched filter bandwidth itself (to avoid the phase noise) the IF bandwidth should be still at least equal to the LPF bandwidth; however this inherently increases the noise levels again. Therefore, the bandwidth of identical to the chip-rate (wide enough regarding to the bit-rate) should be considered for the IF bandwidth as an optimum bandwidth. Therefore, the phase noise impairment can be neglected [42, 47, 99, 115].

Based on the above analysis, the performance (i.e. BER) of the BPSK-OCDMA transceivers is evaluated. Figure 6.10 illustrates the receiver BER variation against the number of simultaneous active users *K* when *P*=23 and 511-chip long Gold-sequence.

The system performs under different received signal power of $P_r = -30$ dBm and $P_r = -25$ dBm. Also in Figure 6.10, the desired BER threshold value of 10^{-9} is apparent to assist the eye. Obviously the system performs better (i.e. lower BER) when the received signal power P_r (or SNR) increases. It is observable when the P_r is -30 dBm and P=23 (i.e. SNR is 13 dB), the maximum number of accommodated simultaneous users in which the $BER = 10^{-9}$ is K_c= 240 (≈45% of 529 total users) and K_c= 310 (≈59% of 529 total users) when P_r increases to -25 dBm (i.e. SNR is 16 dB). The critical accommodated number of users (K_c) for the systems with 511-chip long Gold codes, when P_r is -30 or -25 dBm are 220 (43% of 511 total users) and 300 (58% of 511 total users) respectively. This critical value depends on the system received power, P_r (or SNR) that can be obtained by setting $BER = 10^{-9}$. For further examination, we look at the BER at a certain number of users, e.g. K=240 and $P_r = -30$ dBm, now the BER at the receiver with DPMPC is 1.4×10^{-9}, while it is 3.2×10^{-8} at the receiver with Gold-sequence, i.e. significant improvement.

Figure 6.11 shows the transceivers' BER variations against the received signal power P_r under the different traffics when 50 and 30 percent of total number of users are present. As expected, the higher the P_r (or SNR), the better the receivers perform. In this analysis, 30% and 50% of total number of users are assumed in the communication when P=23 and 511-chip long Gold sequence. As Figure 6.11 indicates, to maintain $BER = 10^{-9}$ the system P_r should be -30 dBm and -27 dBm for 30% and 50% load respectively.

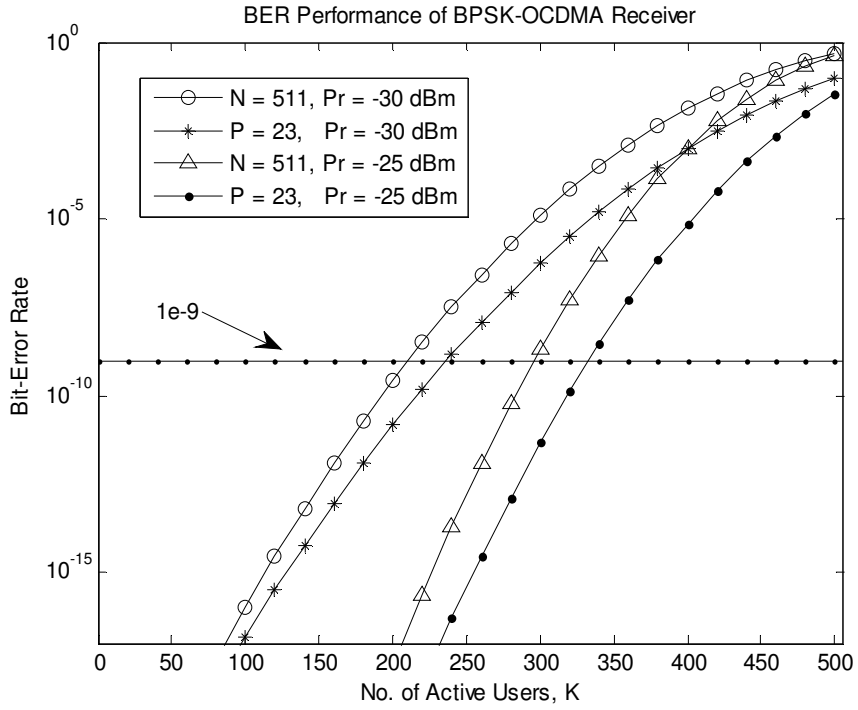

Figure 6.10 BER performance of heterodyne BPSK-OCDMA against the number of simultaneous active users, *K*

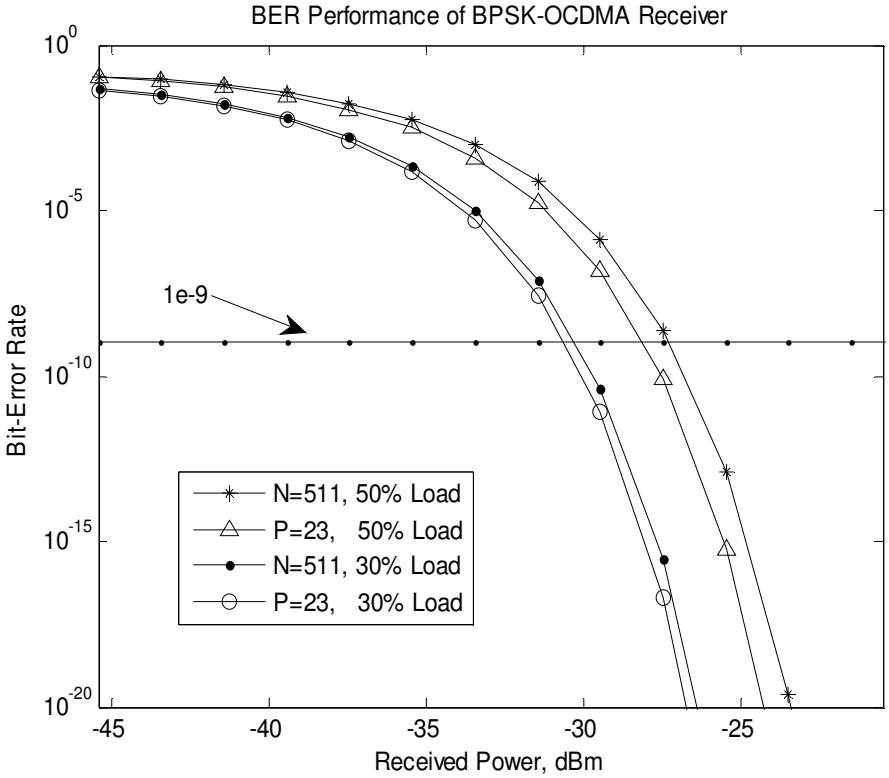

Figure 6.11 BER performance of heterodyne BPSK-OCDMA against the received signal power, P_r

In other words, when the traffic is low the less SNR is required to maintain low BER. It is also apparent that DPMPC outperforms Gold-sequence. For example, at the received power of -27.45 dBm, BER at the receiver with *P*=23 equals 7.8×10^{-11} while it is 2.3×10^{-9} at the receiver with 511-chip long Gold-sequence, i.e. a huge enhancement.

6.4 Conclusion

We have investigated the performance of coherent homodyne and heterodyne OCDMA systems by employing a new prime code family (DPMPC) and coherent dual-balanced detection. The homodyne scheme utilised either the external phase modulation by the use of MZI or the injection-locking of driving current of DFB laser diodes. The results indicate that the analyses are also valid for codes with the same correlation properties. Accordingly, employing DPMPC outperforms the conventional bipolar codes regarding flexible code-lengths and accommodating more simultaneous active users. The limited phase excursion, generated by injection-locking method, caused several complications. Firstly, separate phase tracking is required as it can no longer be accomplished simultaneously with phase modulation; secondly, there is a dc-bias level in the detector output requiring estimation and removal; finally, there is the degradation in BER equivalent to 1.2 dB signal loss. The overall performance of the transceivers shows that by employing the DPMPC the system can be very power efficient and have enhanced network capacity as compared with commonly used Gold-sequences. Above all, the proposed coherent schemes [P3-P7][1] can be a promising scheme for long-haul high-speed transmissions over the OCDMA networks.

[1] See 'List of Publications'

Chapter 7

Analysis of DPMPC in FSK-OCDMA Network

7.1 Introduction

In a conventional OCDMA, each time-slot is divided into chips which are equals to spreading code-length consisting of $\{0, 1\}$-sequences (depending on spreading codes) addressed to each user. The data are modulated and assigned through optical pulses (OP) at the certain chips of each allocated slot either in on-off keying (OOK) [39] or in pulse-position modulation (PPM) formats.

The modulated signal is then transmitted after multiplied by the spreading code in the OCDMA encoder via optical tapped-delay lines (OTDL), i.e. the output OP in the first chip of a slot is spread in time domain to several chips corresponding to 1's of the spreading codes. The OP sequences transmitted from users are multiplexed in the star passive optical network (SPON) couplers as an infrastructure reference and then transmitted over fibre-to-the destination (FTTx). At the receiver, in order to obtain the

intended signal from the received signal, de-spreading is performed in a de-correlator which consists of OTDL with inverse tap coefficients. The OPs are merged at the last chip in a slot, and the desired data is extracted in the demodulator based on the modulation scheme.

As aforementioned, when the number of simultaneous active users increases, the effect of channel interference also inherently raises in incoherent OCDMA. On the other hand, multiple-access interference (MAI) cancellation techniques at the receivers have been widely studied with different modulation schemes such as OOK and PPM. When OOK is used, the interference canceller is unable to completely eliminate the channel interference, since the reference signal has the components of the desired user [39]. In this Chapter we propose and analyse a novel interference cancellation technique in which the reference signal does not contain the component of the desired signal.

Y. Gamachi *et. al* [51] has proposed the *M-ary* FSK-OCDMA and indicated that in the *M-ary* PPM the probability of overlapping pulses can be reduced by increasing the number of symbols (*M*). This is because each symbol is allocated to the corresponding one slot among *M* slots. On the other hand, WDMA techniques assign each user certain wavelengths for upload and download links; accordingly, the more users allocated in the network, the more wavelengths must be assigned. In *M-ary* FSK-OCDMA, $\log_2 M$ encoded bits of data (symbol) are assigned to *M* frequencies (wavelengths) for all users as a result of *M-ary* source coding. Therefore, this brings the network higher spectral efficiency, no wavelength-assignment and fewer set of wavelengths [116].

Since the number of slots in a frame is independent of the number of symbols, the bit-rate of FSK does not decrease as the number of symbols increases. When the number of slots in a frame is γ (which corresponds to the repetition index of the tuneable laser), the bit-rate of *M-ary* FSK becomes M/γ ($\gamma < M$) times higher than that of *M-ary* PPM. Also, the probability of having interference for *M-ary* FSK is $1/M\gamma$, while the corresponding probability for *M-ary* PPM is $1/M$; hence, the probability of having interference can be mitigated by using FSK. Nevertheless, K. Iversen *et. al* [116] have studied an incoherent FSK-OCDMA and used OOC as spreading codes and found that the number of users was limited. Since systems without cancellation schemes have already been analysed and studied [34, 116, 117], we have focused on the transceivers with MAI cancellation as they have been less investigated lately and this novel MAI cancellation technique is part of our research contribution. In the following, the *M-ary* FSK-OCDMA system with the proposed MAI cancellation technique taking advantage of DPMPC is introduced and also the overall system performance in terms of BER is analysed.

7.2 FSK-OCDMA with MAI Cancellation: Coherent Modulation with Incoherent Demodulation

In this Section, we examine and derive BER of the FSK-OCDMA system with an interference canceller in which a reference signal contains no data component of the intended signal.

M-ary FSK allocates *M* symbols to the corresponding *M* wavelengths, whereas *M-ary* PPM allocates the symbols to the slot positions. Figure 7.1 shows *M-ary* FSK pulse

series with $M = 4$, where four wavelengths from λ_0 to λ_3 are assigned to contain 2-bit information such as *00, 01, 10* and *11*, respectively. γ is the repetition index which corresponds to the number of slots between two subsequent transmitted optical pulses by a tuneable laser as shown in Figure 7.1. For the optical source, we consider a step-tuneable mode-locked laser diode with 100 GHz repetition rate [118]. In other words, we have multi-wavelength steps switched with the speed of 100 GHz which makes the *M-ary* FSK modulation possible. On the other hand in the CDMA encoder block in Figure 7.2, a passive OTDL has been used and makes the CDMA encoding at incoming 100 GHz feasible [119].

We show in Section 7.4 when the number of symbols *M* is constant and γ becomes smaller, the bit-rate becomes higher, whereas the channel interference increases.

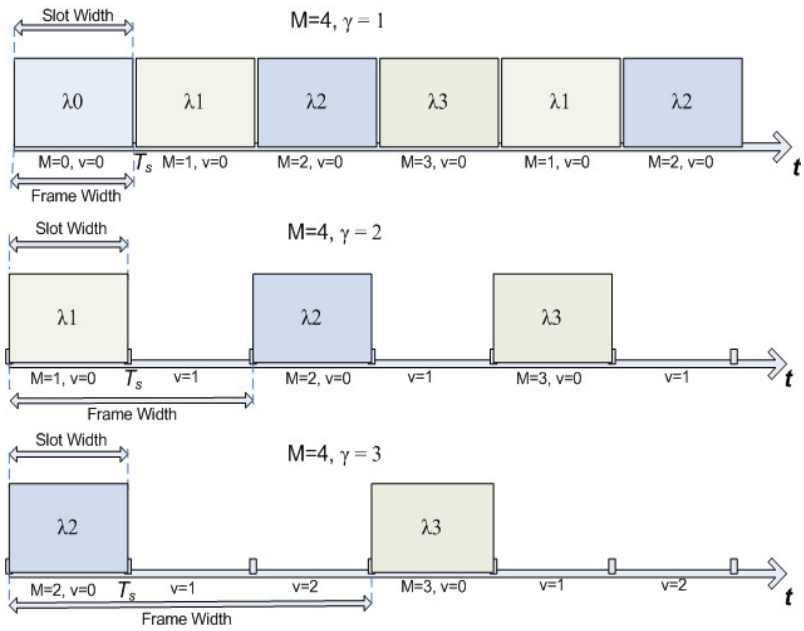

Figure 7.1 *M-ary* FSK signalling format with *M = 4* (T_s is the slot time)

As γ becomes larger, the bit-rate becomes lower; although, the channel interferences are reduced because the interrupted slots at each frame prevent interferences of in-phase correlation functions.

Figure 7.2 shows the transmitter block diagram of this FSK-OCDMA scheme. A frame consists of γ slots, and a slot consists of P^2+2P (code-length) chips. When γ is larger than one, one slot is selected for data transmission among γ slots in a frame. The subsequent data are placed on the same slot positions in the following frames. As shown in Figure 7.1, the data are placed on the desired slot in a frame, and then it is inputted to the tuneable laser diode encoder as in Figure 7.2. The tuneable laser emits the OP with a certain wavelength corresponding to the data at the certain chip positions in a slot came from coherent FSK modulator. Note that the OPs with other wavelengths are not emitted. The OP is time spread in the multiple chip positions corresponding to '1s' of the spreading code by the encoder consisting of OTDLs in CDMA encoder. Then, this desired user's signal is transmitted together with the signals of other users in the SPON.

The FSK-OCDMA with an MAI canceller is similar to the discussed PPM one with an interference canceller; however, the main difference is that only one of the DPMPC sequences which has data-free component of the desired signal is used as a reference signal, and the cancellation is performed by subtracting the reference signal from the received signal of the desired user at each wavelength. The 'one' reference signal is used to cancel the interference for all users. It is noted that, the total number of subscribers increases to P^2-1 as compared with the previously mentioned PPM scheme in Chapter 4, which were P^2-P. This also makes the system operation faster in that it

has to compare the received signal with only one reference than *P* references, and also makes the receiver's structure simpler in that OTDLs configurations in the reference branches are simplified into one instead of *P*.

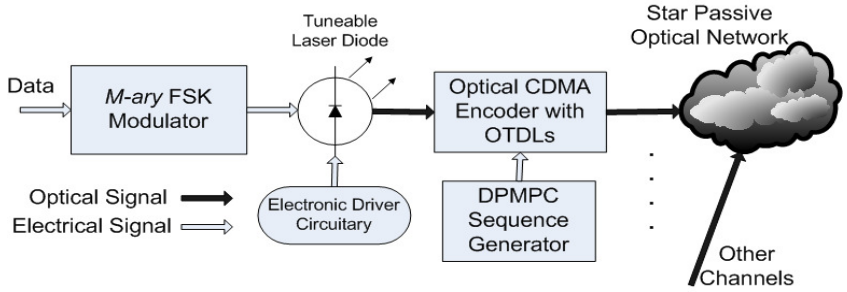

Figure 7.2 Structure of FSK-OCDMA transmitter

Here, we allocate the first spreading code sequence in the first group to the intended user (U_1), and use the P^{th} spreading code as a reference signal. co_1 and co_P denote as the corresponding optical correlators for the main and reference branches, respectively. Figure 7.3 shows the receiver block diagram of the FSK-OCDMA system with this interference canceller. The transmitted signal with *M* wavelengths on the SPON is separated incoherently into *M* signals with different wavelengths by arrayed-waveguide grating (AWG) demultiplexer [102]. Here, we assume the ideal AWG is used and that no interference between adjacent wavelengths occurs. The received signals are separated by *M* wavelengths and each is split into two parts passing through co_1 and co_P respectively. Here, the data of U_1 with wavelength λ_0 are assumed to be in slot 0. Thus, in slot 0 with other wavelengths, there are only interference components of other users in other groups except for group 1 due to the orthogonal sequences in each group. Other slots with λ_0, assigned to U_1, have the data component of U_1 and interference components. Now, since the main branch produces 'data + interference +

noise' and the reference branch produces 'interference + noise', the interference and noise can be cancelled out by subtracting the reference signal from the components of U_1 at all slots. Ideally, only the signal component of U_1 with wavelength λ_0 is kept in slot 0 and there are no components in the other slots. For the other wavelengths, there are no components in all slots, since U_1 has only components with λ_0. In practice, since the output of the photo-detectors (PD) follow the Poisson process, and the PDs used in the branches have the same characteristics, they add similar amount of thermal and shot-noises to the signals; accordingly, it can be assumed that the noises are also cancelled out after subtraction. The outputs of co_1 and co_P for wavelength λ_m and slot *v* are converted from optical signal to electrical signal through the PDs, and the outputs of co_1 and co_P are denoted as $Y_{m,v}(1)$, $Y_{m,v}(P)$, $m \in \{0,...,M-1\}$, $v \in \{0,...,\gamma-1\}$ respectively in Figure 7.3. Since we have focused on slot 0 and assigned λ_0 to U_1, hence *m* = 0 and *v* = 0. After the interference cancellation per wavelength, the signal with the highest power is selected by the maximum likelihood (ML) detector and then the corresponding data is obtained from the *M-ary* FSK detector unit.

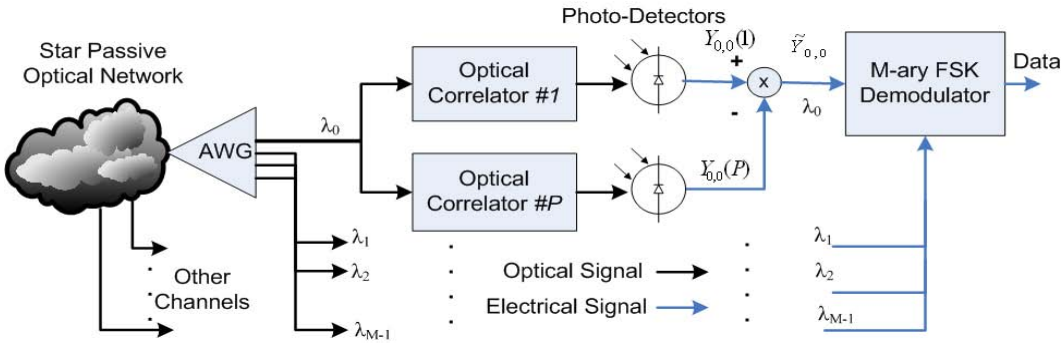

Figure 7.3 Structure of FSK-OCDMA receiver with MAI canceller

7.3 Analysis of *M-ary* FSK-OCDMA with MAI Cancelation

We derive the BER for the proposed FSK-OCDMA with MAI canceller using DPMPC as the spreading codes. Here, we assume that the I/O characteristic of the PD follows the Poisson process, i.e. the number of photons has Poisson distribution. The signal power of the desired user with λ_m in slot *v* and the reference signal, $Y_{m,v}(i),\ i \in \{1,\ P\}$ after PD as shown in Figure 7.3 is given as follows:

$$\begin{aligned} &Y_{m,v}(i) = Z_{m,v}(i) + I_{m,v}(i) \\ &m \in \{0,1,...,M-1\},\ v \in \{0,1,...,\gamma-1\} \end{aligned} \tag{7.1}$$

where $Z_{m,v}(i)$ is the user (data) signal power, and $I_{m,v}(i)$ is the interference power. Since the reference signal has only the reference (P^{th}) sequence multiplied by the received signal, the interference components of $Z_{m,v}(P)$ becomes 0 (i.e. data-free). Also, since all users in the same group receive an equal amount of interference from the users of other groups and no interference from the users from the same group, $I_{m,v}(1)$ equals $I_{m,v}(P)$. Here we assume that U_1 transmits the OP of λ_0 (m = 0) at the first slot (v = 0) in a signal frame as shown in Figure 7.1.

Since the DPMPC sequences are employed as signature codes, the cross-correlation between the first and x^{th} user, $C_{1,x}$, of the same group is equal to *zero*. Thus, *R* users $(0 \le R \le P-2)$ in the first group do not affect the photon count of the first user. The probability density function (PDF) of the random variable *R* is given by [51]:

$$\Pr\{R = r\} = \frac{\binom{P^2-2P+1}{K-r} \cdot \binom{P-2}{r-1}}{\binom{P^2-P-1}{K-1}} \tag{7.2}$$

where $r \in \{r_{\min},...,r_{\max}\}$, $r_{\max} = \min(K, P-1)$ and $r_{\min} = \max\left(1, K-(P-1)^2\right)$.

Here *K* refers to the number of simultaneous active users. Let us define the random variable $\kappa_{m,v}$ to be the number of users who are in groups other than the first group, and have a pulse in the v^{th} slot with wavelength λ_m. The probability that $l_{m,v}$ users have a pulse in the v^{th} slot with wavelength λ_m is $1/(M\gamma)$ and the probability of having no pulse is $1-1/(M\gamma)$ (recalling binomial distribution). Then, the PDF of $\kappa_{m,v}$ can be expressed as:

$$\Pr\{\kappa_{m,v} = l_{m,v} | R = r\} = \binom{K-r}{l_{m,v}} \cdot \left(\frac{1}{\gamma.M}\right)^{l_{m,v}} \cdot \left(1-\frac{1}{\gamma.M}\right)^{K-r-l_{m,v}} \tag{7.3}$$

When U_1 has an optical pulse with wavelength λ_m in the v^{th} slot $\left(b_{m,v}^1 = \{m,v\}\right)$ the expected value of the random variable $Z_{m,v}(i),\ i \in \{1,P\}$ is expressed as:

$$\overline{Z}_{m,v}(i) = \begin{cases} \dfrac{(P+2)\cdot Q \cdot T_c}{2} & if\ b_{m,v}^1 = \{m,v\} \\ 0 & otherwise \end{cases} \tag{7.4}$$

where T_c is the chip-duration. Taking the fibre attenuation coefficient α into account, the average number of received photon count per pulse Q can be expressed as [41]:

$$Q = \frac{\xi P_W}{hf} \cdot \frac{e^{-\alpha L}}{P+2} \approx \mu \cdot \frac{\ln M}{P+2} \tag{7.5}$$

where $P_r = \xi \cdot P_W \cdot e^{-\alpha L}$ is the received signal power, P_W is the transmitted peak power per symbol, ξ is the quantum efficiency of the PDs, *h* is Planck's constant, *f* is the optical frequency, *L* is the fibre-length, and μ ($\mu = P_r/(h \cdot f \cdot \ln M)$) is the average number of photons per pulse (photons/nat) [40]. The experimental values for these

parameters are listed in Table 7.1. The expected value of the random variable $I_{m,v}(i), i \in \{1, P\}$ can be expressed as:

$$\bar{I}_{m,v}(i) = l_{m,v} \cdot Q \cdot T_c \tag{7.6}$$

From 7.4 and 7.6, then the expected value of $Y_{m,v}(i)$, $i \in \{1, P\}$ is expressed as:

$$\bar{Y}_{m,v}(i) = \begin{cases} \dfrac{(P+2+l_{m,v}) \cdot Q \cdot T_c}{2} & b_{m,v}^1 = \{m, v\} \\ \dfrac{l_{m,v} \cdot Q \cdot T_c}{2} & otherwise \end{cases} \tag{7.7}$$

Table 7.1 Link parameters

Descriptions	Symbols	Values
Optical Wavelength	λ_0	1550 nm
PD Quantum Efficiency	ξ	0.8
Linear Fibre-Loss Coefficient	α	0.2 dB/Km
Chip-Rate	$1/T_c$	100 Gchips/s
Fibre Length	*L*	10 Km

In order to cancel the interference, the reference signal is subtracted from the U_1 signal and also as aforementioned, since both PDs have the same characteristics; the signals suffer from the same shot-noise which cancels out after subtraction. The subtracted signal $\tilde{Y}_{m,v}$ is then:

$$\tilde{Y}_{m,v} = \bar{Y}_{m,v}(1) - \bar{Y}_{m,v}(P) \tag{7.8}$$

Since U_1 has an OP with wavelength λ_0 at slot 0, the symbol-error occurs when $\tilde{Y}_{j,0}(1) \geq \tilde{Y}_{0,0}(1), (j \neq 0)$. Suppose P_E denotes the symbol-error rate, and then the BER (P_b) is expressed as [51]:

$$P_b \leq \frac{M}{2(M-1)} \cdot \sum_{r=r_{\min}}^{r_{\max}} P_E \cdot \Pr\{R = r\} \tag{7.9}$$

where:

$$\begin{aligned} P_E &= \sum_{j=0}^{M-1} \Pr\left\{\tilde{Y}_{j,0} \geq \tilde{Y}_{0,0} \middle| R=r, \kappa_{0,0}=l_{0,0},\ldots,\kappa_{M-1,0}=l_{M-1,0}, b_{m,v}^{1}=\{0,0\}\right\} \\ &\quad \times \Pr\left\{\kappa_{0,0}=l_{0,0}, \kappa_{1,0}=l_{1,0}, b_{m,v}^{1}=\{0,0\} \middle| R=r\right\} \\ &\leq (M-1) \sum_{l_{0,0}=0}^{K-r} \sum_{l_{1,0}=0}^{K-r-l_{0,0}} \Pr\left\{\tilde{Y}_{1,0} \geq \tilde{Y}_{0,0} \middle| R=r, \kappa_{0,0}=l_{0,0}, \kappa_{1,0}=l_{1,0}, b_{m,v}^{1}=\{0,0\}\right\} \\ &\quad \times \Pr\left\{\kappa_{0,0}=l_{0,0}, \kappa_{1,0}=l_{1,0}, b_{m,v}^{1}=\{0,0\} \middle| R=r\right\} \\ &\leq \sum_{l_{0,0}=0}^{K-r} \sum_{l_{l,0}=0}^{K-r-l_{0,0}} \Pr\left\{\kappa_{0,0}=l_{0,0}, \kappa_{1,0}=l_{1,0} \middle| R=r\right\} \times \Phi\left(r, l_{m,0}\right) \end{aligned} \quad (7.10)$$

and:

$$\Phi\left(r, l_{m,0}\right) = (M-1) \cdot \Pr\left\{\tilde{Y}_{1,0} \geq \tilde{Y}_{0,0} \middle| R=r, \kappa_{0,0}=l_{0,0}, \kappa_{1,0}=l_{1,0}, b_{m,v}^{1}=\{0,0\}\right\} \quad (7.11)$$

The upper-bounded $\Phi\left(r, l_{m,0}\right)$ is then given by [51]:

$$\Phi\left(r, l_{m,0}\right) \leq (M-1) \cdot E\left[z^{\bar{Y}_{1,0}(1)-\bar{Y}_{1,0}(P) \geq \bar{Y}_{0,0}(1)-\bar{Y}_{0,0}(P)} \middle| R=r, \kappa_{0,0}=l_{0,0}, \kappa_{1,0}=l_{1,0}, b_{m,v}^{1}=\{0,0\}\right] \quad (7.12)$$

where z ($z>1$ and integer) denotes the number of optical interference pulses in slot 0 and $E[\bullet]$ refers to the expected value, and by using the Chernoff bound $\Phi\left(r, l_{m,0}\right)$ can be expressed as [51]:

$$\ln\Phi\left(r, l_{m,0}\right) \leq -\ln(M-1) - \bar{Y}_{1,0}(1)(1-z) - \bar{Y}_{1,0}(P)(1-z^{-1}) - \bar{Y}_{0,0}(1)(1-z^{-1}) - \bar{Y}_{0,0}(P)(1-z) + \bar{Z}_{0,0}(1)(1-z) \quad (7.13)$$

Now, by setting $z-1=\rho$ ($\rho>0$ and integer) we have then $1-z^{-1} \leq 1$ while $\rho-\rho^2 \leq 0$, thus by considering new boundaries, we obtain this lower-bounded equation [51]:

$$1-z^{-1} \geq \rho-\rho^2 \quad (7.14)$$

By substituting 7.4, 7.7 and 7.14 into 7.13, we have:

$$\begin{aligned} \ln\Phi\left(r, l_{m,0}\right) \leq & -\ln(M-1) - \left(\frac{\left(P+2+l_{1,0}\right)QT_c}{2}\right)(-\rho) - \left(\frac{l_{0,0}QT_c}{2}\right)(\rho-\rho^2) \\ & - \left(\frac{\left(P+2+l_{1,0}\right)QT_c}{2}\right)(\rho-\rho^2) - \left(\frac{l_{0,0}QT_c}{2}\right)(-\rho) + \left(\frac{(P+2)QT_c}{2}\right)(-\rho) \end{aligned} \quad (7.15)$$

Then,

$$\ln \Phi\left(r, l_{m,0}\right) \le -\ln\left(M-1\right) + \left(\frac{\left(P+2+l_{1,0}+l_{0,0}\right)QT_c}{2}\right)\rho^2 - \left(\frac{(P+2)QT_c}{2}\right)\rho \qquad (7.16)$$

Now by minimizing the right-hand-side of the new equation with respect to ρ, we will have:

$$\rho = \frac{P+2}{P+2+l_{0,0}+l_{1,0}} \qquad (7.17)$$

By substituting ρ back into 7.16, we have the upper-bounded $\Phi\left(r, l_{m,0}\right)$ as:

$$\Phi\left(r, l_{m,0}\right) \le \left(M-1\right)\exp\left\{-\frac{Q\cdot(P+2)^2}{4\cdot\left(P+2+l_{0,0}+l_{1,0}\right)}\right\} \qquad (7.18)$$

Then, the upper-bound of symbol-error probability P_E in 7.10 is then rewritten as follows:

$$P_E \le \left(M-1\right)\cdot \sum_{l_{0,0}=0}^{K-r}\sum_{l_{1,0}=0}^{K-r-l_{0,0}} \Pr\left\{\kappa_{0,0}=l_{0,0}, \kappa_{1,0}=l_{1,0}, b_{m,v}^1=\{0,0\} \middle| R=r\right\} \cdot \exp\left\{-\frac{Q\cdot(P+2)^2}{4\cdot\left(P+2+l_{0,0}+l_{1,0}\right)}\right\} \qquad (7.19)$$

By substituting 7.3 into 7.19, and then substituting 7.3 and new 7.19 into 7.9, the total upper-bounded probability of error (P_b), depending on the number of active users (K), can be derived as:

$$P_b \le \frac{M}{2}\sum_{r=r_{\min}}^{r_{\max}}\sum_{l_{0,0}=0}^{K-r}\sum_{l_{1,0}=0}^{K-r-l_{0,0}}\binom{K-r-l_{0,0}}{l_{1,0}}\cdot\left(\frac{1}{\gamma.M}\right)^{l_{1,0}}\cdot\left(1-\frac{1}{\gamma.M}\right)^{K-r-l_{0,0}-l_{1,0}}\cdot\exp\left\{-\frac{\rho}{2}\cdot\frac{Q\cdot(P+2)}{2}\right\} \times\binom{K-r}{l_{0,0}}\cdot\left(\frac{1}{\gamma.M}\right)^{l_{0,0}}\cdot\left(1-\frac{1}{\gamma.M}\right)^{K-r-l_{0,0}}\times\frac{\binom{P^2-2P+1}{K-r}\cdot\binom{P-2}{r-1}}{\binom{P^2-P-1}{K-1}} \qquad (7.20)$$

7.4 Discussion of Results

In this section, the numerical results of the BER of the FSK-OCDMA receiver with the interference canceller are presented and discussed based on the theory presented in the previous section. The link parameters used in simulations are listed in Table 7.1. The numerical results are compared with those of PPM-OCDMA employed the DPMPC as the spreading codes in Section 4.4.2. The reference BER of 10^{-9} is also depicted in the Figures for better explanations.

Figure 7.4 shows the BER of FSK and PPM systems with the interference canceller against the average number of photons per pulse μ. In this analysis P = 13, M = 8, $\gamma = 1, 2, 3$ (as shown by j in the graphs). In this analysis we have assumed all interfering users are present i.e. full-load. It is observable that the FSK-OCDMA is more power efficient than PPM scheme, since the BER reaches to 10^{-9} under less average number of photons per pulse μ. On the other hand, repetition index can also enhance the FSK-OCDMA performance; for example at $\mu = 100$, the BER for FSK when $\gamma = 3$ is 4.7×10^{-11}, when $\gamma = 2$ it is 2.1×10^{-9} and 1.6×10^{-7} at $\gamma = 1$; while error-rate is 2.2×10^{-6} for PPM scheme.

Figure 7.5 also illustrates the bit-error probabilities against the number of simultaneous users K, for PPM and FSK receivers. It is clearly observed that the FSK scheme outperforms the PPM one especially for higher repetition index γ. The results indicate this hybrid FSK scheme (i.e. coherent modulation and incoherent demodulation) can mitigate the effect of interference much better. As aforementioned, in the PPM system, the optical pulse of the desired signal overlaps

with the pulse of any other user, having a probability of $1/M$. In contrast, in the FSK, the corresponding probability is reduced by a factor of γ (i.e. $1/(\gamma M)$).

When the repetition index γ becomes large, the probability of pulse overlap decreases and the performance is improved as indicated in Figures 7.4 and 7.5. The reason is that in the PPM the probability of having interference is reduced by increasing the number of slots (corresponding to the number of symbols) in the time domain. On the contrary, in the FSK the probability of having interference is reduced by using both number of wavelengths (corresponding to the number of symbols) and repetition index. When the chip-rate is constant, in order to decrease the probability of having interference in the PPM scheme, the number of slots has to increase, which results in larger frame-length and lower bit-rate.

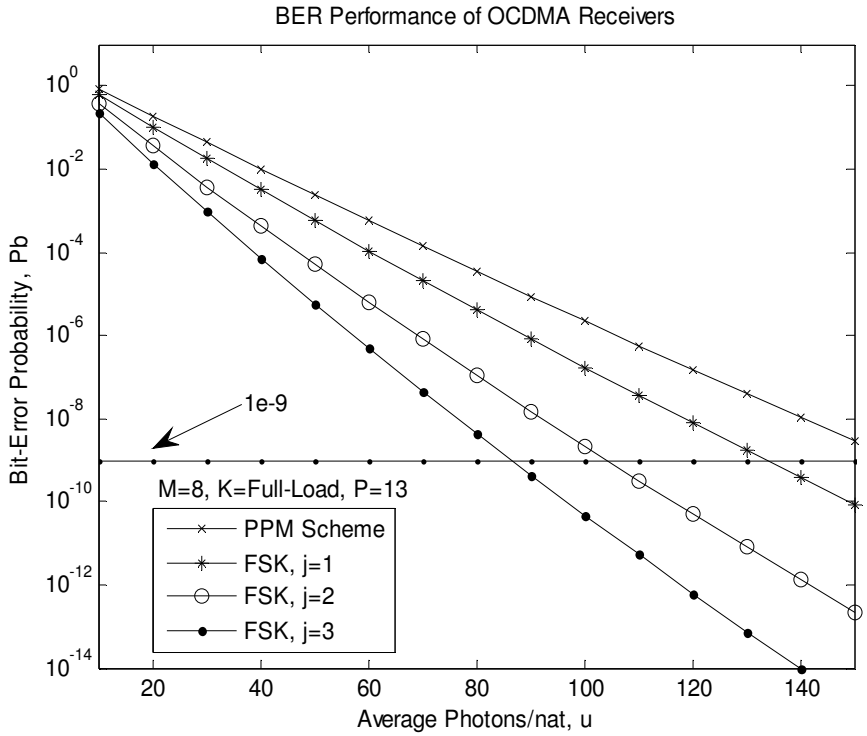

Figure 7.4 BER performances of PPM and FSK-OCDMA transceivers with MAI cancellation against the average no. of photons per pulse, μ

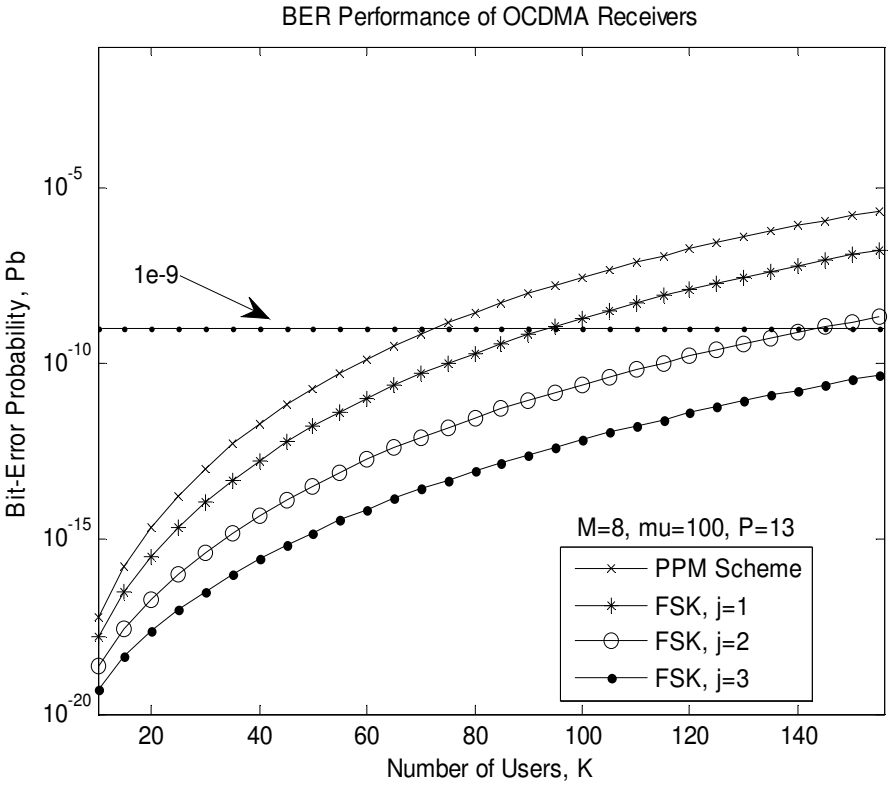

Figure 7.5 BER performances of FSK and PPM transceivers with MAI cancellation against the no. of simultaneous users, *K*

Alternatively, in the FSK scheme, the frame-length depends only on the repetition index which is smaller than *M* as shown in Figure 7.1. It is also shown in Figure 7.5 that the system capacity can be expanded by growth in repetition index γ.

By increasing the number of wavelengths *M*, the probability of having interference can therefore be further reduced in the FSK system with shorter frame-length than PPM; accordingly, FSK can attain higher bit-rate transmission than PPM. The bit-rates R_b, for FSK and PPM systems using DPMPC as spreading codes are rewritten as [40, 51]:

$$R_b = \frac{\log_2^M}{\gamma \cdot T_c \cdot (P^2 + 2P)}, \quad M - ary\ FSK - OCDMA \tag{7.21}$$

$$R_b = \frac{\log_2^M}{M \cdot T_c \cdot (P^2 + 2P)}, \quad M - ary\ PPM - OCDMA \tag{7.22}$$

Additionally, in the FSK the bit-rate decreases as the repetition index increases. For example, the bit-rates of FSK with $P=7,\ M=8,$ and $\gamma=2$ and 3 are 2.381 Gbps and 1.587 Gbps respectively; whereas, the bit-rate of PPM is 595.23 Mbps which is nearly 4 times slower. In other words, $R_{b-FSK}/R_{b-PPM}=M/\gamma$, where always $M>\gamma$.

Figures 7.6 and 7.7 illustrate the BER variations against μ, for both FSK and PPM systems as functions of multiplicity *M* and prime number *P* respectively. All users are assumed to be active in the communications. The results reveal that in the FSK system lower BER as well as higher bit-rate can be achieved as the number of symbols (*M*) increases, while in the PPM system the performance improves whereas the bit-rate decreases. As the number of symbols increases, the probability of having interference decreases, which leads to the improvement of the performance.

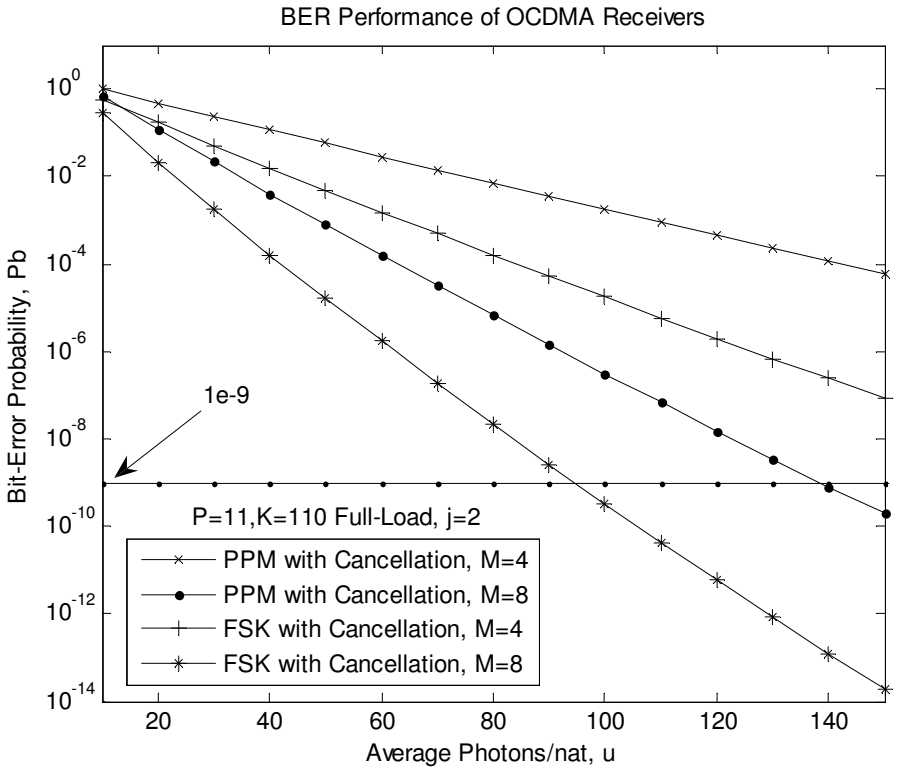

Figure 7.6 BER performances of FSK and PPM transceivers with MAI cancellation against the average no. of photons per pulse μ, with different multiplicities, *M*

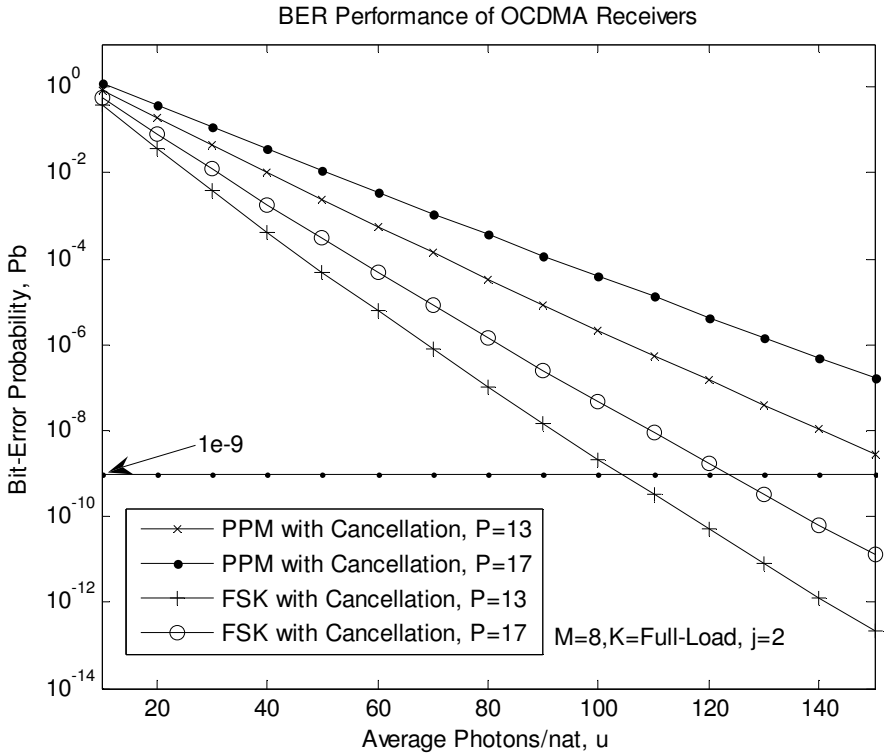

Figure 7.7 BER performances of FSK and PPM transceivers with MAI cancellation against the average no. of photons per pulse μ, with different prime numbers, P

As for the bit-rate, the number of FSK symbols is independent of the frame-length, while in the PPM the frame-length becomes larger as the number of symbols increases. As it can be seen from Figure 7.7, when P becomes larger, the performance is degraded due to the increase in the number of interfering users, and the bit-rate decreases due to the increase in the code-length which corresponds to the increase of frame-length. However, the number of simultaneous active users can be increased in both FSK and PPM systems by utilising the higher prime number P.

Figure 7.8 demonstrates the BER of different receivers with MAI canceller against the number of simultaneous active users K, with different multiplicities M. It is observable from Figure 7.8 that the network capacity can be increased by raising the multiplicity in both PPM and FSK schemes.

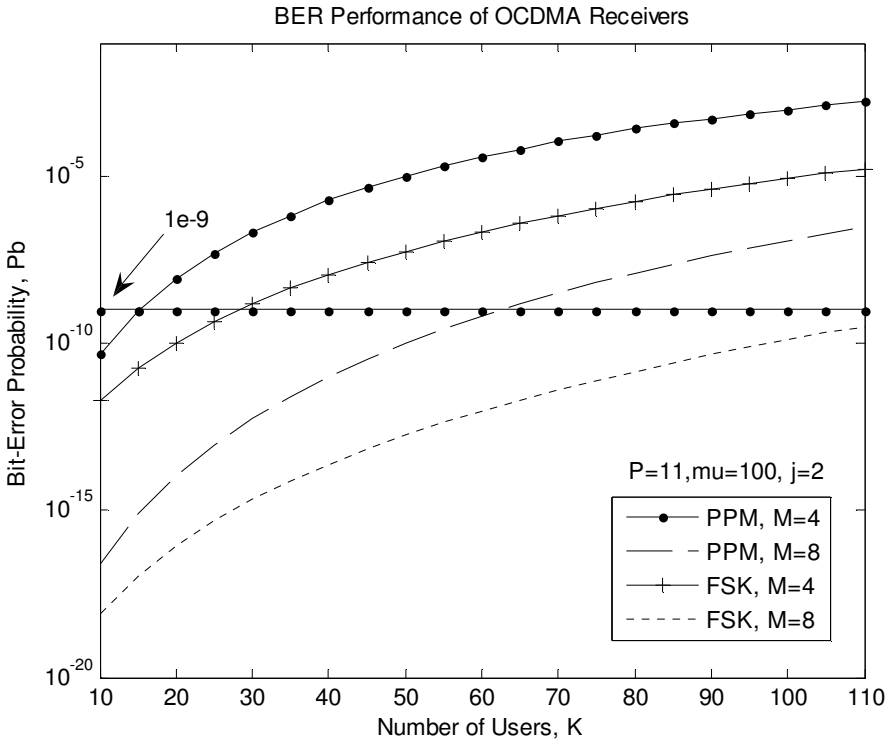

Figure 7.8 BER performances of FSK and PPM transceivers with MAI cancellation against the no. of simultaneous users *K*, with different multiplicities, *M*

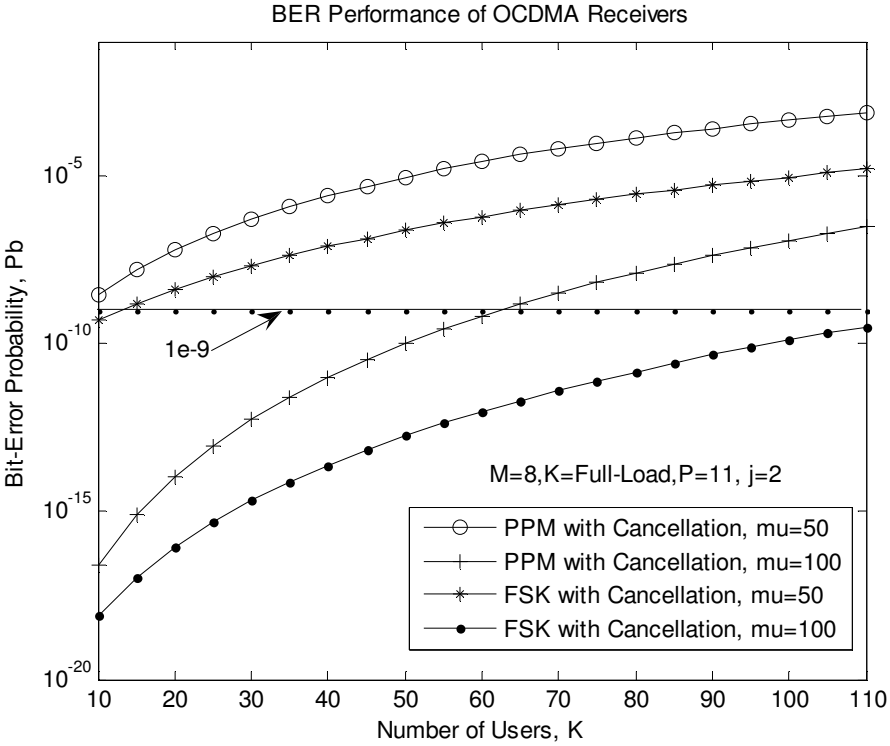

Figure 7.9 BER performances of FSK and PPM transceivers with MAI cancellation against the no. of simultaneous users *K*, with different average no. of photons per pulse, μ

It is clear that the FSK again outperforms; for example, assuming 55 users (50% of total number of users when *P* = 11) are present in the network, the error-rate of the FSK receiver where *M* = 4 and 8 is 1.2×10^{-7} and 4.2×10^{-13} respectively. While the error-rate for PPM receiver where *M* = 4 and 8 is 2×10^{-5} and 2.7×10^{-10} respectively. Figure 7.9 also displays the BER of different receivers with MAI canceller against the number of simultaneous active users *K,* with different average number of photons per pulse μ. As it can be seen, the higher received power makes the detection process more reliable due to elevating sufficient SNR that results in low error-rate and enhanced network capacity. For further examination, the PPM-OCDMA network can support 65 users at $BER = 10^{-9}$ where $\mu = 100$, while the total number of users (i.e. 110 users when *P* = 11) is accommodated with the FSK-OCDMA network under the same given condition.

7.5 Conclusion

A new interference cancellation technique taking advantage of DPMPC correlation properties, which simplifies the receiver structure in the synchronous *M-ary* FSK-OCDMA network, has been proposed and analysed. Coherent FSK modulation along with incoherent demodulation using arrayed-waveguide grating has been examined in the transceivers' structures. As the spreading codes, DPMPC has been considered. A reference signal is constructed by using one of the DPMPC sequences, and cancellation is performed by subtracting the reference signal from the received signal of the desired user. As a result, the cancellation technique along with FSK-OCDMA system, as compared with existing technique with PPM-OCDMA, has more enhanced performance (lower BER, higher bit-rate) under the same given conditions.

Additionally, the results indicated that the FSK scheme is very power efficient and when the bit-rate is constant its network capacity can be expanded to accommodate great number of simultaneous active users with low error-rate. It should be noted that the FSK-OCDMA architecture is more complex than incoherent PPM-OCDMA scheme since driving the tuneable laser diode is challenging; however, as a validation, this scheme has been published [P8, P9][1] as well as implemented and verified by OptiSystem™ a commercial optical communications software package [107].

[1] See 'List of Publications'

Chapter 8

Analysis of Polarization Modulation in OCDMA Network

8.1 Introduction

Polarization shift keying (PolSK) is the only modulation scheme that makes use of the vector nature of the lightwave. Like frequency shift keying (FSK), it is a multiple-array (*M-ary*) signalling transmission scheme, and unlike FSK the spectrum of a PolSK signal corresponds to an equivalent amplitude shift keying (ASK) signal at the same bit-rate [120].

When a polarized lightwave is transmitted through a single-mode fibre-optic (SMF), its state of polarization (SOP) changes due to the presence of waveguide birefringence. However the fibre birefringence only causes a rigid rotation of the lightwave's polarization constellation over the Poincaré sphere [121]. In other words, each signal point is displaced although the Stokes parameters illustrating the spatial relations

among signal points in Poincaré sphere are preserved. Thus, the information is not degraded. To compensate the constellation rotation, some forms of processing are required either optically by a polarization controlling and tracking or electronically by a digital signal processing (DSP) at the decision processor [122]. To perform PolSK detection avoiding optical birefringence compensation, it is necessary to use a receiver that extracts the Stokes parameters of the incoming lightwaves [48]. The receiver which extracts the Stokes parameters can be generally divided into two sections: (i) the optical front-end that probes the input electrical field and produces electric current at the output of its photo-detector (PD) and (ii) the following electrical front-end that generates the Stokes parameters which are proportional to the produced photocurrent. The polarized spreading codes have been considered to increase the number of accommodated users in [87, 123], since the polarization has been utilised to double the communication channel. However, here we employ the signal constellations in the polarization modulation as the information bearing to encode the data taking advantages of vector characteristic of lightwaves.

In this Chapter, we introduce a novel incoherent PolSK-OCDMA receiver which employs the optical correlators i.e. optical tapped-delay lines (OTDL) to simplify the architecture with more privileged performance than those mentioned in [45, 124] for direct-detection (DD) PolSK. Thus, the proposed PolSK-OCDMA transceiver does not require interferometer stability and the complicated DSP, although the polarization controller is needed here and it is very suitable for binary transmission as will be discussed. A comprehensive set of results in [125, 126] showed that the performance of the binary system is approximately 3 dB better than intensity modulation/DD (on

the peak optical power) of other PolSK or equivalent phase shift keying (PSK) modulations. Therefore, we have also considered binary PolSK for the proposed transceiver architecture.

Originally, PolSK was theoretically analysed [126, 127] mostly in conjunction with coherent-detection (CD). The early work on CD-PolSK has revealed that (i) the fibre birefringence does not corrupt polarization-encoded information and in particular the bit-error probability is relatively unaffected, (ii) birefringence compensation at the receiver is necessary, however it can be performed at the decision stage after photo-detection, (iii) binary PolSK has a 40 photons/bit quantum-limited sensitivity [124], whereas coherent ASK requires 80 photons/bit (peak) [128], (iv) PolSK systems are largely insensitive to phase noise [42, 87, 99, 122, 129], (v) for multi-level (*M-ary*) PolSK, quantum-limited performance is even better than differential-PSK when 3 bits/symbol or more are transmitted [125]. DD-OCDMA technique inherently suffers from MAI which requires estimation and removal through cancelation techniques or higher order modulations. In the past few years, advances in photonics technology (e.g. ultra-high-speed lasers, PDs and erbium-doped fibre amplifiers) made it possible for DD systems to approach the sensitivity performance of CD systems. Hence, there has been a considerable shift of interest from CD scheme to constant-power-envelope DD scheme on the part of both research and industry, due to its (i) simple architecture, (ii) cost effectiveness, (iii) high immunity to laser phase-noise, (iv) insensitivity to self- and cross-phase modulations caused by the fibre non-linearity [58, 130, 131].

On the other hand, FSK modulation is attributed with high phase noise insensitivity and high power efficiency. Therefore, it is required to develop an advanced modulation

scheme to take advantages of both modulations: FSK and PolSK. The advantages of FSK-OCDMA system has already been discussed in Chapter 7. Also the merits of hybrid frequency-polarization shift keying (F-PolSK) modulation has been introduced in [128, 132, 133] for the optical transmission.

Also in this Chapter, we propose a novel design structure for the OCDMA transceiver based on the two-dimensional array (*2D-ary*) hybrid F-PolSK modulation, which is based on the combination of both frequency and polarization modulations. This technique enhances distances between modulated signal points on the Poincaré sphere and hence reduces the required transmission power [126]. However, this advantage causes an increase in the transmission bandwidth requirement as a result of using multiple FSK tones. In our analysis we have assumed that the signal is degraded by (i) fibre amplified spontaneous emission (ASE) noise, (ii) electronic receiver noise and (iii) PD shot-noise and mainly (iv) multiple-access interference (MAI). In addition, the intensity-modulated systems are vulnerable in terms of interception, which could easily be broken by simple power detection, even without any knowledge of the code, whereas the security can improve significantly by using 2D advanced modulation (i.e. F-PolSK).

8.1.1 Polarization Shift Keying Fundamentals

Polarization shift keying (PolSK) transmission encodes information on a constellation of signal points in the space of the Stokes parameters. In general, each signal point corresponds to a given SOP and a given optical power. If only the polarization of the lightwave is modulated, and not its power, all the signal points lie on the Poincaré

sphere. Examples of such signal constellations are shown in Figure 8.1. In this Chapter we will restrict to constellations of equal power signal points.

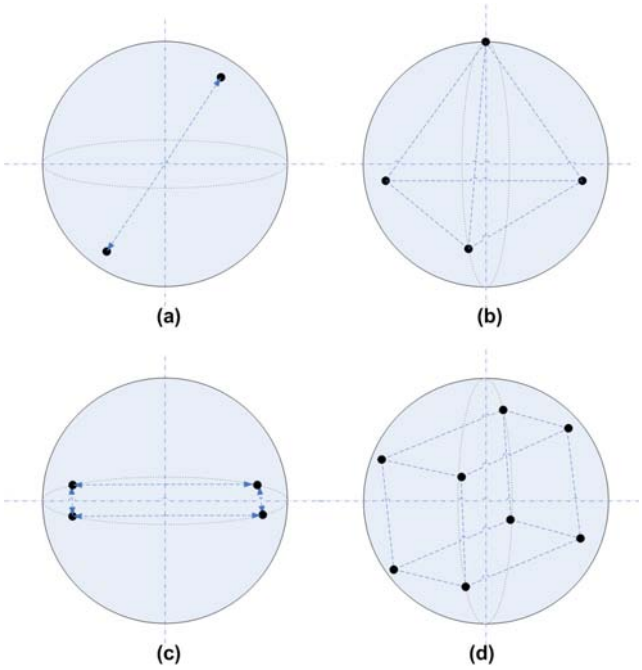

Figure 8.1 Signal-points constellation for multi-array PolSK inscribed into Poincaré sphere (a) binary-PolSK (b) quad-PolSK at the vertices of a tetrahedron (c) quad-PolSK on a maximum circle of the Poincaré sphere (d) 8-PolSK at the vertices of a cube

The SOP of a fully polarized lightwave can be described through the Stokes parameters. Given a reference plane $(\bar{x}, \bar{y})$ normal to the *z* propagation axis of an electromagnetic field, the expression of them is as follows [121]:

$$\begin{aligned} E_x &= a_x(x,y)e^{j(\omega t+\phi_x(t))} \\ E_y &= a_y(x,y)e^{j(\omega t+\phi_y(t))} \\ \overline{E} &= E_x\bar{x} + E_y\bar{y} \end{aligned} \tag{8.1}$$

The Stokes parameters can be calculated as:

$$\begin{aligned} S_1 &= a_x^2 - a_y^2 \\ S_2 &= 2a_x a_y Cos(\delta) \\ S_3 &= 2a_x a_y Sin(\delta) \end{aligned} \tag{8.2}$$

where $\delta = \phi_x - \phi_y$. The dependence on time of the parameters has been omitted for notation simplicity throughout the analysis in all unambiguous cases.

In classical optics, an average is generally taken from the quantities appearing in the right-hand-side of 8.1 which have been utilised to define instantaneous values for the Stokes parameters. The fourth Stokes parameter is also defined as:

$$S_0 = a_x^2 + a_y^2 = S_1^2 + S_2^2 + S_3^2 \tag{8.3}$$

This represents the total electromagnetic power density travelling in the *z*-axis.

The S_i can also be demonstrated in three-dimensional space with vectors $(\bar{s}_1, \bar{s}_2, \bar{s}_3)$, called *Stoke space*. The waves with the same power density $\bar{S}$ lies on a sphere of radius S_0, called *Poincaré Sphere* shown in Figure 8.1 with different signal constellations.

A fundamental feature of this demonstration is that the orthogonal SOPs, according to the Hermitian scalar product of:

$$\left\langle \bar{E}_1 . \bar{E}_2^* \right\rangle = a_{1x}(x,y) \cdot a_{2x}^*(x,y) \cdot a_{1y}(x,y) \cdot a_{2y}^*(x,y) \cdot e^{j(\omega t + \phi_1)} \cdot e^{-j(\omega t + \phi_2)} \tag{8.4}$$

will map onto the points which are antipodal on the Poincaré sphere [121].

A generic transformation of the SOP of a fully polarized lightwave, propagating along the *z-axis* which preserves the degree of polarization, is explained below. Let $\bar{E}$ and $\bar{E}'$ be the electromagnetic field vectors before and after the transformation (i.e. modulation) respectively. Their associated decompositions can be expressed as:

$$\begin{aligned} E_x(t) &= a_x(t) e^{j(\omega t + \Phi_x)} & \qquad E'_x(t) &= a'_x(t) e^{j(\omega t + \Phi'_x)} \\ E_y(t) &= a_y(t) e^{j(\omega t + \Phi_y)} & \qquad E'_y(t) &= a'_y(t) e^{j(\omega t + \Phi'_y)} \end{aligned} \tag{8.5}$$

where ω is the optical angular frequency, a_x, a_x' and a_y, a_y' are the amplitudes of *x* and *y* components, Φ_x, Φ_x' and Φ_y, Φ_y' are the phase of *x* and *y* components before and after the transformation respectively. The electric field vectors are given then by:

$$\overline{E}(t) = E_x(t)\overline{x} + E_y(t)\overline{y} \quad , \quad \overline{E}'(t) = E_x'(t)\overline{x}' + E_y'(t)\overline{y}' \tag{8.6}$$

where $\overline{x}, \overline{y}$ and $\overline{x}', \overline{y}'$ are the transverse reference axis sets before and after the transformation, respectively (i.e. normal to the direction of propagation). Thus, we have:

$$\begin{bmatrix} E_x'(t) \\ E_y'(t) \end{bmatrix} = \mathbf{Q} \begin{bmatrix} E_x(t) \\ E_y(t) \end{bmatrix} \tag{8.7}$$

where **Q** is a complex Jones matrix with unit determinant. A subset of Jones matrices, called the set of matrices of birefringence or optical activity that not only preserves the degree of polarizations, but also has the additional feature of preserving two orthogonal fields (according to the Hermitian scalar product [121]) which were orthogonal before the transformation [122]. Matrices of this kind are complex unitary matrices with unit determinant. Throughout this Chapter we strictly refer to the $\mathbf{J}_j$ as subset of $\mathbf{Q} = [\mathbf{J}_0 \quad \ldots \quad \mathbf{J}_j \quad \ldots \quad \mathbf{J}_{k-1}]$.

By using the Jones notation, the field can be represented by the vector, $\mathbf{J} = [E_x \quad E_y]^T$ and the intensity of the beam can be normalized so that $|E_x|^2 + |E_y|^2 = 1$. Two SOPs represented by $\mathbf{J}_1$ and $\mathbf{J}_2$ are orthogonal if their inner product is *zero*, i.e. $\mathbf{J}_1^H \cdot \mathbf{J}_2 = E_{1x}^* \cdot E_{2x} + E_{1y}^* \cdot E_{2y} = 0$ where *H* is the Hermitian. Any SOP can be transformed into another by multiplying it by Mueller matrices. A list of Mueller matrices that is required for SOP processing can be found in [121, 126].

8.2 PolSK-OCDMA Transceiver Architecture

8.2.1 Signals and System Configuration

A binary PolSK constellation is made up of two points that are antipodal over the Poincaré sphere. If the diameter on which they lie is made to coincide with one of the Stokes axes, then the knowledge of only one of the Stokes parameter is sufficient to demodulate the signal without incurring any penalty [48]. The receiver model in Figure 8.2 extracts only one Stokes parameter and hence it is suitable only for binary systems. Its optical and electronic front-end are remarkably simple but it does require an optical polarization controller to ensure that the axis of the binary constellation is aligned with the Stokes parameter axis at the input of the receiver. It can be seen from Figure 8.2, an optical filter is placed at the input of the receiver to reduce the received ASE noise. For both technical and practical reasons (e.g. minimizing the laser phase-noise or chirp) the bandwidth of this filter (B_o) should be generally wider than a matched filter whose noise bandwidth would be equal to the symbol-rate [120]. In order to reduce the penalty caused by (i) using a wider filter bandwidth and (ii) electrical noise, a tight low-pass filter (LPF) is placed after the polarization-demodulated signal as shown in Figure 8.2. This technique is also widely used in amplified intensity modulated systems [128]. The LPF is assumed to be an integrate-and-dump filter of integration time T_s (i.e. symbol duration) whose bandwidth is $B_{el} = 1/T_s$. For binary systems the bit and the symbol duration coincide, however here every bit is also CDMA encoded at T_c chip duration.

By assuming the complex-envelope representation of band-pass signals, the electric field at the transmitter output in Figure 8.3, can be written as:

$$\overline{E}_t = \sqrt{2P_t} \cdot \begin{pmatrix} e_x \\ e_y \end{pmatrix} \tag{8.8}$$

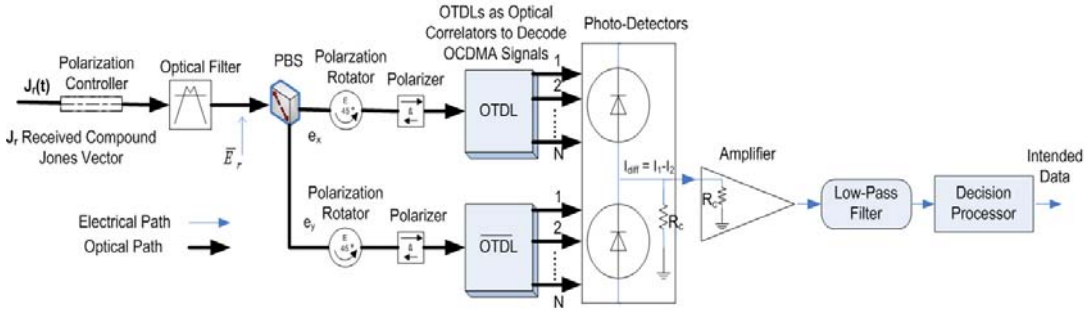

Figure 8.2 Architecture of incoherent PolSK-OCDMA receiver with OTDL

where P_t is the transmitted optical power launched into the fibre and e_x and e_y represent the $(\hat{x},\ \hat{y})$-components of the signal with respect to two orthogonal linear fibre polarizations normalized in such a way that $|e_x|^2 + |e_y|^2 = 1$. They form a vector called Jones vectors shown in Figure 8.3 where the corresponding Stokes parameters $\overline{S} = (S_1, S_2, S_3)$ are derived from them and satisfies the equality $|\overline{S}|^2 = 1$. A vector in the Stokes space $\overline{S}$ is defined as the vector linking the origin to the point (S_1, S_2, S_3) unless otherwise specified. The signal at the output of the optical filter at the receiver, in Figure 8.2, is given by:

$$\overline{E}_r = \sqrt{2P_r} \cdot \begin{pmatrix} e_x \\ e_y \end{pmatrix} + \begin{pmatrix} n_x \\ n_y \end{pmatrix} \tag{8.9}$$

where P_r is the received power and n_x and n_y are complex Gaussian random variables accounting for the total filtered ASE noise with the variance of:

$$\sigma_{ASE}^2 = 2N_0 B_o \tag{8.10}$$

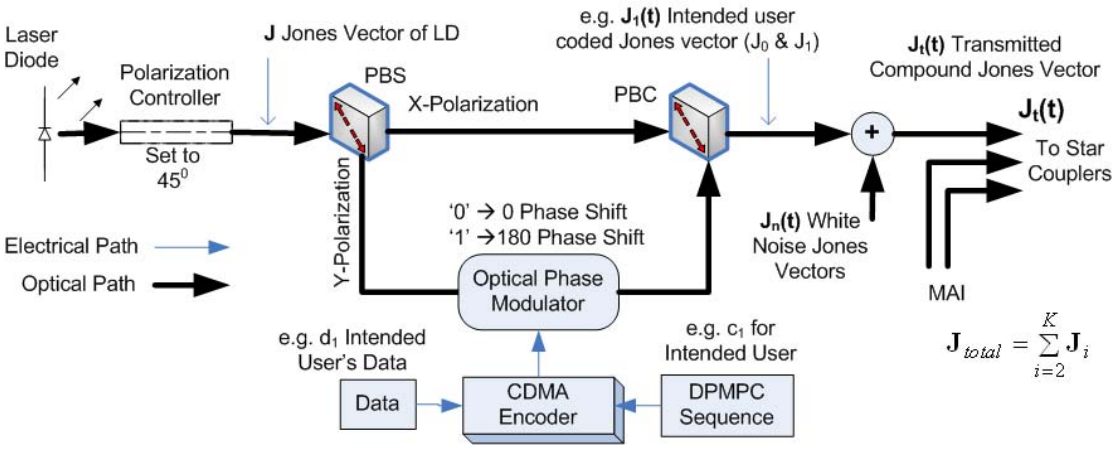

Figure 8.3 Architecture of incoherent PolSK-OCDMA transmitter

where N_0 is the power spectral density (PSD) of the white ASE noise and B_o is optical filter bandwidth. The apparent doubling of the overall ASE noise is due to the complex envelope notation adopted here. The power of the information signal is doubled as well, so that the optical signal-to-noise ratio (SNR) is preserved. As shown in Figure 8.2, the signal $\overline{E}_r$ passes through a polarization beam splitter (PBS) that divides the two linear $\hat{x}$ and $\hat{y}$ polarizations. These signals are subsequently CDMA-decoded through OTDLs and then photo-detected and the following corresponding currents are generated at the outputs of photo-detectors (PD) for decision rule:

$$I_x = \Re \cdot P_r \cdot |e_x|^2$$
$$I_y = \Re \cdot P_r \cdot |e_y|^2 \qquad (8.11)$$

where $\Re = e\eta / hf$ is the responsivity of PD, η is the quantum efficiency of PD ($\eta = 0.9$), h is the Planck constant, f is the optical frequency (λ *=1.55 μm*). Hence, the current I_{diff} at the input of the LPF (after amplifier) is:

$$I_{diff} = \Re \cdot P_r \cdot (|e_x|^2 - |e_y|^2) \qquad (8.12)$$

which is proportional to the Stokes parameter S_1 and as aforementioned it is suitable for binary transmission. Since it extracts only one of the Stokes parameters, this remarkably simplifies the receiver structure. It is assumed, as shown in Figure 8.2, that the PD internal load is matched to the input resistance of the electronic amplifier (R_c). Hence, the output of the final integrate-and-dump LPF can be expressed as:

$$I = \Re \cdot P_r \cdot \left(\left| e_x \right|^2 - \left| e_y \right|^2 \right) * h_{LP}(t) + n_{LP}(t) \tag{8.13}$$

where $h_{LP}(t)$ is the impulse response of the electronic LPF and $n_{LP}(t)$ is a zero-mean Gaussian random variable that represents the receiver noise current with the following variance:

$$\sigma_{LP}^2 = \frac{2kT}{R_c} \cdot B_{el} \cdot F \tag{8.14}$$

where *F* is the noise-figure of the electronic amplifier, T and *k* denote the absolute temperature and the Boltzmann constant respectively. Apart from temperature, the fundamental parameter characterizing the electronic stage of the receiver is the ratio F/R_c . It is noticeable that the thermal noise power on the detected current is doubled if we would place one amplifier after each PD before the subtraction node. Under the hypothesis that the LPF bandwidth is large enough to avoid phase-to-amplitude noise conversion, phase noise is cancelled out within the nonlinear receiver stage extracting the Stokes parameters from currents (i.e. decision processor in Figure 8.2). The only side effect is the bandwidth enhancement of the noise passing through the LPF. This impairment can be almost completely recovered through the use of a post-detection filter, similar to the one used in ASK or FSK schemes [125, 126].

8.2.2 Decision Rule Analysis at PolSK-OCDMA Receiver

In PolSK, the angle of one polarization component is switched relative to the other between two angles; therefore, binary data bits are mapped into two Jones vectors. A block diagram of the proposed PolSK-OCDMA transmitter is illustrated in Figure 8.3. The light source is a highly coherent laser with a fully polarized SOP. If a non-polarized source is used, then a polarizer can be inserted after the laser source. The light beam first passes through the polarization controller that sets the polarization to an angle of $45°$; since the laser phase noise is minimal at this polarization and component's polarization matching (e.g. polarizer, polarization controller and rotator) at this angle is simpler [99, 115, 123]. Then, the lightwave is divided through PBS to become SOP-encoded in PolSK modulator which switches the SOP of the input beam between two orthogonal states, that is referred to $0°$ and $180°$ at the phase modulator, *N* times per bit according to an externally supplied code (i.e. DPMPC) that spreads the optical signal into CDMA format. Thereafter, the PolSK-OCDMA modulated signals are combined through polarization beam combiner (PBC) and transmitted. As displayed in Figure 8.3, for a *K*-user system with the first user as the desired one (for example), the i^{th} user SOP-encoded signal can be written as:

$$\mathbf{J}_i(t) = \begin{cases} \mathbf{J}_0 & if\ \ d_i(t) \oplus c_i(t) = 0 \\ \mathbf{J}_1 & if\ \ d_i(t) \oplus c_i(t) = 1 \end{cases} \tag{8.15}$$

where $d_i(t) = \sum_{j=0}^{D-1} d_{i,j} \cdot u_T(t - jT_s)$ is the data signal with *D* bits (i.e. the data-length with symbol duration of T_s), $c_i(t) = \sum_{j=0}^{N-1} c_{i,j} \cdot u_T(t - jT_c)$ is the code sequence signal with *N* chips (i.e. the code-length with chip duration of T_c) and $d_i(t), c_i(t) \in \{0,1\}$, furthermore $u_T(t)$ denotes a unity rectangular pulse of width *T*, and $\oplus$ denotes the

signal correlation. As the emitted light is initially (linearly) polarized at an angle of $45°$, therefore $\mathbf{J}_0 = \frac{1}{\sqrt{2}}[1 \quad 1]^T$ and $\mathbf{J}_1 = \frac{1}{\sqrt{2}}[-1 \quad 1]^T$ [123]. In other words, we have:

$$\mathbf{Q} = [\mathbf{J}_0 \quad \mathbf{J}_1] = \frac{1}{\sqrt{2}}\begin{bmatrix} 1 & -1 \\ 1 & 1 \end{bmatrix} \tag{8.16}$$

Therefore, the polarization-modulated signal travels a distance of *L* km through an optical SMF. Consequently, the SOP-encoded signal undergoes several impairments such as attenuation, dispersion, polarization rotation and fibre nonlinearity. The polarization rotation can be compensated by polarization tracking and control system, as discussed in [134], that also suppresses the polarization mode dispersion (PMD) as well as rotation, although this will bring complexity to the structure and extra implementation cost. Instead, at this receiver end shown in Figure 8.2, the SOP rotation is compensated by the polarization controller, rotators and polarisers whose functions are to ensure the received signal and the optical components at the receiver to have the same SOP reference axis. Hence, we have the received signal Jones vector $\mathbf{J}_r(t)$; containing the data from desired user $\mathbf{J}_1(t)$ generated at the transmitter and corrupted by other users' transmissions $\sum_{i=2}^{K}\mathbf{J}_i(t)$ (i.e. MAI) plus additive Gaussian white noise (AWGN) as follow:

$$\mathbf{J}_r(t) = \begin{bmatrix} E_{rx} \\ E_{ry} \end{bmatrix} = \mathbf{J}_1(t) + \sum_{i=2}^{K}\mathbf{J}_i(t) + \mathbf{J}_n(t) \tag{8.17}$$

where $\mathbf{J}_n(t) = [E_{nx} \quad E_{ny}]^T$ is the complex Jones vector of the AWGN. In Figure 8.2, it is assumed that the received composite signal undergoes a lossless split after PBS. Thereafter, the signals in the both branches are rotated through the polarization

rotators by $45°$ in order to align the output beam's polarization to the polarizer axis. The polarizer passes only the optical beam matched to its axis; it performs like a polarization filter. Then, the signals are optically correlated through OTDLs. The OTDLs are tuned to the intended user's assigned spreading code to de-spread the CDMA-encoded signals (i.e. OCDMA-decoder). The upper and lower branches signals are presented by $(.)^0$ and $(.)^1$ notation respectively. Therefore, Jones vectors representing the upper and lower branches at the output of the PBS can be expressed as:

$$\mathbf{J}_{PBS}^{z}(t)=\begin{bmatrix} E_{rx} \\ \left|E_{ry}\right|\exp\left[j(\arg(E_{ry})+x_z\pi\right] \end{bmatrix} \tag{8.18}$$

where $z\in\{0,1\}$ denotes upper or lower branch, thus $x_0=c_1$, $x_1=\bar{c}_1$ (complement of c_1) and $\arg(.)$ denotes the phase of E_{ry}. Then, the Jones vectors are applied into the rotators. The function of rotator's Jones vectors is given as:

$$\mathbf{J}_{R}^{z}(t)=\frac{1}{\sqrt{2}}\begin{bmatrix} 1 & 1 \\ -1 & 1 \end{bmatrix}\cdot\mathbf{J}_{PBS}^{z}(t) \tag{8.19}$$

Then the polarizers (i.e. polarization filters) produce only the *x*-polarization at their output corresponding to the first elements of the Jones vector and only allow the signal with assigned polarization to pass. Hence, we have:

$$\mathbf{J}_{P}^{z}(t)=\begin{bmatrix} E_{Rx}^{z} & 0 \end{bmatrix}^{T} \tag{8.20}$$

The output of each polarizer is then:

$$\mathbf{J}_{P}^{z}(t)=E_{Rx}^{z}=\frac{1}{\sqrt{2}}\left\{E_{rx}+\left|E_{ry}\right|\cdot\exp[\,j(\arg(E_{ry})+x_z\pi)]\right\} \tag{8.21}$$

$\mathbf{D}^{z}$ is defined as the decision variable from which the polarizers decision rules can be obtained by:

$$\mathbf{D}^z = \left|E_{Rx}^z\right|^2 = E_{Rx}^z \cdot E^{*z}_{Rx} \tag{8.22}$$

After substituting, it can be written as:

$$\mathbf{D}^z = \frac{1}{2}\left\{E_{rx} + \left|E_{ry}\right|\exp[j(\arg(E_{ry}) + x_z\pi)]\right\} \times \left\{E_{rx}^* + \left|E_{ry}\right|\exp[-j(\arg(E_{ry}) + x_z\pi)]\right\} \tag{8.23}$$

And it can be expanded to:

$$\mathbf{D}^z = \frac{\left|E_{rx}\right|^2 + \left|E_{ry}\right|^2}{2} + \left|E_{rx}\right| \cdot \left|E_{ry}\right| \cdot \cos(\phi + x_z\pi) \tag{8.24}$$

where $\phi = \arg(E_{ry}) - \arg(E_{rx})$. The decision variable **D** is the difference between the upper and lower branch outputs which is given by:

$$\mathbf{D} = \int_0^{T_s}\left|E_{Rx}^1\right|^2 dt - \int_0^{T_s}\left|E_{Rx}^0\right|^2 dt = \int_0^{T_s}(\mathbf{D}^1 - \mathbf{D}^0)dt \tag{8.25}$$

Finally, the decision rule $\tilde{d}$ is defined as below in order to extract the final bit value from the modulated signal:

$$\tilde{d} = \begin{cases} 0 & if \quad \mathbf{D} < 0 \\ 1 & if \quad \mathbf{D} \geq 0 \end{cases} \tag{8.26}$$

8.2.3 PolSK-OCDMA Signal Processing

We previously discussed the configuration of the transceiver. Now we consider the alignment and analysis of the received optical signal. The electric field of the received polarization-modulated optical signal can be expressed as [124]:

$$\overline{E}'(t) = \mathrm{Re}\left\{\overline{E}(t) \cdot \sum_{i=1}^{K}\mathbf{Q} \cdot \begin{bmatrix} d_i(t) \\ 1 - d_i(t) \end{bmatrix} \cdot u_T(t - iT_s) \cdot c_i(t)\right\} \tag{8.27}$$

The channel is represented by the Jones matrix $\mathbf{Q}$ and $\mathrm{Re}\{\bullet\}$ refers to the real part of complex $\overline{E}'(t)$. Equi-power signal constellations have been considered through out our

analysis in this Chapter. That is, we have assumed both orthogonal components have the same power and equally attenuated and dispersed as they travel the same distance in the fibre and suffer from the same noise sources. Because the two polarizations are orthogonal (i.e. reciprocal), the electric field $\overline{E}(t)$ will have a constant amplitude. It has also been discussed in details [122] that the loss in the orthogonality in any linear optical medium is related to the transferred maximum and minimum power coefficients and a bound on this loss is calculated from these coefficients. In this analysis as the power coefficients are clarified later (i.e., 8.35), the orthogonality is therefore preserved with equality as a result of (*x,y*)-components equi-power constellations. While switching time in SOP (i.e. bit-rate) is much slower than the chip-rate, the elements of the Jones matrix can be understood as time-independent (i.e. $T_c << T_s$). The *x*-component of the received electric field vector based on $\mathbf{Q} = [\mathbf{J}_0 \quad \mathbf{J}_1]$ (i.e., 8.16) becomes:

$$E'_x(t) = \mathrm{Re}\left\{ \overline{E}(t) \cdot \sum_{i=1}^{K} \left[\mathbf{J}_0 \cdot d_i(t) + \mathbf{J}_1 (1 - d_i(t)) \right] \cdot u_T(t - iT_s) \cdot c_i(t) \right\} \tag{8.28}$$

Thus, orthogonal components of the *i*th user are given as $E_{xi}(t) = \mathbf{J}_0 \cdot d_i(t) \cdot c_i(t) \cdot \overline{E}(t)$ and $E_{yi}(t) = \mathbf{J}_1 \cdot (1 - d_i(t)) \cdot c_i(t) \cdot \overline{E}(t)$ and the *(x,y)*-components of received modulated PolSK-OCDMA signal are [124]:

$$\begin{aligned} E'_{xi}(t) &= \left(\frac{E_{xi}(t) + E_{yi}(t)}{2} + \sum_{i=1}^{K} c_i(t) \cdot d_i(t) \cdot \frac{E_{xi}(t) - E_{yi}(t)}{2} \cdot u_T(t - iT_s) \right) \cdot \cos(\varphi_{xi}) \\ E'_{yi}(t) &= \left(\frac{E_{xi}(t) - E_{yi}(t)}{2} + \sum_{i=1}^{K} c_i(t) \cdot d_i(t) \cdot \frac{E_{xi}(t) + E_{yi}(t)}{2} \cdot u_T(t - iT_s) \right) \cdot \cos(\varphi_{yi}) \end{aligned} \tag{8.29}$$

where φ_{xi} and φ_{yi} describe the frequencies and phases of transmitting lasers in a general form of $\varphi = \omega \mathrm{t} + \theta$. Based on the concept of OCDMA, the field vectors of all *K*

transmitters are added up and transmitted (i.e. multiplexed) over the same channel. Thus, the overall channel field vector can be expressed as:

$$\overline{E}_{Channel} = \sum_{i=1}^{K} \overline{E}_i'(t) \tag{8.30}$$

Figure 8.2 illustrates the application of the OTDLs as the optical correlator in incoherent PolSK-OCDMA. They correlate the incoming signal with pre-reserved user assigned spreading code to despread the signal. In doing so, the time delays and coefficients in OTDLs are designed to perform as a correlator in both branches. Additionally, OTDL in lower branch is set up with complement of code (i.e. 180 degree phase difference) used in upper branch (i.e. shown by $\overline{\mathbf{OTDL}}$ in Figure 8.2) to decode other symbol (i.e. '1'). As can be observed from Figure 8.2, OTDLs output contain *N* chip pulses that can be assumed as a parallel circuit of many single PDs so that their currents are added and no interference between the pulses is possible. The signals are photo-detected in the balanced-detector format to generate the differential electrical current ($I_{diff} = I_1 - I_2$) ready for data-extraction in decision processor. The individual branch current at a certain chip time T_c in upper branch (i.e. *x*-component) after photo-detection is:

$$I_n^0 = \Re \int_{t=0}^{T_c} \left(\sum_{i=1}^{K} \left(\frac{E_{xi}(t) + E_{yi}(t)}{2} + d_i(t) \cdot c_i(t - nT_c) \cdot \frac{E_{xi}(t) - E_{yi}(t)}{2} \right) \cdot \cos(\varphi_{xi}) \right)^2 dt \tag{8.31}$$

where $\Re$ is responsivity of the PD, $c_i(t - nT_c)$ is the n^{th} chip of assigned spreading code of the i^{th} user. Hence, the total current in upper branch is:

$$I^0 = \Re \int_{t=0}^{T_s} \sum_{n=1}^{N} \left\{ \frac{c(nT_c)+1}{2} \left(\sum_{i=1}^{K} \left(\frac{E_{xi}(t) + E_{yi}(t)}{2} + d_i(t) \cdot c_i(t - nT_c) \cdot \frac{E_{xi}(t) - E_{yi}(t)}{2} \right) \cdot \cos(\varphi_{xi}) \right)^2 \right\} dt \tag{8.32}$$

It can be rewritten as:

$$I^0 = \frac{\Re}{4}\int_{t=0}^{T_s}\sum_{n=1}^{N}\left\{\frac{c(nT_c)+1}{2}\left(\sum_{i=1}^{K}\left(E_{xi}^2(t)+E_{yi}^2(t)+d_i(t)\cdot c_i(t-nT_c)\cdot(E_{xi}^2(t)-E_{yi}^2(t))\right)\cdot(1-\cos 2\varphi_{xi})\right)\right\}dt + \frac{\Re}{8}\int_{t=0}^{T_s}\sum_{n=1}^{N}\left\{\frac{c(nT_c)+1}{2}\left[\sum_{i=1}^{K}\sum_{\substack{j=1\\ j\neq i}}^{K}\left\{\left(E_{xi}(t)+E_{yi}(t)+d_i(t)\cdot c_i(t-nT_c)\cdot(E_{xi}(t)-E_{yi}(t))\right)\times \left(E_{xj}(t)+E_{yj}(t)+d_j(t)\cdot c_j(t-nT_c)\cdot(E_{xj}(t)-E_{yj}(t))\right)\cdot\left(\cos(\varphi_{xi}+\varphi_{xj})+\cos(\varphi_{xi}-\varphi_{xj})\right)\right\}\right]\right\}dt \quad (8.33)$$

Since PD frequency response is similar to an LPF, hence in 8.33 the term $\cos 2\varphi_{xi}$ in the first element and $\cos(\varphi_{xi}+\varphi_{xj})$ in the second element are filtered out as they are outside of the PD frequency range. Furthermore, the term $\cos(\varphi_{xi}-\varphi_{xj})$ can also be removed provided that $\varphi_{xi}-\varphi_{xj} >> \omega_c$ where ω_c is the cut-off frequency of the PD. Hence, the total current of upper branch can be expressed as:

$$I^0 = \frac{\Re}{4}\sum_{n=1}^{N}\left\{\frac{c(nT_c)+1}{2}\left(\sum_{i=1}^{K}\left(E_{xi}^2(t)+E_{yi}^2(t)+d_i(t)\cdot c_i(t-nT_c)\cdot(E_{xi}^2(t)-E_{yi}^2(t))\right)\right)\right\} \quad (8.34)$$

The Stokes parameters are defined as:

$$\begin{aligned} S_i^0 &= E_{xi}^2(t)+E_{yi}^2(t) \\ S_i^1 &= E_{xi}^2(t)-E_{yi}^2(t) \end{aligned} \quad (8.35)$$

where S_i^0 refers to signal intensity part, generated in upper branch of polarization modulator at the transmitter while S_i^1 refers to the linear polarized part, generated in lower branch containing data (see Figure 8.3). These parameters also denote the maximum and minimum transmitted power respectively in order to have a bound on the negligible loss of orthogonality [122]. Thus, 8.34 can be rewritten as:

$$I^0 = \frac{\Re}{4}\sum_{n=1}^{N}\left\{\frac{c(nT_c)+1}{2}\left(\sum_{i=1}^{K}\left(S_i^0+d_i(t)\cdot c_i(t-nT_c)S_i^1\right)\right)\right\}+n_1(t) \quad (8.36)$$

Similarly the total current of the lower branch (i.e. *y*-component) can be derived as:

$$I^1 = \frac{\Re}{4}\sum_{n=1}^{N}\left\{\frac{1-c(nT_c)}{2}\left(\sum_{i=1}^{K}\left(S_i^0 + d_i(t)\cdot c_i(t-nT_c)\cdot S_i^1\right)\right)\right\} + n_2(t) \tag{8.37}$$

where:

$$\begin{aligned} n_1(t) &= n_{1x}(t) + j\, n_{1y}(t) \\ n_2(t) &= n_{2x}(t) + j\, n_{2y}(t) \end{aligned} \tag{8.38}$$

In 8.38 $n_1(t)$ and $n_2(t)$ represent the filtered AWGN with independent Gaussian processes of $n_{1x}(t)$, $n_{1y}(t)$, $n_{2x}(t)$ and $n_{2y}(t)$ with equal variances σ^2 which originate $n_1(t)$ and $n_2(t)$. Thus, the balanced-detector output ($I = I^0 - I^1$) is then derived as follows:

$$I = \frac{\Re}{4}\sum_{n=1}^{N} c(nT_c)\sum_{i=1}^{K}\left(S_i^0 + d_i(t)\cdot c_i(t-nT_c)\cdot S_i^1\right) + n(t) \tag{8.39}$$

The noise $n(t)$ includes both noise contributions from I^0 and I^1 and consists of optical ASE noise mentioned in 8.10, PD shot-noise $\left\langle {i_{av}}^2 \right\rangle = 2eiB_0$ where i_{av} is the average photocurrent and also electronic receiver noise at the output of LPF introduced in 8.14. Thus, the total noise $n(t)$ variance can be represented in total as:

$$\sigma_{n(t)}^2 = \left\langle i^2 \right\rangle + \sigma_{ASE}^2 + \sigma_{LP}^2 \tag{8.40}$$

The differential output current, 8.39, can be modified considering the first user (#1) as the intended user as:

$$\begin{aligned} I = {} & \frac{\Re}{4}\sum_{n=1}^{N} S_1^0 \cdot c(nT_c) + \frac{\Re}{4}\sum_{n=1}^{N} c(nT_c)\cdot c_1(t-nT_c)\cdot d_1(t)\cdot S_1^1 \\ & + \frac{\Re}{4}\sum_{i=2}^{K}\sum_{n=1}^{N} c(nT_c)\cdot c_i(t-nT_c)\cdot d_i(t)\cdot S_i^1 + n(t) \end{aligned} \tag{8.41}$$

The first element in 8.41 is a direct-current (dc) that needs estimation and removal in the balanced-detector. The second element represents the intended data mixed with its assigned spreading code auto-correlation and polarization while the third element assumes the interference (i.e. MAI) caused by other transmitters and the last one is the noise. Thus, the system SNR can be expressed as:

$$SNR = \frac{\left(\frac{\Re}{4} \sum_{n=1}^{N} c(nT_c) \cdot c_1(t - nT_c) \cdot d_1(t) \cdot S_1^1 \right)^2}{\left(\frac{\Re}{4} \sum_{i=2}^{K} \sum_{n=1}^{N} c(nT_c) \cdot c_i(t - nT_c) \cdot d_i(t) \cdot S_i^1 \right)^2 + \sigma_{n(t)}^2} \tag{8.42}$$

Now, according to the DPMPC correlation properties, we have:

$$\sum_{n=1}^{N} c(nT_c) \cdot c_1(t - nT_c) = P + 2 \quad \text{i.e. DPMPC Auto-Correlation} \tag{8.43}$$

By defining the variable X_{li} as the DPMPC cross-correlation value:

$$X_{li} = \sum_{n=1}^{N} c_l(nT_c) \cdot c_i(t - nT_c) \tag{8.44}$$

Its probability density function (PDF) can be obtained from the independent values of random variable X_{li}. The in-phase cross-correlation value is either *zero* or *one* depending on whether the codes are in the same group or from the different groups. Obviously, the *zero* value does not cause the interference due to perfectly orthogonal sequences, while the *one* value causes the interference which is only among intended user and ($P^2 - P$) users from the different groups (i.e. P^2 whole sequences and *P* sequences from the same group of intended user which are orthogonal). As, the cross-correlation values are uniformly distributed among interfering users, thus the PDF of *w*, realization of X_{li}, is:

$$P(w=i)=\frac{i}{P^2-P} \tag{8.45}$$

where $P(w=i)$ is the probability that *w* assumes the value *i* (the number of actively involved users in the transmission). Therefore, by substituting 8.43 and 8.45 into 8.42, the system SNR as a function of the number of active users *K* can be further simplified as:

$$SNR(K)=\frac{1}{\left(\frac{(K+2)\cdot(K-1)}{2\cdot(P^2-P)\cdot(P+2)}\right)^2+\frac{16\sigma_{n(t)}^2}{\Re^2\cdot d_1^2(t)\cdot S_1^{1^2}\cdot(P+2)^2}} \tag{8.46}$$

Note that $SNR(1)=\Re^2\cdot d_1^2(t)\cdot S_1^{1^2}\cdot(P+2)^2\Big/16\sigma_{n(t)}^2=E_b/N_0$, where E_b the energy of one bit and N_0 is the noise PSD, denotes the single-user SNR. Expression 8.46 is one of the main results of this Chapter as it represents the SNR of polarization-modulated OCDMA system.

8.3 Transceiver Architecture for Hybrid F-PolSK-OCDMA

8.3.1 Transmitter Configuration

Here we investigate the two-dimensional array (*2D-ary*) F-PolSK-OCDMA transmitter and its operation. Its structure includes sequentially connected optical M_1*-ary* FSK modulator and M_2*-ary* polarization modulator with the CDMA encoder. In the following, we illustrate the mathematical formulation of the hybrid modulated signals.

The *2D-ary* F-PolSK transmitter for the signal generation is shown in Figure 8.4(a) which consists of a FSK modulator with a tuneable laser diode (TLD) that allocates M_1 symbols (i.e. $k_1=\log_2^{M_1}$ bits per symbol) to the corresponding M_1 wavelengths emitted

from the TLD corresponding to the data. It has been discussed in details in Chapter 7 that both the bit-rate and OCDMA interferences will increase when the number of symbols (M_1) is constant and the repetition ratio of TLD becomes smaller. In contrast, as TLD repetition ratio becomes larger, the bit-rate becomes lower and since the interrupted slots at each data-frame prevent interferences of in-phase correlation, the channel interferences will reduce.

The PolSK-OCDMA modulator, similar to the previously discussed model, is shown in Figure 8.4(b). Having the signal FSK modulated, each wavelength from the TLD is initially linearly polarized and set to $45°$ for simplicity through polarization controller at the beginning of PolSK modulator. Then the wavelengths enter the PolSK-CDMA modulator. The signal is *M_2-ary* PolSK modulated where *M_2* denotes number of the lightwave SOP (i.e. $k_2 = \log_2^{M_2}$ bits per SOP), and CDMA encoded by means of the DPMPC spreading sequences.

At the transmitter output and given a reference plane $(\hat{x}, \hat{y})$ normal to the direction of propagation $\hat{z}$, the transmitted lightwave during *M* symbol intervals can be written, in the complex form as [132]:

$$\bar{v}(t) = \sum_{m=1}^{M} \bar{v}_{m_1 m_2}^{(m)}(t) = \sum_{m=1}^{M} \bar{p}_{m_2}^{(m)} \cdot \exp[\, j(2\pi \cdot (f_c + f_{m_1}^{(m)}) \cdot (t - mT_s)\,] \cdot u_T(t - mT_s) \qquad 0 \le t \le MT_s \tag{8.47}$$

where T_s is the symbol interval, $m_1 = 1, 2 \ldots, M_1$, $m_2 = 1, 2 \ldots, M_2$ as signal multiplicities.

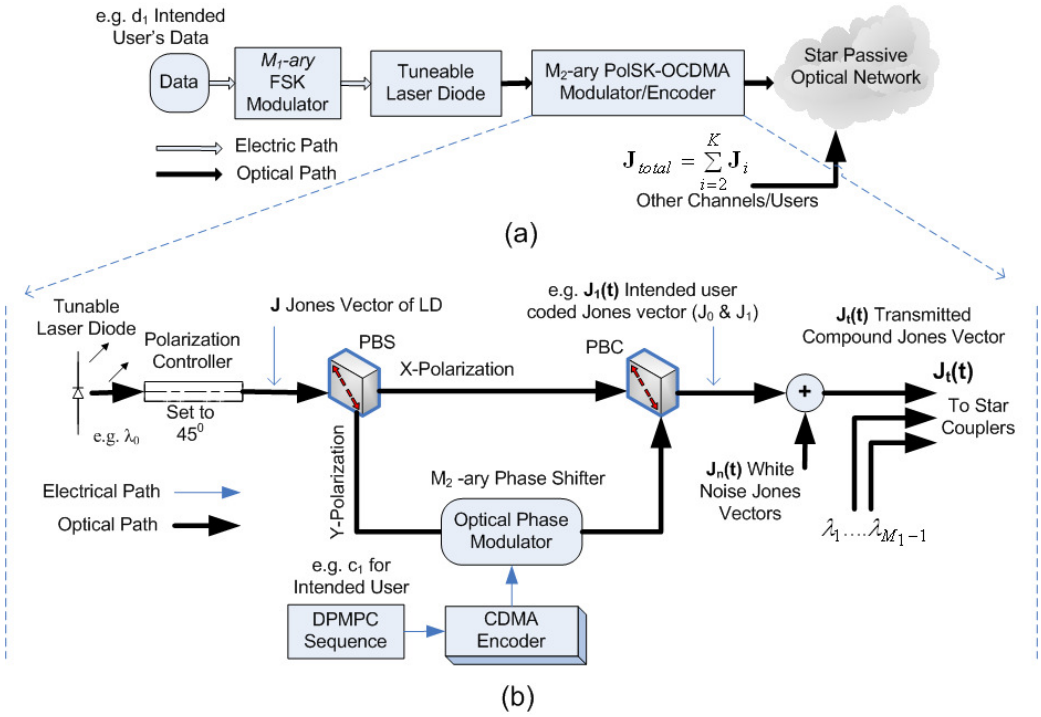

Figure 8.4 (a) Incoherent *2D-ary* F-PolSK-OCDMA transmitter (b) structure of M_2*-ary* PolSK-OCDMA modulator/encoder

Also $\bar{v}_{m_1 m_2}^{(m)}(t)$ is the complex-valued transmitted signal during the m^{th} signalling interval, $\bar{p}_{m_2}^{(m)}$ is the 2D vector that gives the signal amplitudes and phases over $\hat{x}$ and $\hat{y}$ directions where f_c is the carrier frequency with offsets of $f_{m_1}^{(m)}$ (increment or decrement) representing the assigned frequency from the TDL. $u_T(t)$ is a rectangular pulse of unit amplitude. The complex-valued correlation coefficient between two different frequency-polarization modulated signals $\bar{v}_{m_1 m_2}^{(m)}(t)$ and $\bar{v}_{i_1 i_2}^{(m)}(t)$ is defined as [133]:

$$\rho[\bar{v}_{m_1 m_2}^{(m)}(t), \bar{v}_{i_1 i_2}^{(m)}(t)] = \frac{1}{2\sqrt{E_{v_{m_2}} \cdot E_{v_{i_2}}}} \int_{(k-1)T_s}^{kT_s} LP[\bar{v}_{m_1 m_2}^{(m)}(t) \cdot \bar{v}_{i_1 i_2}^{(m)*}(t)]dt \qquad (8.48)$$

where $LP[.]$ denotes the low-pass component of the complex-valued quantity. $E_{v_{m_2}}$ and $E_{v_{i_2}}$ are the signal energies of the transmitted $\bar{v}_{m_1 m_2}^{(m)}(t)$ and $\bar{v}_{i_1 i_2}^{(m)}(t)$

respectively. The asterisk (*) denotes the complex conjugate. The F-PolSK signals satisfy the orthogonality principle if the magnitude of the correlation coefficient $\left|\rho[\bar{v}^{(m)}_{m_1 m_2}(t), \bar{v}^{(m)}_{i_1 j_2}(t)]\right|$ is zero. It can be shown that the orthogonality can be satisfied when the minimum frequency separation between any adjacent frequency tones is $\Delta f = 1/T_s$ [132]. Thus, $f^{(m)}_{m_1}$ can take its value from the set $\{r^{(m)}_{m_1}\Delta f/2\}^{M_1}_{m_1=1}$, where $r^{(m)}_{m_1} = 2m_1 - 1 - M_1$.

In 8.47, $\bar{p}^{(m)}_{m_2}$ defines the transmitted signal amplitudes and phases over the orthogonal $\hat{x}$ and $\hat{y}$ channels during the *m*th signalling interval, given by:

$$\bar{p}^{(m)}_{m_2} = \begin{pmatrix} \bar{p}^{(m)}_{x_{m_2}} \\ \bar{p}^{(m)}_{y_{m_2}} \end{pmatrix} = \begin{pmatrix} a^{(m)}_{x_{m_2}} e^{j\theta^{(m)}_{x_{m_2}}} \\ a^{(m)}_{y_{m_2}} e^{j\theta^{(m)}_{y_{m_2}}} \end{pmatrix} \tag{8.49}$$

where $a^{(m)}_{x_{m_2}}$, $a^{(m)}_{y_{m_2}}$ are the amplitudes of the $(\hat{x}, \hat{y})$-components of the lightwave and $\theta^{(m)}_{x_{m_2}}$, $\theta^{(m)}_{y_{m_2}}$ are their corresponding phases. The discrete random sequences $\{\bar{p}^{(m)}_{m_2}\}^{M_2}_{m_2=1}$ and $\{r^{(m)}_{m_1}\}^{M_1}_{m_1=1}$ are stationary and independent, and are referred to as source symbol sequences. Additionally, $\bar{p}^{(m)}_{m_2}$ determines the SOP of the fully polarized lightwave given in 8.47 during the *m*th symbol interval that is corresponding to symbol number m_2, where $m_2 = 1, 2 \ldots, M_2$.

The electromagnetic wave $\bar{v}^{(m)}_{m_1 m_2}(t)$ consists of two sets of *2D-ary* signals ($M_1 = 2^{k_1}, M_2 = 2^{k_2}$). The signals at each set are uncorrelated and orthogonal (i.e.

orthogonal frequencies and SOP), and all the $M = M_1 \times M_2 \rightarrow k = k_1 + k_2$ signals have the same time duration. Now, the data source emits a data symbol from a set of *M* symbols every $T_s = k \cdot T_b$ seconds, where T_b is the bit duration.

The SOP is described using (S_1, S_2, S_3) as Stokes parameters. Each of which is determined by the amplitudes $a_{x_{m2}}^{(m)}$ and $a_{y_{m2}}^{(m)}$ plus the phase difference $\Delta\theta^{(m)} = \theta_{y_{m2}}^{(m)} - \theta_{x_{m2}}^{(m)}$ of m^{th} symbol. These parameters are given as follow regarding the symbol number m_2 [125]:

$$\overline{S}_{m2}^{(m)} = \begin{pmatrix} S_{1_{m2}}^{(m)} \\ S_{2_{m2}}^{(m)} \\ S_{3_{m2}}^{(m)} \end{pmatrix} = \begin{pmatrix} \left| p_{x_{m2}}^{(m)} \right|^2 - \left| p_{y_{m2}}^{(m)} \right|^2 \\ p_{x_{m2}}^{(m)} \cdot p_{y_{m2}}^{(m)*} + p_{x_{m2}}^{(m)*} \cdot p_{y_{m2}}^{(m)} \\ \left[p_{x_{m2}}^{(m)*} \cdot p_{y_{m2}}^{(m)} - p_{x_{m2}}^{(m)} \cdot p_{y_{m2}}^{(m)*} \right] e^{j\pi/2} \end{pmatrix} = \begin{pmatrix} \left(a_{x_{m2}}^{(m)} \right)^2 - \left(a_{y_{m2}}^{(m)} \right)^2 \\ 2a_{x_{m2}}^{(m)} \cdot a_{y_{m2}}^{(m)} \cdot \cos\left(\Delta\theta^{(m)}\right) \\ 2a_{x_{m2}}^{(m)} \cdot a_{y_{m2}}^{(m)} \cdot \sin\left(\Delta\theta^{(m)}\right) \end{pmatrix} \quad (8.50)$$

The average number of photons representing the energy of the transmitted multi-SOP lightwave is directly proportional to:

$$S_{0_{m2}}^{(m)} = \sqrt{\sum_{i=1}^{3} \left(S_{i_{m2}}^{(m)} \right)^2} = \left(a_{x_{m2}}^{(m)} \right)^2 + \left(a_{y_{m2}}^{(m)} \right)^2 \quad (8.51)$$

where $S_{0_{m2}}^{(m)} = E_{s_{m2}} / T_s$ is the fourth Stokes parameter representing the transmitted optical waveform power with energy of $E_{s_{m2}}$. Only three out of four Stokes parameters are mutually independent since $S_{0_{m2}}^{(m)}$ is expressed in terms of $S_{1_{m2}}^{(m)}, S_{2_{m2}}^{(m)}$ and $S_{3_{m2}}^{(m)}$.

Because of nonlinear effects in the optical fibre, it is very convenient to generate lightwaves with the constant power envelope [125]. Because the constant-envelope

lightwaves are immune from relative intensity and phase noises [125]; additionally, when all electromagnetic signals are transmitted on the same power level (i.e. $S_{0_{m_2}}^{(m)} = S_0$ or equivalently, $E_{s_{m_2}} = E_s$ for $m_2 = 1, 2...., M_2$) and having the same carrier frequency, then they can be assumed as the vectors with the form of $\overline{S}_{m_2}^{(m)} = S_{1_{m_2}}^{(m)} \hat{s}_1 + S_{2_{m_2}}^{(m)} \hat{s}_2 + S_{3_{m_2}}^{(m)} \hat{s}_3$. These vectors are allocated on the surface of the Poincaré sphere with a constant radius of S_0 [128]. For any signal constellation, the upper half of the sphere corresponds to right oriented polarizations and the lower half corresponds to left orientations. Poles of the sphere correspond to circular polarization with two opposite orientations. The right hand circular polarization is presented by the points $S_{1_{m_2}} = S_{2_{m_2}} = 0$ and $S_{3_{m_2}} = S_0$, while the left circular polarization corresponds to the points $S_{1_{m_2}} = S_{2_{m_2}} = 0$ and $S_{3_{m_2}} = -S_0$. Linearly polarized signal points are located on the equator of the Poincaré sphere.

8.3.2 Receiver Configuration and Signal Processing

By assuming negligible nonlinear effects in the fibre and low polarization mode dispersion (PMD), the received optical power $\bar{r}_{m_1 m_2}(t)$ at the receiver input can be expressed as:

$$\bar{r}_{m_1 m_2}(t) = \mathbf{Q} \cdot e^{-(\alpha + j\phi(w))} \cdot \bar{v}_{m_1 m_2}^{(m)}(t) \qquad 0 \le t \le T_s \tag{8.52}$$

where $\bar{v}_{m_1 m_2}^{(m)}(t)$ is the transmitted modulated signal, α and $\phi(w)$ are the fibre attenuation coefficient and phase shift respectively and $\mathbf{Q}$ is the complex Jones matrix. $\mathbf{Q}$ is a unitary operator that takes the polarization variation into account along

the fibre due to coupling between the SOPs. Additionally, due to the low chromatic dispersion over the frequency range of the transmitted field, the value of $\phi(w)$ remains constant. Moreover, α has a negligible effect in the analysis as all transmitted signals have the same power level. In fact, these are some of the PolSK advantages we took in the CDMA-based optical transmission links.

The front-end of the *2D-ary* F-PolSK-OCDMA receiver is initially with frequency selective arrayed waveguide grating (AWG) as illustrated in Figure 8.5(a). In the analysis we have assumed an ideal AWG so that no interference between adjacent wavelengths occurs. The wavelengths assigned to symbols (i.e., $M_1 - ary$) at the transmitter are divided into $\lambda_0, \lambda_1, \ldots \lambda_{M_1-1}$ through AWG. Each wavelength enters the PolSK-OCDMA de-modulator as displayed separately in Figure 8.5(b) and then the symbols are extracted from each wavelength. Thereafter, SOPs are obtained from the SOP extractor block based on generated Stoke parameters in the PolSK-OCDMA decoder. In the data processor block, the FSK part of the signal is demodulated, where the FSK detector determines the part of symbols used to generate the frequency tones $\left\{f_{m_1}^{(m)}\right\}_{m_1=1}^{M_1}$ in every symbol interval *m*. Also, the SOP of the transmitted optical field is estimated similar to the one described previously.

The signal alignment and analysis of the optical signals after passing the fibre channel is investigated when reaching to the receiver end and ready for CDMA-decoding in the OTDL and photo-detection. The delays coefficients in OTDLs are designed in such a way to make them perform as a CDMA chip-decoder in both branches at each wavelength came from AWG which is filtering M_1-FSK wavelengths similar to the PolSK-OCDMA

receiver discussed in Section 8.2.3. However, the only difference is that this receiver works for *M_2-ary* PolSK with variable polarizers' output-function according to the Jones vectors defining the symbols SOPs. Consequently, 8.20 is modified to a $1\times M_2$ matrix instead; while, the rest of the calculation is untouched and the same expression for SNR can be expected throughout the analysis for the PolSK-OCDMA receiver in Figure 8.5(b) [125].

8.4 Analysis of Receivers Error Probability

It is assumed that (i) $\bar{v}^{(m)}_{m_1 m_2}(t)$ is transmitted, (ii) the correct symbols are carried by the correct wavelength and (iii) the decision variables λ_m are calculated at the demodulator for $m = 1,2....,M_1$. Then, the correct decision rule at the FSK demodulator can be expressed as:

$$|\lambda_m|^2 = \begin{cases} \left|E_s + N_{m_1}\right| & m = m_1 \\ |N_m|^2 & m \neq m_1 \end{cases} \tag{8.53}$$

where E_s is the symbol energy and $\{N_m\}_{m=1}^{M_1}$ is an independent Gaussian noise with zero mean and PSDs of σ_n^2.

The correct decision is made if and only if $\left|\lambda_{m_1}\right|$ in the decision rule of $M_1 - ary$ FSK, for $m_1 = 1,\ 2....,M_1$ satisfies:

$$\left|\lambda_{m_1}\right|^2 = \max\left\{|\lambda_m|\right\}_{m=1}^{M_1} \tag{8.54}$$

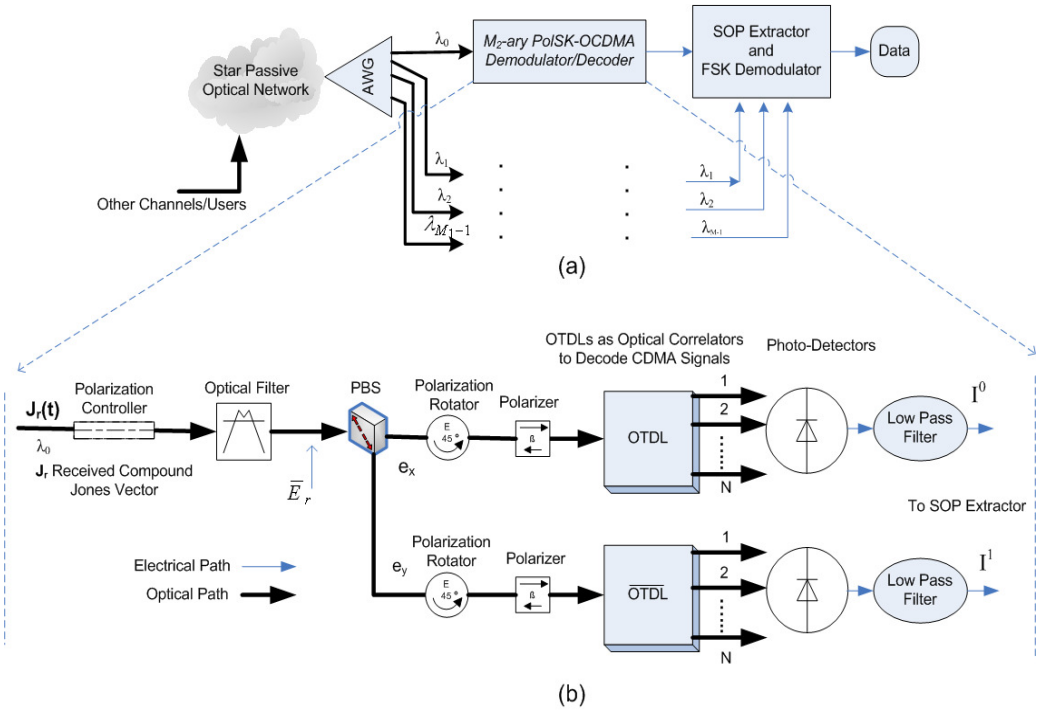

Figure 8.5 (a) Incoherent *2D-ary* F-PolSK-OCDMA receiver (b) structure of M_2*-ary* PolSK-OCDMA demodulator/decoder with OTDL

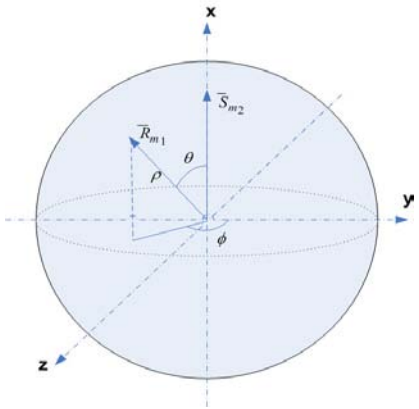

Figure 8.6 Representation of noisy received signal in polar coordinates according to the un-noisy transmitted signals inscribed into Poincaré sphere

Also it is assumed that the received estimated noisy parameters $\bar{R}_{m1} = \left(R_{1m_1}, R_{2m_1}, R_{3m_1}\right)$ are in the decision region of the un-noisy transmitted parameters $\bar{S}_{m_2} = \left(S_{1m_2}, S_{2m_2}, S_{3m_2}\right)$ as shown in Figure 8.6. Based on the maximum likelihood (ML) decision rule and assuming that all possible transmitted vectors $\{\bar{S}_l\}_{l=1}^{M_2}$

are equi-power and equi-probable, the decision metric is implemented for multiple-array signalling as follows:

$$f_{\overline{R}_{m1}|\overline{S}_{m2}}(\overline{R}|\overline{S}_{m2}) = \max\left\{ f_{\overline{R}_{m1}|\overline{S}_l}(\overline{R}|\overline{S}_l) \right\}_{l=1}^{M_2} \tag{8.55}$$

where $f_{\overline{R}_{m1}|\overline{S}_l}(\overline{R}|\overline{S}_l)$, for $l = 1,2....,M_2$ is the conditional PDF of the estimated noisy Stokes vector $\overline{R}_{m1}$ given that $\overline{S}_l$ is transmitted. This PDF was already given in spherical coordinates $(\rho_m, \theta_m, \phi_m)$ [128] in the form of:

$$f_{(\rho_m,\theta_m,\phi_m)}(\alpha_m, \beta_m, \delta_m) = \frac{\alpha_m}{16\pi\sigma_n^4} \cdot \sin(\beta_m) \cdot e^{-\frac{E_s^2+\alpha_m}{2\sigma_n^2}} \cdot I_0\left(\frac{E_s}{\sigma_n^2}\sqrt{\alpha_m}\cos\left(\frac{\beta_m}{2}\right)\right) \tag{8.56}$$
$$\alpha_m > 0 \ , \ \beta_m \in [0,\pi] \ , \ \delta_m \in [0,2\pi]$$

where $m = 1,2....,M_2$ and $I_0(.)$ is the 0^{th} order modified Bessel function of the first kind. The random variables ρ_m and θ_m are statistically independent of ϕ_m, which is uniformly distributed over $[0,2\pi]$ [128]. Based on the ML rules, particularly $\overline{S}_{m2}$ was chosen as the transmitted vector when it satisfies:

$$\overline{R}_{m1} \,.\, \overline{S}_{m2} = \max\left\{ \overline{R}_{m1} \,.\, \overline{S}_l \right\}_{l=1}^{M_2} \equiv \max\left\{ \cos(\beta_m) \right\}_{m=1}^{M_2} \tag{8.57}$$

Since birefringence polarization transformation only causes a rigid rotation of the signal constellation, the decision metric in 8.57 is insensitive to this perturbing effect [126]. In the absence of noise, the index m in 8.54 and l in 8.55 should be equal to m_1 and m_2 of $\overline{v}_{m_1 m_2}^{(m)}(t)$ respectively.

The probability of the correct decision for the system equals the probability that satisfies 8.54 times the probability that satisfies 8.57 conditional to 8.54. That is given by:

$$P_c = \Pr\left(\left|\lambda_{m_1}\right|^2 = \max\left\{\left|\lambda_m\right|\right\}_{m=1}^{M_1}\right) \times \Pr\left(\overline{R}_{m_1} \,.\, \overline{S}_{m_2} = \max\left\{\overline{R}_{m_1} \cdot \overline{S}_l\right\}_{l=1}^{M_2} \;\middle|\; \left|\lambda_{m_1}\right|^2 = \max\left\{\left|\lambda_m\right|\right\}_{m=1}^{M_1}\right) \quad (8.58)$$

The first probability term in 8.58, for $m = 1,2....,M_1$ is the probability that a correct decision is made on the transmitted frequency at the FSK demodulator shown in Figure 8.5(b). It is noted that the normalized decision variables $\chi_m = \left|\lambda_m\right|^2 / 2\sigma_n^2$ for $m = 1, 2...., M_1$, are mutually statistically independent and chi-square distributed random variables with two degrees of freedom [132]. It was also shown that their PDFs, conditioned on the transmitted signal $\overline{v}_{m_1 m_2}^{(m)}(t)$ are given by:

$$f_{\chi_m|\overline{v}_{m_1 m_2}}(\mu|\overline{v}_{m_1 m_2}) = \begin{cases} e^{-(\mu+\gamma(K))} I_0(\sqrt{4\mu \cdot \gamma(K)} & m = m_1, \mu \geq 0 \\ e^{-\gamma(K)} & m \neq m_2, \mu \geq 0 \end{cases} \quad (8.59)$$

where $\gamma(K)$ represents the system SNR per transmitted symbol, which is directly proportional to the number of photons representing a transmitted symbol and number of users derived as 8.46. Based on 8.59, the probability of the correct decision on the transmitted frequency tone is obtained as:

$$\begin{aligned} P_c^{FSK} &= \int_0^\infty e^{-(z+\gamma(K))} I_0(\sqrt{4\gamma(K) \cdot z}) \left[\prod_{m=1}^{M_1} P(\chi_{m_1} \geq \chi_m | \chi_{m_1} = z)\right] dz \\ &= \int_0^\infty e^{-(z+\gamma(K))} I_0(\sqrt{4\gamma(K) \cdot z})(1 - e^{-z})^{M_1 - 1} \\ &= \sum_{i=0}^{M_1 - 1} (-1)^i \binom{M_1 - 1}{i} \frac{1}{i+1} e^{-\frac{i}{i+1}\gamma(K)} \end{aligned} \quad (8.60)$$

The second probability term in 8.58 is the probability that the transmitted SOP is correctly chosen at the SOP extractor shown in Figure 8.5(b), as well as the correct decision is made on the transmitted frequency at the frequency demodulator. The probability of the correct detection was evaluated in [125] for some regular equi-power $M_2 -$ PolSK modulations with different variables of n, θ_0 and θ_1 which are

constant referring to different modulation levels as shown in Table 8.1, reproduced from [125], and given by:

$$P_c^{PolSK} = F_\theta(\theta_1) - \frac{n}{\pi}\int_{\theta_0}^{\theta_1} \cos\left(\frac{\tan\theta_0}{\tan\tau}\right)\cdot f_\theta(\tau)d\tau \tag{8.61}$$

$f_\theta(\tau)$ is the marginal PDF and $F_\theta(\tau)$ is the cumulative distribution function (CDF) of θ, which can be derived from the joint PDF (i.e., 8.56) by integrating over ρ_m and ϕ_m, then we have:

$$\begin{aligned} f_\theta(\tau) &= \frac{\sin\tau}{2} e^{-\frac{\gamma(K)}{2}\cdot(1-\cos\tau)\cdot\left[1+\frac{\gamma(K)}{2}(1+\cos\tau)\right]} \\ F_\theta(\tau) &= 1-\frac{1}{2} e^{\frac{-\gamma(K)}{2}\cdot(1-\cos\tau)\cdot(1+\cos\tau)} \end{aligned} \tag{8.62}$$

where $\tau \in [0,\pi]$.

Table 8.1 The values for n, θ_0 and θ_1 for M_2-PolSK

M_2-PolSK	n	θ_0	θ_1
4-PolSK Circular	2	$\pi/4$	$\pi/2$
4-PolSK Tetrahedron	3	$[\pi-\tan^{-1}(2\sqrt{2})]/2$	$\pi-2\theta_0$
6-PolSK Octahedron	4	$\pi/4$	$\pi/2-\tan^{-1}(1/\sqrt{2})$
8-PolSK Cube	3	$\tan^{-1}(1/\sqrt{2})$	$\pi/2-\theta_0$

In the binary signalling format (BPolSK), as shown in Figure 8.1(a), the signal set consists of two antipodal points on the Poincaré sphere. The un-noisy received signals are $S_{1_{m2}}$, $S_{2_{m2}}$ where $S_{1_{m2}} = -S_{2_{m2}}$. Given a transmitted SOP such that the un-noisy received SOP is $\overline{S}_{m2}$, chosen within the decision region, and the received vector $\overline{R}_{m1}$, an error occurs each time the scalar product $\overline{R}_{m1}.\overline{S}_{m2}$ becomes negative. This is due to the fact that the ML criterion implies in this binary case a decision based on the sign of the scalar product as discussed in Section 8.2.2. Hence, the error event turns out to be:

$$\{E\} = \left\{\theta > \frac{\pi}{2}\right\} \tag{8.63}$$

where $\theta = \cos^{-1}\left(\overline{R}_{m1} \cdot \overline{S}_{m2} \Big/ \left(\left|\overline{R}_{m1}\right| \cdot \left|\overline{S}_{m2}\right|\right)\right)$.

It is noted that the error event is independent of both ρ and ϕ with this signal set. Therefore, by using $F_\theta(\tau)$ in 8.62, the error probability of BPolSK can be obtained as:

$$P_e^{BPolSK} = P(\theta > \frac{\pi}{2}) = \frac{1}{2} e^{-\gamma(K)} \tag{8.64}$$

In the higher order signalling format, the analysis presents the upper bounds on the actual probability of errors in that the error is function of both θ and ϕ. The system probability of error now is chosen based on the following upper bound:

$$P_e^{MPolSK} \le P_e \left| \max \phi \right. \tag{8.65}$$

Now for circular-quad-PolSK (CQPolSK), as shown in Figure 8.1(b), the error condition is assumed based on 8.65 and signal constellation as:

$$\{E\}_{upper\ bound} = \left\{\theta > \frac{\pi}{4}\right\} \tag{8.66}$$

Thus, the error probability for CQPolSK is obtained as:

$$P_e^{CQPolSK} = 1 - F_\theta(\frac{\pi}{4}) = \frac{1}{2}\left(1 + \frac{\sqrt{2}}{2}\right) e^{-\gamma(K)\left(1 - \frac{\sqrt{2}}{2}\right)} \tag{8.67}$$

This scheme has a SNR penalty of 2.5 dB with respect to BPolSK in a generic polarization-modulated system [125].

Similarly for tetrahedron-quad-PolSK (TQPolSK), as shown in Figure 8.1(c), the error condition can be derived by half the angle subtended between the centre of the sphere and two adjacent signal points as follows:

$$\{E\}_{upper\ bound} = \{\theta > 0.304\pi\} \tag{8.68}$$

Thus the probability of error can be calculated as:

$$P_e^{TQPolSK} = 1 - F_\theta(0.304\pi) = (0.7882)\cdot e^{-\gamma(K)(0.4226)} \tag{8.69}$$

It is again mentioned that this scheme has a SNR penalty of 0.8 dB with respect to BPolSK in a generic polarization-modulated system.

Also for the cubic-PolSK (8-PolSK), as shown in Figure 8.1(d), the error condition, derived as above, is:

$$\{E\}_{upper\ bound} = \{\theta > 0.196\pi\} \tag{8.70}$$

And the resulting error probability bound is thus:

$$P_e^{8-PolSK} = 1 - F_\theta(0.196\pi) = (0.9082)\cdot e^{-\gamma(K)(0.1835)} \tag{8.71}$$

This scheme also has a SNR penalty of 2.6 dB with respect to BPolSK in generic polarization-modulated system.

These bounds indicate that the multi-level polarization modulation in transmission lines can be accomplished with high performance in cost of relatively small SNR penalties, however to overcome the phase and shot noises instead.

Finally, having the probability of $M_1 - \text{FSK}$, $M_2 - \text{PolSK}$ and CDMA encoded SNR $\gamma(K)$, the overall system error probability, which denotes the BER of the transceivers, is derived as:

$$P_e^{F-PolSK} = 1 - P_c = 1 - [\sum_{i=0}^{M_1-1}(-1)^i \binom{M_1-1}{i} \frac{1}{i+1} e^{-\frac{i}{i+1}\gamma(K)}] \times [F_\theta(\theta_1) - \frac{n}{\pi}\int_{\theta_0}^{\theta_1} \cos(\frac{\tan\theta_0}{\tan\tau}) f_\theta(\tau)\, d\tau] \tag{8.72}$$

8.5 Transceivers Performances

8.5.1 PolSK-OCDMA Transceiver

In this section, the numerical results of the BER performance of the proposed incoherent PolSK-OCDMA transceiver based on the above detailed analysis, resulted in the system SNR, are demonstrated and discussed. The $BER = 10^{-9}$ is also depicted on the graphs for further clarification.

Figure 8.7 shows the BER of the proposed structure against the single-user SNR (shown as *Sdb*). Different trends of traffic like 10%, 20%, 30% and 40% of full-load as the number of simultaneous active users when *P = 13* have been evaluated. It is obvious from Figure 8.7 that the higher values of *Sdb* offer lower error-rates. The analysis shows the system that can accommodate 30% of all users (46 users) is able to meet $BER = 10^{-9}$ with $Sdb = 16dB$; while at $Sdb = 7.2dB$ the system can support 20% of all users (32 users) which is superior enough to deliver the network services in this case. However, the system is unable to guarantee a reliable communication for more than 35% of all users. The system introduced in [124], employed Gold-sequences with lengths of 511 and 1023 to accommodate 40 and 80 users (i.e. 8% of the full-load in both cases) respectively. However, in the proposed system with *P* = 13 the code-length will be only 195. Obviously by applying longer code (greater *P*) the performance will also be improved. That means this system also provide higher throughput, data-rate and capacity.

Figure 8.8 also displays the BER performance against the number of simultaneous active users, *K* for the proposed architecture. As it is apparent from Figure 8.8, when

the great number of users exists, the higher error-rate occurs due to the growing interferences. It is indicated that the system employed DPMPC with *P*=13 and $Sdb = 16dB$ can tolerate 48 simultaneous users which equals 32% of full-load. While, 44 and 39 users (28% and 25% of full-load respectively) are guaranteed reliable communication link ($BER \le 10^{-9}$) with only $Sdb = 12dB$ and $Sdb = 8dB$ respectively. This implies a cost effective link-budget that consumes less power to compare with the previous coding schemes and architectures introduced in [123, 124].

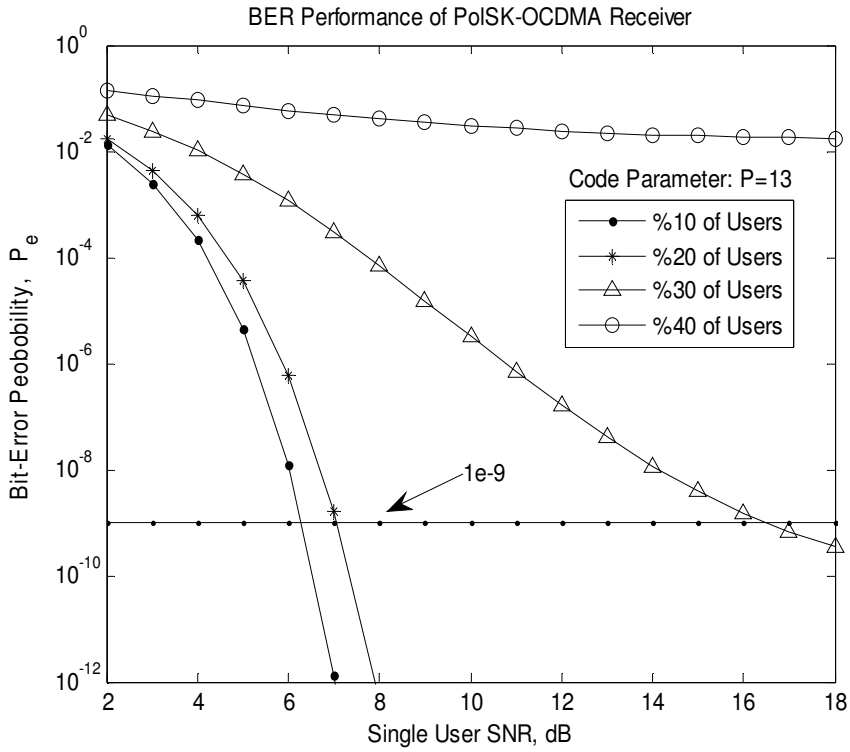

Figure 8.7 BER performance of PolSK-OCDMA transceiver against the single-user SNR, *Sdb*

On the other hand, this polarization-based OCDMA transceiver architecture is easily able to accommodate 10-25 percent of all active users (which is more than expected in a networking side considerations) with as little as less than single-user SNR of 10 dB. Although, it is recommended to deploy DPMPC with greater *P* value to support higher

number of users and to apply higher *Sdb* for lower BER. For further examination from Figure 8.8 and focusing on 46 users residing in the network, the BER at Sdb = 8, 12 and 16 dB, the error-rate becomes 3.2×10^{-5}, 2.3×10^{-8} and 7.4×10^{-11} respectively.

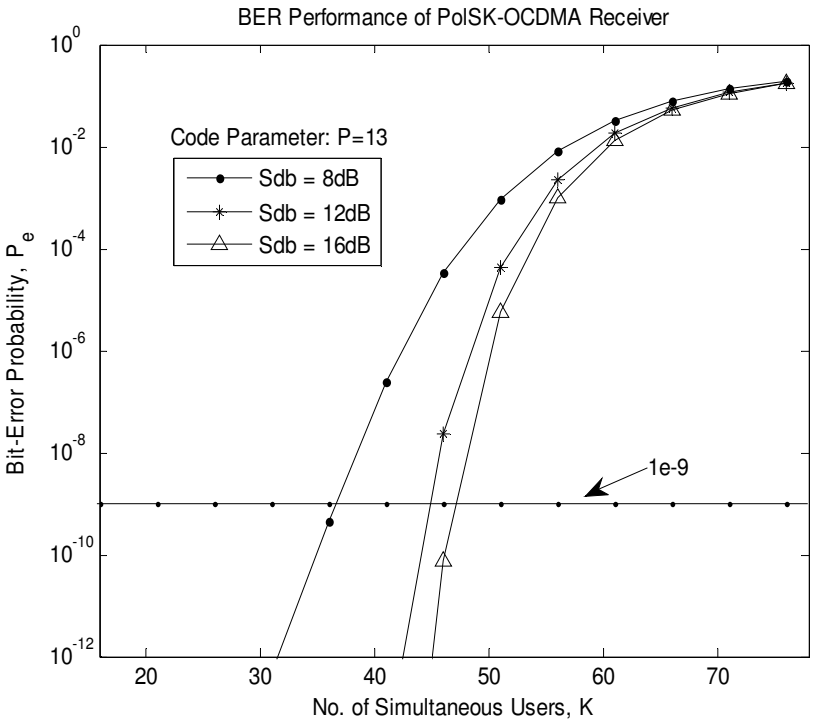

Figure 8.8 BER performance of the PolSK-OCDMA transceiver against the number of simultaneous users, *K*

8.5.2 Hybrid F-PolSK-OCDMA Transceiver

In this section, the BER probability of hybrid F-PolSK-OCDMA transceivers as a function of single-user SNR $\gamma(1)$ (shown as *Sdb* on the graphs) has been evaluated based on the above analysis. The numerical results of the proposed architecture are demonstrated in Figure 8.9 to 8.11. As a reference, $BER=10^{-9}$ is also displayed for comparison purposes.

Figure 8.9 explains the performance of the hybrid transceiver under conditions of *P*= 19, *Sdb*= 15 dB and binary FSK modulation with different polarization constellations. It can be observed from Figure 8.9 that binary FSK with binary PolSK enhances the

overall BER as compared with the other polarization constellations. The 2-FSK/2-PolSK configuration is able to accommodate 20% of full-load (i.e. 70 users, with respect to *P*=19) simultaneous users. On the other hand, the 2-FSK / 4-PolSK with circular constellation can also tolerate 45 users (i.e. 13% full-load). It has been shown that by increasing the polarization constellation, not only the system complexity grows also the performance degrades. This is because the decision region for higher degrees of polarization become smaller and subsequently the demodulation process becomes more complicated and requires precisely designed components. The proposed coding scheme and architecture can support more throughput as the spreading code is much smaller than Gold-sequences of 511 or 1023 employed in the literature [123, 124].

The BER comparison of BPolSK modulation with various frequency tones in M_1-*ary* FSK signalling format is demonstrated in Figure 8.10 under conditions of *P* = 19, *Sdb* = 15 dB and M_1= 2, 4, 8 and 16. The results again indicate that the combination of two binary modulations is promising. The number of accommodated users at $BER = 10^{-9}$ at receivers of 2-FSK/BPolSK, 4-FSK/BPolSK, 8-FSK/BPolSK and 16-FSK/BPolSK are 70, 65, 60 and 55 respectively. Furthermore, focusing at 20% of the total number of users (70 users) accommodated in the network, corresponding error-rates to the above receivers are 1.1×10^{-9}, 3.2×10^{-9}, 7.4×10^{-9} and 1.5×10^{-8} respectively.

It is observed that the combination of two binary modulations has the potential as a secure, efficient and accommodating OCDMA architecture. Therefore, the variation of binary F-PolSK-OCDMA transceiver's BER against the number of active users with different single-user SNR is illustrated in Figure 8.11. As it can be seen, the higher SNR values reduce the error-rate as well as enhance the network capacity. The employed

SNR values are still adequate for a given circumstances to make the proposed architecture very power efficient.

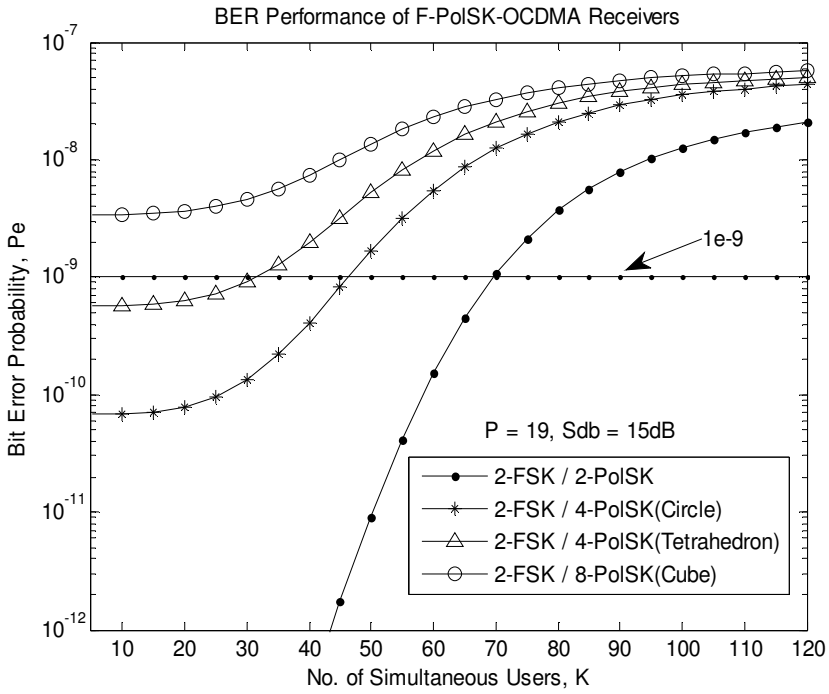

Figure 8.9 BER performances of BFSK / M_2-PolSK-OCDMA receivers against the number of simultaneous active users, K

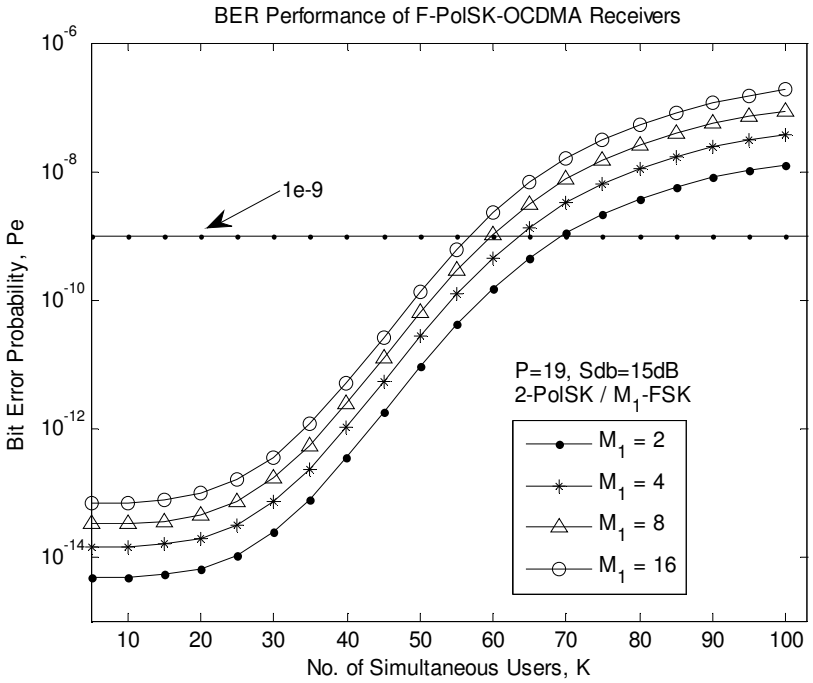

Figure 8.10 BER performances of M_1-FSK / BPolSK-OCDMA receivers against the number of simultaneous active users, K

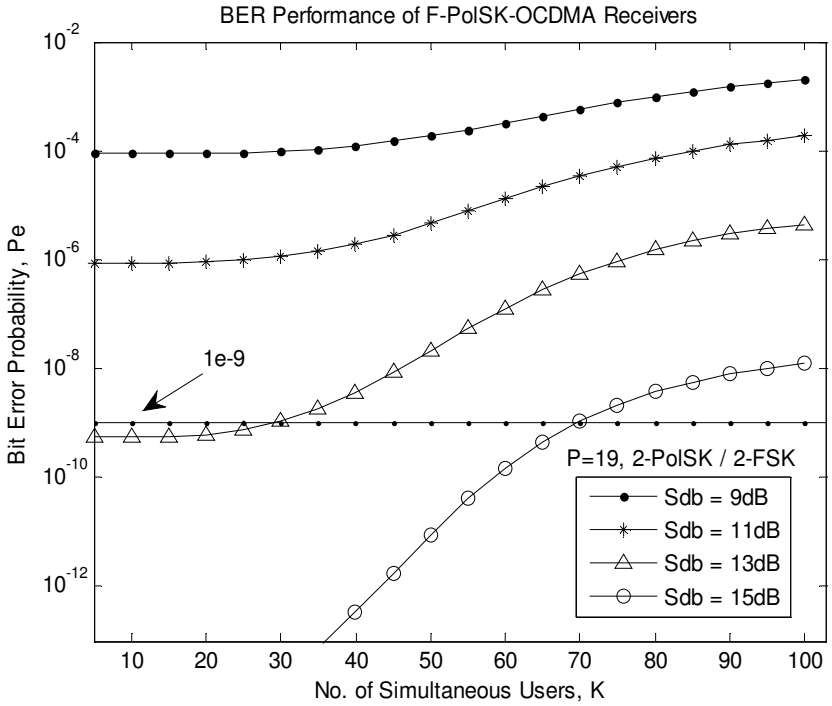

Figure 8.11 BER performances of binary F-PolSK-OCDMA receivers with different single-user SNRs against the number of simultaneous active users, *K*

8.6 Conclusion

The polarization-modulated OCDMA technique has been introduced followed by a novel incoherent transceiver architecture which employed OTDLs to decode CDMA signals. From a detailed analysis, we obtained the system SNR and accordingly demonstrated the overall network BER performance.

Furthermore, the transceiver design of the proposed *2D-ary* frequency-polarization modulated OCDMA has also been presented. The generated signals have the advantage of spreading over higher dimensional constellation which provides greater geometric distances between the transmitted signals. The results demonstrated that the binary combination of two modulations remarkably improves the transceivers performance that can reliably and power-efficiently accommodate greater number of simultaneous users that implies capacity enhancement of 10 to 15 percent as

compared with the similar system with existing coding scheme [P10-P12][1]. It should be mentioned that the overall promising performance of PolSK modulation is a trade-off with complex architecture and physical implantation.

Moreover, the system security also boosted due to two-dimensional advanced modulation in the optical domain. The performance of OCDMA receivers in cooperation with DPMPC as the spreading code have been presented taking into account the effects of optical ASE noise (i.e. optical filter), electronic receiver noise (i.e. LPF), photo-detectors shot-noise and mainly the multi-user interferences (i.e. MAI). The results indicated that the architectures can reliably and power-efficiently accommodate greater number of simultaneous users. In other word, the proposed architectures enhanced the system capacity in a less power consuming regime [P13, P14][1].

[1] See 'List of Publications'

Chapter 9

Analysis of OCDMA-PON and IP over OCDMA Network

9.1 Introduction

Similar to the OCDMA technique, passive optical network (PON) is a point-to-multipoint optical access in which the optical components are passive, such as optical fibre, splices and splitters that potentially reduce the cost of operations and maintenances. The first mile is a network with a central office (CO) where serves multiple users. There are several multipoint topologies suitable for the access network, including tree, ring or bus [19]. All transmissions in a PON are performed between an optical line terminal (OLT) and optical network units (ONU) which are premises or general end users. The architecture of PON using single fibre link is illustrated in Figure 9.1. The OLT may contain all encoder-decoder pairs required for communication with each ONU or a smaller number of tuneable encoders-decoders. The OLT resides in the CO and connects the optical access to the backbone or long-haul transport network.

Time-division multiple-access (TDMA)-PON and wavelength-division multiplexing (WDM)-PON have also been enabled to date. Even though TDMA-PON utilizes the bandwidth of fibre efficiently, it has limitations in its increased transmission speed, difficulty in burst synchronisation and traffic control, low security and complex dynamic bandwidth allocation requirement [16]. The emerging WDM-PON took over TDMA due to required bandwidth growth, whereas it came with extravagant cost from precise wavelength-dependent components. In addition, the effect of statistical multiplexing is insignificant in multimedia communications environments [11]. Although WDM-PON has several advantages over TDMA-PON, it founds its way hardly to industries due to high operation and maintenance expenses.

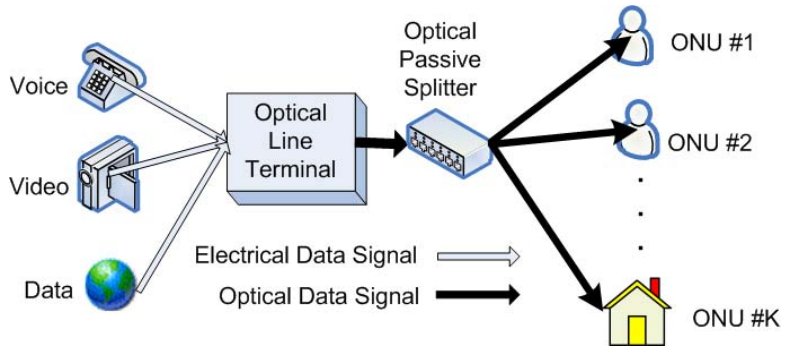

Figure 9.1 PON architecture using single fibre link

OCDMA-PON, where each subscriber's channel is given its own code for spreading and de-spreading, is a good alternative in view of cost, simplicity and noise reduction [50]. OCDMA link is transparent to the input channel's data protocol with security. It supports bursty traffics and random access protocols. Furthermore, the optical beat noise problem, which often arises in a system using several laser diodes as in optical subcarrier multiplexing or WDM, does not have much effect on the OCDMA-PON [54].

In this Chapter, two of previously introduced and analysed transceiver architectures have been considered. The coherent homodyne BPSK-OCDMA (Chapter 6) is utilised in the proposed OCDMA-PON line terminal and network units. Also, a network node configuration featured with Internet protocol (IP) traffic transmission in hybrid *M-ary* FSK-OCDMA network (Chapter 7) is proposed.

9.2 OCDMA-PON Architecture

The architectures of transmitter, receiver, optical network unit (ONU) and optical line terminal (OLT) as part of the proposed OCDMA-passive optical network (PON) are explained in detail in this Section. The transmitter structure of the coherent homodyne BPSK-OCDMA with external Mach-Zehnder (MZ) phase modulator as an electro-optic modulator (EOM) shown in Figure 9.2. The outgoing data is first BPSK encoded generating the in-phase and quadrature-phase (IQ) signals electrically to drive the MZ modulator as an active MZ modulator [135]. Then, the encoded BPSK-signal drives the MZ modulator to phase modulate the lightwave. Finally, the lightwaves are CDMA encoded by means of the DPMPC sequences and multiplexed via couplers and transmitted over the PON as a network infrastructure.

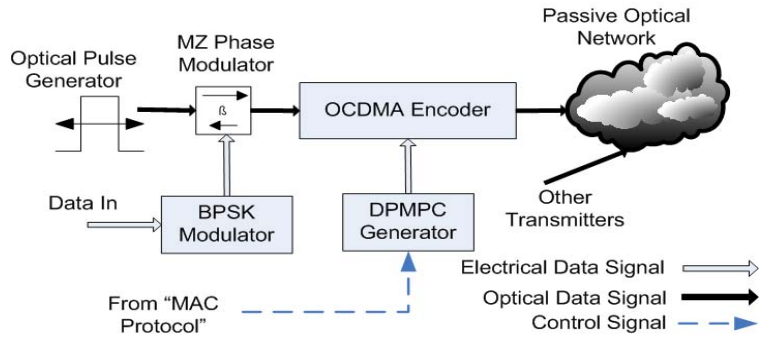

Figure 9.2 Proposed coherent OCDMA transmitter in PON architecture

At the receiver the local oscillator, which is modulated with the pre-reserved DPMPC address code as shown in Figure 9.3, is combined coherently with the received OCDMA signal. The polarization controller makes sure all users have the same polarization to reduce any polarization sensitive noises on the photo-detectors (PD). In CDMA decoding process, the portion of the received signal encoded with the same DPMPC spreading code sequence at the transmitter (i.e. intended data for the intended receiver) is de-spread, whereas signals encoded with other DPMPC spreading code sequences (i.e. MAI) are further spread and reduced. The coherently mixed optical signals are incident on a dual-balanced detector whose electrical output conserves the phase information. The generated bipolar electrical signal is integrated over a bit interval and the result is compared to a reference to form the final bit estimation.

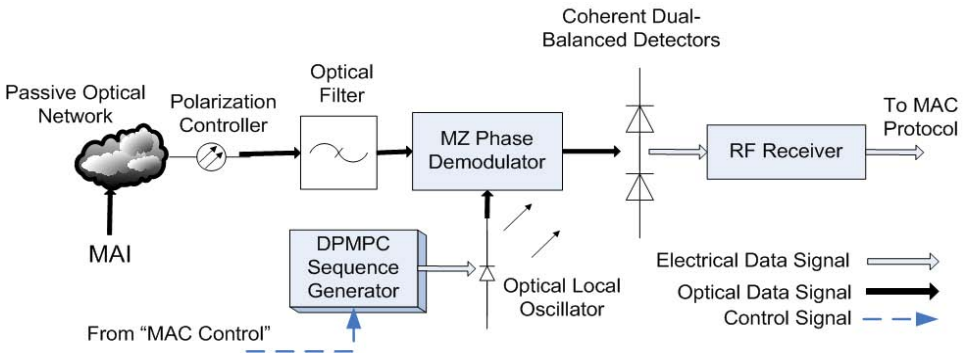

Figure 9.3 Proposed coherent OCDMA receiver in PON architecture

Now, the passive optical network architecture in which the coherent OCDMA is employed as a multiple-access technique is investigated. The optical line terminal configuration of this OCDMA-PON is shown in Figure 9.4.

The multiple-access is achieved by using DPMPC sequences as the address code to identify users in the all-optical domain. In the downstream from optical line terminal (OLT) to optical network unit (ONU), at the 1550 nm wavelength, the optical pulses are

encoded at the OLT by means of MZ external modulator driven by DPMPC generator at the transmitters and every user is assigned with one unique sequence code.

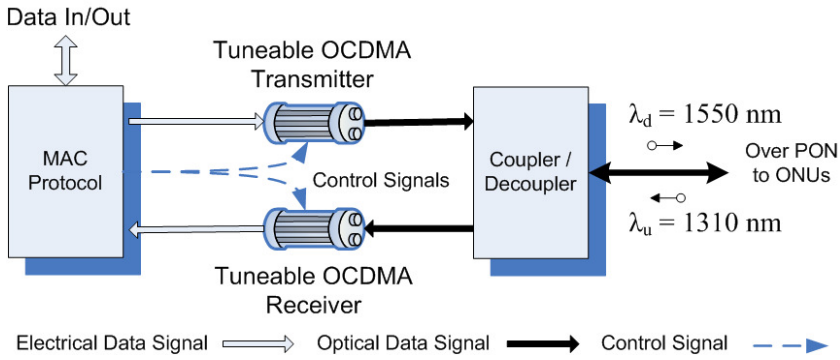

Figure 9.4 Configuration of OLT in the OCDMA-PON architecture

Since OLT serves number of ONUs, it contains multiple transceivers consisting reconfigurable DPMPC generator. The signal is then coupled and transmitted over fibre link to the receivers i.e. ONUs where each user is separated and identified by optical address and medium access control (MAC). The ONU configuration of this OCDMA-PON is shown in Figure 9.5. In upstream channel from ONU to OLT, at the 1310 nm wavelength, the signals are optically decoupled and divided to the decoder at the OLT where the information from each user is obtained together with the MAC signal control from the ONUs to OLT.

The MAC signal is also fed back to the access protocol transmitter to manage the network operation, for example, for the allocation of the DPMPC to each user as shown in Figures 9.4 and 9.5. Usually, a stable upstream wavelength is required with a stabilized laser source at the transmitter of the ONU. The downstream signal from the passes through the de-coupler and goes into the detector, then the data information for the user is separated by optical correlation operation with their unique address sequence. The downstream control signal is also obtained and passed to the network

control unit. For the upstream, the signal from the ONU to the OLT is encoded by the DPMPC for user identification by the optical encoder and is then transmitted towards the OLT through the fibre link. The MAC protocol can be the carrier-sense multiple-access collisions detect (CSMA/CD).

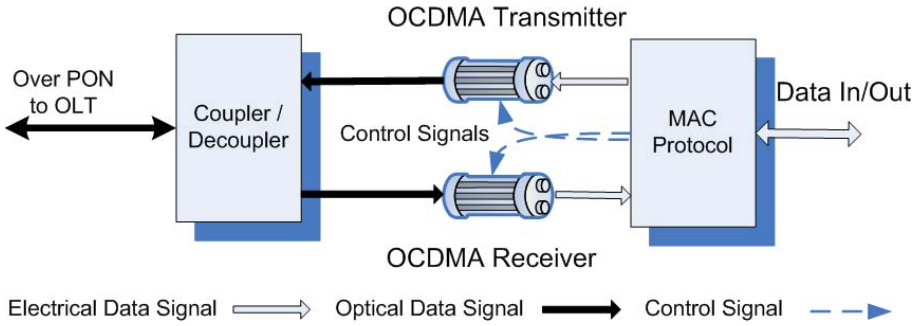

Figure 9.5 Configuration of ONU in the OCDMA-PON architecture

In this OCDMA-PON, the signal can be potentially modulated by frame information for data load switching as well as address code sequences for user identification. This brings the compatibility of the architecture to work also with IP and label switching techniques for routing and traffic managements. By considering the ring topology with number of nodes (i.e. OLT), the OLT can be treated as one of the nodes where generally links to the number of ONUs. The downstream and upstream traffics are at the different wavelengths and then can be broadcasted on the same fibre link. For example, one node can add/drop data traffic by a 2×2 coupler. One port of the coupler is connected to a 2×2 optical cross connector (OXC) and the other port links to the fibre ring attached to the nodes based on the OCDMA-PON. The OXC control signals can be generated through an optical routing table or a label switch paradigm [112]. The downstream traffic from a node and the upstream traffic from the ONU pass through the same optical coupler, where the former is directed to the OLT and the

latter is directed to an ONU or a user. This architecture proposes a transparent protocol, flexible user allocation and mainly all-optical operations with cost effective solution since it reduces wavelength-sensitive devices with complex operations and control used in the other schemes.

9.2.1 OCDMA-PON Transmission Analysis

Before OCDMA-PON can be considered for use in large-scale networks, it must demonstrate scalability in terms of fibre transmission distance. Scaling is a concern because the encoding process broadens the spectra of individual OCDMA tributaries, resulting in increased sensitivity to frequency-dependent transmission impairment. The power-budget-based analysis of the network scalability relatively mitigates that impairment and is more practical to study. Now, the impact of coding parameters, number of nodes (i.e. number of ONU per OLT), channel link length and optical components characteristics on the system bit-error rate (BER) are now investigated.

If we assume each node supports up to N_u users (i.e. ONUs), then the number of nodes in the network (N_n) can be expressed as:

$$N_n = \frac{N_T}{N_u} \tag{9.1}$$

where N_T is the total number of users in the network. The upstream signal power, from ONU to OLT, must satisfy the following power budget [136]:

$$R_S \le P_{UT} - \alpha_c \cdot N_n - \alpha_F \cdot L - \alpha_{IL} - \delta^2_{other} \tag{9.2}$$

where P_{UT} is the upstream transmitter output power of ONU, α_c is coupler/de-couplers' loss, α_F is the fibre attenuation coefficient, *L* is the length of the fibre link, α_{IL} is the optical filter's insertion loss, and R_S is the photo-detectors (PD)

sensitivity. Similarly, the down-stream traffic power, from OLT to ONU, must satisfy the following power budget:

$$R_S \le P_{DT} - \alpha_c \cdot N_n - \alpha_F \cdot L - \alpha_{IL} - C \cdot \log_2^{S_P} - \delta^2_{other} \tag{9.3}$$

where P_{DT} is the downstream transmitter power of OLT, *C* is the filtering index and S_P is the splitters' splitting ratio. In the above two power budget analysis equations, the equivalent noise power budget term, shown as δ^2_{other}, includes the noise contribution from the CDMA en/decoder δ^2_{coder} and the noise contribution from the MAI δ^2_{MAI}. Thus:

$$\delta^2_{other} = \delta^2_{coder} + \delta^2_{MAI} \tag{9.4}$$

The en/decoder noise δ^2_{coder} is relative to the MZ modulator, number of chips and chip duration that can be approximated as an average by 1dB [114]. δ^2_{MAI} can be introduced as:

$$\delta^2_{MAI} = (K-1) \cdot \delta^2_{MAI-\sin gle} \tag{9.5}$$

where K is the number of active users in the network (i.e. sending and receiving data). $\delta^2_{MAI-\sin gle}$ has been discussed and introduced in [115, 136] as follow:

$$\delta^2_{MAI-\sin gle} = \Re^2 \cdot P_{UT} \cdot P_{DT} \cdot Var[C_{mn} \cdot \cos(\theta_i - 2\pi f \tau_i)] \big/ N^4 \tag{9.6}$$

where $\Re$ is the responsivity of the PDs, $Var[.]$ is the variance function, θ_i is the CDMA encoded phase angle of the i^{th} user, f is the optical carrier frequency, τ_i is the propagation delay between the i^{th} user transmitter and the corresponding receiver. *N* is the spreading code-length. And finally, $\delta^2_{MAI-\sin gle}$ is the variance of an interfering

signal of a single user i.e. cross-correlation value. Based on the above analysis, the network scalability for this OCDMA-PON architecture will be discussed later.

To conserve the information contained in the phase of the optical carrier, coherent detection is deployed, whereby a local optical source is coherently combined with the received information-bearing signal. By following the same procedure analysed in Chapter 6, the integration of the detector output, over a bit interval T, will result in (i.e., 6.7):

$$\begin{aligned} S_{out} &= \Re \sum_{i=1}^{K} \int_0^T l(t)s(t)dt + \sqrt{N_0}\int_0^T n(t)dt \\ &= \Re \hat{L}\hat{S}b_0^1 T + \sqrt{\Re T}\hat{L}\int_0^T n(t)dt + \Re \hat{L}\hat{S}\sum_{i=2}^{K}\left[b_{-1}^i R_{i,1}(\tau_i) + b_0^i \hat{R}_{i,1}(\tau_i)\right]\cos\theta_i \end{aligned} \tag{9.7}$$

where $l(t)$ is local oscillator's signal with power of $\hat{L}$, $s(t)$ is the received signal with power of $\hat{S}$, b_0^1 represents the information bit being detected, b_{-1}^i and b_0^i are overlapping of the previous and the following bits of the i^{th} user. N_0 is the noise power spectral density (PSD). $R_{i,j}(\tau)$ and $\hat{R}_{i.j}(\tau)$ are the continuous-time partial correlation functions. The noise $n(t)$ at the optical receiver include mainly the thermal and shot noises, the relative intensity noise and the fibre attenuation e.g. amplified spontaneous emission (ASE) noise. The thermal noise δ_{th}^2 is given by:

$$\delta_{th}^2 = (2k_B^{B_r} T_r T)\big/(e^2 R_L) \tag{9.8}$$

where k_B is the Boltzmann constant, B_r is the ration of the equivalent receiver bandwidth to the signal bandwidth, T_r is receiver noise temperature, R_L and *e* are receiver load resistance and fundamental electron charge respectively. When a relatively high-power local oscillator is employed, the receiver operates under shot-

noise limited regime. Then the noise has one-sided power spectral density of $N_0 = \Re\, T\hat{L}^2$. Nevertheless, the shot noise δ_{sh}^2 is introduced by [115]:

$$\delta_{sh}^2 = \hat{S}^2(2+m^2)\big/(8G_{PD}B_s^2) \tag{9.9}$$

where *m* is the modulation index, G_{PD} is the PD processing gain ratio ($G_{PD} = 60$) and B_s is the baseband signal bandwidth.

The relative intensity noise, δ_{RIN}^2 is also introduced as [56]:

$$\delta_{RIN}^2 = 2P_{RIN}.\hat{S}^2.R_b \tag{9.10}$$

where P_{RIN} is the intensity PSD and R_b is the data bit-rate.

The fibre link noise, δ_{link}^2 such as ASE from optical amplifiers is also defined as:

$$\delta_{link}^2 = \sum_{i=1}^{K}\frac{1}{2}i.e.R_L.P_P.\Re.B_w + 2B_w\Re^2[(\eta_{sp}(G_{amp}-1)h\nu)\big/(\eta G_{amp})]^2 \tag{9.11}$$

where P_P is the optical power per pulse, B_w is the optical components bandwidth, η_{sp} is the spontaneous emission factor, $h\nu$ is the photon energy, η is the PD quantum efficiency and G_{amp} is the gain of optical amplifiers.

Now with all the main contributing noises, the total noise, $n(t)$, can be considered as:

$$\delta_{n(t)}^2 = \delta_{th}^2 + \delta_{sh}^2 + \delta_{RIN}^2 + \delta_{link}^2 \tag{9.12}$$

The noise $n(t)$ is assumed a Gaussian random variable with zero mean and unit variance; all data bits are independent, equi-probable and the delays are independent and uniformly distributed over a bit interval. By following the analysis for coherent homodyne system, the OCDMA-PON transmission signal-to-noise ratio (SNR), with respect to the number of active users *K*, is derived as the following:

$$SNR(K) = \frac{\Re^2 \hat{L}^2 \hat{S}^2 T^2}{\Re^2 \hat{L}^2 \hat{S}^2 T^2 \frac{K-1}{3N} + N_0.\delta_{n(t)}^2} = \frac{1}{\frac{K-1}{3N} + \frac{\delta_{n(t)}^2}{\hat{S}^2 \Re T}} \quad (9.13)$$

It should be noted that the signal-to-noise ratio for a single-user is: $SNR(1) = \hat{S}^2 \Re T / \delta_{n(t)}^2$.

9.2.2 Performance Discussion of OCDMA-PON

The numerical results are presented based on the above analysis. The parameters used for the simulation are listed in Table 9.1 [136]. For spreading code, DPMPC with $P = 19$ is employed that makes the code-length and total number of users 399 and 361 respectively.

Now, we can obtain the maximum reachable fibre length regarding to acceptable receiver sensitivity. The number of nodes in this network architecture and the number of tolerable ONU per node are shown in Figures 9.6 and 9.7 respectively with different downstream transmitter power. It is clearly seen that the maximum reachable length of fibre link is shortened with increasing number of nodes in the network, in Figure 9.6, and also increasing number of ONU per node, in Figure 9.7.

The maximum accessible length of fibre link also increases with higher transmitter's output optical power. To compare with a similar trend as in a WDM-PON [11] this architecture accommodates greater number of users and accordingly nodes even for a longer distance. It is observable from Figure 9.6, by decreasing the number of nodes in the network, the distant between central office (CO) and ONUs can be increased remarkably. For example, when the downstream transmitter output power is 5 dBm and network is able to support 10 nodes (i.e. $N_T / N_u = 10$), the OLT and ONUs can be

maximum 30 Km apart which indicates the enhanced power efficiency and practically worthwhile to compare with the schemes in [54, 56, 136].

Table 9.1 OCDMA-PON link parameters

Descriptions	Symbols	Values
Downstream Transmitter Output Power	P_{DT}	4-5 dBm
Upstream Transmitter Output Power	P_{UT}	-4 dBm
Photo-Detectors Sensitivity	R_S	-35 dBm
Couplers Coefficient Loss	α_c	1 dB
Fibre Attenuation Coefficient	α_F	0.2 dB/Km
Optical Filter Insertion Loss	α_{IL}	1 dB
Filtering Index	C	3
Splitting Ratio	S_P	16-64
Receiver Load Resistor	R_L	1030 Ω
Amplifier Gain	G_{amp}	20 dB
Photo-Detectors Processing Gain	G_{PD}	60
Photo-Detectors Quantum Efficiency	η	0.8
Ration of the Equivalent Receiver's Bandwidth	B_r	100 MHz
Chip Duration	T_c	0.1 ns
Receiver's Baseband Bandwidth	B_s	1 GHz
Receiver's Noise Temperature	T_r	600 K
Modulation Index	m	100
Fibre Length	L	0-45 Km

On the other hand, the investigation of the scalability with respect to the number of users is illustrated in Figure 9.7. It is apparent that the accessibility reduces by growth in the number of ONUs (i.e. users).

A reasonable number of 100 active users (i.e. 28% total number of users when *P*= 19) can be accommodated up to 17 or 23 Km fibre link as shown in Figure 9.7 when transmitter power is only 4 dBm or 5 dBm respectively.

The overall network performance in terms of BER against the number of active users and received signal power (i.e. $\hat{S}^2$) is investigated in Figures 9.8 and 9.9. It is shown in Figure 9.8 that the BER degrades as the number of users increases due to increasing

multiple user interferences from which CDMA inherently suffers and obviously the higher the received power, the lower BER is obtained.

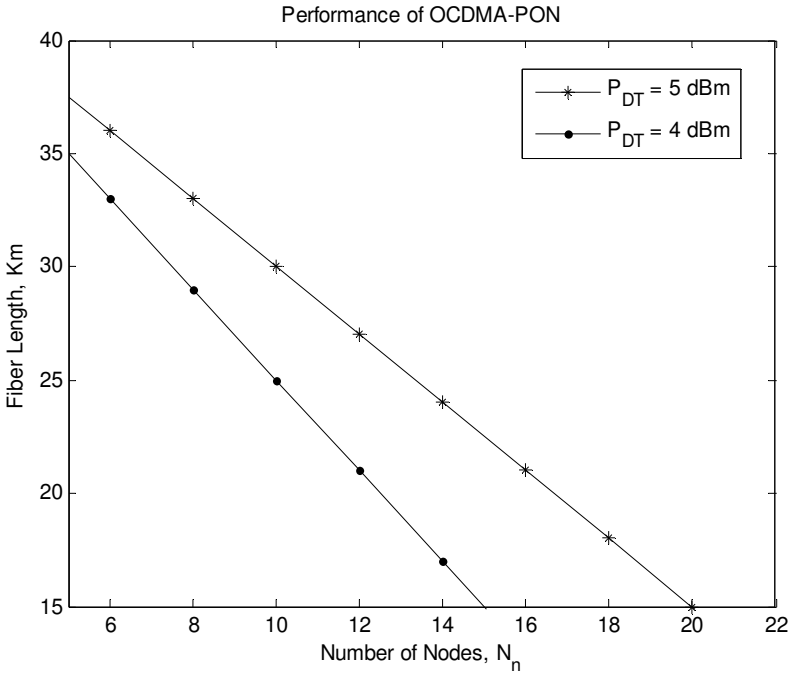

Figure 9.6 Fibre length against the tolerable number of nodes, N_n

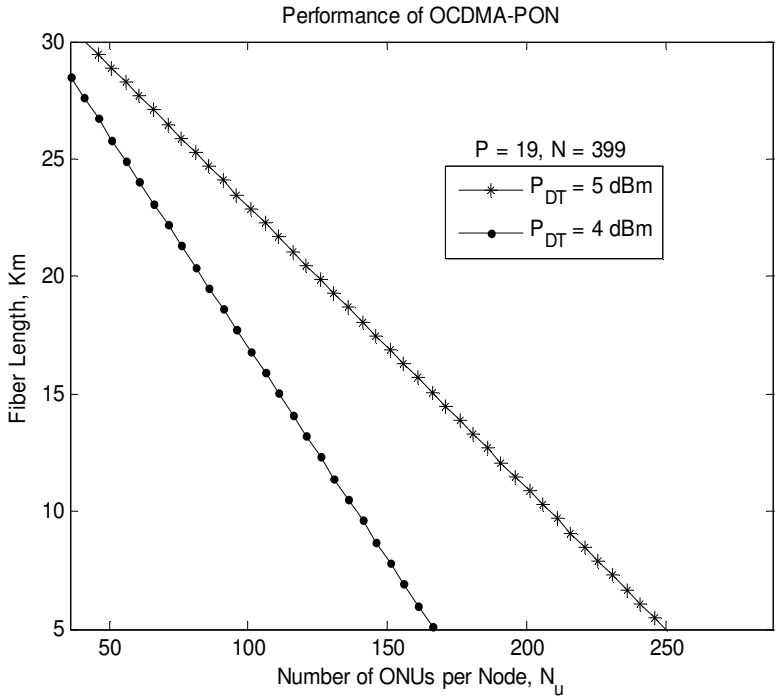

Figure 9.7 Fibre length against the tolerable number of ONUs per node, N_u

As illustrated in Figure 9.8, 100 users can be reliably accommodated when $P_r = -20dBm$ at $BER = 10^{-9}$.

To support greater number of users, higher P value and higher received power should be considered; however there will be then a balance in the network throughput and the number of users since the greater P means longer code-length. The results are comparable with the CDMA-PON and WDM-PON studied in [11, 54, 56], since they indicate that this coding scheme and architecture enhanced the network capacity and also decreased the power consumption.

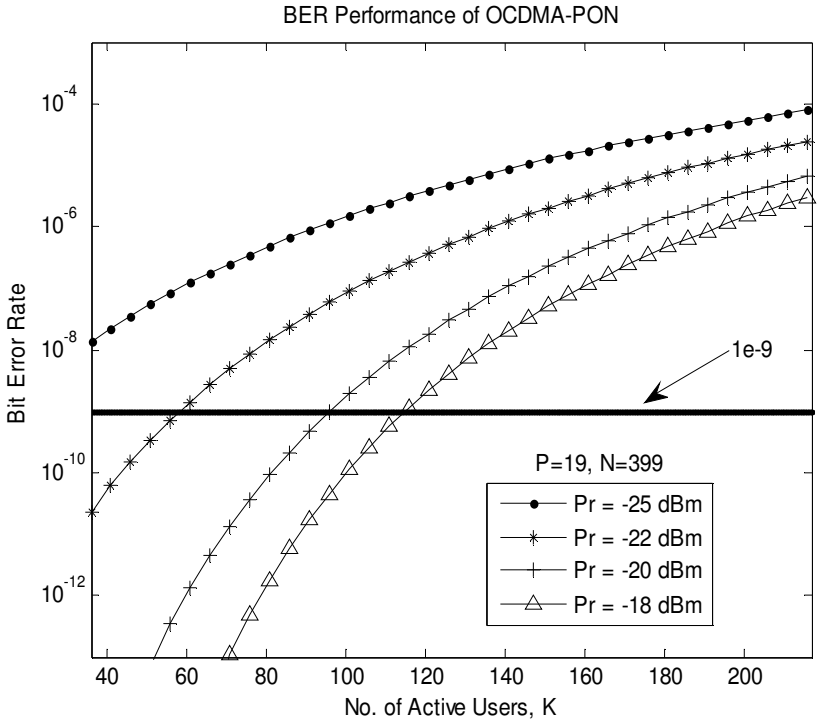

Figure 9.8 BER performance of the OCDMA-PON against the number of active users, *K*

Figure 9.9 explains the BER performance of the network against the received signal power under the presence of various numbers of active users to share the channel from 10% to 40% of total number of users. It is observable from Figure 9.9 that the lower received power is required for fewer users (e.g. 10% and 20%) to

maintain $BER = 10^{-9}$, since fewer users mean less interference and accordingly higher SNR.

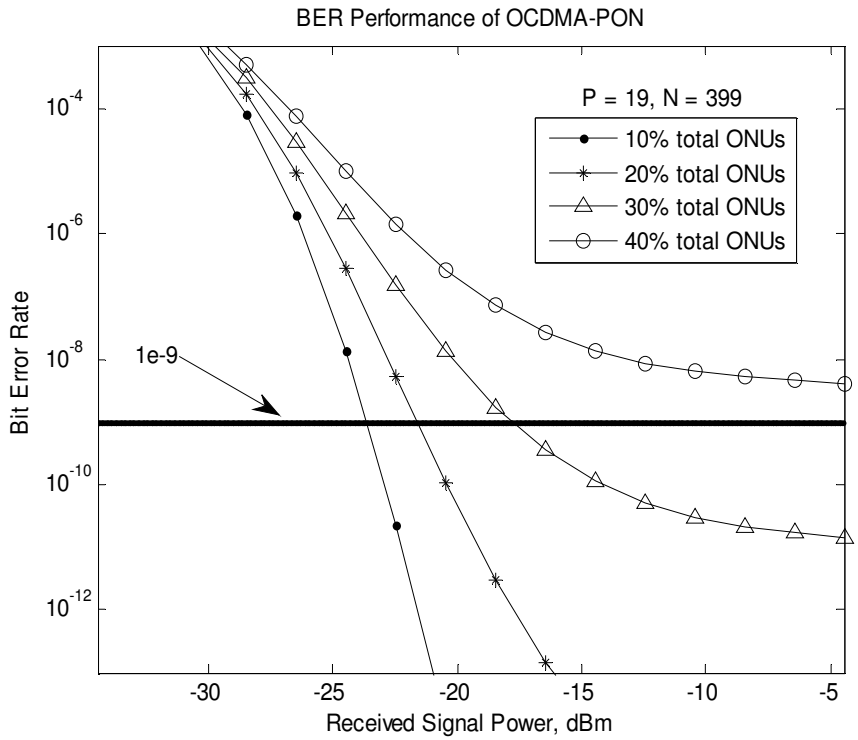

Figure 9.9 BER performance of the proposed OCDMA-PON against the received signal power

The BER can reach to 10^{-9} by accommodating 30% of total number of users with the received power of -18.5 dBm which is still very power efficient. To further improve the performance of the OCDMA-PON, we need to consider the degradation problems from the MAI and improvement in the optical encoder/decoders.

9.3 IP Traffic over OCDMA Network

The IP routing operates electrically in the network layer and then it cannot be processed at the speed matched with the huge transmission offered by the fibre optic, it thus became the main challenge in the optical networking.

The labels can be used to establish end-to-end paths that are called label switched paths (LSP). Multi-protocol label switching (MPLS) is a switching protocol between layers 2 and 3, adding labels in packet headers and forwarding labelled packets in corresponding paths using switching instead of routing [9]. This is what exactly performed in OCDMA concept if it is utilised as network access protocol and then has the potential to support label switching as well. Major applications of MPLS are traffic engineering. Generalized MPLS (GMPLS) extends MPLS to add a signalling and routing control-plane for devices in packet domain, time domain or wavelength domain, providing end-to-end provisioning of connections, resources, and quality of services (QoS).

Even though (G)MPLS forms a good and fast solution, it does not by itself solve the mismatch between the switching speed of the router and the data speed of the fibre in that lookup table processing are still time consuming. In an attempt to overcome this, research started focusing on optical packet switching (OPS) [137] and optical label swapping (OLS) [138], where the packet header (label) is processed (all) optically. OLS implements the packet-by-packet routing and forwarding functions of (G)MPLS directly in the optical domain. Ideally, this approach can route packets independent of bit-rate, packet format and packet-length. Advantages of OPS are particularly evident in core networks, where OLS can be used to replace both OXCs and IP core routers. With regard to OXCs, OLS is a multi-client transport platform used by IP, SDH, gigabit and Ethernet (GbE) clients to manage the bandwidth more efficiently [139]. With regard to IP routers, OLS offers an aggregation layer; it implies using multiple network cables/ports, e.g. Ethernet, in parallel to increase link speed [140]. The IP network is

simplified (avoiding core devices) through the transport infrastructure realized by OPS nodes. From a networking perspective, an all-optical node is defined as a high-throughput packet-switched node. However, processing capabilities are rather limited, and the node essentially limits itself to a forwarding function based on the label of the incoming packets. In metro-regional networks, transport functionality is currently realized by means of different solutions like SDH or WDM rings, etc.

MPLS can be then a solution [9] since at the intermediate nodes a packet is forwarded only according to its label. Since network layer label analysis is avoided, significant processing time is saved at each hop. The end-to-end delay can also be significantly reduced because IP routing is only needed at the edge routers. Although MPLS partially relieves the IP routing, the electrical routing scheme will still become a bottleneck as IP traffic increases. OPS can be another solution by use of pure optical signal processing. There are though many difficulties in contention resolution and optical buffers [137] that make OPS still an immature technology.

In current WDM networks [141] the electronic IP router receives the selected wavelength channels at its input ports, converts the data from optical to electronic form, and finally routes the packets by forwarding them through the output ports. In the wavelength routed networks [142] the direct wavelength path can be established by introducing OXC switches at each node. The chance to establish better routing increases as the number of wavelengths increases that means wider bandwidth and greater set of wavelengths and wavelength sensitive devices will be required. Therefore, it will be very advantageous in the future to execute as many tasks as

possible in the optical domain such as routing/switching [143] and dynamic signal processing [144] whereas they are still under development.

9.3.1 IP Transmission over OCDMA Network

The architecture of IP transmission in the OCDMA network is shown in Figure 9.10. At every transmitter network node, the destination of each incoming IP packet is recognized, the packet recognition can be performed by address correlation process and then the packet is saved into the buffer. The buffer is divided into *K* first-in-first-out (FIFO) subparts where *K* is the total number of users accommodated in the network. IP packets that are destined for different receivers are stored in different subparts accordingly. When IP packets are to be routed to the same receiver, they are saved in one FIFO subpart in order.

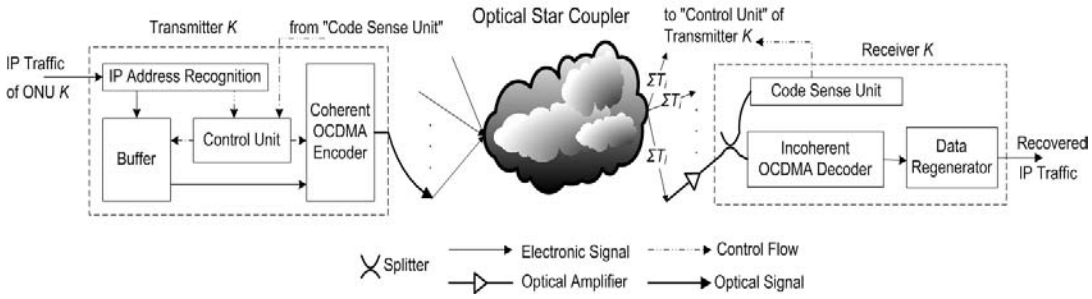

Figure 9.10 IP routing and transmission over OCDMA network architecture

It is important to note that the purpose of storing IP packets separately according to their destination address is to transmit all the IP traffic to the same receiver at one time and at a high speed, once the total length reaches a predefined threshold. Thus, the optical encoder is adjusted for number of packets belonged to the same user rather than being tuned for every incoming IP packet individually. As a result, the encoder adjusting time requirement is significantly reduced. The control unit is

responsible to record the total traffic of each subpart. When the total traffic is greater than a certain value i.e. a threshold, the control unit tries to send the packets to the assigned address. Before sending, the optical encoder has to be adjusted according to the desired address sequence i.e. DPMPC generator in Figure 9.11(a). It should be noted that with a higher threshold, each packet has to wait for a longer time in the buffer before transmission. When the threshold is large, the buffer delay becomes predominant. However, due to the higher transmission speed, proper selection of a threshold value will make this delay acceptable, even for real-time services. The star coupler mixes all the incoming optical signals and this superimposed signal is amplified and transmitted to the receiver of each user.

At the receiver network node, the optical decoder retrieves the right signal and regenerates the original data stream. When the DPMPC is employed, the number of users can be as large as the size of the code (i.e. $K = P^2$). It should be noted that when two (or more) transmitters send signals to the same receiver at the same time, a collision may occur. In order to prevent the collision, a code sense unit is used to sense whether others are sending data to the same address. In fact, the sense unit can be a correlator to recognize the address sequence configured with the code that the intended user should be checked, the same as IP recognition at the transmitter. The sensing procedures can be similar to CSMA/CD protocol; however, a modified one is required to fit in the timing and packet-lengths specifications that can be a future work. Other functions of the code sense unit are both to check whether the optical encoder is adjusted correctly to the desired address code and to prioritize the users to avoid collision. It is noted that there must be one user that we can send data to,

immediately after a collision, since *K* different code sequences are assigned to *K* users separately.

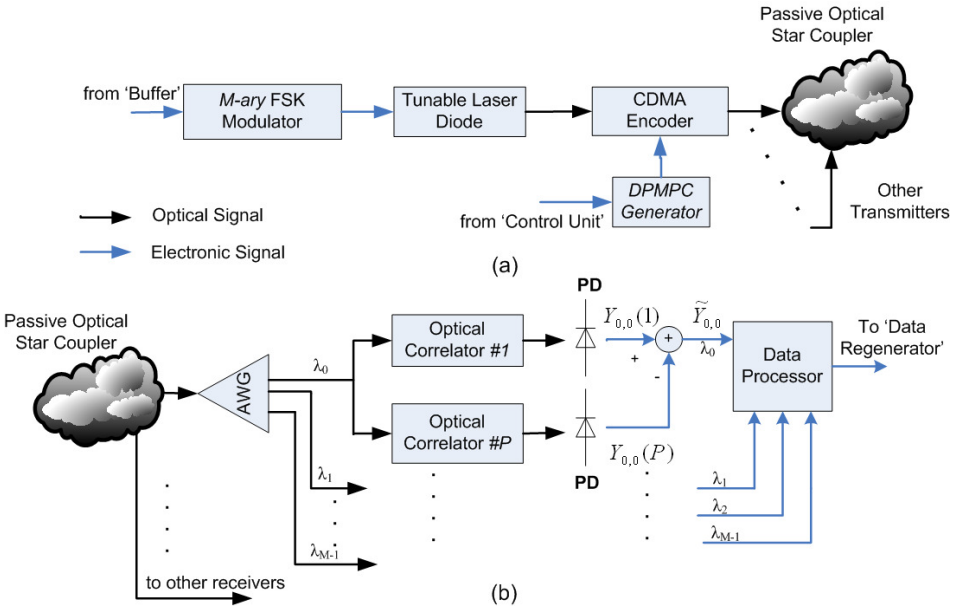

Figure 9.11 Inside OCDMA en/decoder block (a) transmitter and (b) receiver architectures

In addition, the probability of a collision is small because of the large number of available code sequences; although, it can also be analysed and consider in the future work. In this network, owing to the use of coherent OCDMA technique, not only is fibre bandwidth utilized efficiently, but also IP traffic routing is automatically performed. It means that the OCDMA-encoded IP packets are broadcasted through star coupler and only intended user recognises the desired data by its assigned spreading code sequence. Since each IP packet is buffered only twice at the edge of the OCDMA network, the same as in an MPLS network, the buffer delay is significantly reduced compared with traditional routing schemes where IP packets are buffered at each hop.

While the FSK-OCDMA technique is considered, Figure 9.11 illustrates the inside of the optical encoder/decoder blocks as introduced in Figure 9.10 and analysed in details in Chapter 7. As aforementioned, a step-tuneable mode-locked laser diode with 100 GHz repetition rate can be utilised for the optical source to make the 100 Gchips/s feasible [118, 119].

9.3.2 Analysis of IP over OCDMA

The performance analysis for the FSK-OCDMA scheme with the MAI canceller is derived using DPMPC in details in Chapter 7. It is assumed that the input/output characteristic of the PDs follows the Poisson process. Since the reference signal has only the P^{th} sequence (reserved at the receiver, i.e. there is no reference channel) multiplied by the received signal, the data components of reference signal becomes 0 due to further spreading. Also, since all users in the same group receive an equal amount of MAI from the users of other groups and no interference from the users from the same group, i.e. DPMPC correlation properties, the interference signal of intended user u_1, equals the interference signal of *P*. It is assumed that u_1 transmits the optical pulse of λ_0 at the first slot in a data frame.

Since the DPMPC sequences are employed as signature codes and considering number of interfering users in each group based on its correlation properties and using various probability distribution functions based on interfering users and interference estimation, the final bit-error probability (P_b) is derived as (i.e., 7.18):

$$P_b \le \frac{M}{2} \sum_{r=r_{\min}}^{r_{\max}} \sum_{l_{0,0}=0}^{K-r} \sum_{l_{1,0}=0}^{K-r-l_{0,0}} \binom{K-r-l_{0,0}}{l_{1,0}} \times \left(\frac{1}{\gamma.M}\right)^{l_{1,0}} \times \left(1-\frac{1}{\gamma.M}\right)^{K-r-l_{0,0}-l_{1,0}} \times \exp\left\{-\frac{\rho}{2}.\frac{Q.(P+2)}{2}\right\} \times \binom{K-r}{l_{0,0}} \times \left(\frac{1}{\gamma.M}\right)^{l_{0,0}} \times \left(1-\frac{1}{\gamma.M}\right)^{K-r-l_{0,0}} \times \binom{P^2-2P+1}{K-r} \times \binom{P-2}{r-1} \Big/ \binom{P^2-P-1}{K-1} \quad (9.14)$$

where *P* is a prime number, *r* is the number of interfering users in a same group in which $r \in \{r_{\min},...,r_{\max}\}$, $r_{\max} = \min(K, P-1)$ and $r_{\min} = \max\left(1, K-(P-1)^2\right)$. Here K refers to the number of simultaneous active users. $l_{m,v}$ is the number of users who are in groups other than the first group and have a pulse in the v^{th} slot with wavelength λ_m. Taking the fibre attenuation coefficient of α into account, the average received photon count per pulse (*Q*) can be expressed as:

$$Q = \frac{\eta P_w}{hf}.\frac{e^{-\alpha L}}{P+2} \approx \mu.\frac{\ln M}{P+2} \quad (9.15)$$

where $P_r = \eta.P_W e^{-\alpha L}$ is the received power to the detector, P_w is the transmitted peak power per symbol, η is the quantum efficiency of the PDs, *h* is Planck's constant, *f* is the optical frequency, *L* is the fibre-length, and μ ($\mu = P_r/(h.f.\ln M)$) is the average number of photons per pulse (photons/nat). As introduced in Chapter 7, ρ is the parameter minimizing the interference that equals:

$$\rho = \frac{P+2}{P+2+l_{0,0}+l_{1,0}} \quad (9.16)$$

On the other hand, when the bursty IP traffic is implemented to the OCDMA concept, to obtain the acceptable performance without overload, the designed transmission rate for each user should be larger than the average traffic arrival rate. Hence each code channel cannot be fully utilized. It is easy to see that the average number of

active users in the network changes when different channel utilisations are applied. Since the performance of an OCDMA network is a function of the number of active users, the channel utilisation will have a significant effect on the network performance. For this impact analysis, all users (i.e. ONUs) are assumed to have the same channel utilisation in the network as defined by:

$$B = \frac{Average\ Output\ Bitrate}{Maximum\ Transmission\ Bitrate} \tag{9.17}$$

Taking into account that the *zero* and *one* data bits are equi-probable, then the probability of each transmitted bit is $1/2$. Since the ONUs are sending data independently, so the distribution of *K* as a number of active users is K/U where *U* is the total number of users accommodated in the network. Consequently, the probability that *K* users are active ($P_{ac.}$) equals the probability of a transmitted data-bit times the probability of users involved in the transmission times the channel utilisation. This can be expressed as:

$$P_{ac.} = \frac{1}{2} \times \frac{K}{U} \times B \tag{9.18}$$

As being active (sending IP packet) has the binomial behaviour, the active users out of all users can be treated as a binomial distribution. Thus, the PDF of *K* active users are sending IP packet is obtained by:

$$P_{IP}(K) = \binom{U}{K} P_{ac.}^{K} (1 - P_{ac.})^{U-K} \tag{9.19}$$

Accordingly, the total probability of error function of number of active users *K*, $P_T(K)$ denoting BER, can be expressed by the decoder probability of error (P_b) times probability of error stating the *K* active users (P_{IP}). This is then derived by:

$$P_T(K) = \sum_{k=1}^{K} P_{IP}(k).P_b(k) \tag{9.20}$$

The packet-error rate (PER) of the IP traffic over this OCDMA network can be expressed as [30]:

$$PER = 1 - (1 - P_T(K))^w \tag{9.21}$$

where the average IP packet length is w bits.

9.3.3 Performance Discussion of IP over OCDMA

The numerical results are presented based on the above analysis. The parameters used for the simulation are found in Table 9.2. For spreading code, DPMPC with *P*= 13 is employed that makes the code-length and total number of users 169 and 195 respectively. The repetition ratio (γ) is shown by *j* in the graphs and the BER threshold of 10^{-9} is also displayed in all graphs as a reference.

Table 9.2 IP-over-OCDMA link parameters

Descriptions	Symbols	Values
Optical Wavelength	λ_0	1550 nm
PD Quantum Efficiency	η	0.8
Linear Fibre-Loss Coefficient	α	0.2 dB/Km
Chip-Rate	$1/T_c$	100 Gchips/s
Fibre Length	L	10 Km
Packet Length	w	12000 bits

Figure 9.12 shows the performance (BER) comparison of PPM and FSK schemes against the number of users, *K* involved in the transmissions. The analysis for PPM-OCDMA employed DPMPC has also been analysed in Chapter 4. It is obvious that the performance degrades when the MAI increases by growing the number of users as a result of CDMA concept. The received power (P_r) is set to -26 dBm in this analysis. It is apparent that the FSK outperforms PPM in that the repetition ratio γ and *M-ary*

frequency signal distribution mitigate the interference better than the signal position distribution. As introduced and analysed previously, the results explain the scheme is remarkably power efficient. Figure 9.12 demonstrates two different cases when the channel utilisation is fully and 50% occupied. It can be seen that when the channel utilisation is moderate, i.e. *B*= 0.5, the FSK network is able to accommodate 100 active users while PPM supports only 40 users at $BER = 10^{-9}$. In the worst case, when *B* = 1, the IP-over-FSK-OCDMA network still tolerates 40 users at $BER = 10^{-9}$ while only 14 users are supported by PPM scheme. Interestingly, it is indicated that FSK in the worst case (i.e. *B*=1) accommodate the same number as the PPM does when the channel utilisation is halved.

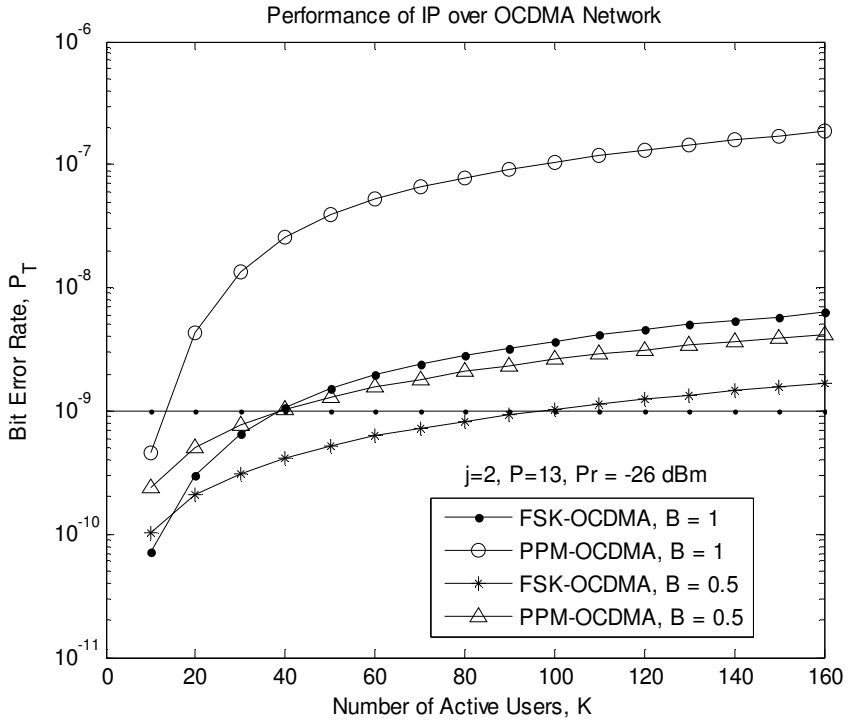

Figure 9.12 BER performance of IP over Different OCDMA against the number of active users, *K*

Figure 9.13 illustrates the performance of IP-over-FSK against the number of active users in different conditions of signal multiplicity *M*, laser repetition ratio γ and the

channel utilisation. The received power is again set to -26 dBm. It is shown that increasing the repetition ratio improves the performance remarkably, though by the cost of throughput, Section 7.4.

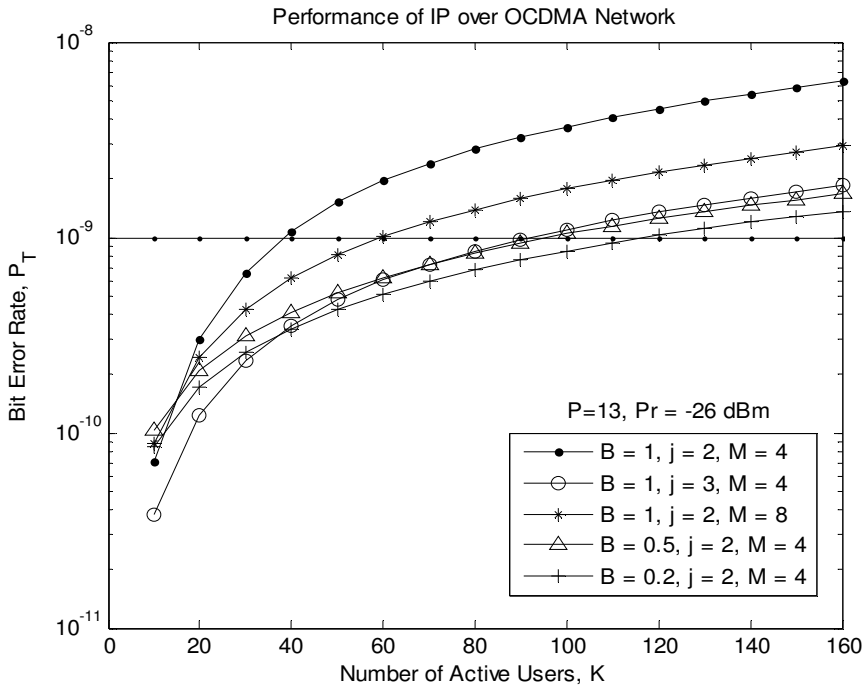

Figure 9.13 BER performance of IP over OCDMA against the number of active users, *K* under different multiplicities, *M* channel utilisations, *B* and repetition ratios, γ

It is indicated from Figure 9.13 that under the same conditions, the system with $\gamma = 3$ and *B* = 1 behaves very similar $\gamma = 2$ and *B* = 0.5, which presents the effect of repetition ratio on the performance. Increasing multiplicity means greater number of positions to distribute the signal and higher number of symbols to transmit; therefore, as seen in Figure 9.13, it can suppress the effect of co-channel interference (i.e. MAI). The number of users accommodated under $BER = 10^{-9}$ when *M*=8 (60 users) is 50% greater than that of *M*=4 (40 users) in the worst case (i.e. *B*=1). Also obviously, it is presented that the performance can be enhanced by reduction in the users' channel utilisation.

In Figure 9.14, the variations of packet-error rate (PER) against the number of active users for different channel utilisations have been presented. The received power and repetition ratio are set to -26 dBm and 2 respectively. In this analysis, it has been assumed that the IP traffic has a packet-length of 1500 bytes (i.e. in Ethernet local area network). Therefore, the calculated PER is estimated in the worst condition. It is clearly shown that the performance of IP traffic becomes better with the reduction in the channel utilisation. As observable from Figure 9.14, while *B* = 1 the performance degrades dramatically however 25 users (15% of total users) are still accommodated at $BER = 10^{-9}$. When the probability that a user is active becomes relatively low i.e. *B* = 0.2, the network is able to hold $BER = 10^{-9}$ with serving 115 users. To compare with the scheme and conditions previously used, it should be noted that here *P* = 13 and received power is only -26 dBm whereas *P* = 17 and 19 (i.e. longer code-length) and effective power equals -10 dBm (i.e. more power consumption) in [29, 30].

When the channel utilisation is 50% the network is still able to provide a reliable communication link for 58 users (35% of total users). To achieve a consistent overall network performance when each user in the network has a fixed average bit-rate, optimal channel utilisation can be set for the network based on the network preferences and link-budgets at the design stage. To support greater number of users, it is obviously recommended to employ higher *P* and P_r values.

The performance presented in Figure 9.15 is against the received signal power (P_r) for different channel utilisations. In this analysis 100 users (60% of total users) are assumed being involved in the transmission. It is obvious that by increasing the received power the detection is performed with assurance and BER becomes lower. As

Figure 9.15 noticeably shows, in order to mitigate the BER in worse cases higher power consumption can be a solution. Although the overall performance reveals that the system is very power efficient.

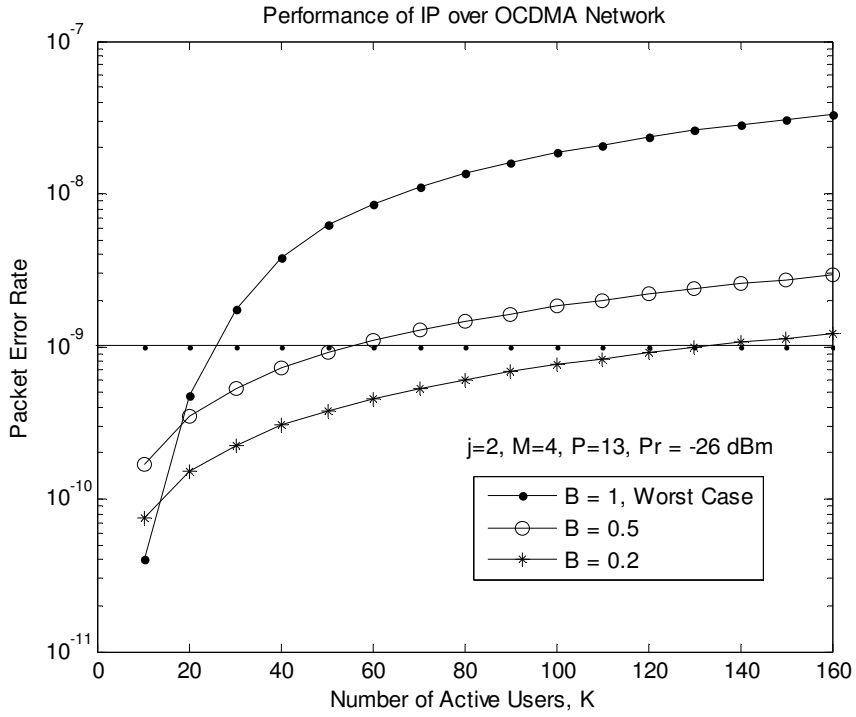

Figure 9.14 PER performance of IP over OCDMA against the number of active users, *K*

When *B* is low, the probability that a user is sending traffic becomes relatively small. On the average, there are fewer active users sending data in each unit data frame, therefore the performance is enhanced. This means when the traffic burden is light, the network performance will be automatically improved. Further examination at P_r = -26 dBm in Figure 9.15 reveals that the error-rates become 3.1×10^{-10}, 1.2×10^{-9} and 6.4×10^{-9} when the channel utilisation is 20%, 50% and fully occupied.

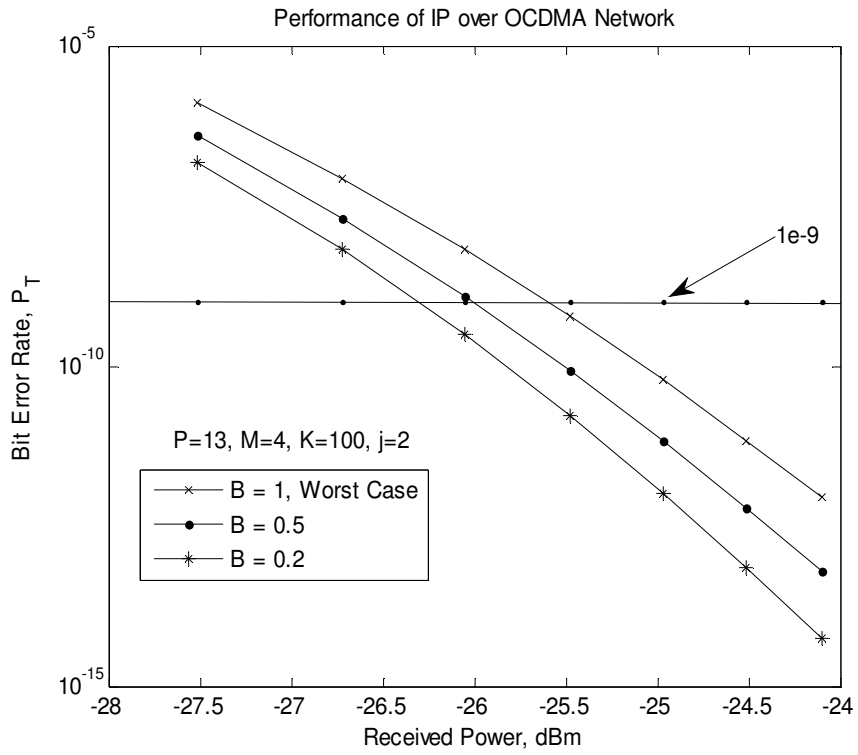

Figure 9.15 BER performance of IP over OCDMA against the received signal power, P_r

9.4 Conclusion

This Chapter introduced a coherent OCDMA-PON architecture including transceivers in the optical line terminal and the optical network units. The scalability of this architecture based on the power-budget analysis has been evaluated. The supportable number of nodes in the network and accessible number of users against the fibre link (i.e. how far they can be from central office) have been investigated and shown that the proposed architecture is more scalable to compare with the schemes and structures introduced in [56, 136].

The overall SNR has been analysed based on degradation of the received signal by (i) fibre link noise e.g. amplifier spontaneous emission noise, (ii) thermal noise, (iii) photo-detectors' shot-noise (iv) phase to intensity noise and (v) mainly multiple-access

interference. The results indicated that the proposed architecture is power efficient and able to accommodate greater number of users which are quite distant from the central office as compared with schemes studied in the literature [56, 136]. It should be noted that the overall promising performance in this architecture is a trade-ff with driving an active EOM and complex implementation to compare with spectral-amplitude-coding (SAC) schemes introduced in the literature. However, this architecture does not need unique transceivers for every user due to generic time-spreading manner imposed by the electric signals, whereas every transceiver needs a specific fibre Bragg grating (FBG) or spectra sensitive components in SAC architectures.

In this Chapter, we have also analysed a novel IP routing and transmission architecture over the OCDMA network taking advantage of coherent modulation and incoherent demodulation. The performance has been considered for different cases in terms of the channel utilisation. To compare with previous schemes [29, 30], since each IP packet is buffered only twice at the edge of the proposed network node, similar to multi-protocol label switching, the buffer delay is significantly reduced as compared with traditional routing schemes where IP packets are buffered at each hop. Additionally, the optical encoder is adjusted for number of packets belonged to the same user instead of getting tuned for incoming IP packet individually. Accordingly, the encoder adjusting time is significantly reduced. As a validation, it should be noted that the results in this Chapter has also been accepted for publication [P15, P16][1].

[1] See 'List of Publications'

Chapter 10

Conclusion and Future Work

10.1 Conclusion and Contributions

In this thesis, we have investigated synchronous time-spreading incoherent and coherent optical CDMA (OCDMA) architectures and reviewed the latest developments on OCDMA coding, multiple-access interference (MAI) cancellation techniques, transceiver architectures and applications. A wide investigation showed that the current state of OCDMA networks inherently suffers from high signal interference (caused by users' simultaneous transmission) and thus cannot be scaled to a large number of users. In order to relax the effect of user interferences, we have proposed a novel spreading code in Chapter 3 referred to as the double padded modified prime code (DPMPC) which can be used in both coherent and incoherent OCDMA systems. Furthermore, based on the correlation properties of the DPMPC, we have introduced a novel co-channel interference (i.e. MAI) cancellation technique that consequently improved the network capacity. The DPMPC assists the OCDMA to operate in more

secure regime under the longer code-length. It can also raise the system performance by increasing auto-correlation peak that enhances the detection process at the receiver in which reduces MAI and accordingly bit-error rate (BER).

The detailed performance of DPMPC when applied to an incoherent PPM-OCDMA network is explained in Chapter 4. Three different types of receivers including (i) simple receiver (ii) receiver with MAI cancellation and (iii) receiver with Manchester coded MAI cancellation, have been analysed. The results indicated that receivers with the DPMPC are able to accommodate greater number of simultaneous users (up to 40-50% of total users depending on *P*, the prime number) as well as low error-rate and less power consumption as compared with existing coding schemes.

We have also analysed the DPMPC in overlapping PPM (OPPM) architecture in Chapter 5 taking into account the effect of self-interferences (SI) which degrades the performance of such a system. Finally, the throughput limitations of PPM and OPPM schemes are studied and evaluated. As observed in Chapter 5, the overlapping index plays a significant role in the improvement of the system performance. Both PPM and OPPM transceivers employed Manchester coding and it was shown when the signal multiplicity restricts the system implementation, Manchester coding is able to recover this limitation at the cost of transceivers bandwidth. The performance of the OPPM-OCDMA transceivers with Manchester coding indicated that the system can accommodate easily up to 50-60% (depending on *P*, prime number) simultaneous users under the lowest error-rate ($<<10^{-9}$).

To examine the DPMPC performance in coherent OCDMA, we have analysed homodyne and heterodyne transceivers with dual-balanced detection in Chapter 6.

The homodyne scheme utilised either a Mach-Zehnder interferometer (MZI) as an external phase modulator (i.e., MZM) or a distributed feedback (DFB) laser diode whose driving current phase-modulated the data signal (so–called injection-locking method). Accordingly, employing the DPMPC outperformed the conventional bipolar codes regarding flexible code-lengths and accommodating more simultaneous active users. The limited phase excursion, generated by injection-locking method, caused several complications including: (i) requirement of separate phase tracking as it can no longer be accomplished simultaneously with phase modulation, (ii) requirement for estimation and removal (or minimisation) of the dc-bias level in the detector output, and (iii) the signal in this method degrades 1.2 dB in total at transmitter and receiver. The overall performance of the transceiver showed that by employing DPMPC the system not only becomes more power efficient but also enhances the network capacity as compared with the commonly used Gold-sequences or optical orthogonal codes.

A novel multiple user interference cancellation technique taking advantage of the DPMPC correlation properties, which simplified the receiver structures in the FSK-OCDMA network, was proposed and analysed in Chapter 7. The coherent FSK modulation along with incoherent demodulation (i.e. hybrid-detection method) using arrayed-waveguide-grating has been examined. It was observed that the cancellation method, as compared with existing techniques, has provided lower error-rate and higher bit-rate. Additionally, the results indicated that when the bit-rate is constant its network capacity can be expanded.

The potential application of optical tapped-delay lines (OTDL) in conjunction with polarization-modulated OCDMA transceivers has been evaluate and analysed in Chapter 8. From a detailed analysis, we have obtained the system signal-to-noise ratio (SNR) and accordingly demonstrated the overall network BER performance. Furthermore, the transceivers design of the proposed two-dimensional (2D) frequency-polarization-modulated OCDMA has been proposed for the first time to the best of our knowledge. The generated signals have the advantage of spreading over higher dimension constellation which provides greater geometric distances between the transmitted signals. Since the polarization-modulated signals have the constant envelope, the transceivers are more robust to nonlinear fluctuations introduced by optical fibres. The results demonstrated that the binary combination of two modulations remarkably enhanced the transceivers performance as well as the security due to 2D advanced modulation in the optical domain.

Chapter 9 unveiled the potential application of OCDMA in the passive optical network (PON) concept as OCDMA-PON architecture. The proposed architecture includes configurations of the transceivers, optical line terminals and optical network units. The network scalability as an important parameter based on power-budget which indicates the network ability to manage growing amounts of workload or users has been introduced and analysed. The results finally revealed that the proposed architecture is able to accommodate greater number of users which are quite distant from the central office (i.e. fibre-link distance) as compared with the schemes surveyed in the literature.

Finally, in Chapter 9 a novel IP traffic transmission over OCDMA network has been introduced and analysed. The channel utilisation, which has a significant impact on the network's throughput, has been considered to evaluate the overall network performance. Since each IP packet is buffered only twice at the edge of the introduced transmission technique, the buffer delay is remarkably reduced as compared with traditional IP traffic managements. Since the optical encoder has been adjusted for number of packets that are belonged to the same user instead of getting tuned for incoming IP packet individually, thus the encoder adjusting time has been considerably reduced as well.

Therefore, the major contributions of this thesis in the field of optical CDMA communications and network can be listed as follows:

- A novel spreading code, i.e. DPMPC, appropriate for both incoherent [P1, P2][1] and coherent [P3-P7] fibre-optic CDMA systems has been proposed. The DPMPC increased the accommodated number of simultaneous users as well as providing securer communication channel.
- A novel co-channel interference cancellation technique [P8] has been introduced into the novel hybrid-detection FSK-OCDMA architecture that reduces the interference noise and accordingly enhances the overall system performance as well as the cost and power efficiency [P9].
- A novel two-dimensional hybrid frequency-polarization modulation taking advantages of vector property of lightwave has been introduced and employed

[1] See 'List of Publications'

into the OCDMA architecture for the first time to the best of our knowledge [P10-P14].

- And finally, a novel network node based on the proposed architectures, for IP traffic transmission over OCDMA networks has been proposed and analysed [P15, P16].

10.2 Future Works

Specific topics for further works have been identified throughout the thesis and the focus of the development should be on the practical implementation of the modulators, correlators and finally transceivers.

Additionally, to further improve the OCDMA communication link, forward error-correcting (FEC) techniques like Turbo code can extremely reduce the co-channel interference and the error-rate. The progressive introduction of in-line optical amplifiers accelerated the use of FEC up to the point that it should be considered almost routine in optical communications [145]. Channel coding is seen as an efficient technique to reduce systems costs and to improve margins against various line impairments such as beat noise, channel cross-talk, or nonlinear dispersion [146]. On the other hand, the design of channel codes for optical communications poses remarkable challenges to the system implementations. Furthermore, the issue of decoding complexity should not be overlooked since data rates are intended to reach tens of gigabits per second and beyond, calling for FEC devices with low power consumption as well. Therefore, there is a need to investigate efficient and fast algorithms of FEC encoding/decoding for OCDMA communications.

From the networking side, the throughput of an OCDMA network at any instant of time depends on the sequences that are on the line at that time instant. The chip-offset between any two sequences is defined as the difference in chip-times between the start of transmission of the sequences, this is so-called out-of-phase or asynchronous transmission. The interference depends on the exact sequences on the line and the chip-offsets with respect to each other at the decoder e.g. OTDL. As discussed in Chapter 9, when two (or more) transmitters send signals to the same receiver at the same time, a collision may occur. To prevent the collision in the asynchronous communication, a medium access control (MAC) protocol is required to fix the correct timing and packet-lengths depending on the network size and specifications [147].

Furthermore, the service-oriented optical network can be a research focused on the evolution of optical networks based on automated-switched transport network (ASTN) infrastructure. In particular, it defines a reference framework for a service-oriented architecture (SOA) by introducing the service-plane that is an intermediate functional plane which contains the intelligence for service provisioning [148, 149].

ASTN has a distributed control-plane (along with the centralised management-plane), which is able to provide dynamic connection to the client networks. Clients are able to request simple connectivity service through the user-network interface (UNI). The analysis of current UNI characteristics reveals some aspects that can be further improved. Currently, the UNI-signalling and UNI-data are more ASTN-specific rather than client-specific. Thus, they need an adaptation at the client network side. In other words, since OCDMA is a promising access technology for the future optical networks

[150, 151] and the quality-of-service policies are well established at various network layers, e.g. differentiated services (DiffServ) and Ethernet [58, 130, 131], a customer-flexible service-oriented OCDMA network will be an intensive future research area.

References

1. K. M. Sivalingam and S. Subramanian, *Emerging optical network technologies*. 2005: Springer Science+Business Media Inc.

2. W. Goralski, *ADSL and DSL Technologies*. 1998: McGraw-Hill.

3. R. Ramaswami and K. N. Sivarajan, *Optical Networks: a practical perspective*. 1998: Morgan Kaufmann.

4. K. Ohara. *Traffic analysis of Ethernet-PON in FTTH trial service*. in *OFC'03*. 2003.

5. K. Kitayama, X. Wang, and N. Wada, *OCDMA over WDM PON - solution path to gigabit symetric FTTH.* J. Lightw. Technol., 2006. **vol. 24**(no. 4): p. 1654-1662.

6. G. Eisenstein, R. S. Tucker, and S. K. Korotky, *Optical time-division multiplexing for very high bit-rate transmission.* J. Lightw. Technol., 1988. **vol. 6**(no. 11): p. 1737–1749.

7. M. S. Borella, et al. *Optical components for WDM lightwave networks*. in *Proceedings of the IEEE*. 1997.

8. M. Fujiwara, et al. *Novel polarization scrambling technique for carrier-distributed WDM networks*. in *ECOC*. 2002.

9. R. Xu, Q. Gong, and P. Ya, *A novel IP with MPLS over WDM-based broadband wavelength switched IP network.* J. Lightw. Technol., 2001. **vol. 19**(no. 5): p. 596-602.

10. A. Sneh and K. M. Johnson. *High-speed tunable liquid crystal optical filter for WDM systems*. in *Proc. IEEE/LEOS Summer Topical Meetings on Optical Networks and Their Enabling Technologies*. 1994.

11. K. Iwatsuki, J. I. Kani, and H. Suzuki, *Access and metro networks based on WDM technologies.* J. Lightw. Technol., 2004. **vol. 22**(no. 11): p. 2623-2630.

12. H. Kobrinski and K. W. Cheung, *Wavelength-tunable optical filters: applications and technologies.* IEEE Comm. Mag., 1994. **vol. 32**(no. 12): p. 50–54.

13. T. P. Lee and C. E. Zah, *Wavelength-tunable and single-frequency lasers for photonic communications networks.* IEEE Comm. Mag., 1989. **vol. 27**(no. 10): p. 42–52.

14. C. A. Brackett, *Dense wavelength division multiplexing networks: principle and applications.* IEEE J. on Selected Areas in Comm., 1990. **vol. 8**(no. 8): p. 948–964.

15. W. T. Tsang, et al., *Control of lasing wavelength in distributed feedback lasers by angling the active stripe with respect to the grating.* IEEE Photonics Tech. Letters, 1993. **vol. 5**(no. 9): p. 978-980.

16. C. Assi, Y. Ye, and S. Dixit, *Dynamic bandwidth allocation for quality of service over Ethernet PON.* IEEE J. on Selected Areas in Comm., 2003. **vol. 21**(no. 11): p. 1467-1477.

17. U. Killat, *Access to B-ISDN via PON - ATM communication in practice*. 1996: Wiley Teubner Communications.

18. C. F. Lam, *Passive optical network: principles and practice*. 2007: Academic Press, Elsevier.

19. G. Kramer, *Ethernet passive optical network*. 2005: McGraw Hill.

20. M. Azizoghlu, J. A. Salehi, and Y. Li, *Optical CDMA via temporal codes.* IEEE Trans on Comm., 1992. **vol. 40**(no. 8): p. 1162-1170.

21. J. P. Heritage, J. A. Salehi, and A. M. Weiner, *Coherent ultrashort light pulse code-division multiple access communication systems.* J. Lightw. Technol., 1990. **vol. 8**(no. 3): p. 478–491.

22. J. A. Salehi, *Code division multiple-access techniques in optical fiber networks - part I: fundamental principles.* IEEE Trans. on Comm., 1989. **vol. 37**(no. 8): p. 824-833.

23. J. A. Salehi and C. A. Brackett, *Code division multiple-access technique in optical fiber networks - part II: system performance analysis.* IEEE Trans. on Comm., 1989. **vol. 37**(no. 8): p. 834-842.

24. W. C. Kwong, P. A. Perrier, and P. R. Prucnal, *Performance comparison of asynchronous and synchronous code-division mutiple-access techniques for fiber-optic local area networks.* IEEE Trans. on Comm., 1991. **vol. 39**(no. 11): p. 1625-1634.

25. Z. Wei and H. Ghafouri-Shiraz, *Proposal of a novel code for spectral amplitude coding optical CDMA systems.* IEEE Photonics Tech. Letters, 2002. **vol. 14**(no. 3): p. 414-416.

26. E. D. J. Smith, R. J. Blaikie, and D. P. Taylor, *Performance enhancement of spectral-amplitude-coding optical CDMA using pulse position modulation.* IEEE Trans. on Comm., 1998. **vol. 46**(no. 9): p. 1176-1185.

27. Z. Wei, H. Ghafouri-Shiraz, and H. M. H. Shalaby, *Performance analysis of optical spectral-amplitude-coding CDMA systems using super-fluorescent fiber source.* IEEE Photonics Tech. Letters, 2001. **vol. 13**(no. 8): p. 887-889.

28. M. Kaverad and D. Zaccarin, *Optical code division-multiplexed systems based on spectral encoding of noncoherent sources.* J. Lightw. Technol., 1995. **vol. 13**(no. 3): p. 534-545.

29. Z. Wei and H. Ghafouri-Shiraz, *IP transmission over spectral-amplitude-coding CDMA links.* J. Microw. & Opt. Technol. Letteres, 2002. **vol. 33**(no. 2): p. 140-142.

30. Z. Wei and H. Ghafouri-Shiraz, *IP routing by an optical spectral-amplitude-coding CDMA network.* IEE Proc. Communications, 2002. **vol. 149**(no. 5): p. 265-269.

31. A. B. Cooper, et al. *High spectral efficiency phase diversity coherent optical CDMA with low MAI*. in *Conference on Lasers and Electro-Optics (CLEO)*. 2007.

32. P. R. Prucnal, *Optical code division multiple access*. 2005: Taylor & Francis Group.

33. H. M. H. Shalaby, *Synchronous fiber-optic CDMA systems with interference estimators.* J. Lightw. Technol., 1995. **vol. 17**(no. 11): p. 2268-2275.

34. H. M. H. Shalaby, *Performance analysis of optical synchronous CDMA communication systems with PPM signaling.* IEEE Trans. on Comm., 1995. **vol. 43**(no. 2/3/4): p. 624-634.

35. H. M. H. Shalaby, *A performance analysis of optical overlapping PPM-CDMA communication systems.* J. Lightw. Technol., 1999. **vol. 19**(no. 2): p. 426-433.

36. T. S. Lee, H. M. H. Shalaby, and H. Ghafouri-Shiraz, *Interference reduction in synchronou fiber optical PPM-CDMA systems.* J. Microw. & Opt. Technol. Letteres, 2001. **vol. 30**(no. 3): p. 202-205.

37. H. M. H. Shalaby, *Direct-detection optical overlapping PPM-CDMA communication systems with double optical hard-limiters.* J. Lightw. Technol., 1999. **vol. 17**(no. 7): p. 1158–1165.

38. M. M. N. Hamarsheh, H. M. H. Shalaby, and M. K. Abdullah, *Design and analysis of dynamic code division multiple access communication system based on tunable optical filter.* J. Lightw. Technol., 2005. **vol. 23**(no. 12): p. 3959-3965.

39. H. M. H. Shalaby, *Complexities, error probabilities and capacities of optical OOK-CDMA communication systems.* IEEE Trans on Comm., 2002. **vol. 50**(no. 12): p. 2009-2017.

40. H. M. H. Shalaby, *Cochannel interference reduction in optical PPM-CDMA systems.* IEEE Trans. on Comm., 1998. **vol. 46**(no. 6): p. 799-805.

41. H. M. H. Shalaby, *Chip-level detection in optical code division multiple access.* J. Lightw. Technol., 1998. **vol. 16**(no. 6): p. 1077-1087.

42. W. Huang, I. Andonovic, and M. Tur, *Decision-directed PLL for coherent optical pulse CDMA system in the presence of multiuser interference, laser phase noise, and shot noise.* J. Lightw. Technol., 1998. **vol. 16**(no. (10)): p. 1786-1794.

43. M. Ito, et al., *Fabrication and application of fiber bragg gratinga review.* J. Optoelectron. Devices Technol., 1995. **vol. 10**(no. 3): p. 119–130.

44. X. Liu, et al., *Tolerance in-band coherent crosstalk of differetial phase-shift-keyed signal with balanced detection and FEC.* IEEE Photonics Tech. Letters, 2004. **vol. 16**(no. 4): p. 1209-1211.

45. S. Betti, G. D. Marchis, and E. Iannone, *Polarization modulated direct detection optical transmission systems.* J. Lightw. Technol., 1992. **vol. 10**(no. 12): p. 1985-1997.

46. T. Ohtsuki, *Performance analysis of direct-detection optical CDMA systems with optical hard-limiter using equal-weight orthogonal signaling.* IEICE Trans. on Comm., 1999. **vol. E82-B**(no. 3): p. 512-520.

47. X. Wang, et al. *Demonstration of DPSK-OCDMA with balanced detection to improve MAI and beat noise tolerance in OCDMA systems*. in *OFC, Paper JThB57*. 2006.

48. S. Benedetto, et al. *Coherent and direct-detection polarization modulation system experiment*. in *ECOC*. 1994.

49. M. Y. Liu and H. W. Tsao, *Cochannel interference cancellation via employing a reference correlator for synchronous optical CDMA system.* J. Microw. & Opt. Technol. Letteres, 2000. **vol. 25**(no. 6): p. 390-392.

50. F. Yamamoto and T. Sugie, *Reduction of optical beat interference in passive optical networks using CDMA technique.* IEEE Photonics Tech. Letters, 2000. **vol. 12**(no. 12): p. 1710-1712.

51. Y. Gamachi, et al., *An optical synchronous M-ary FSK/CDMA system using interference canceller.* J. Electro. & Comm. in Japan, 2000. **vol. 83**(no. 9): p. 20-32.

52. C. C. Yang, *Optical CDMA passive optical network using prime code with interference elimination.* IEEE Photonics Tech. Letters, 2007. **vol. 19**(no. 7): p. 516-518.

53. C. L. Lin and J. Wu, *Channel interference reduction using random Manchester codes for both synchronous and asynchronous fiber-optic CDMA systems.* J. Lightw. Technol., 2000. **vol. 18**(no. 1): p. 26-33.

54. B. Ahn and Y. Park, *A symmetric-structure CDMA-PON system and its implementation.* IEEE Photonics Tech. Letters, 2002. **vol. 14**(no. 9): p. 1381-1383.

55. G. C. Gupta, et al., *A simple one-system solution COF-PON for metro/access networks.* J. Lightw. Technol., 2007. **vol. 25**(no. 1): p. 193-200.

56. C. Zhang, K. Qui, and B. Xu, *Passive optical networks based on optical CDMA: design and system analysis.* Chinese Science Bulletin, 2007. **vol. 52**(no. 1): p. 118-126.

57. A. Stok and E. H. Sargent, *The role of optical CDMA in access networks.* IEEE Comm. Mag., 2002. **vol. 40**(no. 9): p. 83-87.

58. W. Liang, et al., *A new family of 2D variable-weight optical orthogonal codes for OCDMA systems supporting multiple QoS and analysis of its performance.* Photonic Network Communications, 2008. **vol. 16**(no. 1): p. 53-60.

59. U. N. Griner and S. Arnon, *A novel bipolar wavelength-time coding scheme for optical CDMA systems.* IEEE Photonics Tech. Letters, 2004. **vol. 16**(no. 1): p. 332-334.

60. F. Gu and J. Wu, *Construction of two-dimensional wavelength/time optical orthogonal codes using difference family.* J. Lightw. Technol., 2005. **vol. 23**(no. 11): p. 3642-3652.

61. A. L. J. Teixeira, et al. *All-optical time-wavelength code router for optical CDMA networks*. in *LEOS, The 14th Annual Meeting of the IEEE*. 2001.

62. K. Fouli and M. Maier, *OCDMA and optical coding: principles, applications, and challenges.* IEEE Comm. Mag., 2007. **vol. 45**(no. 8): p. 27-34.

63. J. E. Baron, et al., *Multiple channel operation of an integrated acousto-optic tunable filter.* Eletronics Letters, 1989. **vol. 25**(no. 6): p. 375–376.

64. P. R. Morkel, et al., *Erbium-doped fiber amplifier with flattened gain spectrum.* IEEE Photonics Tech. Letters, 1991. **vol. 3**(no. 2): p. 118–120.

65. A. R. Chraplyvy, et al., *Reduction of four-wave mixing crosstalk in WDM systems using unequally spaced channels.* IEEE Photonics Tech. Letters, 1994. **vol. 6**(no. 6): p. 754–756.

66. H. S. Hinton, *Photonic switching fabrics.* IEEE Comm. Mag., 1990. **vol. 28**(no. 4): p. 71–89.

67. H. G. Perros, *Connection-oriented networks: SONET/SDH, ATM, MPLS, and optical networks*. 2005: John Wiley & Sons.

68. B. Mukherjee, S. Yao, and S. Dixit, *Advances in photonic packet switching: an overview.* IEEE Comm. Mag., 2000. **vol. 38**(no. 2): p. 84-94.

69. M. Ilyas and H. T. Moftah, *Handbook of optical communication networks*. 2003: CRC Press.

70. J. G. Proakis, *Digital communications*. 1995: McGraw Hill.

71. I. J. Meel, *Spread spectrum - introduction and application*. 1999: Siruis Communication.

72. A. J. Viterbi, *CDMA, principles of spreading spectrum communication*. 1995: Addison Wesley Publishing Company.

73. R. Prasad, *CDMA for wireless personal communications*. 1996: Artech House publisher.

74. W. W. Diab and H. M. Frazier, *Ethernet in the first mile: access for everyone*. 2006: Standards Information Networks, IEEE Press.

75. D. Reed, *Copper evolution*. 2003, Federal Communications Commission, Technological Advisory Council III.

76. M. Beck, *Ethernet in the first mile: the IEEE 802.3ah standard*. 2005: McGraw-Hill.

77. W. G. Phoel and M. L. Honig. *MMSE space-domain interference suppression for multi-rate DS-CDMA*. in *Vehicular Technology Conf.* 1999.

78. F. R. K. Chung, J. A. Salehi, and V. K. Wei, *Optical orthogonal codes: design, analysis and application.* IEEE Trans. on Info. Theory, 1989. **vol. 35**(no. 3): p. 595-605.

79. L. L. Jau and Y. H. Lee, *Optical code-division multiplexing systems using Manchester coded Walsch codes.* IEE Optoelectronics, 2004. **vol. 151**(no. 2): p. 81-86.

80. F. Liu, *Estimation of new-modified prime code in synchronous incoherent CDMA network*, in *MPhil Dissertation at School of EECE*. 2006, University of Birmingham.

81. S. V. Maric, *New family of algebraically designed optical orthogonal codes for use in CDMA fiber optic networks.* Eletronics Letters, 1993. **vol. 29**(no. 6): p. 538-539.

82. C. S. Weng and J. Wu, *Perferct difference codes for synchronous fiber-optic CDMA communication systems.* J. Lightw. Technol., 2001. **vol. 19**(no. 2): p. 186-194.

83. G. C. Yang and W. C. Kwong, *Performance analysis of optical CDMA with prime codes.* Eletronics Letters, 1995. **vol. 31**(no. 7): p. 569-570.

84. G. P. Agraval, *Fiber-optic communication systems*. 1992: John Wiley & Sons Inc.

85. H. Chung and P. Kumar, *Optical orthogonal codes - new bounds and an optimal construction.* IEEE Trans. on Info. Theory, 1990. **vol. 36**(no. 4): p. 886-873.

86. W. C. Kwong and G. C. Yang, *Multiple-length multiple-wavelength optical orthogonal codes for optical CDMA systems supporting multirate multimedia services.* J. on Selected Areas in Comm., 2004. **vol. 22**(no. 9): p. 1640-1647.

87. J. Huang, et al. *Multilevel optical CDMA network coding with embedded orthogonal polarizations to reduce phase noises*. in *ICICS, Paper F2E.2*. 2005.

88. N. Tarhuni, et al., *Multiclass optical orthogonal codes for multiservice optical CDMA networks.* J. Lightw. Technol., 2005. **vol. 24**(no. 2): p. 694-704.

89. H. M. Kwon, *Optical orthogonal code-devision multiple-access system–part i: APD noise and thermal noise.* IEEE Trans on Comm., 1994. **vol. 24**(no. 7): p. 2470–2479.

90. R. J. Mcyntyre, *The distribution of gains in uniformly multiplying avalanche photodiods: Theory.* IEEE Trans. Electron Devices, 1972. **vol. ED-19**(no. 6): p. 703–713.

91. J. B. Abshire, *Performance of OOK and low-order PPM modulations in optical communications when using APD-based receivers.* IEEE J. on Comm., 1984. **vol. COM-32**(no. 10): p. 1140–1143.

92. G.-C. Yang, *Performance analysis for synchronization and system on CDMA optical fiber networks.* IEICE Trans. on Comm., 1994. **vol. E77B**(no. 10): p. 1238–1248.

93. J. A. Salehi and A. Keshavarzian, *Multiple-shift code acquisition of optical orthogonal codes in optical CDMA systems.* IEEE Trans on Comm., 2005. **vol. 53**(no. 4): p. 687–697.

94. J. G. Zhang and W. C. Kwong, *Design of optical code-division multiple-access networks with modified prime codes.* Eletronics Letters, 1997. **vol. 33**(no. 3): p. 229-230.

95. F. Liu and H. Ghafouri-Shiraz. *Analysis of PPM-CDMA and OPPM-CDMA communication systems with new optical code*. in *Proc. of SPIE*. 2005.

96. C. C. Yang, *The application of spectral-amplitude-coding optical CDMA in passive optical networks.* Optical Fiber Techonlogy, 2008. **14**(2): p. 134-142.

97. A. Gumaste and S. Zheng, *Light-frames: A pragmatic solution to optical packet transport - extending the ethernet from LAN to optical networks.* J. Lightw. Technol., 2006. **vol. 24**(no. 10): p. 3598-3615.

98. D. A. Chapman, P. A. Davies, and J. Monk, *Code-division multiple-access in an optical fiber LAN with amplified bus topology: the SLIM bus.* IEEE Trans on Comm., 2002. **vol. 50**(no. 9): p. 1405-1408.

99. G. J. Foschini and G. Vannucci, *Noncoherent detection of coherent lightwave signals corrupted by phase noise.* IEEE Trans on Comm., 1988. **vol. 36**(no. 3): p. 306–314.

100. T. Koshi, K. Kikuchi, and H. Kikuchi, *Coherent optical fiber communications*. 1988: KTK Scientific Publisher.

101. X. Wang, et al. *10-user, truly-asynchronous OCDMA experiment with 511-chip SSFBG en/decoder and SC-based optical thresholder*. in *OFC, paper PDP33*. 2005.

102. C. C. Yang. *Optical CDMA-based passive optical network using arrayed-waveguide-grating*. in *IEEE Int'l Conf. on Communications, Circuits and Systems*. 2006.

103. J. Huang, et al. *Hybrid WDM and optical CDMA implementation with M-sequence coded waveguide grating over fiber-to-the-home network*. in *IEEE Int'l Conf. on Communications, Circuits and Systems*. 2006.

104. C. C. Chang, H. P. Sardesai, and A. M. Weiner, *Code-division multiple-access encoding and deconding of femtosecond optical pulses over a 2.5-km fiber link.* IEEE Photonics Tech. Letters, 1998. **vol. 10**(no. 1): p. 171–173.

105. A. E. Weiner, *Femtosecond optical pulse shaping and processing.* Progr. Quantum Electron, 1995. **vol. 3**(no. 9): p. 161.

106. Z. Wei and H. Ghafouri-Shiraz, *Codes for spectral-amplitude-coding optical CDMA systems.* J. Lightw. Technol., 2002. **vol. 20**(no. 8): p. 1284-1291.

107. A. Lal-Mohammad, *Synchronous Optical CDMA Networks*, in *MEng Dissertation, School of Electrical, Electronic and Computer Engineering*. 2009, The University of Birmingham.

108. D. J. G. Mestdagh, *Fundamentals of multi-access optical fiber networks*. 1995: Artech House Inc.

109. X. Wang, et al. *Demonstration of 12-user, 10.71 Gbps truly asynchronous OCDMA using FEC and a pair of multi-port optical-encoder/encoders*. in *ECOC, paper Thu 4.5.3*. 2005.

110. Z. Jiang, et al., *Four-User, 2.5-Gb/s, spectrally coded OCDMA system demonstration using low-power nonlinear processing.* J. Lightw. Technol., 2005. **vol. 23**(no. 1): p. 143-158.

111. F. Ayadi and L. A. Rusch, *Coherent optical CDMA with limited phase excursion.* IEEE Comm. Letters, 1997. **vol. 1**(no. 1): p. 28-30.

112. A. H. Gnauck. *40-Gb/s RZ-differential phase shift keyed transmission*. in *OFC'03*. 2003: Paper ThE1.

113. X. Wang, et al., *Coherent OCDMA system using DPSK data format with balanced detection.* IEEE Photonics Tech. Letters, 2006. **vol. 18**(no. 7): p. 826-828.

114. S. Benedetto and G. Olmo, *Performance evaluation of coherent code division multiple access.* Eletronics Letters, 1991. **vol. 27**(no. 22): p. 2000-2002.

115. X. Wang and K. Kitayama, *Analysis of beat noise in coherent and incoherent time-spreading OCDMA.* J. Lightw. Technol., 2004. **vol. 22**(no. 10): p. 2226-2235.

116. K. Iversen, et al. *M-ary FSK signalling for incoherent all-optical CDMA networks*. in *IEEE GlobeCom*. 1996.

117. K. Iversen, T. Kuhwald, and E. Jugl. *D^2-ary signalling for incoherent all-optical CDMA systems*. in *IEEE ISIT Conf.* 1997. Ulm-Germany.

118. J. F. Lemieux, et al., *Step-tunable (100GHz) hybrid laser based on Vernier effect between Fabry-Perot cavity and sampled fibre Bragg grating.* Eletronics Letters, 1999. **vol. 35**(no. 11): p. 904-906.

119. J. Schröder, et al., *Passively mode-locked Raman fiber laser with 100 GHz repetition rate.* Optics Letters, 2006. **vol. 31**(no. 23): p. 3489-3491.

120. A. Carena, et al. *Polarization modulation in ultra-long haul transmission system: a promising alternative to intensity modulation*. in *ECOC'98 Conf.* 1998.

121. M. Born, E. Wolf, and A. B. Bhatia, *Principles of optics*. 7th ed. 1999: Cambridge University Press.

122. L. J. Cimini, et al., *Preservation of polarization orthogonality through a linear optical system.* Eletronics Letters, 1987. **vol. 23**(no. 25): p. 1365-1366.

123. N. Tarhuni, T. O. Korhonen, and M. Elmustrati, *State of polarization encoding for optical code division mutiple access networks.* J. Electromagnetic Waves and Applications (JEMWA), 2007. **vol. 21**(no. 10): p. 1313-1321.

124. K. Iversen, J. Mueckenheim, and D. Junghanns. *Performance evaluation of optical CDMA using PolSK-DD to improve bipolar capacity*. in *Proc. SPIE (Amsterdam)*. 1995.

125. S. Benedetto and P. Poggiolini, *Multilevel polarization shift keying: optimum receiver structure and performance evaluation.* IEEE Trans. on Comm., 1994. **vol. 42**(no. 2/3/4): p. 1174-1186.

126. S. Benedetto and P. Poggiolini, *Theory of polarization shift keying modulation.* IEEE Trans. on Comm., 1992. **vol. 40**(no. 4): p. 708-721.

127. S. Betti, et al., *Homodyne optical coherent systems based on polarization modulation.* J. Lightw. Technol., 1991. **vol. 9**(no. 10): p. 1314-1320.

128. S. Benedetto, R. Guadino, and P. Poggiolini, *Direct detection of optical digital transmission based on polarization shift keying modulation.* IEEE J. on Selected Areas in Comm., 1995. **vol. 13**(no. 3): p. 531-542.

129. N. Gisini, B. Huttner, and N. Cyr. *Influence of polarization dependent loss on birefringent optical fiber networks*. in *OFC 2000*. 2000. Baltimore USA.

130. M. Batayneh, et al., *Optical network design for a multiline-rate carrier-grade Ethernet under transmission-range constraints.* J. Lightw. Technol., 2008. **vol. 26**(no. 1): p. 121-130.

131. C. C. Yang, J. F. Huang, and T. C. Hsu, *Differentiated service provision in optical CDMA network using power control.* IEEE Photonics Tech. Letters, 2008. **vol. 20**(no. 20): p. 1664-1666.

132. M. M. Matalgah and R. M. Radaydeh, *Hybrid frequency-polarization shift keying modulation for optical transmission.* J. Lightw. Technol., 2005. **vol. 23**(no. 3): p. 1152-1162.

133. S. Pun, C. Chan, and L. Chen, *A novel optical frequency-shift keying transmitter based on polarization modulation.* IEEE Photonics Tech. Letters, 2005. **vol. 17**(no. 7): p. 1528-1530.

134. S. Shin, et al. *Real-time endless polarization tracking and control system for PMD compensation*. in *OFC, paper TuP7-1*. 2000.

135. Y. L. Guennec, G. Maury, and B. Cabon, *BER Performance Comparision Between an Active Mach–Zehnder Modulator and Passive Mach-Zehnder Interferometer for Conversion of Microwave Subcarrier of BPSK Signals.* J. Microw. & Opt. Technol. Letteres, 2003. **vo. 36**(no. 6): p. 496-498.

136. C. Zhang, K. Qui, and B. Xu. *Investigation on performance of passive optical network based on OCDMA*. in *IEEE Int'l Conf. on Communications, Circuits and Systems*. 2006.

137. S. Yao, S. J. B. Yoo, and B. Mukherjee, *All-optical packet switching for metropolitan area networks: opportunities and challenges.* IEEE Comm. Mag., 2001. **vol. 39**(no. 3): p. 142-148.

138. P. Seddighian, et al. *Time-stacked optical labels: an alternative to label-swapping*. in *OFC*. 2008.

139. P. Seddighian, et al. *All-Optical Swapping of Spectral Amplitude Code Labels for Packet Switching*. in *Photonics in Switching*. 2007.

140. A. Gumaste, et al., *Light-mesh: A pragmatic optical access network architecture for IP-centric service oriented communication.* Opt. Switching and Networking, 2008. **vol. 5**(no. 2-3): p. 63-74.

141. K. Kitayama, N. Wada, and H. Sotobayashi, *Architectural considerations for photonic IP router based on upon optical code correlation.* J. Lightw. Technol., 2000. **vol. 18**(no. 12): p. 1834-1844.

142. R. Dutta and G. N. Rouskas, *A survey of virtual topology design algorithms for wavelength routed optical networks.* Opt. Networks Mag., 2000. **vol. 1**(no. 1): p. 73-89.

143. M. Meenakshi and I. Andonovic, *Code-based all optical routing using two-level coding.* J. Lightw. Technol., 2006. **vol. 24**(no. 4): p. 1627-1637.

144. A. L. J. Teixeira, et al. *All-optical routing based on OCDMA header*. in *LEOS, The 16th Annual Meeting of the IEEE*. 2003.

145. R. Le Bidan, et al., *Reed-Solomon Turbo product codes for optical communications: from code optimization to decoder design.* EURASIP Journal on Wireless Communications and Networking, 2008. **vol. 2008**(Article ID 658042).

146. S. Ayotte and L. A. Rusch, *Increasing the capacity of SAC-OCDMA: forward error correction or coherent sources.* J. on Selected Topics in Quantum Electronics, 2007. **vol. 13**(no. 5): p. 1422-1428.

147. Z. A. El-Sahn, et al., *Performance of the R3T random-access OCDMA protocol in noisy environment.* J. on Selected Topics in Quantum Electronics, 2007. **vol. 13**(no. 5): p. 1396-1402.

148. M. Hayashi, H. Tanaka, and M. Suzuki. *Advanced reservation-based network resource manager for optical network*. in *OFC*. 2008.

149. J. Perelló, et al., *Resource discovery in ASON/GMPLS transport networks.* IEEE Comm. Mag., 2007. **vol. 45**(no. 10): p. 86-92.

150. Y. F. Wang and J. F. Huang, *Optimal lightpath placement on a metropolitan-area network linked with optical CDMA local nets.* Optical Fiber Techonlogy, 2008. **vol. 14**(no. 1): p. 72-78.

151. J. Berthold, et al., *Optical networking: past, present, and future.* J. Lightw. Technol., 2008. **vol. 26**(no. 9): p. 1104-1118.

List of Publications

P1. ***M. M. Karbassian*** *and H. Ghafouri-Shiraz*, "Fresh prime codes evaluation for synchronous PPM and OPPM signaling for optical CDMA networks", *J. Lightw. Technol., vol. 25, no. 6, pp. 1422-1430, June 2007*

P2. ***M. M. Karbassian*** *and H. Ghafouri-Shiraz,* "Capacity enhancement in synchronous optical overlapping PPM-CDMA network by a novel spreading code", *in Proc. IEEE GlobeCom, pp. 2407-2411, Washington D.C, USA, Nov. 2007*

P3. ***M. M. Karbassian*** *and H. Ghafouri-Shiraz*, "Phase-modulations analyses in coherent homodyne optical CDMA network using a novel prime code family", *in Proc. WCE (ICEEE), pp. 358-362, London, UK, July 2007*

P4. ***M. M. Karbassian****, F. Liu and H. Ghafouri-Shiraz,* "Performance analysis of novel prime code family in coherent optical CDMA network", *in Proc. IEEE ChinaCom, pp. 393-396, Shanghai, China, August 2007*

P5. ***M. M. Karbassian*** *and H. Ghafouri-Shiraz, "*Performance analysis of heterodyne detected coherent optical CDMA using a novel prime code family*", J. Lightw. Technol., vol. 25, no. 10, pp. 3028-3034, Oct. 2007*

P6. ***M. M. Karbassian*** *and H. Ghafouri-Shiraz, "*Evaluation of coherent homodyne and heterodyne optical CDMA structures*", J. Optical and Quantum Electronics, vol. 40, no. 7, pp. 513-524, May 2008*

P7. ***M. M. Karbassian*** *and H. Ghafouri-Shiraz,* "Study of phase modulations with dual-balanced detection in coherent homodyne optical CDMA network", *J. Lightw. Technol., vol 26, no. 16, pp. 2840-2847, August 2008*

P8. ***M. M. Karbassian*** *and H. Ghafouri-Shiraz,* "Novel channel interference reduction in optical synchronous FSK-CDMA networks using a data-free reference", *J. Lightw. Technol., vol. 26, no. 8, pp. 977-985, April 2008*

P9. ***M. M. Karbassian*** *and H. Ghafouri-Shiraz,* "Frequency-shift keying optical code-division multiple-access system with novel interference cancellation", *J. Microw. and Opt. Techno. Lett., vol. 50, no. 4, pp. 883-885, April 2008*

P10. ***M. M. Karbassian*** *and H. Ghafouri-Shiraz*, "Novel PolSK-OCDMA transceiver architecture"*, in Proc. WCE (ICEEE), pp. 411-415, London, UK, July 2008*

P11. ***M. M. Karbassian*** *and H. Ghafouri-Shiraz,"*Transceiver architecture for incoherent optical CDMA networks based on polarization modulation*", J. Lightw. Technol., vol. 26, no. 24, pp. 3820-3828, Dec. 2008*

P12. ***M. M. Karbassian*** *and H. Ghafouri-Shiraz***,** "Optical CDMA transceiver architecture: polarization modulation with dual-balanced detection", *Chapter 5 in* Advances in Electrical Engineering and Computational Science*, Prof. Len Gelman and Dr. Sio-Iong Ao (Eds), Springer Science+Business, pp. 47-57, April 2009 (ISBN: 978-90-481-2310-0)*

P13. ***M. M. Karbassian*** *and H. Ghafouri-Shiraz,* "Hybrid F-PolSK tranceiver architecture for CDMA-PON", *in Proc. WCECS (ICCST), pp. 331-336, San Francisco, USA, Oct. 2008*

P14. ***M. M. Karbassian*** *and H. Ghafouri-Shiraz,* "Incoherent two-dimensional array modulation transceiver for photonic CDMA", *J. Lightw. Technol., vol. 27, no. 8, pp. 980-988, April 2009*

P15. ***M. M. Karbassian*** *and H. Ghafouri-Shiraz,* "IP routing and traffic analysis in coherent optical CDMA networks", *J. Lightw. Technol., vol. 27, no. 10, pp. 1262-1268, May 2009*

P16. ***M. M. Karbassian*** *and H. Ghafouri-Shiraz,* "IP routing and transmission analysis over optical CDMA networks: coherent modulation with incoherent demodulation", *J. Lightw. Technol., In Press*